R72-54

Structures Publication No. 349

Optimum Seismic Protection
and
Building Damage Statistics

Report No. 3

NON-LINEAR DYNAMIC RESPONSE AND DUCTILITY REQUIREMENTS OF BUILDING STRUCTURES SUBJECTED TO EARTHQUAKES

by

Stavros Aristidou Anagnostopoulos

Supervised by

José M. Roesset

John M. Biggs

SCHOOL OF ENGINEERING
MASSACHUSETTS INSTITUTE OF TECHNOLOGY
Cambridge, Massachusetts 02139

September 1972

Sponsored by National Science Foundation

Grants GK-27955 and GI-29936

50272-101

REPORT DOCUMENTATION PAGE	1. REPORT NO. NSF-RA-E-72-261	2.	3. Recipient's Accession No. PB296886

4. Title and Subtitle
Nonlinear Dynamic Response and Ductility Requirements of Building Structures Subjected to Earthquakes (Optimum Seismic Protection and Building Damage Statistics) Report No. 3

5. Report Date
September 1972

6.

7. Author(s)
S.A. Anagnostopoulos

8. Performing Organization Rept. No.
R 72-54

9. Performing Organization Name and Address
Massachusetts Institute of Technology
School of Engineering
Department of Civil Engineering
Cambridge, Massachusetts 02139

10. Project/Task/Work Unit No.

11. Contract(C) or Grant(G) No.
(C)
(G) GK27955
GK29936

12. Sponsoring Organization Name and Address
Applied Science and Research Applications (ASRA)
National Science Foundation
1800 G Street, N.W.
Washington, D.C. 20550

13. Type of Report & Period Covered

14.

15. Supplementary Notes
Structures Publication No. 349

16. Abstract (Limit: 200 words)
The dynamic response of single and multi-degree of freedom systems under earthquake excitation is studied. Some new models that include stiffness and/or strength degradation are introduced, and their response is compared with other frequently used models. Expressions are derived relating the natural period of simple systems (whose properties are estimated by using code procedures) to the required ductility factors for earthquakes of the El Centro intensity. Curves are obtained relating strength-motion intensity to the ductility requirements and are further used to obtain base shear coefficient laws for prespecified values of the ductility factor. A mathematical model, which combines shear and bending springs in three dimensions, is developed and implemented for studies of multi-degree of freedom systems. The formulation has included gravity loads and soil flexibility. Results obtained from the analysis of several buildings are presented and compared to those obtained by other investigators with more accurate models.

17. Document Analysis a. Descriptors

Earthquakes
Earthquake resistant structures
Mathematical models
Dynamic structural analysis
Degrees of freedom
Factor analysis
Dynamic response
Ductility

b. Identifiers/Open-Ended Terms

El Centro

c. COSATI Field/Group

18. Availability Statement	19. Security Class (This Report)	21. No. of Pages 312
NTIS	20. Security Class (This Page)	22. Price A14-A01

(See ANSI-Z39.18) See Instructions on Reverse

OPTIONAL FORM 272 (4-77)
(Formerly NTIS-35)
Department of Commerce

OPTIMUM SEISMIC PROTECTION AND BUILDING DAMAGE STATISTICS

Sponsored by National Science Foundation
Grants GK-27955 and GI-29936

Report No. 3

NON-LINEAR DYNAMIC RESPONSE AND DUCTILITY REQUIREMENTS OF BUILDING STRUCTURES SUBJECTED TO EARTHQUAKES

by

STAVROS ARISTIDOU ANAGNOSTOPOULOS

Supervised by
José M. Roesset
John M. Biggs

September, 1972

R72-54 Structures Publication No. 349

Previous Reports

1. Whitman, R.V., Cornell, C.A., Vanmarcke, E.H., and Reed, J.W.: "Methodology and Initial Damage Statistics," Department of Civil Engineering Research Report R72-17, M.I.T., March 1972.

2. Leslie, S.K., and Biggs, J.M., "Earthquake Code Evolution and the Effect of Seismic Design on the Cost of Buildings," Department of Civil Engineering Research Report R72-20, M.I.T., May 1972.

ABSTRACT

The dynamic response of single and multi-degree of freedom systems under earthquake excitation is studied. Some new models that include stiffness and/or strength degradation are introduced, and their response is compared with other frequently used models.

Expressions are derived relating the natural period of simple systems (whose properties are estimated by using code procedures) to the required ductility factors for earthquakes of the El Centro intensity. Curves are obtained relating strength-motion intensity to the ductility requirements and are further used to obtain base shear coefficient laws for prespecified values of the ductility factor.

A simple mathematical model, which combines shear and bending springs in three dimensions, is developed and implemented for studies of multi-degree of freedom systems. The formulation has included gravity loads and soil flexibility. Results obtained from the analysis of several buildings are presented and compared to those obtained by other investigators with more accurate models.

Preface

This is the third report prepared under National Science Foundation grants GK-279SSK and GI-29936. This report is identical with a thesis written by Stavros A. Anagnostopoulos in partial fulfillment of the requirements for the degree of Doctor of Science. The research was supervised by J. M. Roesst and J. M. Biggs, professors of Civil Engineering at the Massachusetts Institute of Technology. Some of the design data were provided by the firm of LeMessurier Associates, Inc. (Cambridge, Mass.)

TABLE OF CONTENTS

TABLE OF CONTENTS (Continued)

LIST OF TABLES

LIST OF TABLES (Continued)

LIST OF FIGURES

LIST OF FIGURES (Continued)

LIST OF FIGURES (Continued)

LIST OF FIGURES (Continued)

LIST OF SYMBOLS

Notes: 1. In trying to use standard notation we run into the problem of using the same symbols for different quantities. In such cases, however, the notation is always explained in the text, unless no danger of confusion exists.

2. For matrices, capital symbols have always been used.

3. Dots stand for differentiation with respect to time.

I. ENGLISH

A = Area or
= Matrix as defined in 4.23

a = Numerical coefficient or
= Angle of an element with respect to X axis

B = Diagonal matrix with elements $2\beta_i\omega_i$ or
= Constant for shear deformation

b = Numerical coefficient

C = Damping matrix

c = Damping constant or
= Base-shear coefficient

D = Diagonal matrix with elements the distances of the resisting components from the origin

d = Distance of a resisting component from origin or
= Term of modified stiffness matrix for bending springs

E = Modulus of elasticity

e = Term of modified stiffness matrix for bending springs

LIST OF SYMBOLS (Continued)

F = Force vector or
= Shear force

$F(u)$ = Force function

f = Inertia force or
= Flexibility coefficient

$f(\dot{z})$ = Nondimensional resistance function

G = Shear modulus

g = Acceleration of gravity

H = Vector of heights measured from the base

h = Height as defined in the appropriate figures

I = Moment of inertia or
= Matrix of moments of inertia or
= Earthquake intensity or
= Unit vector

K = Stiffness matrix or
k = Stiffness coefficient

ℓ = Length of a strut or
= Bay width

M = Mass or
= Mass matrix or
= Moment

m = Mass

P = Shear force or
= Matrix as defined in 4.23

p = Density

Q = Matrix with columns the eigenvectors of the system

R = Vector of inertia forces

LIST OF SYMBOLS (Continued)

r = Exponent of Ramberg-Osgood model or
$= k_2/k_1$

S = Mass moment of a slab about reference axis

$s = 1 - r$

T = Natural period

t = Time

U = Displacement vector relative to ground in X-Direction

u = Displacement relative to ground in X-Direction

V = Base Shear or
= Displacement vector relative to ground in Y-Direction

v = Displacement relative to ground in Y-Direction

W = Section modulus

X = Vector of x coordinates

x = Coordinate in x-direction

Y = Vector of y coordinates

y = Coordinate in y-direction

$z = u/u_y$

II. GREEK

β = Percentage of critical damping

Δt = Time step

δ = Displacement

θ = Angle of rotation (twist)

λ = .32/ak (as defined in 3.3.4)

μ = Ductility factor

LIST OF SYMBOLS (Continued)

σ = Normal stress

τ = Shear stress

ϕ = Angle of rotation (bending, rocking)

ψ = Chord rotation

Ω = Frequency of periodic excitation

ω = Natural circular frequency

III. SUBSCRIPTS

B - Refers to Base (foundation

b - Refers to Base (foundation) or

- Refers to Bending

c - Refers to Columns

cr - Refers to Cracking

g - Refers to Ground or

- Refers to Girder

ga - Refers to Girder in floor above

gb - Refers to Girder in floor below

i = Subscript for summation

j = Subscript for summation

k = Subscript for summation

ℓ = Subscript for summation

L - Refers to lateral stiffness matrix

m - Refers to Center of mass

n - Refers to n^{th} time step

LIST OF SYMBOLS (Continued)

t - Refers to Tangent stiffness matrix

x - Refers to X axis

y - Refers to Y axis

z - Refers to Z axis

δ - Refers to Displacements

θ - Refers to Rotational component (twist)

ϕ - Refers to Rotational component (bending, rocking)

CHAPTER 1

INTRODUCTION

1.1 Scope

The problem of inelastic response of a complete building which is excited by an earthquake-type loading is a complicated one. Even if the load were completely known, the response would still be highly uncertain, due to the many idealizations that are made, in order to arrive at a workable mathematical model. Some of these idealizations and uncertainties are:

1. Replacement of the actual structure with a set of linear members.
2. Disregard of non-structural or "architectural" components such as partitions, facades, etc.
3. Uncertainty about the load deformation characteristics of the components used, especially under dynamic reversals of loading.
4. Reduction of the actual degrees of freedom to a number which is almost always determined by the available computational capacity and corresponding costs.
5. Disregard of the continuous change of stiffness and/or strength of the structure at levels of deformation above yielding.
6. Disregard of sudden changes of stiffness and strength due to brittle failure of structural and non-structural components.

Almost all the research done in the past few years on the inelastic response of multistory structures has been limited to the

study of simple multistory plane frames (7), (8), (9). Because of tremendous computational requirements, the frames studied were chosen most of the time with one bay, a factor that imposes limitations on the general applicability of the results obtained. Very often results obtained by one investigator are in conflict with those obtained by another, or in other cases they cannot be compared due to different assumptions, different models or different earthquake inputs.

In this work we approach the problem from a different angle. Instead of dealing with one frame, we are trying to determine, from experimental results available in the literature, simple non-linear models, which would best reproduce the interstory behavior of different structural components such as: braced or unbraced steel frames, reinforced concrete frames, shear walls, masonry partitions and infilled frames. In this way a set of equivalent non-linear springs can be determined for each floor, each spring corresponding to one of the components mentioned above. This provides the flexibility of using various load-deflection characteristics for the non-linear springs and incorporates some of the factors listed earlier in the analysis. On the other hand, dealing with components rather than with single members, it is expected that the overall behavior of a certain class of buildings (namely those for which axial shortening of the columns is not important) will be reproduced at computational costs lower than those incurred in the detailed analysis of simple plane frames. Our analysis, of course, will not yield de-

tailed information such as maximum ductility requirements of one particular member in one particular frame, but rather average overall ductilities for the various components in each story. The simplified model employed combines a set of close-coupled springs, arbitrarily arranged on a floor plan, with far-coupled shear-wall type components. Several real buildings will be analyzed using this model.

Another objective of this study is to gain better insight and understanding of ductility requirements of structures by studying single degree of freedom non-linear systems. It is suspected that the Uniform Building Code does not produce earthquake resistant structures equally safe for all categories of buildings. We will investigate this claim, and we will try to gain a clearer picture of how the base-shear coefficient law influences the ductility requirements of structures.

1.2 Thesis Organization

In chapter 2 results of an extensive literature survey on experimental work concerning the behavior of various structural components are presented. Various mathematical idealizations are discussed, and some new non-linear models are introduced. Finally approximate methods to determine the basic parameters of the various models are suggested.

Chapter 3 contains the studies with one degree of freedom systems. First we compare responses of the systems introduced in chapter 2, and then we make ductility studies for a wide range of systems

and earthquake inputs. Curves relating the strength of the structure, the intensity of the earthquake and the ductility factor are obtained for a wide range of systems and are used to derive base shear-coefficient laws that will produce uniform ductility requirements over the complete spectral range. Another set of curves is also derived, which relates ductility factors of 1-DOF systems designed by the U.B.C. to their natural period of vibration.

Chapter 4 contains the mathematical formulation for the multidegree of freedom systems, discussion and comparisons of several numerical methods, and some comparisons in the elastic range with exact methods of analysis. We have also included the formulation that accounts for gravity loads and a matrix formulation for the soil flexibility. The capabilities and limitations of the computer program are also discussed.

Chapter 5 contains results for multidegree of freedom systems which confirm general trends and conclusions obtained in chapter 3 for 1-DOF systems. The effect of torsion on inelastic response is also given some consideration, but not very extensive. Finally results are presented from the analysis of 3 actual buildings: a 13-story steel frame, an 11-story concrete frame, and a 17-story concrete shear wall building.

Chapter 6 contains a summary of the results and recommendations for future research.

CHAPTER 2

LOAD-DEFLECTION CHARACTERISTICS OF VARIOUS STRUCTURAL COMPONENTS

2.1 Introduction

In this chapter we will present the results of an extensive literature survey on the experimental work concerning the behavior of different structural components, we will discuss various mathematical idealizations frequently used and we will introduce new models that describe the behavior of some of these components. Some of these models will be used, as was described in chapter 1, for the modeling of complete buildings that are to be presented in later parts of this work. There is a large amount of experimental work in countries all over the world and different investigators have tried to incorporate results of their experiments in mathematical models. It seems, however, that many of them did so based on their own experiments only and this has resulted in a wide variety of models and formulas. For this particular work, we tried to be as general as possible, looking at results from various sources. In cases where there was a lack of sufficient data we give ranges for possible values of our parameters and keep the models more general. In what follows we will first discuss the behavior of reinforced concrete frames, braced and unbraced steel frames, block walls and infilled concrete and steel frames, giving at the same time the different idealizations devised

to simulate their loading and unloading paths. At the end of this chapter we will give approximate formulas that one can use to determine the basic parameters of the various models, namely the initial stiffness K_o and the maximum force the component can attain at yield F_y.

2.2 Reinforced Concrete Frames

Most of the experimental work on the behavior of reinforced concrete frames comes from three sources: Japan, University of California at Berkeley and PCA-University of Illinois. The PCA tests are on concrete joints which in essence are half portal frames, so the results are directly comparable with those in Japan or Berkeley which are on complete portal frames. Before proceeding with our discussion, we should clarify that some of the tests done were static, some others dynamic. However, it has been found that the loops obtained from a dynamic test are for all practical purposes the same as those obtained from a static test (Shiga et al, (11), Higashi and Ohkubo (12)). So no further consideration will be given to this point.

The behavior of portal frames under cyclic loading is much more complicated than that of a single member. This is due to the fact that factors such as joint details, presence of compressive or tensile axial loads etc. alter the theoretically predicted behavior. Bad design of the connection and inadequate shear strength of the columns are the two main factors that reduce significantly the bending

resistance of the frame and cause brittle failure in many cases. Diagonal (shear) cracks due to inadequate spacing of the stirrups can change drastically the overall behavior and reduce the strength to a minimum, in a very small number of cycles. This was consistently observed in all the cases that showed a considerable decrease of ultimate load capacity with the increase of displacements and loading cycles.

The frames and the joints usually tested are shown below (Fig. 2-1).

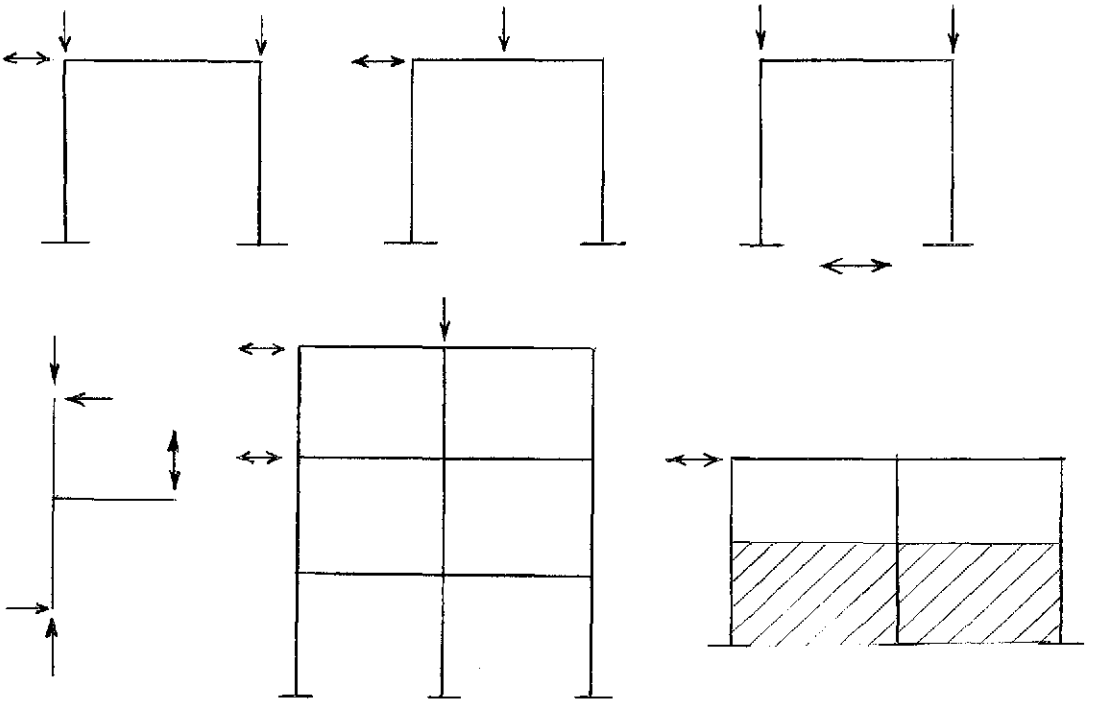

Figure 2-1 Test Configurations of Concrete Frames

No difference was observed in the general shape of the loops for the portal frames and the multistory-multibay ones. Qualitatively, they all showed the same tendencies. A continuous decrease of stiffness is present in all the experiments and the envelope curve of the load-deflection loops can have any of the following three shapes (Fig. 2-2).

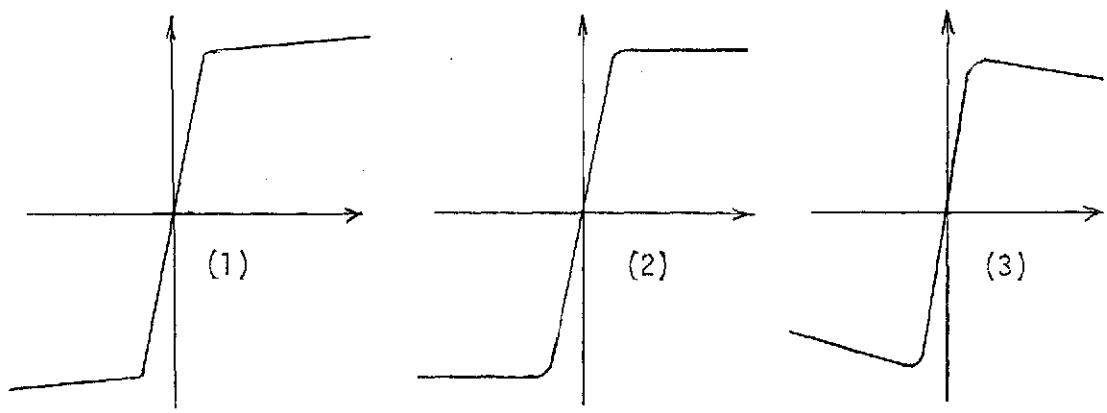

Figure 2-2 Typical Load Deflection Curves for Concrete Frames

Case 1 applies to the well designed, under-reinforced frames with adequate shear resistance. In this case the shear capacity of any section is at any instant greater than the applied shear. The upward slope of the second branch varies and is a function of the excess capacity after the reinforcement has yielded, strain hardening of the reinforcement, etc. It can be conservatively taken as zero and then we are in case 2 that marks the transition between 1 and 3. Case 3 is a typical case of inadequate shear strength. The negative slope

of the second branch can become very steep and in such cases we can have brittle failure.

It is suggested (Bertero and McClure (17), Shiga et al (11), N. Hanson and Conner (19)) that the envelope curve can be well approximated by the curve obtained from a monotonic static increase of the load.

Ultimate strength is not affected (or very little) by the number of cycles or increased displacements, provided again that shear strength is adequate (12), (17), (27), (28).

The stiffness however decreases continuously with increased number of cycles and displacements, ((11) ÷ (37)).

Sketched below (Fig. 2-3) are two typical sets of hysteresis loops for a well designed portal frame.

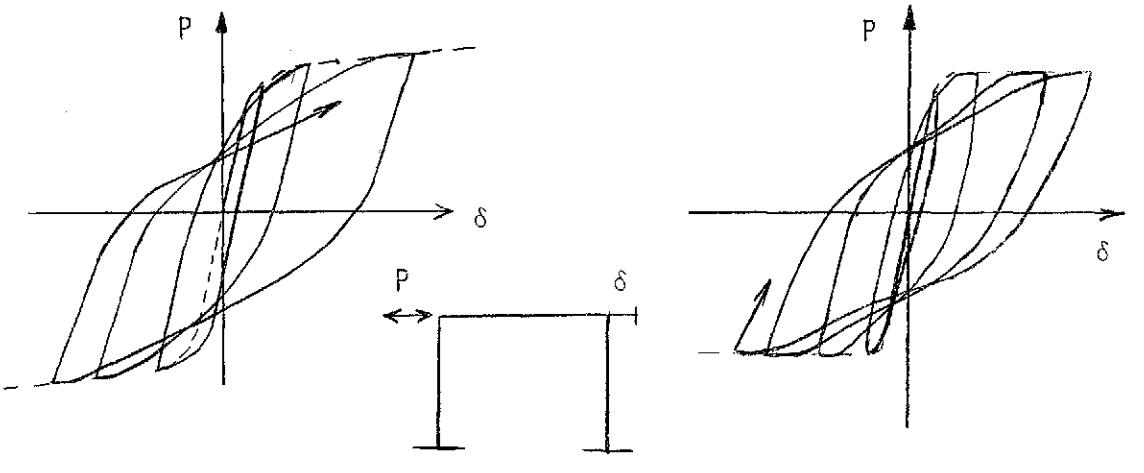

Figure 2-3 Hysteresis Loops for Concrete Portal Frame

From these loops one can observe that there is practically no reduction in stiffness before yielding of the reinforcement has taken place, but after this has happened, the stiffness decreases rapidly with increased displacements and number of cycles.

Analytical models with a varying degree of sophistication have been proposed by different authors. The simplest model that has been used is the typical elastoplastic or bilinear hysteretic, whose loading and unloading is always parallel to the initial slope, if the force is below the yield level.

Tani et al (27), (28) propose a very complex model of the form:

$$Q(x) = A_1 \tan h(A_2 x)$$

and

$$f(x) = C_1(x+1)^{1/s} - 1 - C_2 \tan h(C_3 x - C_4) - C_5 + C_6 \cdot \tan h(C_7 x - C_8) + C_9$$

The first equation is for the envelope curve and the second for the loading-unloading loops.

Shiga et al (11) use the virgin static curve as envelope curve and a cubic equation for the loops (Fig. 2-4).

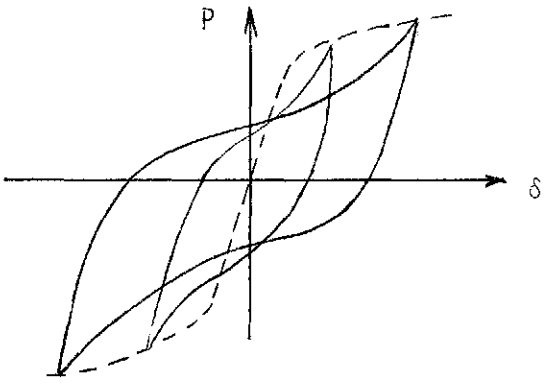

Figure 2-4 Shiga's Curve

Nielsen and Imbeault (29) use a bilinear envelope curve with linear loading and unloading branches. The slope of these branches is degrading with increased displacements (Fig. 2-5). They claim that this model gives satisfactory prediction of the dynamic behavior of reinforced concrete beam-column assemblies, but at low levels of excitation, they had to assume 5% viscous damping because the system does not account for energy absorption in the elastic range. Change in stiffness takes place only when a prior maximum displacement is exceeded.

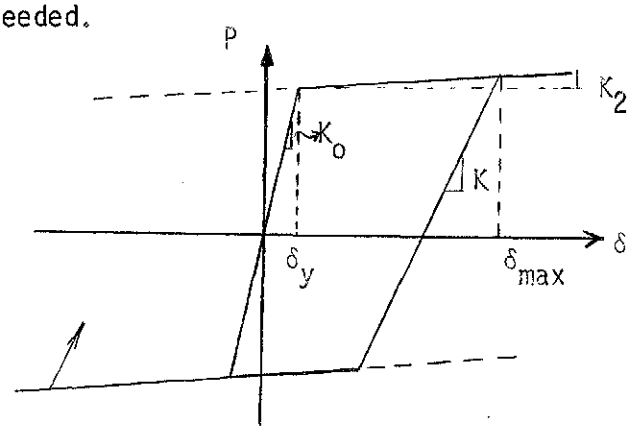

$$\frac{K}{K_o} = \left(\frac{\delta_y}{\delta_{max}}\right)^a$$

$$0.5 \leq a \leq 0.6$$

$$K_2 = .03\ K_o$$

Figure 2-5 Nielsen's Model

Clough and Johnston (69) have also used a degrading stiffness model which is based on the PCA tests. The envelope curve of this model is elastoplastic and the unloading is always parallel to the initial slope. Each reloading however is done with a reduced slope, based on the last point on the envelope curve previously achieved. It is shown schematically below (Fig. 2-6).

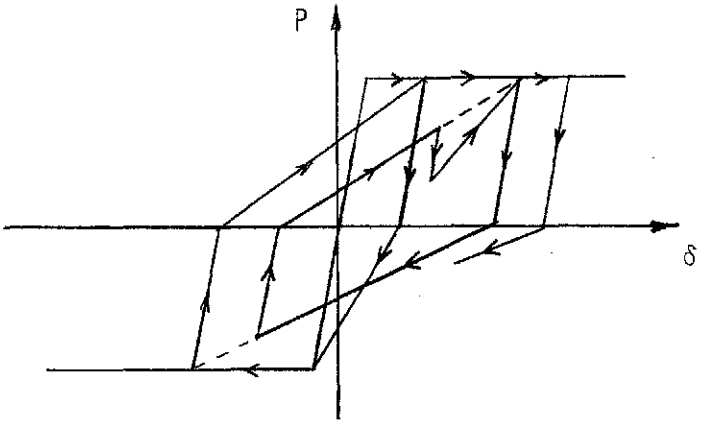

Figure 2-6 Clough's Model

This model has the advantage that each reloading tends to reach the same point in the P-δ plane from which unloading started, which agrees with the experimental data. Nielsen's model does not simulate this. However, Clough's model fails to reproduce the continuously changing slope of the unloading parts of the loops. There is a continuous decrease of the slope of the unloading curves with increased displacements, as can be seen from Figure 2-3.

A new model is proposed here, that combines the advantages of both Clough's and Nielsen's models. This model has an elastoplastic envelope curve (it could have been bilinear with slope of the

second branch same as Nielsen's, i.e. 3% of the initial stiffness); it loads the same way as Clough's model, i.e. with degrading stiffness as determined by the maximum displacement ever reached beyond yielding; and it unloads with a reduced slope. After analyzing several of the reported experimental curves, it was found that the change of slope of the unloading curves follows approximately the law:

$$\frac{K}{K_o} = \left(\frac{\delta_y}{\delta_{max}}\right)^{.35} \qquad 2.1$$

The proposed model is shown below (Fig. 2-7):

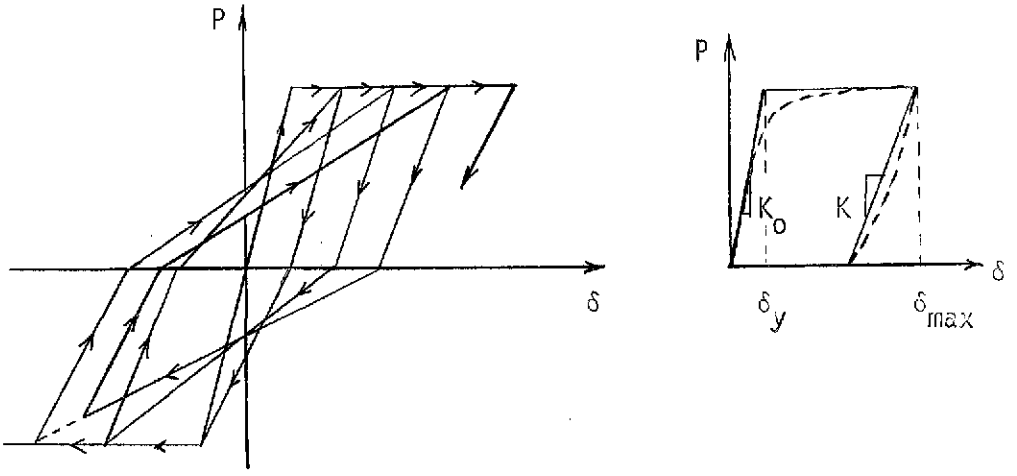

Figure 2-7 Modification of Clough's Model

The new model approximates better than any of the other two, the experimental loops, and is as easy to use as Clough's. The only information needed at any point in order to find the loading or unloading path is the coordinates (in the P-δ plane) of the point

defining the maximum displacement attained up to that moment. The envelope curve can be elasto-plastic or bilinear with positive or negative slope for the second branch.

The slope of the first branch is the one corresponding to the frame's stiffness. The second branch starts after the tension reinforcement of the beams or columns has yielded. It should be mentioned here that different people define stiffness differently. When they plot for example stiffness reduction vs. deflection or number of cycles, what they call stiffness is usually the slope of the straight line connecting the two peaks of the loop. This is different from the average slope of the loading and unloading branches taken separately.

2.3 Unbraced Steel Frames

The basic characteristics of the load-deflection curves for steel frames or beam-column assemblies is that there is practically no decrease of strength or stiffness as the number of loading cycles increases. The loops obtained are stable even after 30 cycles, with distortions well beyond first yielding (46), (48), (49), (51). Local buckling of the flanges near the panel zone however could materially affect the shape of the loops (47), (48). No significant difference was observed between curves obtained under static and curves obtained under dynamic loading (39), (46). A very important characteristic is that a considerable increase of lateral load capacity (up to 40%) over that expected from a monotonic analysis is possible (47). This

is primarily due to strain hardening, which plays a very important role in the overall post-elastic behavior. Spreading of yielding in the plastic hinge locations and Bauschinger effect in the material can cause come reduction of stiffness which will affect the shape of the hysteresis loops, but for all practical purposes this reduction can be neglected (48).

Typical load deflection curves for frames and beam-column assemblies are shown below (Fig. 2-8).

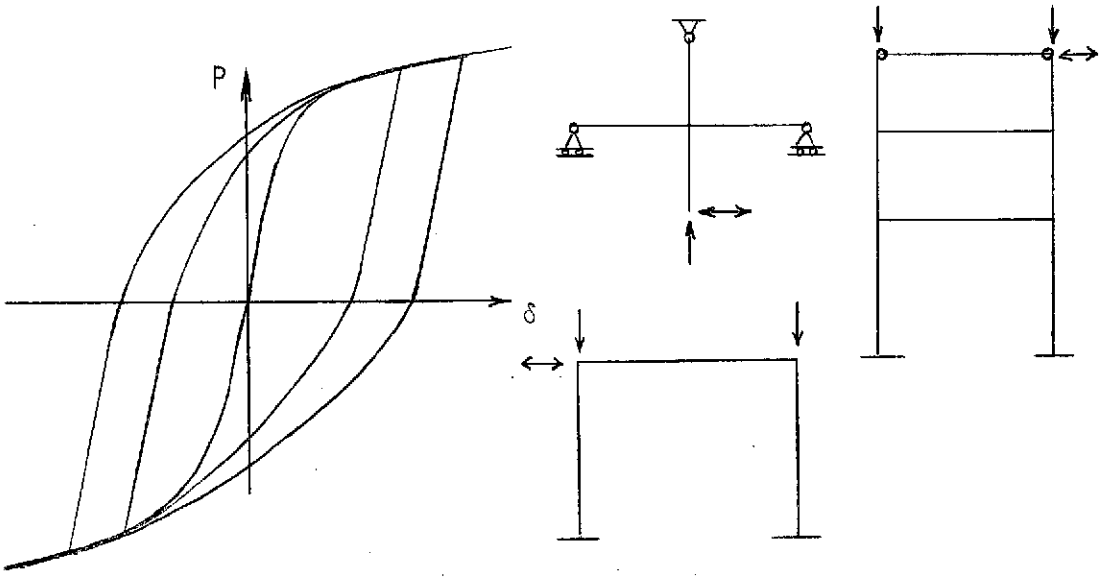

Figure 2-8 Test Configurations and Hysteresis Loops for Steel Frames

Ramberg-Osgood functions of the form:

$$\frac{\delta}{\delta_y} = \frac{P}{P_y}\left(1 + \left|\frac{P}{P_y}\right|^{r-1}\right)$$

can best represent these loops. Depending on the degree of sophistication that one desires, one can use a bilinear hysteretic model which will approximate with straight lines the observed behavior. The parameters of the bilinear model are the slopes of the two branches and the yield level. The slope of the first branch (initial stiffness) is determined as it will be discussed later in this chapter, while the second slope is typically taken as 3 to 5 per cent of the initial slope. The determination of the yield level can be approximately determined by ultimate-load theory, as it will be discussed at the end of this chapter.

Two of the three parameters of the Ramberg-Osgood function, i.e. initial stiffness and yield level, can be determined in the same way as for bilinear models. The third parameter, the exponent r, has a typical value of 8, 9 or 10 (8), (44). The larger the exponent the more flat the curve becomes.

Another model--trilinear in shape--that accounts for a smoother transition due to the gradual formation of hinges will be discussed later.

If the connections of the frame are bolted, the load deflection loops are of the so-called slip-type, similar to those for braced frames (Fig. 2-9). The larger the difference between the nominal diameter of the bolt and the hole, the larger the slip. Such a case could possibly be treated with the model used for a braced frame.

2.4 Braced Steel Frames

Bracing in steel frames increases not only their stiffness and strength but changes considerably the basic shape of the hysteretic

loops. During a cycle the compression braces usually buckle, contributing less or nothing (depending on the type) to the lateral stiffness. Shown below (Fig. 2-9) are some typical experimental curves taken from reference (45) and obtained for zero and one half yield axial load.

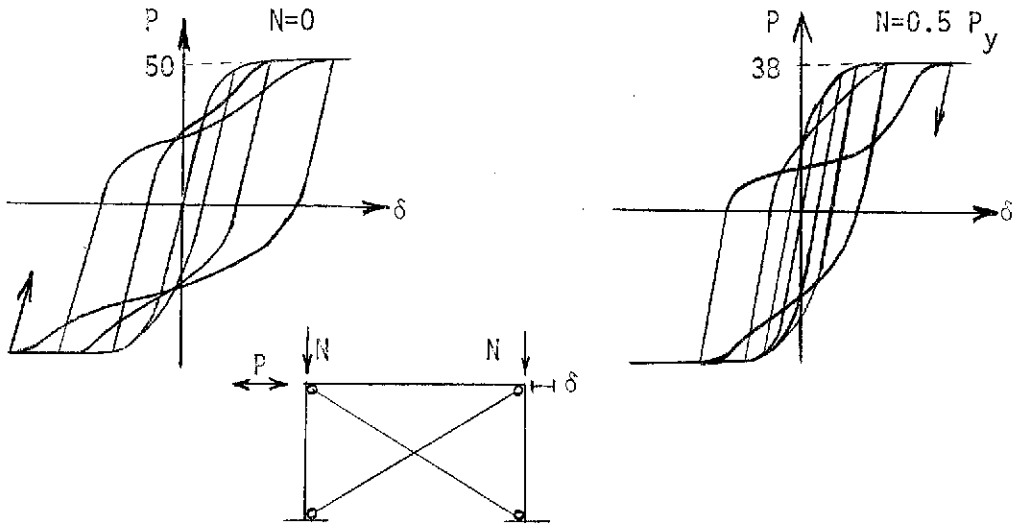

Figure 2-9 Hysteresis Loops for Braced Steel Frames

The usual mathematical model frequently used to simulate this behavior is the so-called "slip-model" which is shown in Figure 2-10.

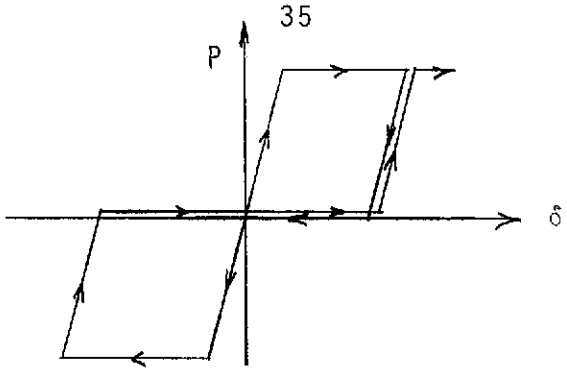

Figure 2–10 Slip Model

It seems however that a degrading stiffness model like those discussed in the paragraph for concrete frames (Clough's model) approximates the experimental loops better. It is worth noting that the slip model neglects the resistance of the frame completely during unloading cycles.

2.5 Walls Without Bounding Frames

Plain walls can be either brick masonry or plain concrete walls. In both cases, if the wall is not reinforced, the load deflection curve is practically a straight line up to the first crack (which occurs at the foundation) and then we have complete failure, since the carrying capacity drops to the frictional resistance of the wall sliding along the foundation. Structurally speaking, this can be neglected (52), (53), (54). This is shown below in Figure 2–11.

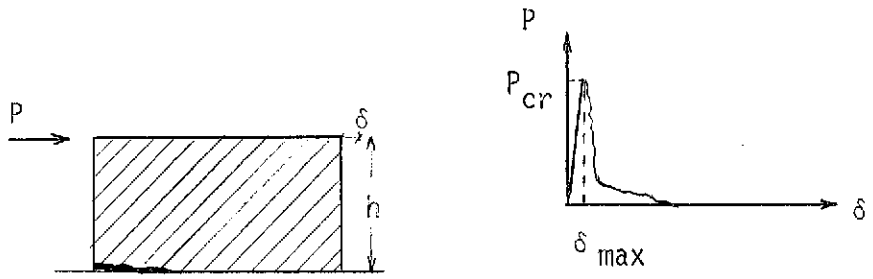

Figure 2-11 Load-Deflection Curve for Plain Walls

If the wall is reinforced, the first crack will force the steel to yield and the carrying capacity will be reduced to the load the steel alone can carry. Reinforced concrete walls with a steel ratio of $p = 0.0025$ have a shear load capacity of the steel alone, which is about 1/3 of that required to produce first cracking. The tensile strength of the base will usually be critical for walls with length-height ratios of approximately 4 or less. If the ratio rises above 4 the shear stress at the center of the wall may be larger than the maximum tensile stress.

However tests show that brick masonry has a strength in bond several times greater than its direct tensile bond strength. The practical solution of the problem will then be found by assuming that foundation cracks in all walls will occur as a result of normal stresses rather than shear stresses.

Unbound walls like the ones discussed above will very rarely be used as load carrying structural components, even for one or two story structures. They were included here for completeness and in order to distinguish their behavior from that of the walls bound by frames.

Their mathematical model is shown below (Fig. 2-12).

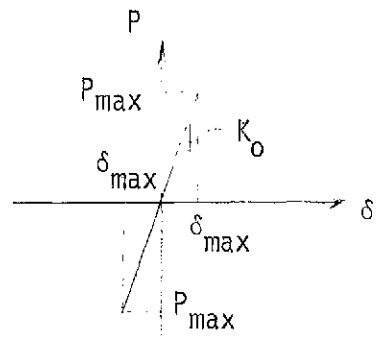

Figure 2-12 Mathematical Model for Plain Walls

Determination of K_o and P_{max} will be discussed in the last paragraph of this chapter.

2.6 Infilled Frames

Infilled frames cannot be considered as a simple superposition of a frame and a wall. Quite the contrary, both components act as an integral unit, with a resulting strength much larger than the sum of the individual strengths. Once cracking occurs, however, there is a considerable decrease in strength and stiffness which is aggravated with increasing number of cycles and magnitude of deformation (52) ÷ (57), (92), (93). It has been proposed to idealize the infill walls with equivalent bracing that extends from the corner where the load acts to the opposite one (this would be a special kind of bracing, acting in compression rather than in tension). When the horizontal load increases, the bond between the wall and the infill deteriorates at the corners and when the tensile strength of the infill is exceeded, diagonal cracks appear, forming a series of parallel struts.

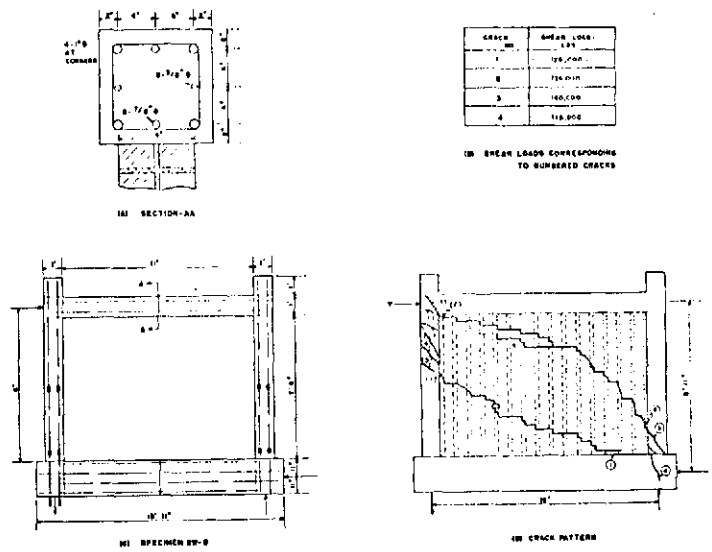

FULL SCALE MODEL OF BRICKWALLED BENT BW-8

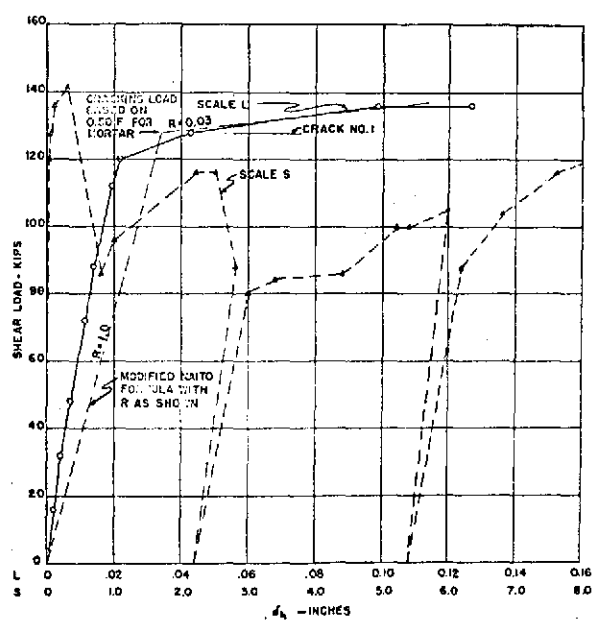

SHEAR LOAD VS. LATERAL DEFLECTION FOR BENT BW-8.

Figure 2-13 Behavior of Infilled Concrete Frames (Adapted from Reference (52))

This is clearly shown in Figure 2-13, which was taken from reference (52). Load deflection curves for the structure at the top part of the figure are also shown there. It is interesting to observe that the cracks initiated in the infill extended into the columns of the frame. It is actually this behavior that causes the deterioration of the complete unit, after the infill starts cracking. In the case of steel frames, the propagation of the crack will not continue in the columns of the frame and the unit will remain with a minimum strength and stiffness, equal to those of the frame alone, after the infill has completely deteriorated (50). In any case, the stronger the bond between the frame and infill and the stronger the infill itself, the higher is the probability that the combination of the two elements will act as a single unit, with very high stiffness and strength. Figure 2-14, taken from reference (5), also indicates the same behavior.

Esteva (55) gives a series of experimentally obtained load-deflection curves for square masonry diaphragms framed by reinforced concrete members and subjected to alternating static loading. His main conclusions are that although the stiffness decreases significantly with increasing deflections and cycles of loading, the strength decreases but not significantly. These conclusions however are restricted to the cases in which the material of the infill is not excessively brittle and diagonal tension cracking of the frame does not occur.

All the above discussion applies to the case of one-story panels, in which the ratio of the applied shear to the base moment

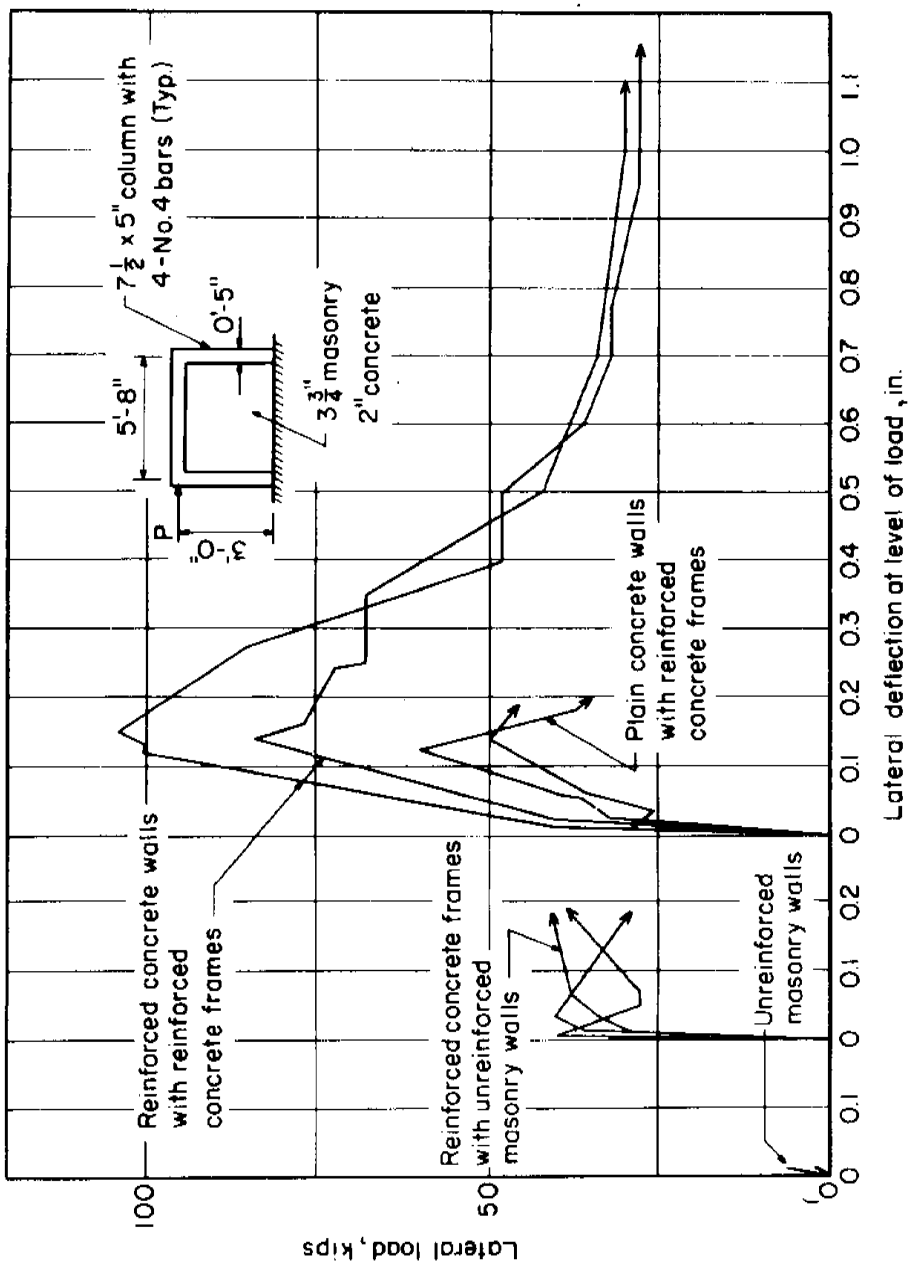

Figure 2-14 Different Cases of Infilled Frames and Walls (Adapted from Reference (5))

is excessively high. In a case of a multistory infill frame, this ratio is low and the unit should be expected to act as a cantilever, provided of course that there is good construction and sufficient bond between frame and infill. That this is actually the case was confirmed by a full scale test, performed in Johannesburg, South Africa. Two frames were tested: one with infill and another without. The cracks in the two cases and the corresponding load deflection curves are shown below in Figure 2-15, taken from reference (5).

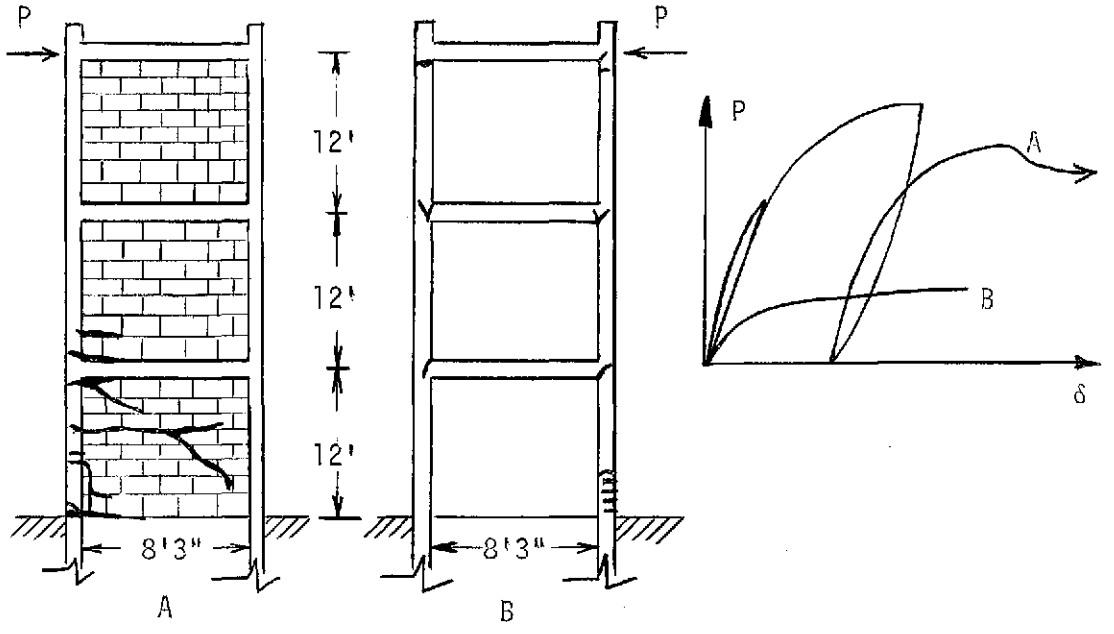

Figure 2-15 Behavior of 3-Story Infilled Frame
(Taken from Reference (5))

The location of the cracks in the case A shows that the infilled frame behaves as a cantilever, while in case B we have a typical

case of rigid frame action. The load capacity of the simple frame was only 20% of the infilled one. In the right of the picture we see that in the second cycle, the maximum capacity has been reduced by 10-20% of the initial. Model tests in Japan show similar behavior.

Selection of an appropriate mathematical model for an infilled frame (steel or concrete) has to depend on the slenderness of the frame (height to width ratio), the type of the infill and the quality of the bond (in some cases, infills are built as floating partitions, in order to avoid this combined action and the ensuing degradation of strength). While more experimental work in this area seems warranted, for most usual buildings a stiffness and strength degrading model seems appropriate. Ohsaki et al (31) have used a stiffness and strength degrading model, whose reduction factors for strength and stiffness are functions of the number of loading cycles. A new model is proposed here, that accounts not only for the number of cycles but also for the maximum displacement.

If we call K_o and F_o the initial stiffness and strength and K, F the stiffness and strength at the nth cycle the new model is described by the following laws:

$$\frac{K}{K_o} = \left(1 - \frac{1}{a} \cdot \frac{\delta_{max}}{\delta_y}\right) b^n \qquad 2.2$$

$$\frac{F}{F_y} = \left(1 - \frac{1}{a^2} \cdot \left(\frac{\delta_{max}}{\delta_y}\right)^2\right) c^n \qquad 2.3$$

and in addition for steel frames:

$$K_{min} = K_{(frame\ alone)}$$

$$F_{min} = F_{(frame\ alone)}$$

where: δ_{max} = maximum absolute displacement occurred

δ_y = yield displacement (or displacement at cracking)

n = number of complete loading cycles

a, b, c = parameters

The value of the parameter a should be determined from the reduction of strength and stiffness, in half cycle of static loading (n =0), a little before collapse. It should always be

$$a \geq \left(\frac{\delta_{max}}{\delta_y}\right) \qquad \text{at static collapse}$$

For example if $\left(\frac{\delta_{max}}{\delta_y}\right)_{\text{at static collapse}} = 10$

and we take a = 15, it will mean that a little before collapse the strength reduction factor from displacement alone is:

$$1 - \frac{10^2}{15^2} = .555$$

and the stiffness:

$$1 - \frac{10}{15} = .333$$

Values of a in the range of 10 to 40 seem reasonable. b and c could have the following values:

$$b = .75 \div .90$$

$$c = .90 \div .95$$

The values suggested for the above parameters are a "little more" than guesses. As more experimental evidence becomes available, different and more specific values might be more appropriate. The proposed model implies faster degradation of stiffness than strength, which is consistent with the existing experimental data. Figure 2-16 shows the variation of the different factors.

From computer runs which will be described in the next chapter, it was found that the proposed model is sensitive mainly to b and c and not so much to a.

Williams and Benjamin (53) give detailed formulas for the determination of F_y and K_o. We will give some cruder approximations at the end of this chapter.

Before closing this section, it is worth mentioning that a particularly important (and dangerous) case is that of concrete frames with partial infill (up to a certain height, the remaining space being used for windows). The bottom of the frame acts then essentially as an integral unit (if there is bond between the columns and the infill), whereas the top is left as a frame with very short columns. If this condition is not properly accounted for in the design, the short columns will probably fail in shear.

$$K,F = (K_o,F_o) \cdot f_\delta \cdot f_n$$

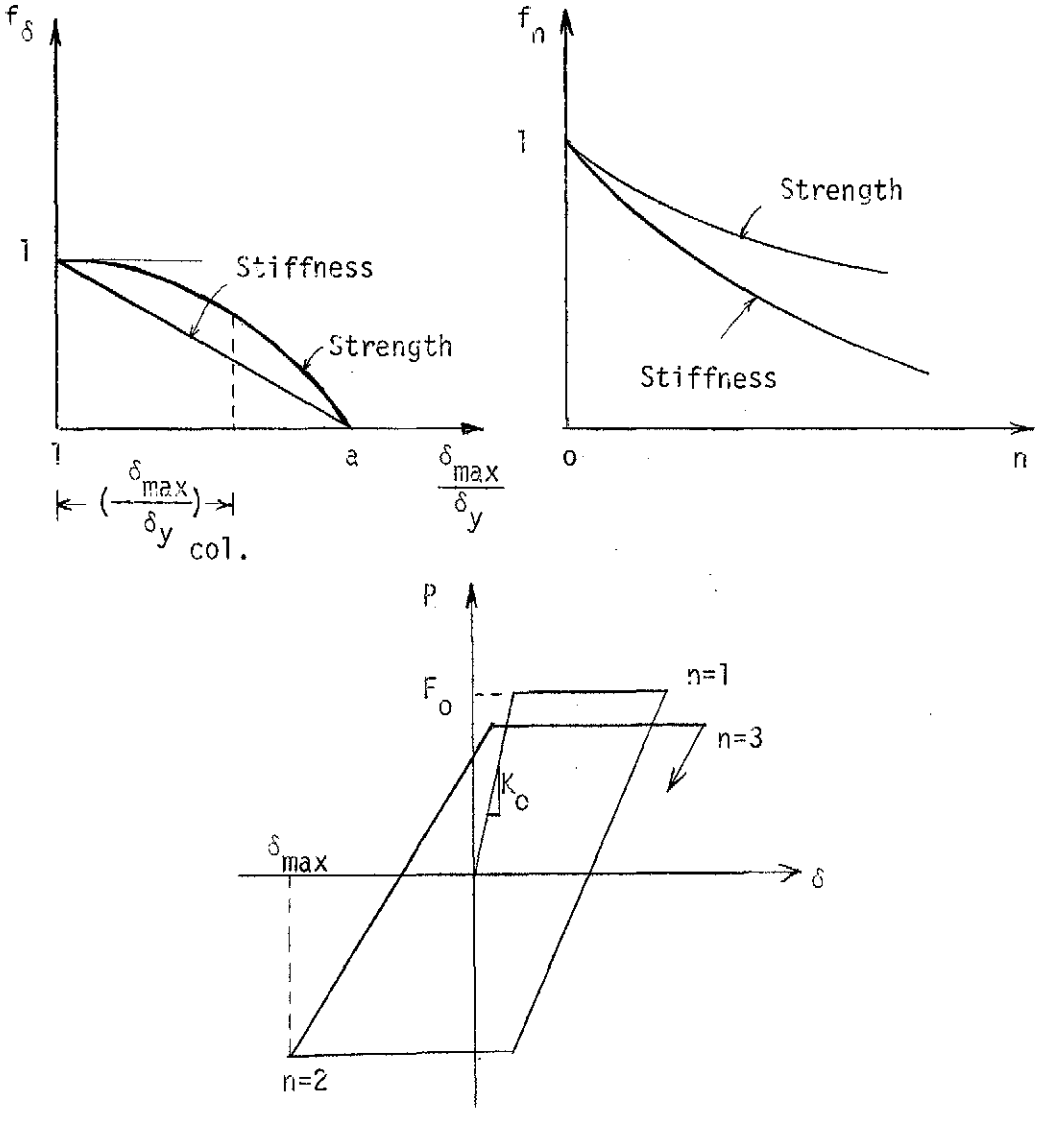

Figure 2-16 Proposed Model for Strength and Stiffness Degradation

2.7 Shear Walls

Shear walls properly designed should behave as cantilever beams. If the shear resistance is not exceeded, they can be considered as a series of members between floor slabs with moment-curvature relation for each joint (at the slab level) given by a constant strength-stiffness degrading model. The effect of the rigidity of the slab could be accounted for.

The same comments essentially apply to box-type elements such as elevator shafts. Initially they will act as a cantilevers connected to the slab at the floor levels, with bending in both directions and considerable torsional stiffness. However for the element to behave as an integral unit, the corners should be properly reinforced, because otherwise they will crack and the different sides will act independently of each other.

2.8 Approximate Determination of Initial Stiffness and Yield Level

In the previous pages we described the behavior of various structural components under alternating loading and we gave straight line mathematical idealizations which approximate this behavior. Here we will give approximate formulas with which the two basic parameters of the various models, namely the initial stiffness K_o and the yield level F_y, could be estimated. It is believed that the confidence level of this approximation is consistent with the rest

of the assumptions about the loading and the modelling of the building.

2.8.1 Initial Stiffness of a Story in a Multistory Frame

We can estimate the stiffness of a particular story by making the following assumptions:

a) Column shears above and below a joint equal
b) Inflection points in columns above and below at same location
c) Rotation of all joints in a floor equal

With these assumptions and using slope-deflection equations, we can obtain:

$$K_o = \frac{24E}{h^2} \cdot \frac{1}{\frac{2}{\Sigma K_c} + \frac{1}{\Sigma Kg_a} + \frac{1}{\Sigma Kg_b}} \qquad 2.4$$

where:

E = modulus of elasticity

h = story height

ℓ = beam length

I = moment of inertia

$\Sigma K_c = \Sigma \frac{I}{h}$ for all columns in the story

$\Sigma Kg_a = \Sigma \frac{I}{\ell}$ for all beams in floor above

$\Sigma Kg_b = \Sigma \frac{I}{\ell}$ for all beams in floor below

The derivation of this formula is given in Appendix A. In the case of concrete frames one difficulty that arises is that of the moment of inertia to be used. This is due to the following three factors.

a) At the section level, the effective moment of inertia is not constant but a function of the axial force and moment.

b) At the member level, the moment of inertia is variable due to the variation of the moment along the member.

c) Being a function of the loading, it varies from one time step to another.

Some people have suggested using the moment of inertia of the cracked section, where the moment is maximum, computed from gravity loads only. This results in using the gross moment of inertia for the columns and the reduced, due to cracking of the section, for the girders. Another approach is to use the formula suggested by the 1971 ACI code, which however does not account for gravity loads. A somewhat more accurate approach is suggested here, which is based on reference (20) by Medland and Taylor. Shown in Figure 2-17 are plots of the ratio $\frac{EI}{EI_{gross}}$ vs $\frac{M}{My}$ for various values of the ratio $\frac{P}{Py}$ taken from reference (20).

My is the ultimate moment capacity of the section for zero axial load.

Py is the ultimate axial load capacity of the section for zero moment.

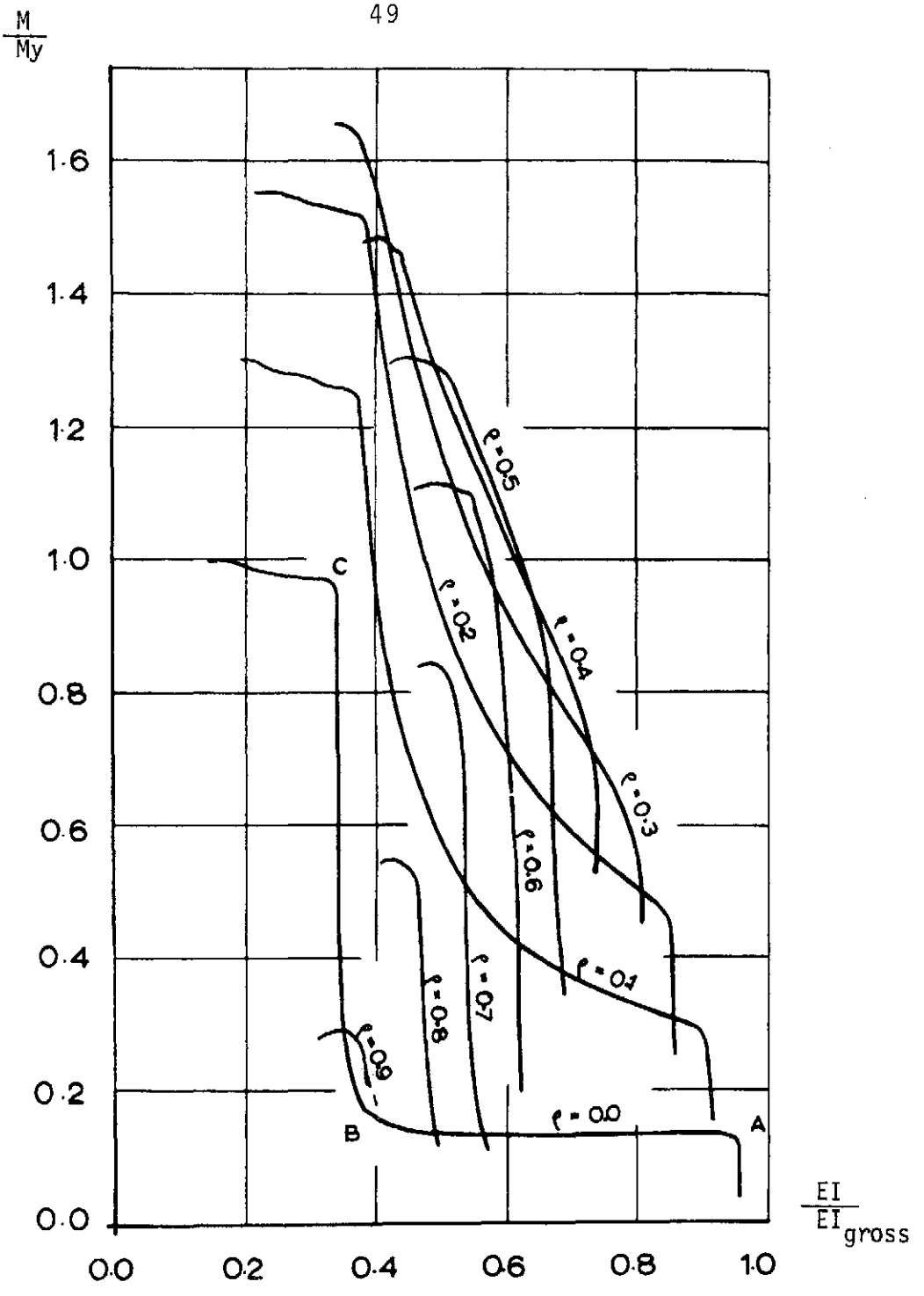

Figure 2-17 Moment of Inertia of Reinforced Concrete Sections (Adapted from Reference (20))

I_{gross} is the moment of inertia of the uncracked section.

From this figure we see that for P = 0, the ratio $\frac{EI}{EI_{gross}}$ is relatively constant and equal to 0.35 for $0.2 \leq \frac{M}{My} \leq 0.95$. This could be used for the moment of inertia of girders.

For columns and for $0.1 \leq \frac{P}{Py} \leq 0.5$ the ratio $\frac{EI}{EI_{gross}}$ varies between 0.5 and 0.9 for $0.2 \leq \frac{M}{My} \leq 1.4$.

if we take into account the extreme complexity of the problem due to the factors mentioned earlier and the fact that sometimes the columns of the structure could be put in tension due to the earthquake, the following simple rules for the effective moment of inertia of concrete members seem justified.

Beams: Use $I_{eff} = 0.40\ I_{gross}$

Columns: Use $I_{eff} = 0.80\ I_{gross}$

2.8.2 Stiffness of Braced Frames

For braced frames we could use:

$$K_o = K_{ofr} + K_{BR}$$

where K_{ofr} is computed from 2.4 and

$$K_{BR} = \Sigma \frac{AE}{\ell} \cos^2 a \qquad 2.5$$

where A = area of bracing

ℓ = length of bracing

a = angle between bracing and beam

Σ = summation over all the braces working in tension.

The above formula is not as accurate as in the case of the unbraced frames and depending on the particular configuration (e.g. number of bays braced) a more accurate approach might be desirable.

2.8.3 Walls and Infilled Frames

For plain walls a formula derived from elastic theory could be appropriate. For example one could write:

$$K_o = \frac{1}{\frac{h}{AG} + \frac{h^3}{\lambda EI}} \qquad 2.6$$

h = height of the wall

A = area of the wall

I = moment of inertia of the section in bending

E, G = elasticity constants

λ = parameter depending on conditions of fixity at the ends. It could vary from 3 to 12.

The stiffness of infilled frames could be found by summing the stiffnesses computed from 2.4 and 2.6 for the two elements. However if the frame has a height to width ratio which is large (tall frame, small number of bays), this superposition will not be valid and the unit will have to be treated as a bending element rather than as a shear beam. The comments made in paragraph 2.6 are pertinent in this case.

2.8.4 Yield Levels for Frames

An upper bound of the strength of one particular story could be estimated by assuming that this story has been transformed into a mechanism. There are two possibilities: hinges in the girders and hinges in the columns. In the case that we have hinges in the girders the story is not exactly a mechanism but its additional strength after the girders have yielded is very small. So we can write

$$Fy_{max} = \min \left\{ 2 \frac{\Sigma Myc}{h}, \quad 2 \frac{\Sigma Myg}{h} \right\} \qquad 2.7$$

where h = story height

ΣMyg = sum of plastic moment capacities for all girders in the floor

ΣMyc = sum of plastic moment capacities for all columns in the floor, reduced for the effect of axial load.

Again the reduction of the ultimate capacity due to the axial loads could be accounted for, in an exact analysis (see for example reference (9)). For the approximate model used in this thesis however, this is not possible except in a rather crude way. This is by using the ultimate moment capacity of the columns as modified for the effect of gravity loads.

Another point worth mentioning is that the yield level computed from 2.7 is an upper bound. Due to the gradual formation of hinges, the load deflection curve will start deviating from the straight line before the total shear reaches the value of Fy_{max}. The value of the story shear when the 1st hinge forms could be as low

as half the amount computed from 2.7 (see for example reference (38)). To account for this phenomenon, a trilinear model was developed as a combination of two elastoplastic ones. It is shown schematically in Figure 2-18 and described in more detail in Appendix B.

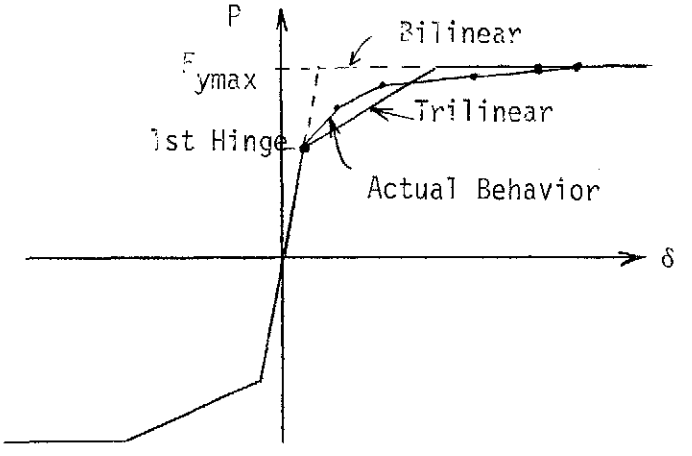

Figure 2-18 Trilinear and Bilinear Model

The value Fy_{max} computed from 2.7 should be lower than the shear strength of the columns. If this is not the case it is possible to have a shear failure before this value is ever attained. However, frames designed by the code and well detailed should not have such a problem.

In the case of bracing an additional term should be added to the value computed from 2.7. We could write:

$$Fy_{(\text{Braced frame})} = Fy_{(\text{Unbraced})} + \Sigma\sigma_y A_{br} \cos a \qquad 2.8$$

where $\Sigma \sigma_y$ = yield stress of the member

A_{br} = area of bracing

a = angle between bracing and beams

Σ = summation over all braces working in tension.

The second term comes from the contribution of the diagonal members to the ultimate capacity.

2.8.5 Yield Levels for Walls and Infilled Frames

For plain walls we can write:

$$P_{max} = \min \left\{ \tau_{max} \cdot bt, \sigma_{max} \cdot \frac{W}{h} \right\} \qquad 2.9$$

where τ_{max} = maximum shear stress the wall can stand

σ_{max} = maximum tensile stress the wall can stand

W = section modulus

h,b,t, = wall dimentions

For infilled frames we can assume that the wall acts as a series of diagonal struts and then we can write:

$$Fy_{max} = Fy_{frame} + \Sigma P_{max} \cos a \qquad 2.10$$

where Fy_{frame} is computed from 2.7

P_{max} is computed from 2.9

a is the angle that the diagonal forms in a bay with the horizontal.

2.9 Comparisons of Deflections Obtained Using the Approximate Formulas with Exact Values

In order to examine how accurate results one could obtain using the approximate formulas for stiffness suggested in this chapter, several frames were analyzed using these formulas and by an exact computer program. The frames examined are shown in Figure 2-19

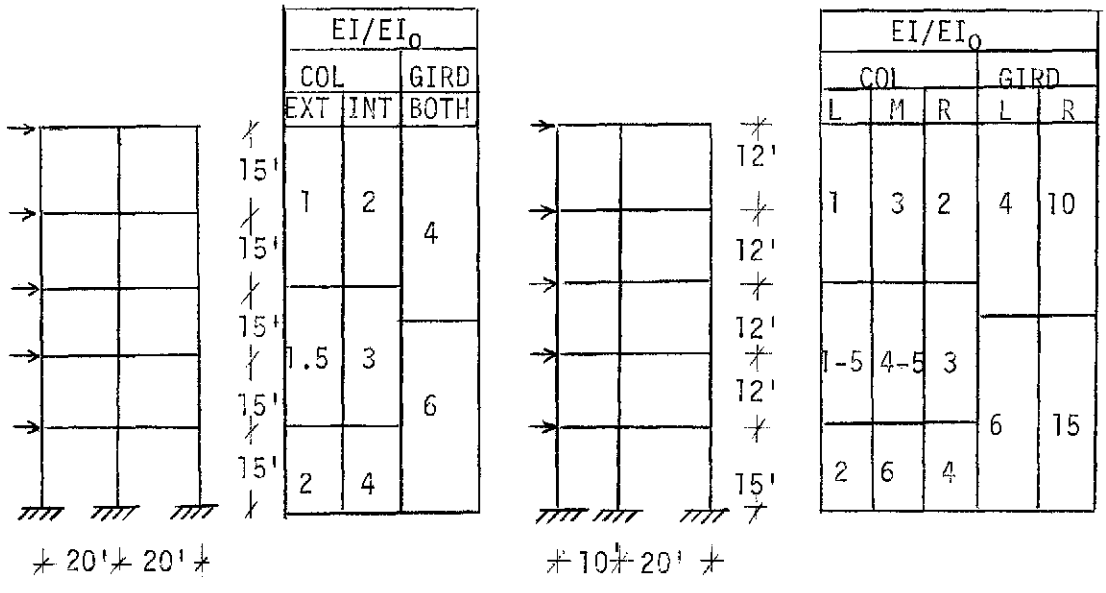

FRAME A

FRAME B

FRAME C Identical to A but with Bracing in the Left Bays
Area of Bracing per Story = 4 in^2

$EI_o = 24 \times 10^6$ (kips in^2)

Figure 2-19 Frames A,B,C

Two types of loadings were used: a) uniform over the height and b) triangular decreasing from top to bottom. Since there was almost no difference in the comparisons of the two cases with the results obtained from the exact analysis, we will give here only the comparison for the uniform load. These results are tabulated in Table 2-1.

INTERSTORY DISPLACEMENTS						
FLOOR	FRAME A		FRAME B		FRAME C	
	APPROX	EXACT	APPROX	EXACT	APPROX	EXACT
1	.875	.849	.526	.523	.454	.461
2	1.08	1.11	.345	.400	.443	.523
3	.895	.943	.282	.344	.345	.452
4	.805	.884	.258	.331	.256	.394
5	.403	.494	.129	.207	.128	.269
TOTAL DISPLACEMENT AT TOP						
	4.058	4.281	1.54	1.80	1.626	2.10
RATIO OF $\delta^{top}_{exact} / \delta^{top}_{approx}$						
	1.05		1.17		1.29	

Table 2-1 Comparisons of Deflections Obtained by Using Approximate Formula for the Stiffness

From the above table we see that the results obtained using the approximate formula are better for the lower stories than the top

ones. Also they are better for regular frames than for irregular or frames with bracing. In all the cases the approximate displacements are smaller than the exact. This is something to be expected, since the approximate method does not account for column shortening. In cases where this is not important, the agreement should be better.

CHAPTER 3

STUDIES OF ONE-DEGREE-OF-FREEDOM SYSTEMS

3.1 Introduction

The inelastic dynamic response of one-degree-of-freedom systems (1 D.O.F.), with the spring characteristics introduced in Chapter 2, will be presented here, in order to compare the effect of the different nonlinearities. This will have first only a qualitative character, although later in this chapter quantitative comparisons will be made for some of the systems. The excitation used for this part is the NS EL CENTRO 1940 accelerogram, the N69W TAFT 1952 (factored to an intensity equal to that of the EL CENTRO record) and finally a sinusoidal motion. Extensive studies on ductility requirements for the nonlinear systems that best represent frame behavior will then be presented, and the possibility of drawing conclusions from these results for multi-degree-of-freedom systems will be discussed. Five different historical records were used for this part of the investigation. Finally, some comments on the effect of gravity loads on the dynamic behavior will be made. Housner (61), (62) and Berg and Thomaides (63) studied the response of single elasto-plastic systems, using energy considerations. Veletsos and Newmark (64), Veletsos, Newmark and Chelapati (65) and Veletsos (66) have done extensive studies on the response of a 1 D.O.F. with various nonlinear force displacement characteristics. They have derived response spectra for such systems, and they suggested practical rules to derive these spectra from those of an associated elastic system.

These rules will be discussed later in this chapter together with their range of application. Clough and Johnston (69) compared the response of a stiffness degrading model with that of an elastoplastic system, and their main conclusion was that the ductility requirements of a stiffness degrading system with natural periods greater than 0.5 seconds are not materially different from those observed in ordinary elastoplastic structures. Ductility requirement (or ductility factor) is defined in general as the ratio of the maximum deformation to the yield one. For systems with periods less than 0.5 seconds, the differences might be significant. For long period structures, the loss of stiffness results in an increase of the period of vibration that leads to a decrease of the response. Jennings (67) studied the response of simple structures with Ramberg-Osgood type characteristics. Kaldjian and Fan (60) derived response spectra for elastoplastic and Ramberg-Osgood systems, and one of their conclusions is that the maximum displacement and the maximum energy input for the two systems are comparable. Husid (68) has studied the effect of gravity on the response of simple, idealized structures, and some of his conclusions will be discussed later in this chapter.

3.2 Nonlinear Response of 1 D.O.F. Systems under Earthquake Excitation

The equation of motion for a 1 D.O.F. system (Fig. 3-1) subjected to a ground excitation is:

$$m\ddot{u} + c\dot{u} + kF(u) = - m\ddot{u}_g$$

or dividing by the mass

$$\ddot{u} + 2\beta\omega\dot{u} + \omega^2 F(u) = -\ddot{u}_g \qquad (3.1)$$

where:

m = mass

u = displacement of the mass relative to ground

c = coefficient of viscous damping

$\beta = c/2\sqrt{km}$ percentage of critical damping

k = initial stiffness of the spring

$\omega = \sqrt{k/m}$

$F(u)$ = force in the spring divided by k (Fig. 3-1)

$\ddot{u}_g$ = ground acceleration

$\dot{}$ → denotes differentiation with respect to time.

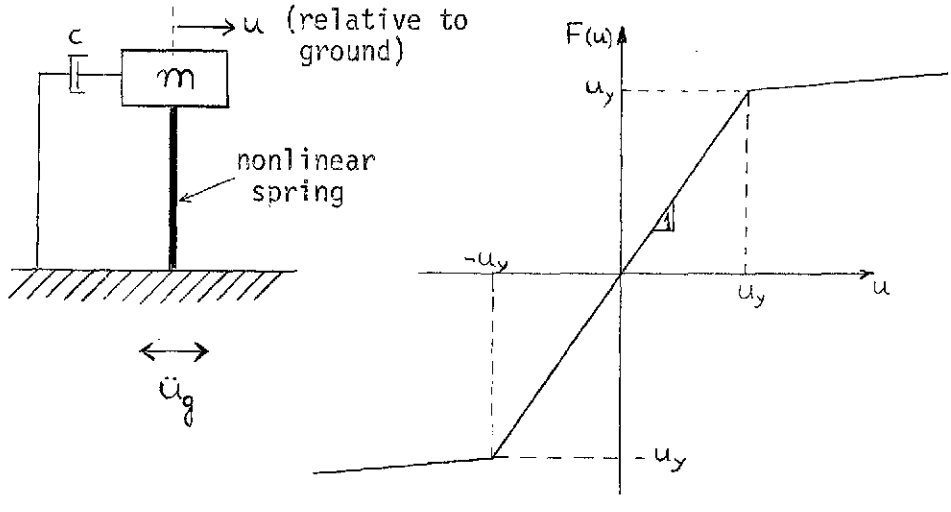

Figure 3-1 1 D.O.F. System with non-linear Resistance Function

The function F(u) for the nonlinear spring follows any of the laws discussed in chapter 2 and is characteristic of the particular type of the resisting element.

Equation 3.1 can be solved numerically for any kind of input ground motion. The numerical method used here is the so-called "impulse acceleration" or "constant velocity method," (see for example Biggs (1), Roesset (6)), which was checked for its accuracy against exact solutions. Because we have only one degree of freedom, the method is almost as accurate as any other, provided that the time step used is small enough. One tenth of the elastic natural period of the system is usually a good guess for the time step to be used, provided of course that it reproduces the input function well. In all the studies reported in this chapter, the time interval used was 0.01 second.

Figures 3-2 - 3-9 give the time history of the displacement response and the force vs. deformation in the springs for the different nonlinear systems discussed in chapter 2. The ground motion used was the first 10 seconds of the N-S component of the 1940 El Centro record. The properties of the different systems used are summarized in Table 3-1, according to notation introduced in chapter 2. In general k stands for stiffness, F_y for yield force, and a, b, c are factors for the degrading models, as defined in 2.6.

Since this part of the study was aimed mainly at a qualitative evaluation of the behavior of the different systems, it was considered appropriate not to include any viscous damping. The stiffness

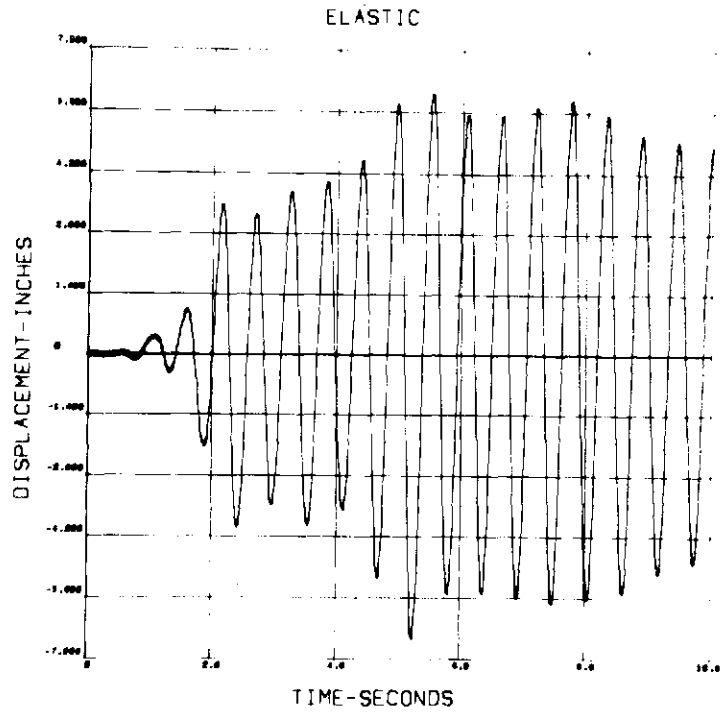
ELASTIC
DISPLACEMENT-INCHES
TIME-SECONDS

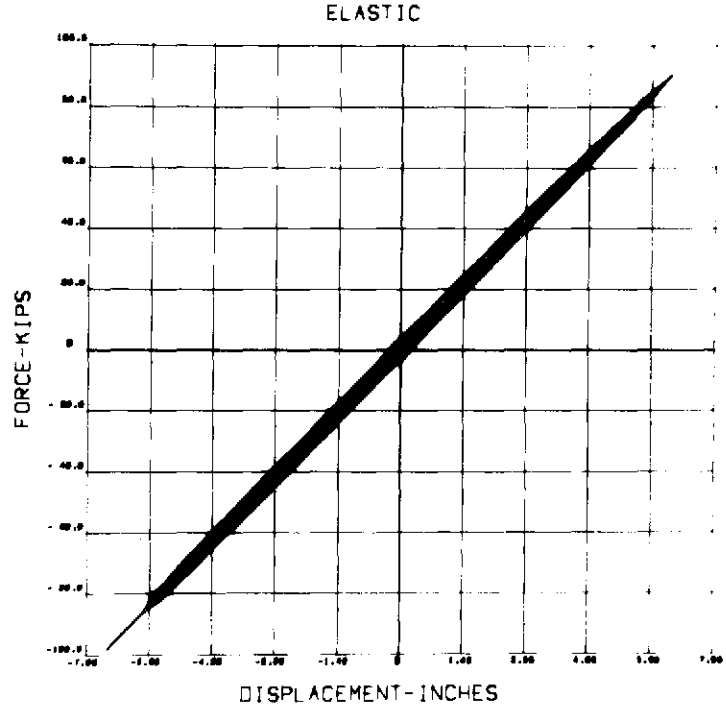
ELASTIC
FORCE-KIPS
DISPLACEMENT-INCHES

Figure 3-2

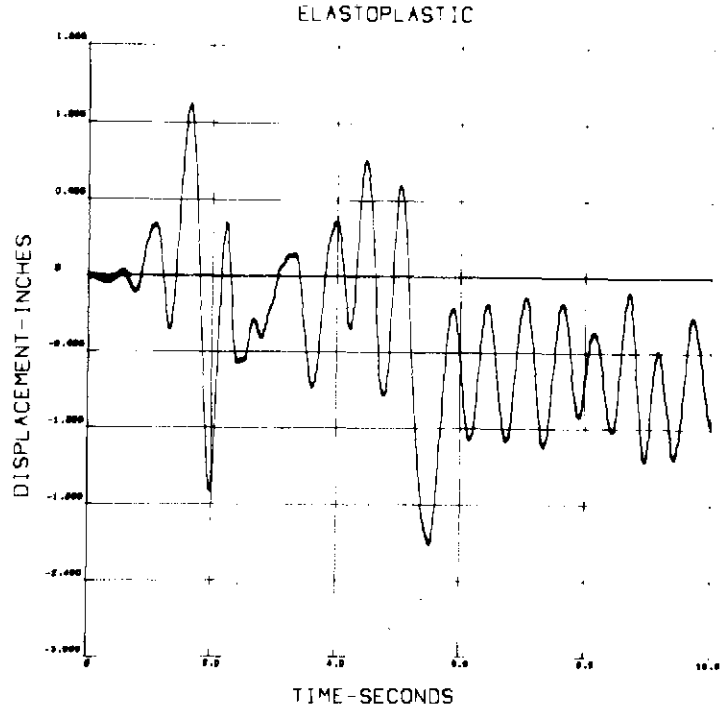
ELASTOPLASTIC
DISPLACEMENT-INCHES
TIME-SECONDS

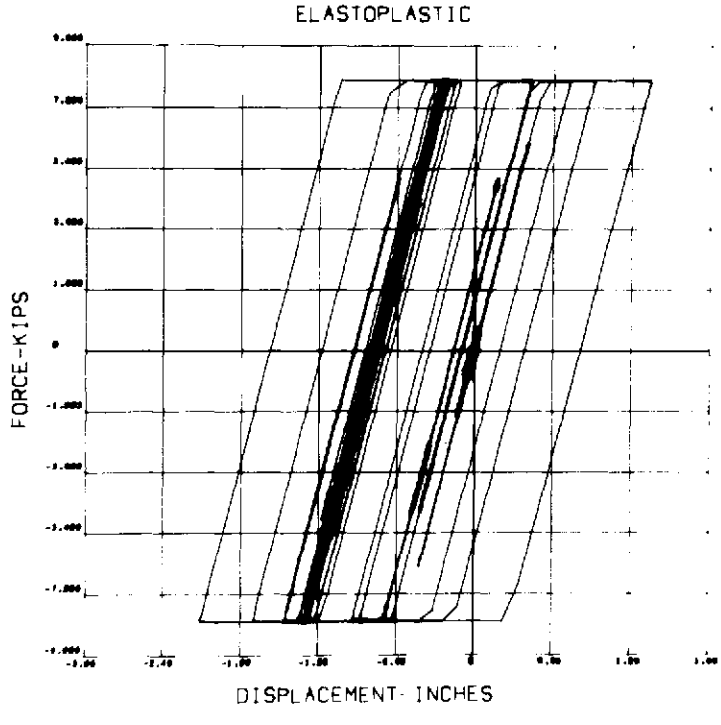
ELASTOPLASTIC
FORCE-KIPS
DISPLACEMENT-INCHES

Figure 3-3

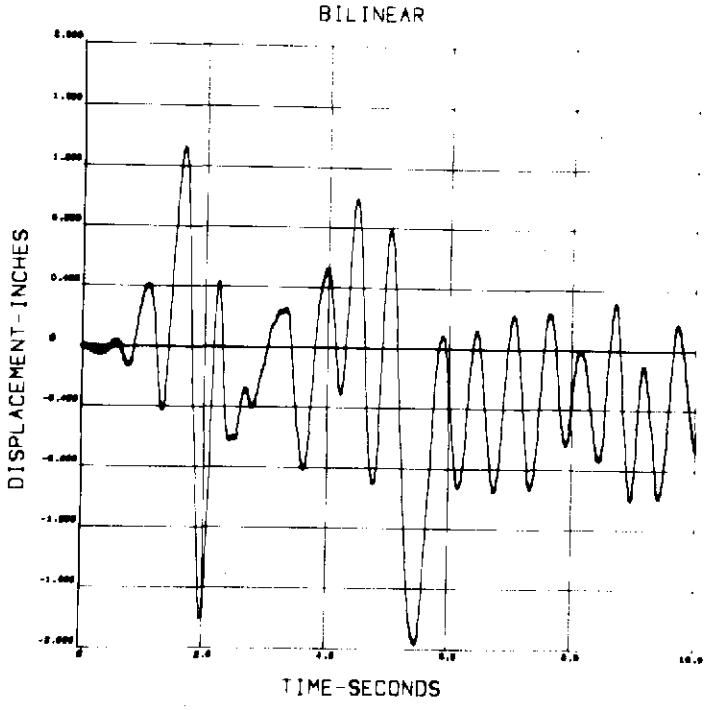
BILINEAR
DISPLACEMENT-INCHES
TIME-SECONDS

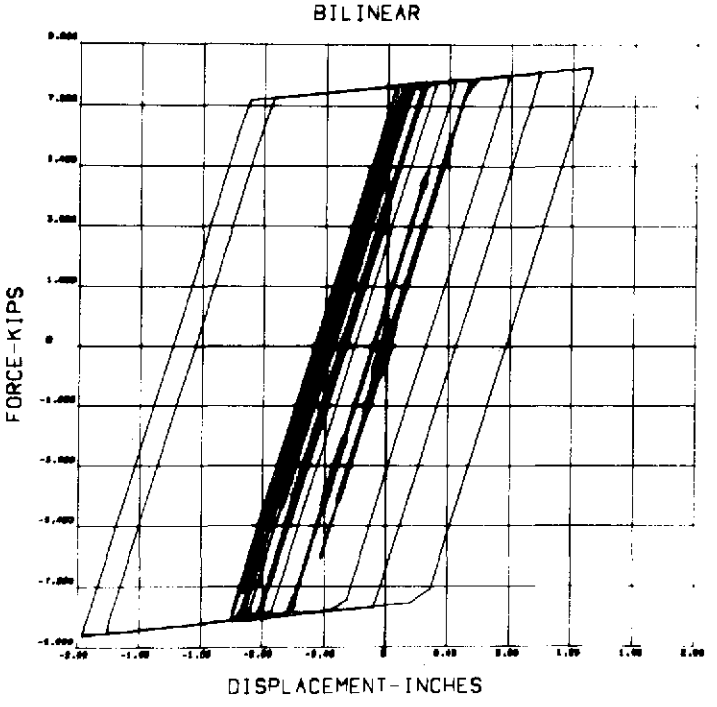
BILINEAR
FORCE-KIPS
DISPLACEMENT-INCHES

Figure 3-4

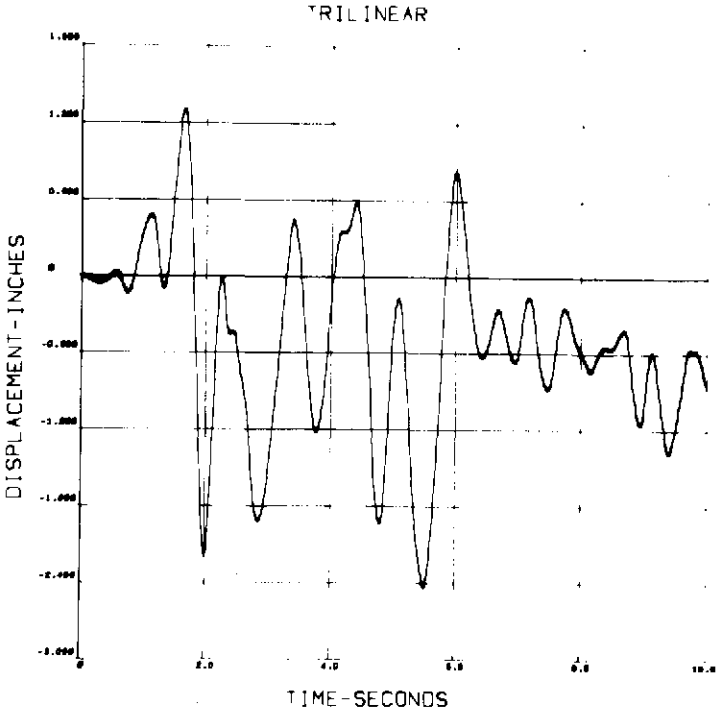
TRILINEAR
DISPLACEMENT-INCHES
TIME-SECONDS

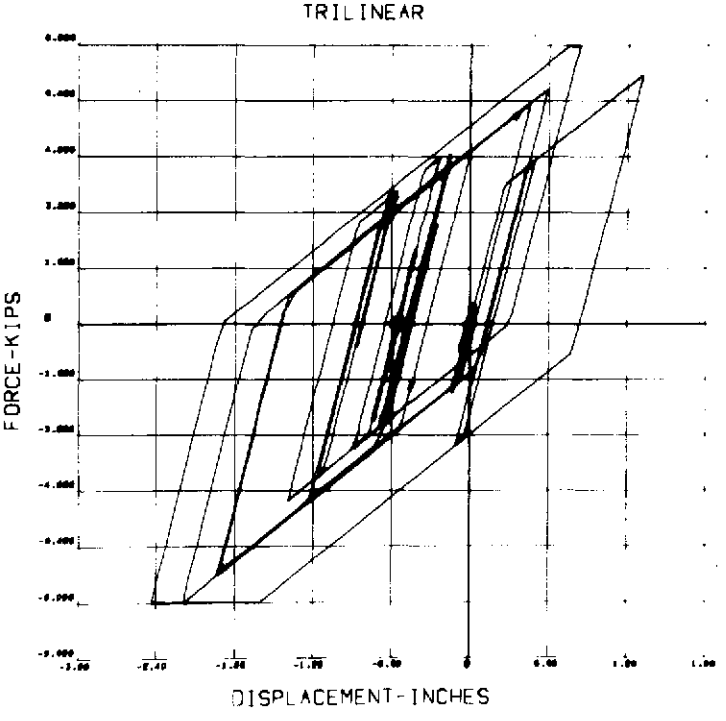
TRILINEAR
FORCE-KIPS
DISPLACEMENT-INCHES

Figure 3-5

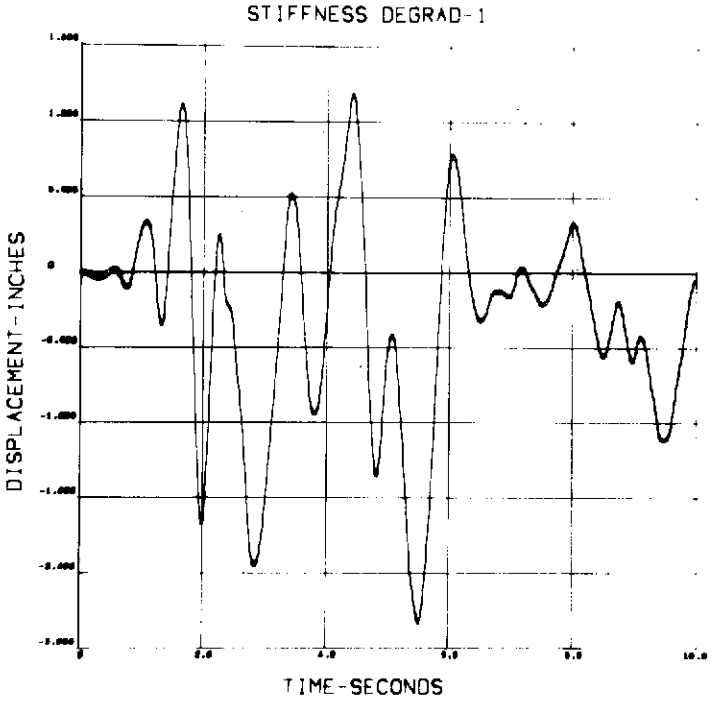
STIFFNESS DEGRAD-1
DISPLACEMENT-INCHES
TIME-SECONDS

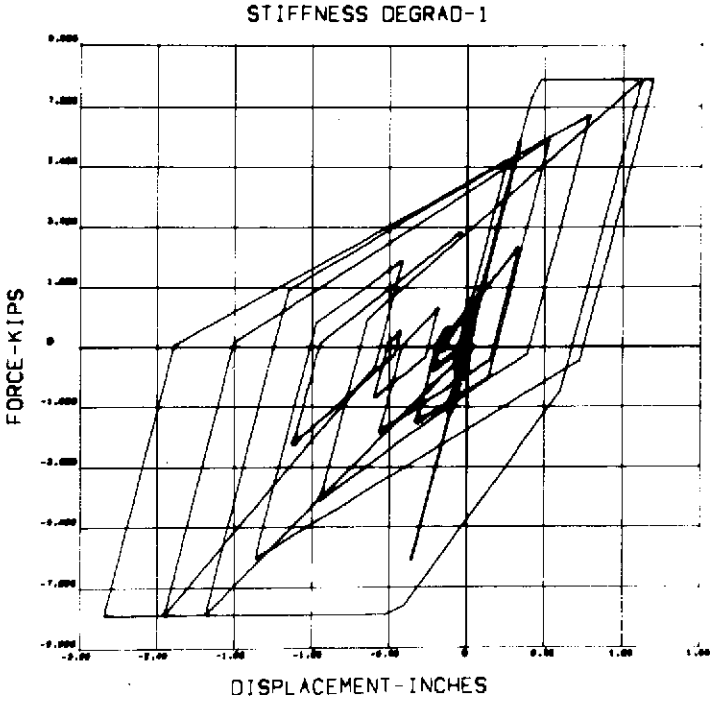
STIFFNESS DEGRAD-1
FORCE-KIPS
DISPLACEMENT-INCHES

Figure 3-6

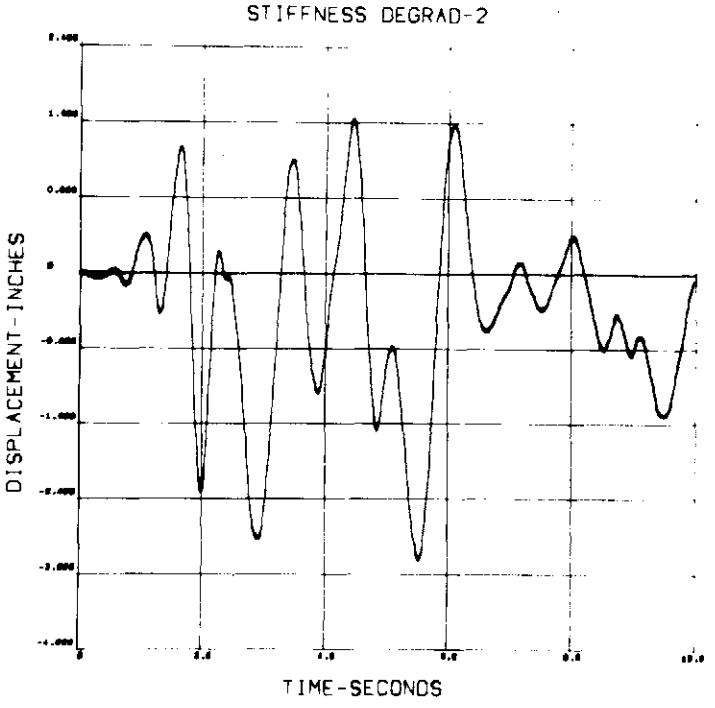
STIFFNESS DEGRAD-2
DISPLACEMENT-INCHES
TIME-SECONDS

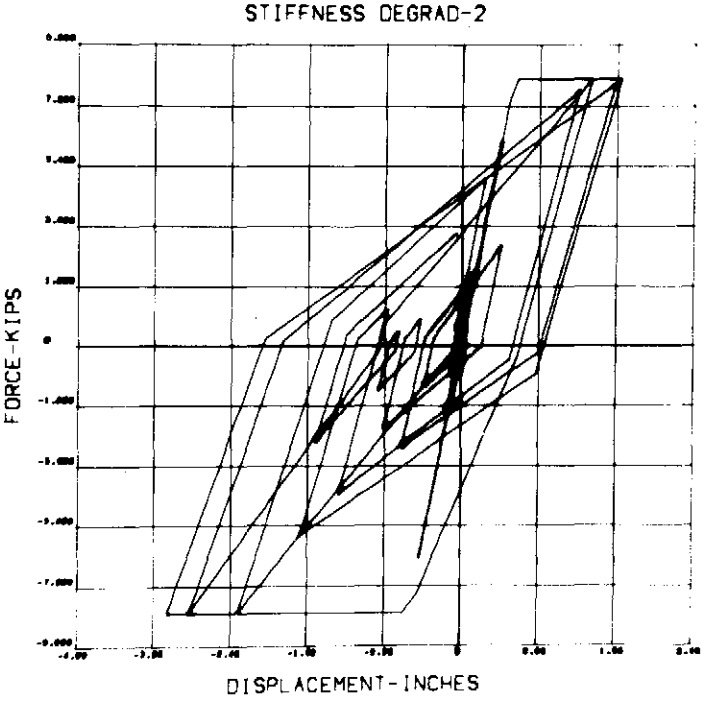
STIFFNESS DEGRAD-2
FORCE-KIPS
DISPLACEMENT-INCHES

Figure 3-7

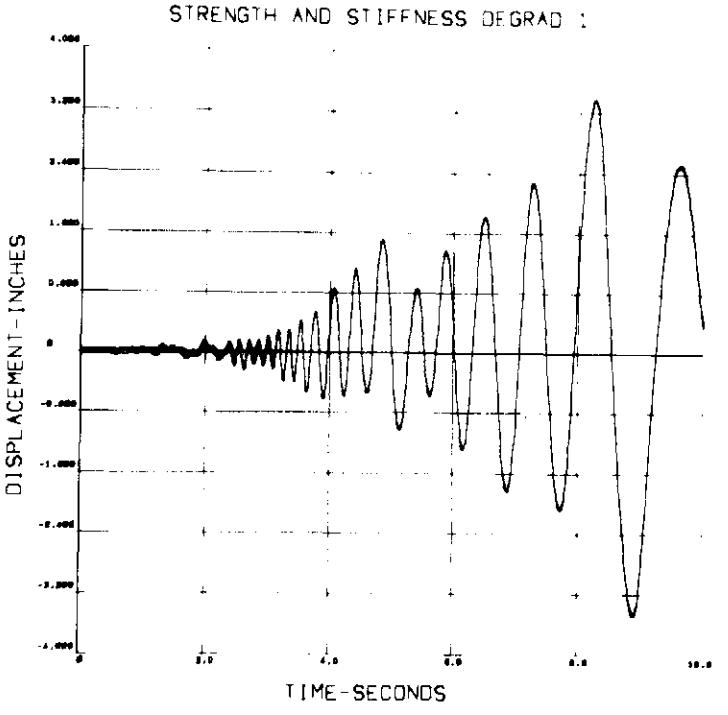
STRENGTH AND STIFFNESS DEGRAD 1
DISPLACEMENT-INCHES
TIME-SECONDS

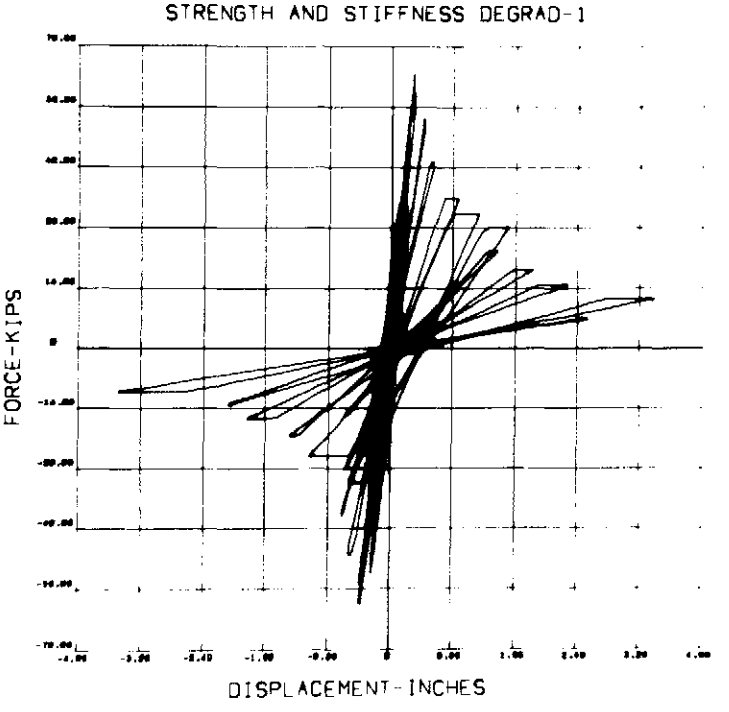
STRENGTH AND STIFFNESS DEGRAD-1
FORCE-KIPS
DISPLACEMENT-INCHES

Figure 3-8

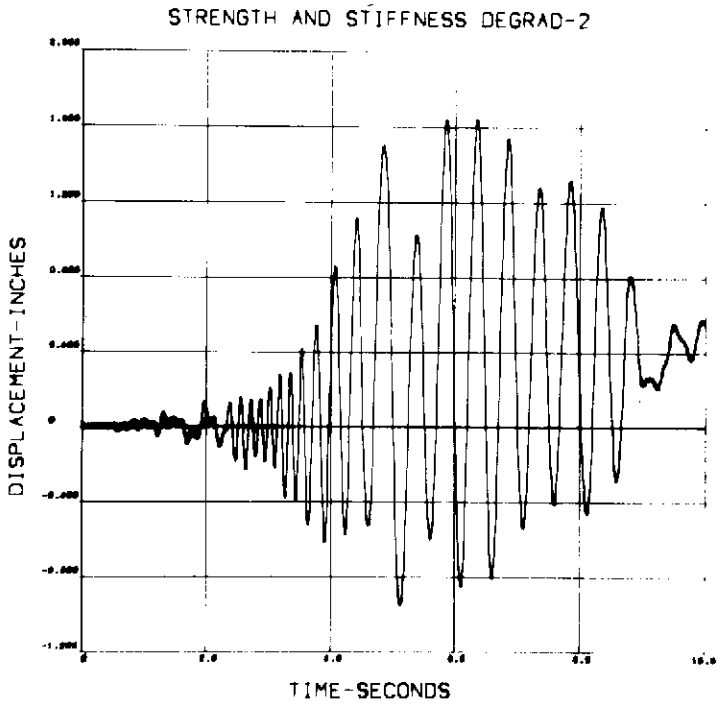
STRENGTH AND STIFFNESS DEGRAD-2
DISPLACEMENT-INCHES
TIME-SECONDS

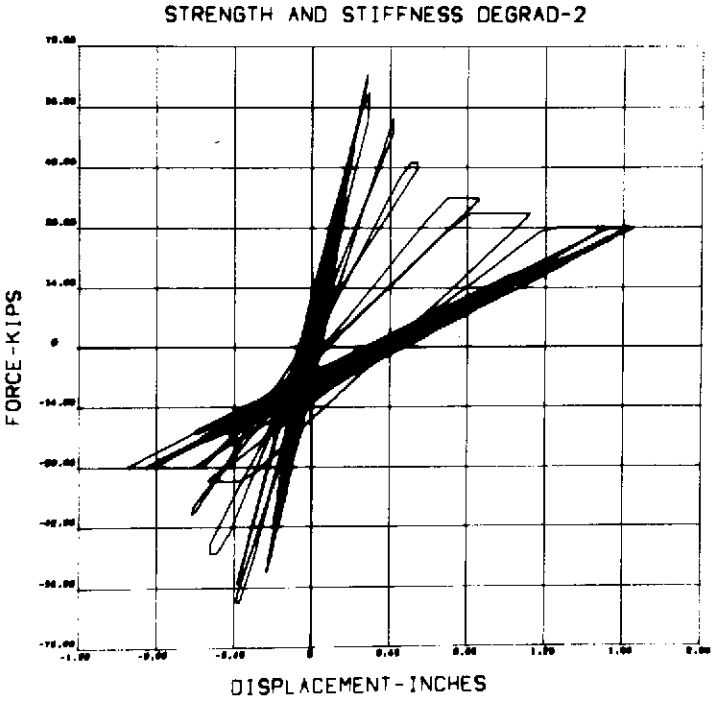
STRENGTH AND STIFFNESS DEGRAD-2
FORCE-KIPS
DISPLACEMENT-INCHES

Figure 3-9

TYPE	$T_{init.}$ (sec)	k_2	F_{y1} (kips)	F_{y2} (kips)	δ_y (in)	a	b	c	k_{min}	Fy_{min}
ELASTIC	.56	—	8	—	.533	—	—	—	—	—
ELASTOPLASTIC	.56	—	8	—	.533	—	—	—	—	—
BILINEAR	.56	$.03k_1$	8	—	.533	—	—	—	—	—
TRILINEAR	.56	$.2k_1$	4	8	.267	—	—	—	—	—
STIFF.DEGR.1	.56	—	8	—	.533	—	—	—	—	—
STIFF.DEGR.2	.56	—	8	—	.533	.35	—	—	—	—
STREN.& STIFF. DEGRAD.1	.156	—	66	—	.29	40.	.9	.8	—	—
STREN.& STIFF. DEGRAD.2	.156	—	66	—	.29	40.	.9	.8	22.5	28.

Table 3-1 Properties of 1 D.O.F. Systems Analyzed

of the last two models, which are for infilled frames, was chosen much larger than the stiffness of the others, so their initial period of vibration is much smaller. Yield levels for the first six systems were chosen so that the ductility factor would be in the order of 3 - 6 (except for the trilinear model whose ductility is with respect to the first yielding level). For the last two, yield levels were chosen by assuming certain properties for the frame and the infill and using formulas from chapter 2.

Figure 3-2 is the response of an undamped elastic system with period .56 seconds. The force-deformation function is a straight line as shown in the bottom part. The maximum displacement is 6.52 in.

Figure 3-3 and 3-4 are the responses of the elastoplastic and bilinear systems, respectively. They are quite similar except that the elastoplastic has a bigger permanent set than the bilinear. Their

ductility factors are 3.95 and 3.68 respectively. The irregularities in their response are of course due to yielding.

The response of a trilinear model is shown in Figure 3-5, and one can observe that it is controlled more from the second slope. Figure 3-10 shows the envelopes of the elastoplastic and the trilinear system. This effect makes the system softer and is probably the rea-

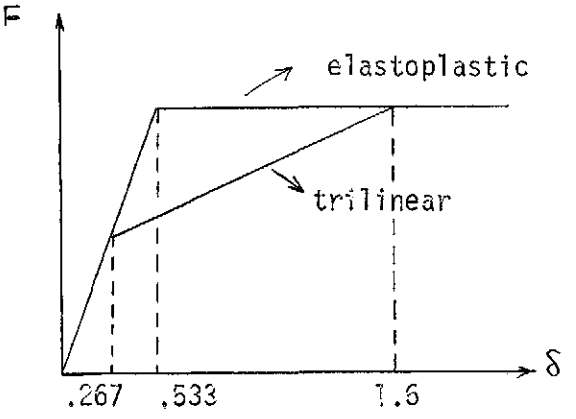

Figure 3-10 Trilinear Model

son for the initiation of some plastic drift after the 8^{th} second. The maximum displacement here is 2.43 in. (larger than that of the elastoplastic and bilinear) and the ductility factor with respect to 1^{st} yield level is 9.12, while with respect to the 2^{nd}, is only 1.51.

The next two figures, 3-6 and 3-7, correspond to the two stiffness degrading models. As it was mentioned in chapter 2, their only difference is in the slope of their unloading branches. For

all practical purposes, however, their responses can be considered identical, as one can observe from the top parts of the figures. Their ductility factors are 5.26 and 5.73, respectively: i.e., 33% and 45% larger than that of the elastoplastic. This is in agreement with Clough's results discussed in the introduction. The increase in the period of vibration is due to the continuous decrease in stiffness after 1^{st} yielding. The increase of the period alters the response significantly only if the system has a period either very small or very large. If the initial period of the system is near the beginning of the horizontal plateau of the spectrum, (plotted against period), then no significant changes in the response should be expected. Due to the close similarity of the response of the two stiffness degrading models, the conclusion that the second model is insensitive to the values of a at least in the range 0 - 35, is evident.

Figure 3-8 corresponds to the stiffness and strength degrading model that is proposed for an infilled concrete frame. Before first yielding occurs, the response is insignificant, but after that it deteriorates very fast, in contrast to Figure 3-9, which corresponds to an infilled steel frame, in which there is a minimum of stiffness and strength, that of the bare frame alone. The following should be made clear, however. Several computer runs were performed, in which the three basic parameters of the model were varied. It was found that the model is rather insensitive to the value of a, but the same is not true for b and c (the parameters that associate degradation to the number of cycles of loading). Appropriate adjustment of these

two parameters could produce any desired behavior. Due to the limited amount of experimental data, the numbers used are only a "little more" than guesses. As new experimental evidence becomes available, more realistic values for these two parameters could be determined. The bottom part of all the previous plots give the force vs. deformation curves for the system considered. They are interesting in the sense that one can see the effect of load reversals, the amount of yielding taking place in each cycle; and they also serve as a check of the analysis.

Figures 3-11, 12, and 13 show the response of the degrading models to the first 10 seconds of the Taft 1952 N69W earthquake scaled to an intensity equal to that of El Centro, 1940. Figure 3-14 shows the response of the strength and stiffness degrading model 1 to a sinusoidal motion with period .5 seconds and maximum acceleration 320 in/sec^2. These additional plots were included to see whether any significant difference in the shape of the loops from those for El Centro would be observed. It is only for the sinusoidal motion that the shape of the loop is different, but this comes from the regularity of the excitation which makes the system stay in the plastic range longer.

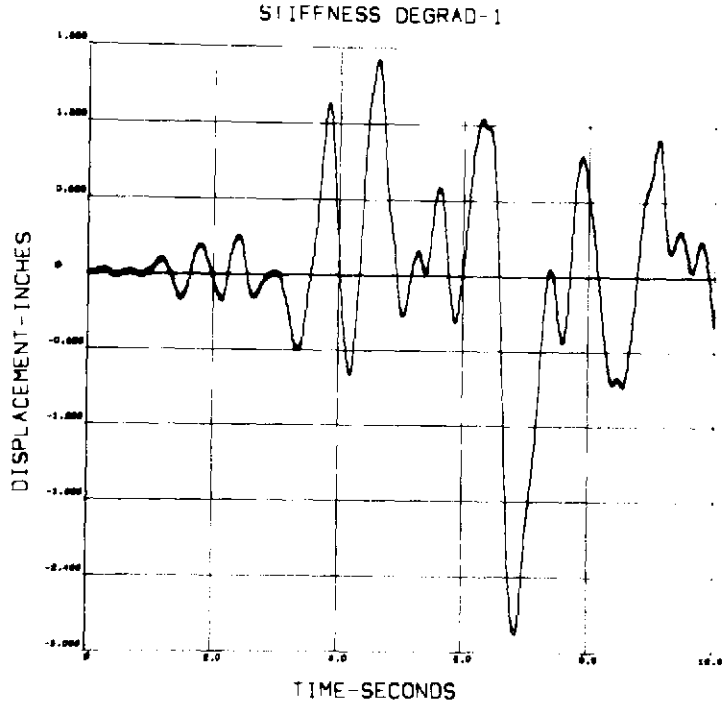
STIFFNESS DEGRAD-1
DISPLACEMENT-INCHES
TIME-SECONDS

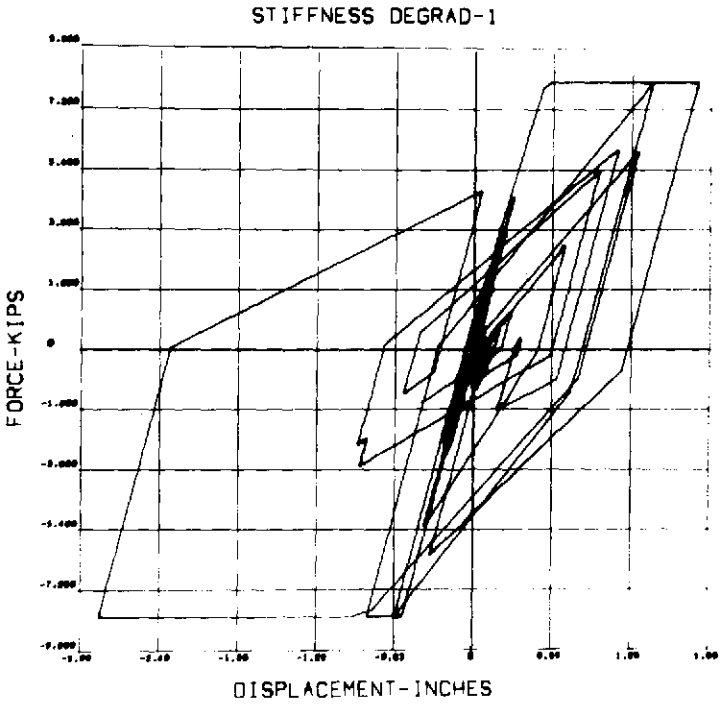
STIFFNESS DEGRAD-1
FORCE-KIPS
DISPLACEMENT-INCHES

Figure 3-11

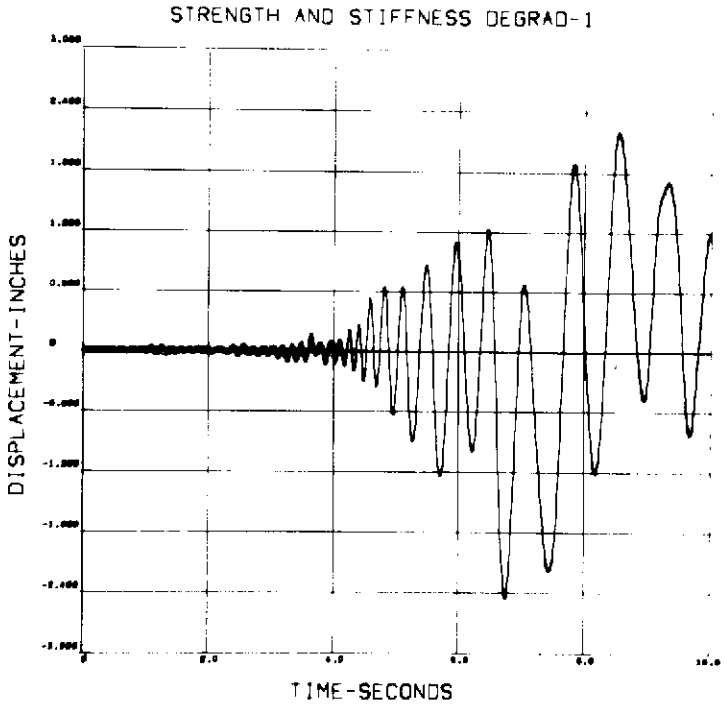
STRENGTH AND STIFFNESS DEGRAD-1
DISPLACEMENT-INCHES
TIME-SECONDS

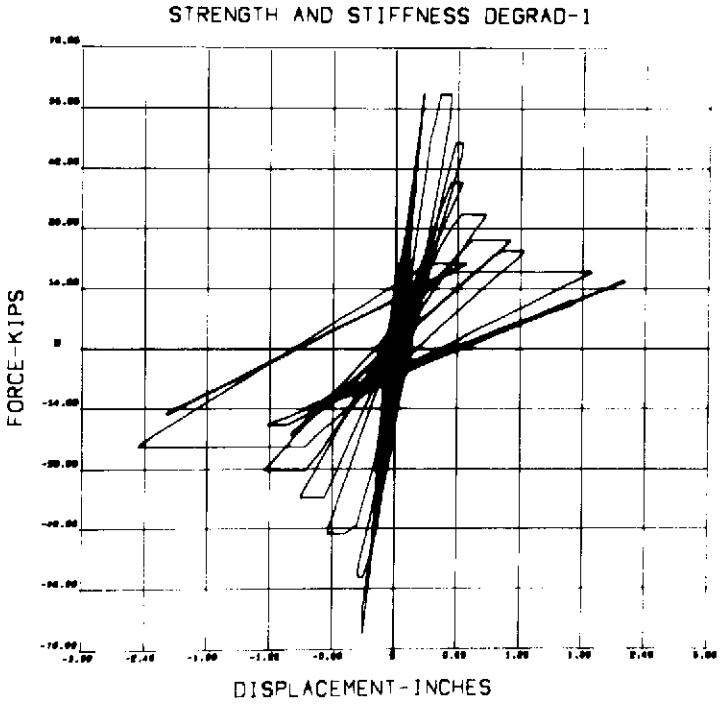
STRENGTH AND STIFFNESS DEGRAD-1
FORCE-KIPS
DISPLACEMENT-INCHES

Figure 3-12

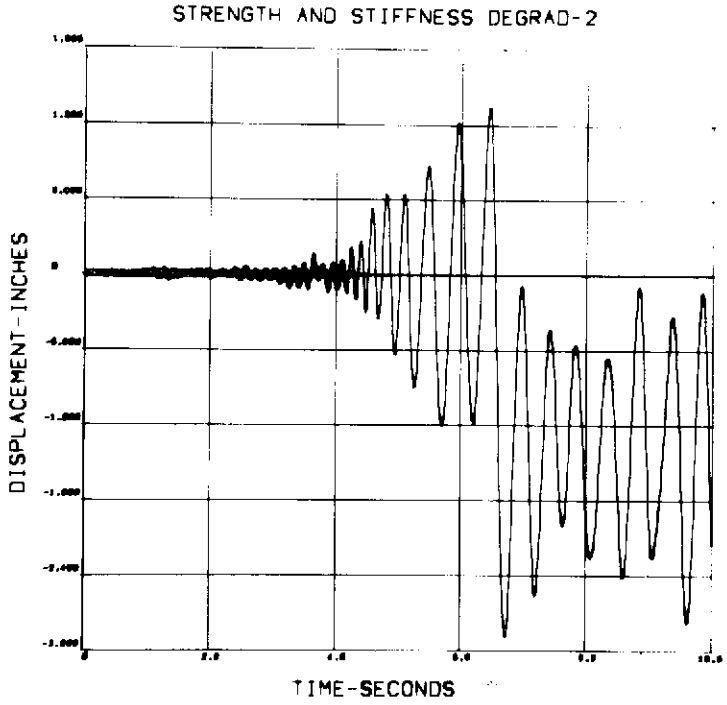
STRENGTH AND STIFFNESS DEGRAD-2
DISPLACEMENT-INCHES
TIME-SECONDS

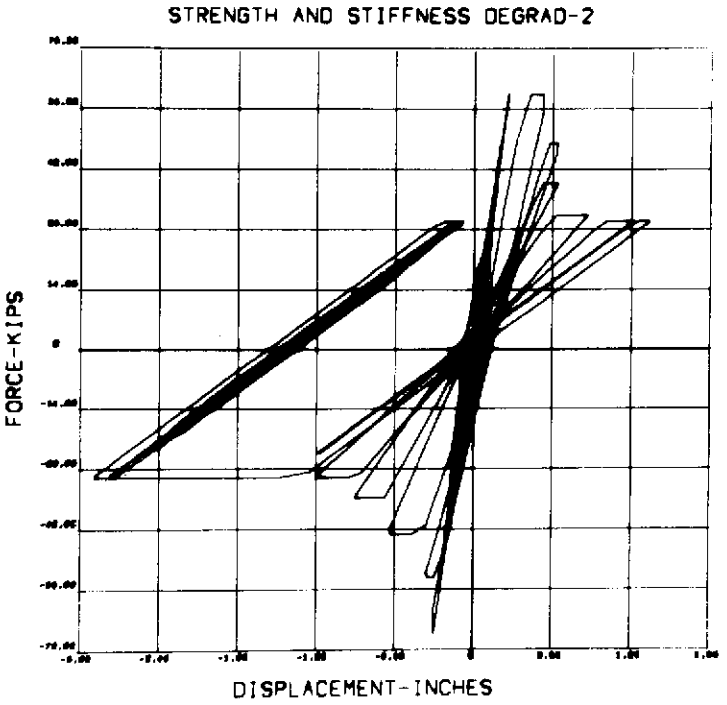
STRENGTH AND STIFFNESS DEGRAD-2
FORCE-KIPS
DISPLACEMENT-INCHES

Figure 3-13

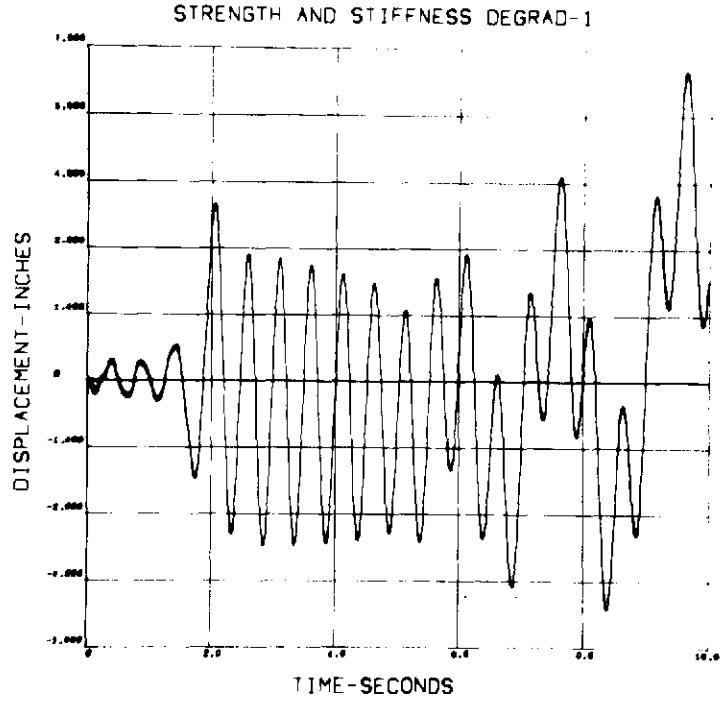
STRENGTH AND STIFFNESS DEGRAD-1
DISPLACEMENT-INCHES
TIME-SECONDS

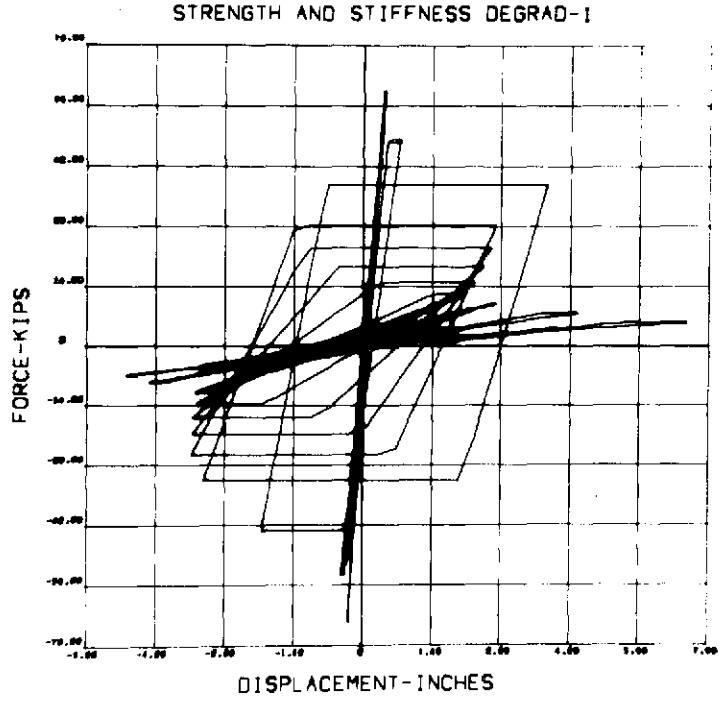
STRENGTH AND STIFFNESS DEGRAD-1
FORCE-KIPS
DISPLACEMENT-INCHES

Figure 3-14

3.3 Studies on Ductility Requirements of Simple Systems

3.3.1 Importance of Ductility

It has been long recognized that ductility is a highly desired property for a structure, to resist strong earthquakes and to avoid possible collapse. A structure that possesses ductility has the ability to accommodate large inelastic deformations and to absorb a substantial amount of energy through inelastic action. But use of a ductile material is not sufficient to guarantee this behavior. Other factors such as the complexity of the structure, the degree of indeterminacy, detailing of the joints and connections, speed of loading and temperature are also important for the overall ductile behavior. Structural steel and reinforced concrete designed in accordance with the code can behave as ductile materials, so for usual structures it is the other reasons that influence the ductility. Simple members usually possess more ductility than entire structures. Usual structures consisting of frames from ductile materials designed and detailed according to the codes can exhibit ductility factors between 3 and 8 (5). Experience from structural failures, however, indicates that very often the construction is very poor, especially at those locations (namely structural joints) that more than any others need good and careful detailing to ensure the overall ductility.

From the point of view of the designer the first question is to determine the amount of ductility required by the structure to endure safely (and with a minimum of damage) a strong earthquake.

And if this ductility is excessive, how can it be reduced

Ideally a building should have enough stiffness to resist wind loads and small or moderate earthquakes with little or no damage. Under a very strong earthquake it should be ductile enough to avoid collapse.

3.3.2 Inelastic Response Spectra

The idea of the elastic response spectra has been extended to nonlinear systems. Although they cannot be readily used for multi-degree-of-freedom systems through a modal analysis, they are useful in that trends can be observed and some general conclusions can be drawn. Veletsos (66) has obtained spectra for several types of non-linear models, and Kaldjian (60) has compared the responses of elasto-plastic and Ramberg-Osgood systems. The trends in all of them are more or less the same, so we will limit ourselves in this part to the elastoplastic springs (which are the ones most widely used.) Inelastic spectra are drawn for constant values of the ductility factor μ (being defined as the ratio of the maximum deformation to the yield deformation) and having continuously decreasing ordinates for increasing values of μ over the whole frequency range (Figure 3-15). This does not mean, however, that the maximum displacement of the elasto-plastic system is smaller than the elastic. It may or it may not be. To find the maximum displacement from the response spectra, the spectral value must be multiplied by the corresponding ductility factor μ. What the decreasing ordinates actually say is that the smaller the yield level F_y, the more yielding will take place.

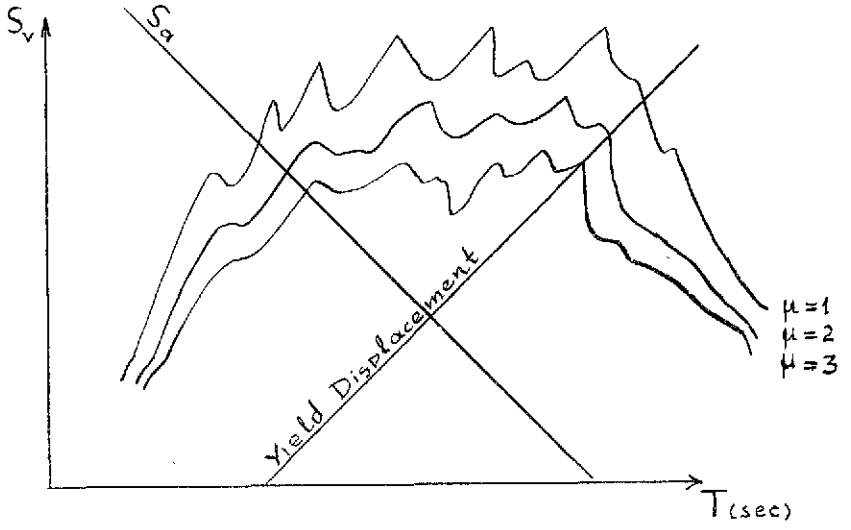

Figure 3-15 Response Spectra for Elastoplastic Systems

Veletsos, Newmark and Chelapati (65) derived elastoplastic response spectra for several inputs and came to the following conclusions: In the long period range of the spectrum, the maximum deformation of the elastoplastic system is approximately equal to that of the elastic. In the short period range, it is the maximum acceleration that is approximately equal and in the medium range it is energy that is preserved. These conclusions are closely related to the basic properties of the elastic spectra in the corresponding regions (i.e., spectral displacements close to ground displacements for long periods, spectral accelerations close to ground acceleration for short periods, and conservation of energy for intermediate range). Following the above conclusions, detailed rules for

deriving elastoplastic spectra from corresponding elastic spectra are suggested in the same reference. Here we will give a simplified version of these rules: For long periods, obtain ordinates of elastoplastic spectra from those of the elastic, dividing the second by the desired ductility factor. (In other words, assume the same maximum displacement for both systems.) In the short period range, assume the acceleration of the two systems to be the same, and in the intermediate, divide the elastic spectra by the quantity $\sqrt{2\mu - 1}$. This quantity can be easily derived, as shown below, by equating the maximum strain energies of the two systems. (Figure 3-16).

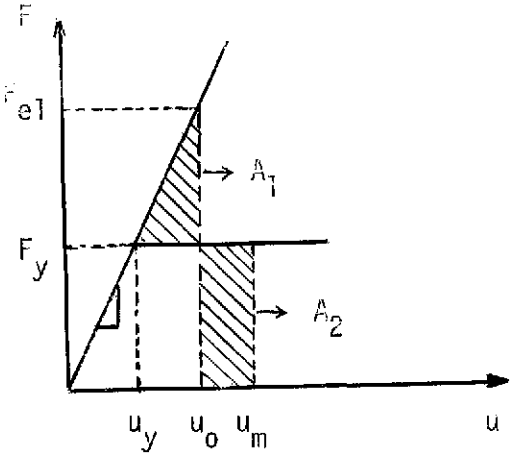

u_y = yield displacement for elastoplastic system

u_o = maximum displacement for elastic system

u_m = maximum displacement for elastoplastic system

Figure 3-16 Derivation of Factor $\sqrt{2\mu-1}$

We want to express u_m in terms of u_o by equating the corresponding energies. This means that the two shaded areas should be equal. Then:

$$A_1 = A_2$$

$$A_1 = \frac{1}{2}(F_{el} - F_y)(u_o - u_y) = \frac{1}{2}\left(\frac{F_y}{u_y}\, u_o - F_y\right)(u_o - u_y)$$

$$= \frac{F_y}{2u_y}(u_o - u_y)^2$$

$$A_2 = (u_m - u_o)\, F_y$$

So: $$(u_m - u_o) = \frac{(u_o - u_y)^2}{2u_y}$$

Dividing both members of the above equation by u_y and setting $\frac{u_m}{u_y} = \mu$

$$\mu = \frac{u_o}{u_y} + \frac{1}{2}\left(\frac{u_o}{u_y} - 1\right)^2$$

$$\frac{u_o}{u_y} = \sqrt{2\mu - 1} \qquad (3.2)$$

One useful observation that can be made, based on the above conclusions, is that for long period structures one could get reasonable values of the required ductility by dividing the forces obtained from an elastic dynamic analysis by the design forces.

The above conclusions, looked upon from a different point of view, suggest that structures in the short or even in the intermediate period range may require excessive ductilities if they are not provided with adequate strength. Newmark, in a discussion of a paper by Clough, Benuska and Wilson (70), notes that presently (1965) available codes do not provide the same amount of ductility over the whole range of building periods that the designer might encounter. This is a serious problem for strong earthquakes, because the factor of safety

against collapse is very closely related to the amount of ductility built into the structure. We address this problem in the following paragraph.

3.3.3 Ductility Requirements of Structures Designed by Code Procedures.

In this paragraph we will try to answer the question posed in 3.3.1: i.e., "What will the ductility requirements of a structure be, for a strong earthquake?" To do this, we chose a set of structures in the range of .1 to 4. seconds natural period. The masses were varied proportional to the natural periods in an attempt to simulate multistory buildings. This was done by assuming a mass of 0.1 kips-sec^2/in. per floor and a variation of periods in proportion to the number of floors. The corresponding stiffnesses were then computed from the natural periods and the masses. The design shears were computed according to the Uniform Building Code provisions for a z = 1 and k = .67 (we will comment later on the possibility of varying k). The code states that "for all one- and two-story buildings, the value of c shall be considered as 0.1." In the case of the .1 period, we chose the most conservative value of c = 0.108, as determined from the formula. Finally, the ultimate shear was assumed to be twice the design shear. This assumption was based on the following facts: a) We designed according to the code several columns as 1-D.O.F. with different periods, for gravity loads coming from the corresponding masses and earthquake loads as determined by the

U.B.C. Sections were selected from the steel manual and ultimate capacities were computed using the interaction formulas. In the cases examined, the ratio of the ultimate to the design shear was 2.04, 1.96, 1.86. b) It is recognized that in a column of a multi-story frame this number will vary with height, being a function of the ratio of the design moment to the design axial load. For girders that carry very little axial load, this number is about constant and very closely equal to 2. Given then that the desired behavior is to have the columns elastic by forcing yielding into the girders, this assumption looked reasonable. c) Clough (69), in his studies for inelastic dynamic response, used the same number for the 1-D.O.F., and also the same number for the girders of his multistory frame (7). The properties of the systems are given in Table 3-2. The units are kips, inches and seconds.

T	m	w	k	kc	V_{des}	F_y	F_y/w
0.10	0.10	38.6	395.00	.0722	2.79	5.60	.145
0.25	0.25	96.5	158.00	.0532	5.14	10.28	.106
0.50	0.50	193.0	79.00	.0422	8.15	16.30	.085
1.00	1.00	386.0	39.50	.0335	12.92	25.84	.067
2.00	2.00	882.0	19.75	.0266	20.50	41.00	.053
3.00	3.00	1160.0	13.20	.0232	26.90	53.80	.046
4.00	4.00	1540.0	9.88	.0211	32.50	65.00	.042

Table 3-2 Properties of 1 D.O.F. for Ductility Studies

The notation is:

T = period
m = mass
w = weight
k = stiffness
kc = U.B.C. coefficient for design shear
V_{des} = earthquake design shear
F_y = ultimate capacity (2 V_{des})

Results were obtained for five different accelerograms which were brought to an intensity equal to that of the 1940 NS El Centro earthquake. The definition of intensity used is that given by Arias (71). It is defined as

$$I(\beta) = \frac{\arccos \beta}{g\sqrt{1 - \beta^2}} \int_0^{t_o} \ddot{u}_g(t)\, df \qquad (3.3)$$

and has the advantage that its variation with respect to β, the percentage of critical damping, is very small. For $\beta = 0.20$, results were also obtained by using Housner's definition of intensity and were quite similar. For two cases the peak ground acceleration was used as a measure for intensity and the results presented a bigger scatter than using Arias' intensity. Table 3-3 gives the different earthquakes and the corresponding scaling factors.

EQ.	$\frac{\ddot{u}_G(\text{El Cen})}{\ddot{u}_G \text{ EQ}}$	$\frac{I^{\text{Housn.}}_{\text{El Cen.}}}{I^{\text{Housn.}}_{\text{EQ}}}$	$\sqrt{\frac{I^{\text{Arias}}_{\text{El Cen.}}}{I^{\text{Arias}}_{\text{EQ}}}}$	Scale Factors for $\ddot{u}_G$	Scale Factors for Arias	Scale Factors for Housner
EL CENTRO (NS)	1	1	1	386.	386.	386.
EL CENTRO (EW)	1.46	1.15	1.21	562.	466.	445.
OLYMPIA (S80W)	.97	1.48	1.24	386.	480.	572.
TAFT (S69E)	2.00	1.85	1.87	772.	720.	715.
TAFT (N21E	1.77	1.97	1.90	685.	735.	760.

Table 3-3 Factors to Multiply Accelerograms

The duration of the earthquakes in Table 3-3 is as follows:

El Centro NS	First 10 sec.	Taft S69E	First 19.20 sec.
El Centro EW	First 19.2 sec.	Taft N21E	First 19.36 sec.
Olympia S80W	First 19.60 sec.		

Before presenting the results obtained, it is interesting to write the equation of motion (3.1) in a nondimensional form, in terms of a new variable $z = u/u_y$ (note that for $u > u_y$, $z_{max} = \mu$) and draw some conclusions from it:

If we define a function $f(z)$ such that $f(z) = 1/u_y \, F(u)$ (where $F(u)$ has been defined in paragraph 3.2), then $F(u) = u_y f(z)$, i.e., the new function $f(z)$ is obtained from $F(u)$ by dividing its ordinates by u_y. This function is sketched in Fig. 3.17 for an elasto-plastic system:

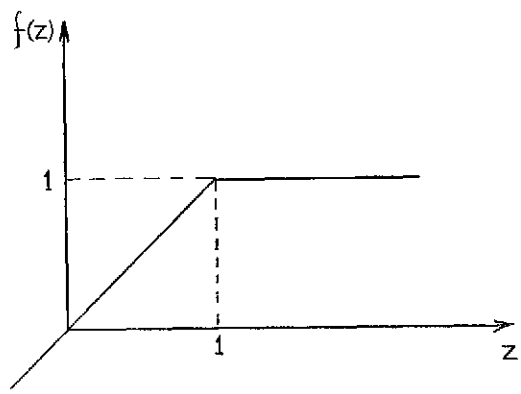

$$\left.\begin{aligned} f(z) &= z \\ f(z) &= 1 \end{aligned}\right\} \quad \begin{aligned} &\text{for } z \leq 1 \\ &\text{for } z \geq 1 \end{aligned}$$

Figure 3-17 Resistance Function in Nondimensional Form

Introducing z in 3.1 we obtain:

$$u_y \ddot{z} + 2\beta\omega u_y \dot{z} + \omega^2 u_y f(z) = -\ddot{u}_g$$

or

$$\ddot{z} + 2\beta\omega \dot{z} + \omega^2 f(z) = -\frac{\ddot{u}_g}{u_y}$$

or

$$\ddot{z} + 2\beta\omega \dot{z} + \omega^2 f(z) = -k\left(\frac{\ddot{u}_g}{F_y}\right) \qquad (3.4)$$

From this equation we see that the dimensionless response $z = u/u_y$ of a nonlinear system depends on the amount of viscous damping, the natural period of the system and the ratio of the maximum acceleration of the motion to the yield level. This means that if we have a nonlinear system and we want to study the effect of the yield level or of the earthquake intensity, we only need to vary one of them. Note also that the above is true for any of the nonlinear models introduced in chapter 2, since the loading and unloading laws governing these models do not affect the validity of equation 3.4.

From the same equation we can make the observation that if we multiply the mass, the stiffness and the yield level of a nonlinear system by some factor a, and use the same earthquake motion, the nondimensional response z remains unchanged. This is because in the left side ω is left unchanged and in the right side the ratio k/F_y remains also unchanged.

In the next pages the results of our investigation are presented in a graphical form. They are for three different systems: elastoplastic, bilinear and stiffness degrading. For the bilinear, the

slope of the second branch was chosen as 3% of the first. The degrading stiffness model is the simplified one that unloads parallel to the initial slope. The two other models that include strength degradation as well were not included in this study because ductility cannot be defined for the complete unit: i.e., the frame and the infill, which the model is designed to simulate. Four different values of viscous damping were selected corresponding to: $\beta = 0, 0.05, 0.10$ and 0.20. We will not elaborate on which of these values is a more realistic one, but we will mention that for a ductility analysis that is done for a strong earthquake, nonstructural elements might have cracked, and substantial damage might have occurred, which suggests that the viscous damping present at that stage of the response (in addition to the hysteretic damping of the yielding structure) could be significant.

Figures 3-18 through 3-23 show the variation of the required ductility factor μ as a function of the natural period of the system. Under each figure the law that describes the appropriate straight lines that best fitted the data is written. The solid line is the "average" line, and the dotted is an "upper-bound" line. In almost all the cases the solid lines are a little conservative for the long period range, and a little unconservative for the intermediate. This of course could be eliminated by a more elaborate curve fitting. From the expressions at the bottom of the figures, the decrease of the response with increase of the viscous damping becomes apparent. No significant difference appears between the undamped response of the elastoplastic and the bilinear model. For all the damped cases, how-

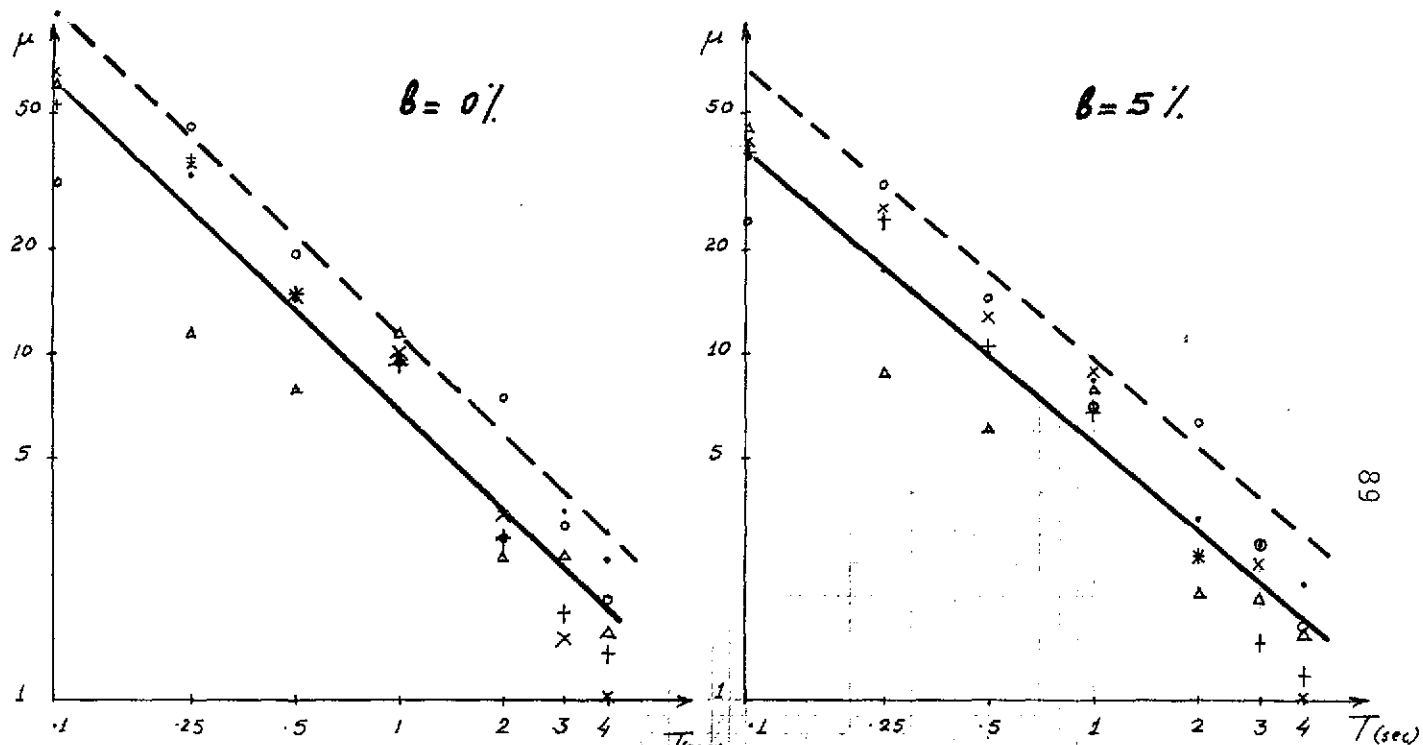

NOTE: All records have been scaled to give the intensity of the NS EL CENTRO, 1940

Figure 3-18

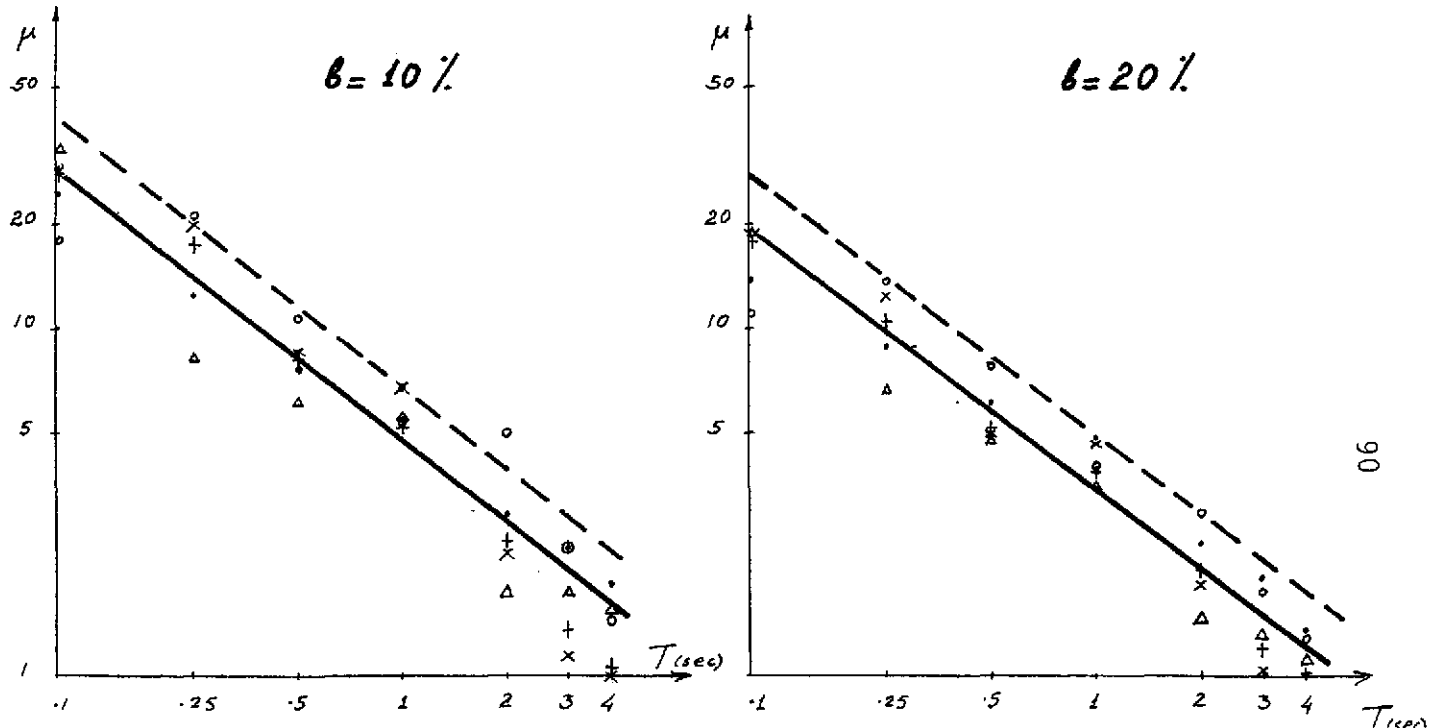
μ
50
20
10
5
1
β = 10 %
T (sec)
.1
.25
.5
1
2
3
4
μ = 4.8/T^.75
μ = 6.8/T^.75 (upper bound)
β = 20 %
μ = 3.4/T^.73
μ = 5./T^.73 (upper bound)
ELASTOPLASTIC
(EQUATE ARIAS' INTENSITY)

Figure 3-19

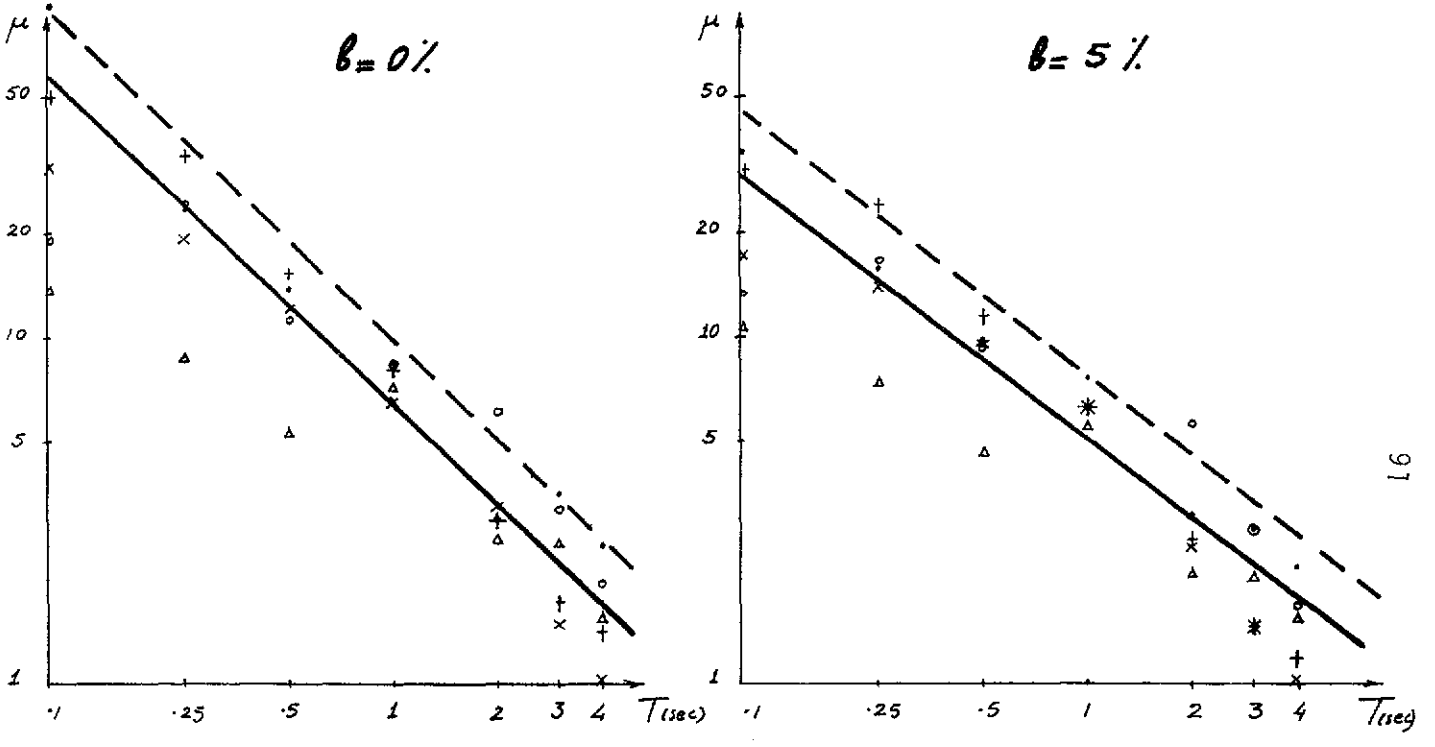

$\mu = 6.5/T^{.95}$

$\mu = 10./T^{.95}$ (upper bound)

$\mu = 5.2/T^{.76}$

$\mu = 7.8/T^{.76}$ (upper bound)

BILINEAR

(EQUATE ARIAS' INTENSITY)

Figure 3-20

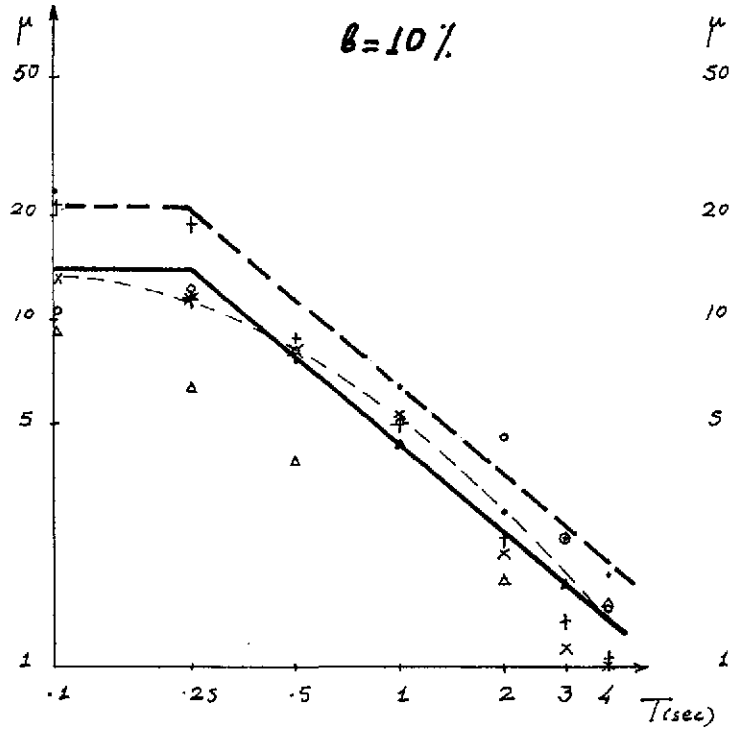

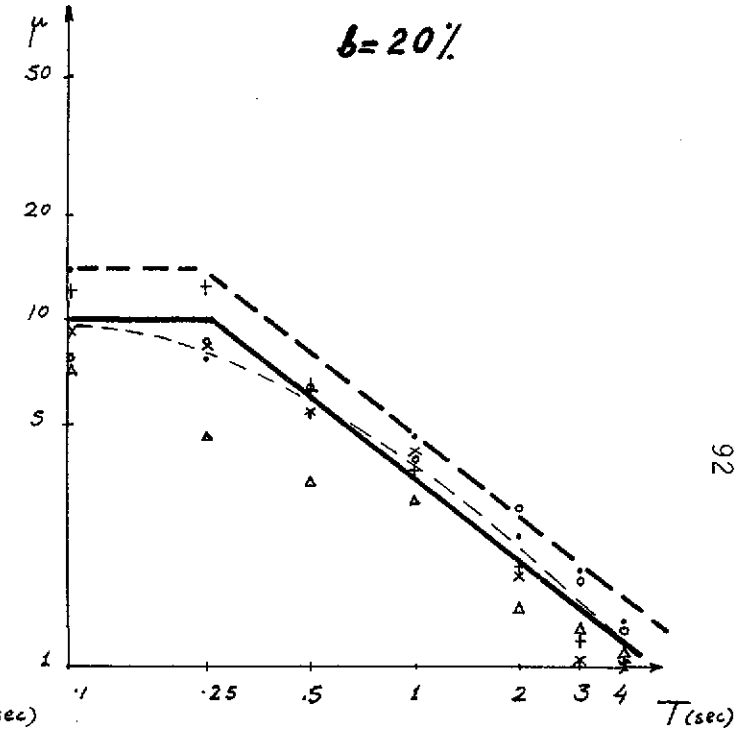

$\mu = 4.4/T^{.83}$

$\mu = 6.4/T^{.83}$ (upper bound)

$\mu = 3.5/T^{.78}$

$\mu = 4.6/T^{.78}$

BILINEAR

(EQUATE ARIAS' INTENSITY)

Figure 3-21

STIFFNESS DEGRADING

(EQUATE ARIAS' INTENSITY)

$\mu = 7.8/T^{1.09}$

$\mu = 12.8/T^{1.09}$ (upper bound)

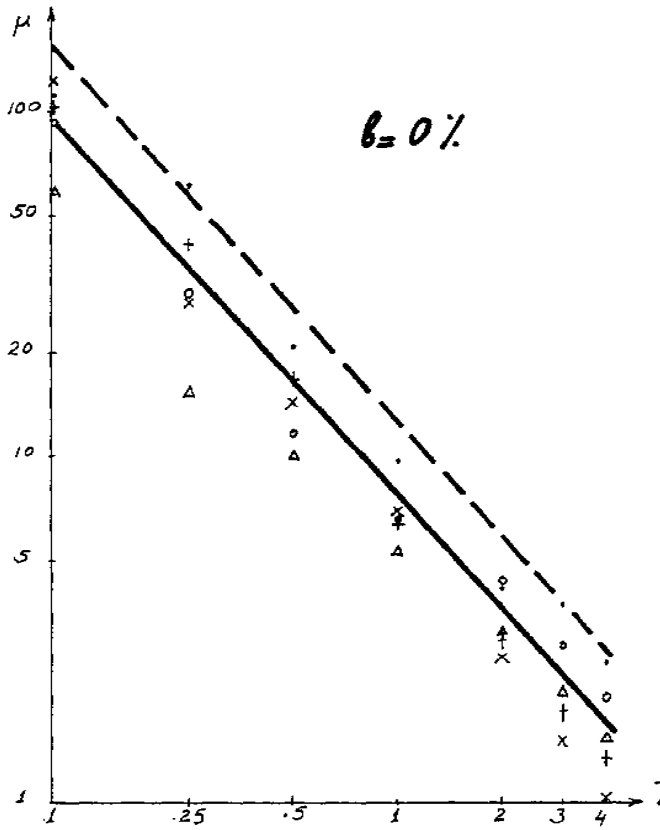

$\mu = 5.4/T^{.92}$

$\mu = 8./T^{.92}$ (upper bound)

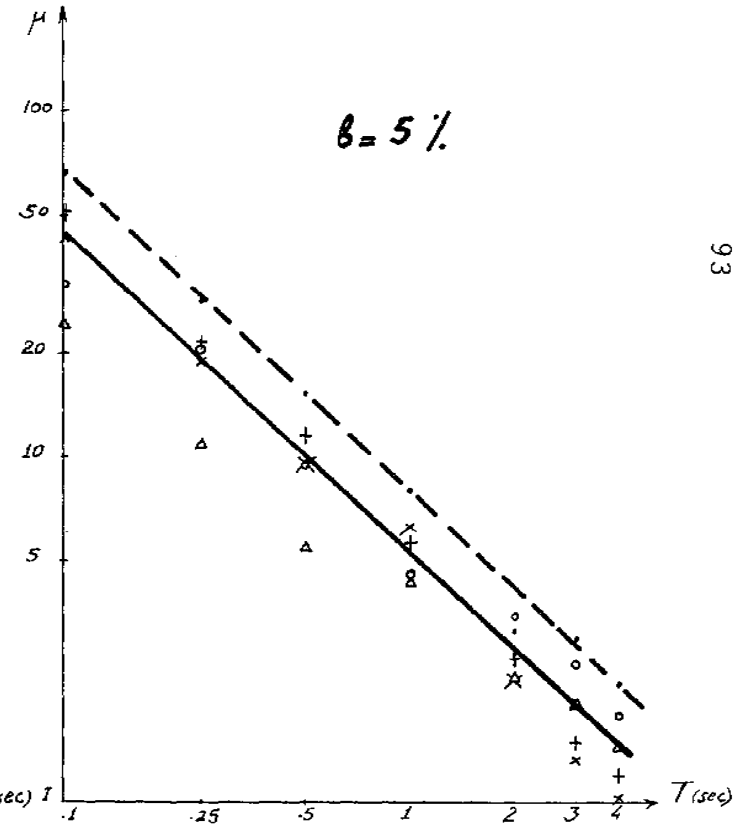

Figure 3-22

STIFFNESS DEGRADING

(EQUATE ARIAS' INTENSITY)

$\mu = 4.3/T^{.76}$

$\mu = 6.3/T^{.76}$ (upper bound)

$\mu = 3.5/T^{.75}$

$\mu = 4.5/T^{.75}$ (upper bound)

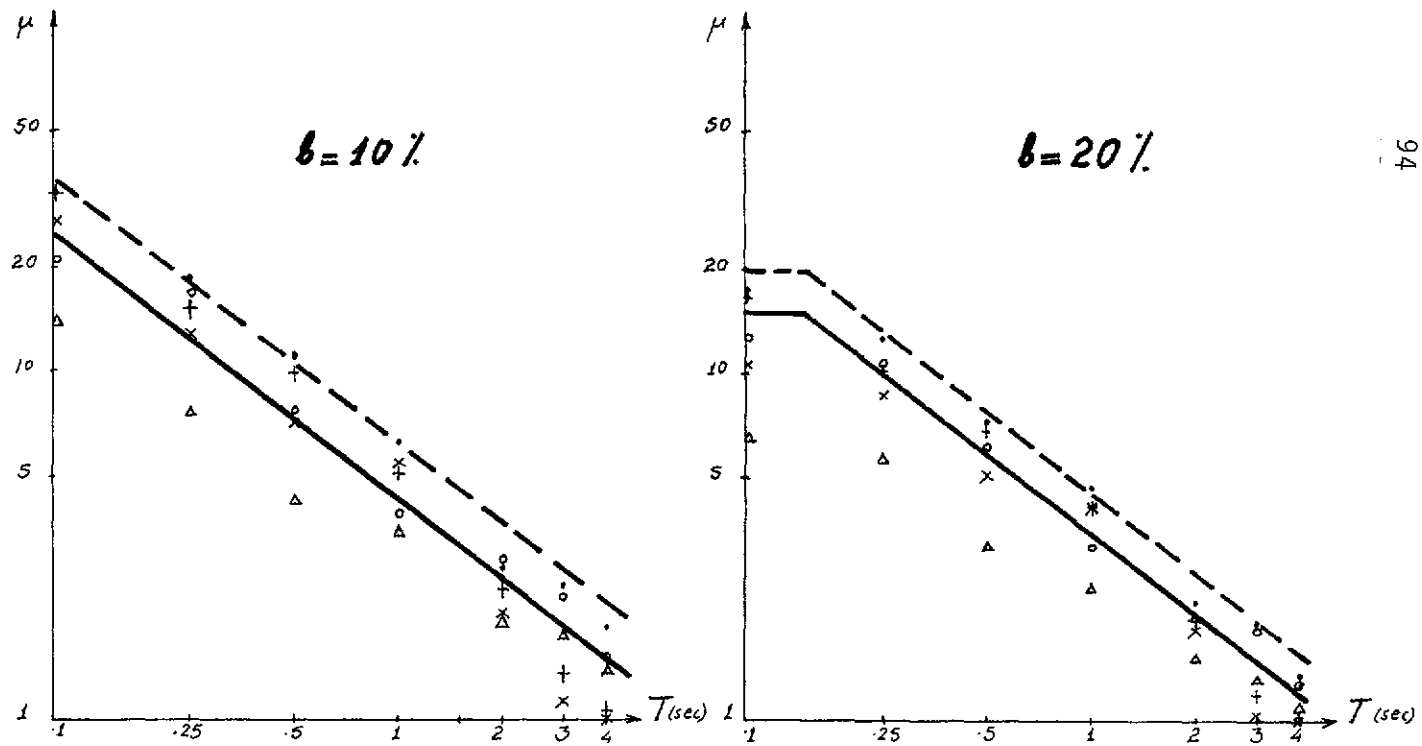

Figure 3-23

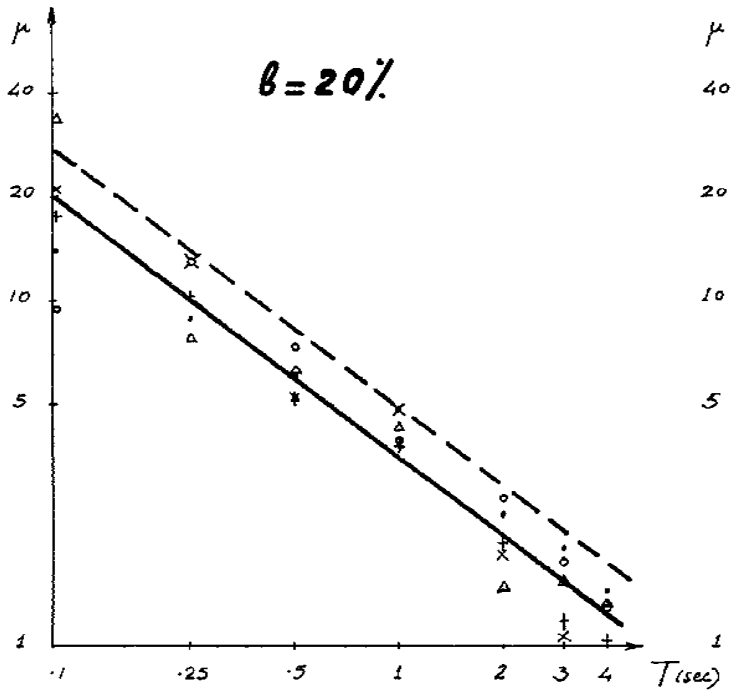

$\mu = 3.4/T^{.73}$

$\mu = 5./T^{.73}$ (upper bound)

ELASTOPLASTIC

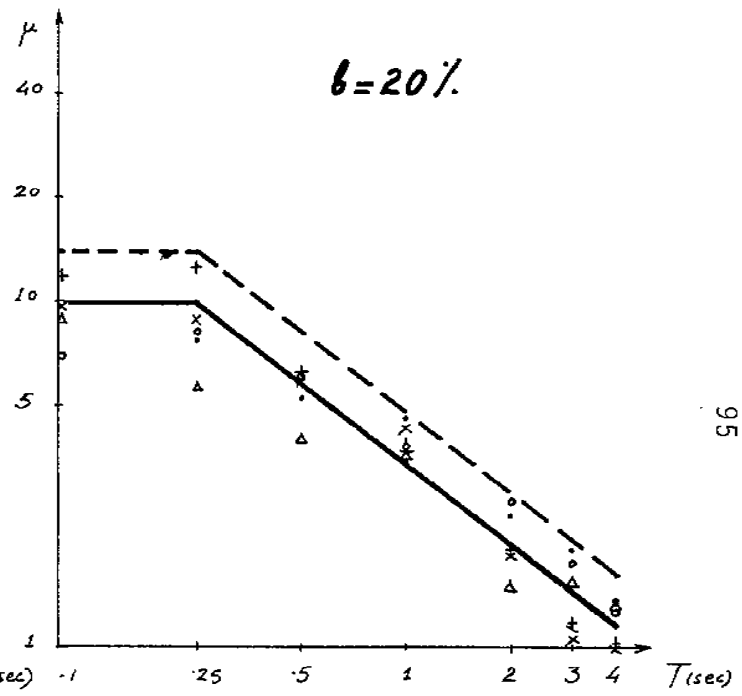

$\mu = 3.5/T^{.78}$

$\mu = 4.6/T^{.78}$

BILINEAR

(EQUATE HOUSNER'S INTENSITY)

Figure 3-24

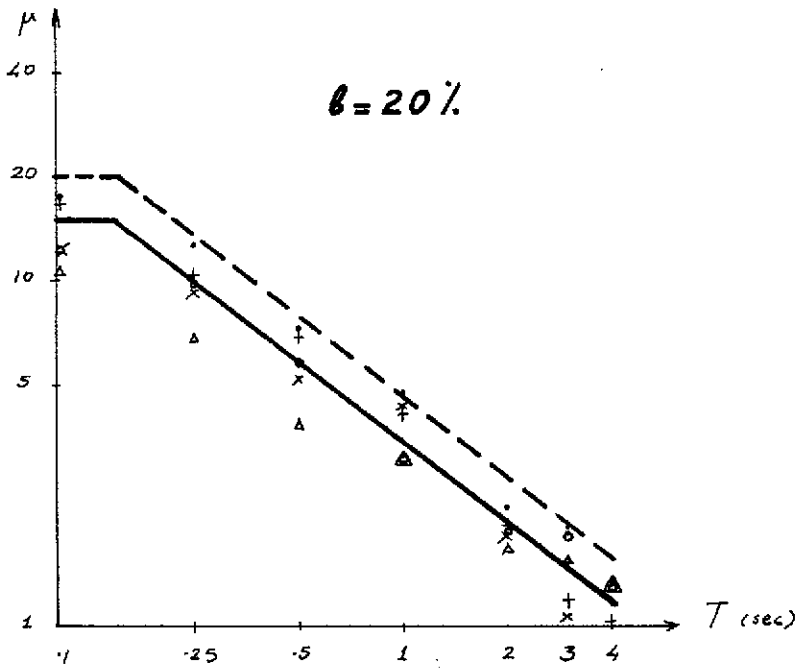

$\mu = 3.5/T^{.75}$

$\mu = 4.5/T^{.75}$ (upper bound)

STIFFNESS DEGRADING

(EQUATE HOUSNER'S INTENSITY)

Figure 3-25

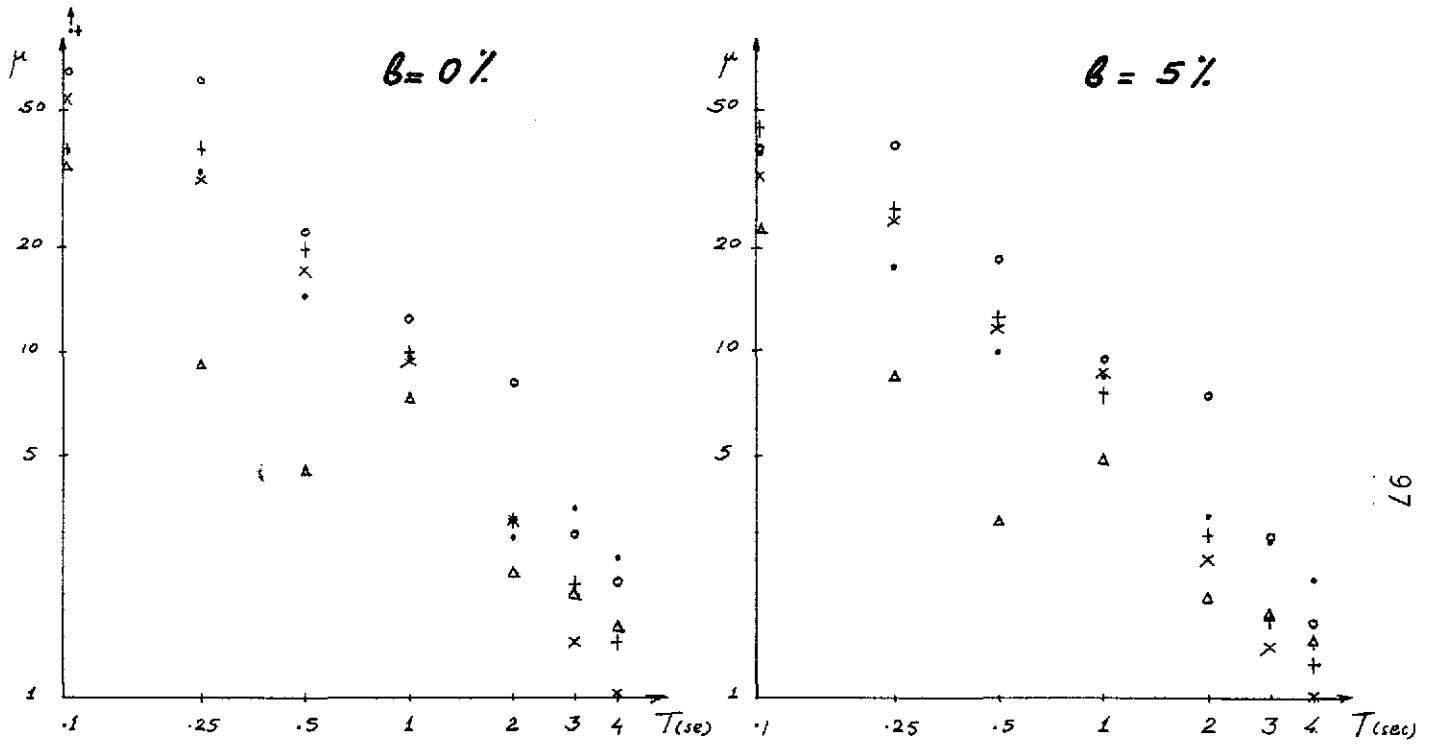

ELASTOPLASTIC

(EQUATE PEAK GROUND ACCELERATION)

Figure 3-26

ever, the bilinear has smaller ductility requirements in the low period regions, while it is almost identical to the elastoplastic in the long periods. This confirms the observations of Veletsos and Newmark in their comparisons of elastic and inelastic response in the same period ranges (see paragraph 3.3.2). The stiffness degrading model, compared to the elastoplastic, has slightly less ductility requirements in the long period region and slightly higher in the short period region. Again this is as expected and in agreement with comments made in paragraph 3.2 about the behavior of such a model in the different frequency ranges.

The most important conclusions, however, independent of the particular system, is that the ductility requirements for these structures are not uniform and increase as we go from long periods to short ones. While it can be argued that it is hard to find buildings designed as ductile frames (as this analysis has assumed with $k = .67$), in the period range, where the curves indicate extremely high ductility requirements, a three- to ten-story frame could very well lie in the region of .3 to 1 seconds, for which case the plots indicate an average value of ductility requirements from 5 to 10, even with 10% viscous damping. We consider this range of ductility to be high and difficult to attain, even for well designed and constructed structures.

A desirable situation would be to have a rather uniform distribution of ductility requirements over the complete range of natural periods in which framed buildings could be. In that case the lines

of the previous figures would tend to be horizontal or at least with a slope smaller than that in the figures. Given that the ductility requirements decrease with an increase of strength (as it will be seen in the following set of curves), it would seem that the design shear should be increased for stiff structures. In other words the coefficient 1/3 in the expression:

$$c = \frac{0.05}{T^{1/3}}$$

should increase to a value a, where a > 1/3.

The value of a could easily be determined, as it will be suggested later, given that an acceptable level of ductility has been established. In a more general sense the ideal kind of a relationship for the design shear coefficient should have the form of:

$$c = f(\mu,\beta) \cdot \frac{1}{T^{a(\mu,\beta)}} \qquad (3.5)$$

where T is the natural period of the structure and f, a are functions of the desired ductility factor μ and the percentage of critical damping β. The functions f and a could also be obtained either through some reasonable idealization of inelastic response spectra, or through random vibration theory.

At this point it seems that additional studies should be made to obtain similar curves for other values of the U.B.C. coefficient "k" (e.g. for k = 0.80, 1.00, 1.33 etc.) in order to include cases of buildings that include shear walls and if possible to use a closer

interval of natural periods examined, and maybe more earthquake records. The cost of computer runs for these studies is small, because we have only a one-degree-of-freedom system, and the numerical method used is very efficient and fast.

As a final remark before closing this section, figures 3-24 and 3-25 show the same curves for 20% viscous damping, determined by using Housner's definition of intensity, and are almost identical with the corresponding ones using Arias' definition. Figure 3-26 shows similar curves obtained by equating peak ground accelerations rather than intensities. The scatter here is bigger than in the other cases.

3.3.4 Ductility Variation as a Function of Strength

The most important factor that influences the ductility requirements of a structure for a given earthquake motion is the strength, defining as such the maximum force it can sustain at yielding. Here we will try to answer the second question posed in 3.3.1: i.e., "What is the required strength for a structure, so that the ductility factor will be within a specified range?" To do this, we computed again the time history response through a step-by-step numerical integration of the systems examined in the previous section, but this time for several values of the yield level F_y. So we obtained the maximum deformations and through them the corresponding ductility factors dividing by the deformation at yielding. This analysis was performed again for the same earthquakes as before, and

the same systems. The results are plotted in dimensionless form for the different values of natural periods, viscous damping, and for the three systems: elastoplastic, bilinear and stiffness degrading. The ordinate is the ductility factor μ and the abscissa is the dimensionless quantity $(m\ddot{u}_g/F_y)$. (Figures 3-27 - 3.68).

If we recall equation 3.4, μ is only a function of the ratio $\ddot{u}_g/F_y$. The earthquake records were multiplied again by the factors given in Table 3-3 and the $\ddot{u}_g$ used was that of El Centro: i.e., 0.32g. The complete set of curves is aimed to be a design aid. For values of period between those in the charts one could interpolate linearly.

One possible use for these curves could be the determination of appropriate laws for base shear coefficients so that we could have uniform ductility requirements for the complete range of the spectrum. This could be done as follows:

Write:

$$V_{des} = kcmg$$

$$F_y = a\, V_{des}.$$

Then:

$$c = \frac{F_y}{akmg} = \left(\frac{F_y}{m\ddot{u}_g}\right) \cdot \frac{\ddot{u}_g}{akg} \tag{3.6}$$

For the curves in this chapter $\ddot{u}_g = .32g$.

So 3.6 becomes:

$$c = \frac{.32}{ak} \cdot \left(\frac{F_y}{m\ddot{u}_g}\right) = \lambda \cdot \left(\frac{F_y}{mu_g}\right) \tag{3.7}$$

where $$\lambda = \frac{.32}{ak}$$

•	EL CENTRO	NS	, 10 sec
o	〃	〃	EW 19.12 first sec
△	OLYMPIA	SOOW	19.60 〃 〃
+	TAFT	S69E	19.20 〃 〃
×	〃	N51E	19.36 〃 〃

ELASTOPLASTIC $T = .1$ sec

$\beta = 0\%$

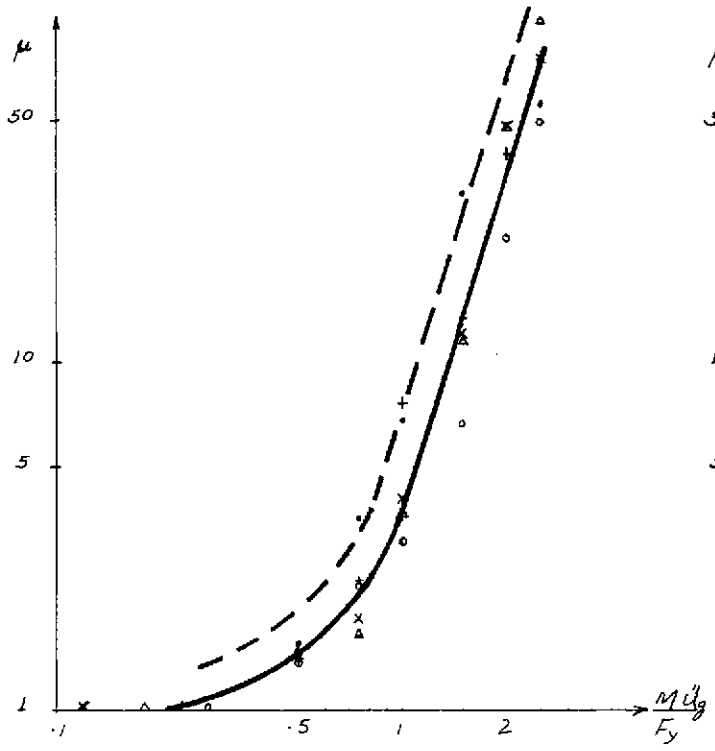

$\beta = 5\%$

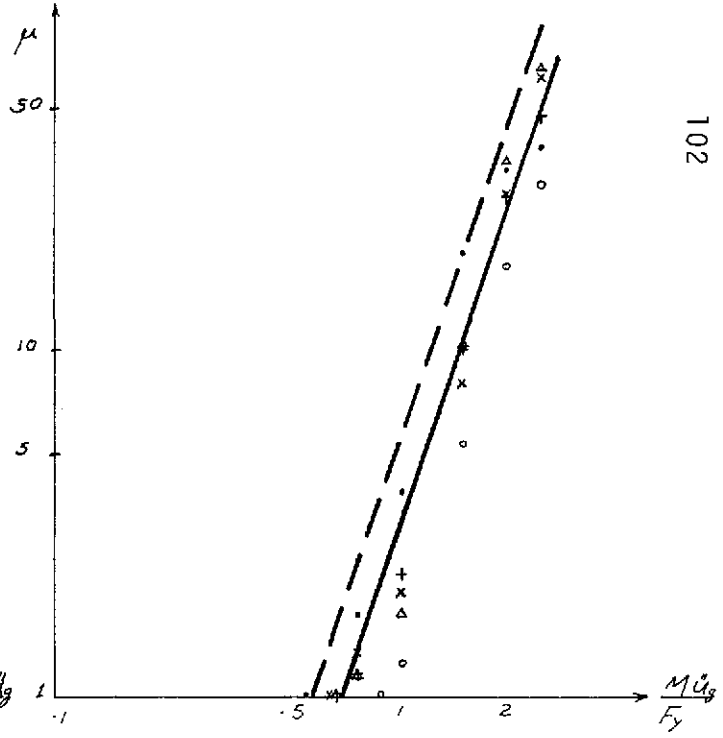

Figure 3-27

ELASTOPLASTIC $T = .1$ sec

$\beta = 10\%$ $\beta = 20\%$

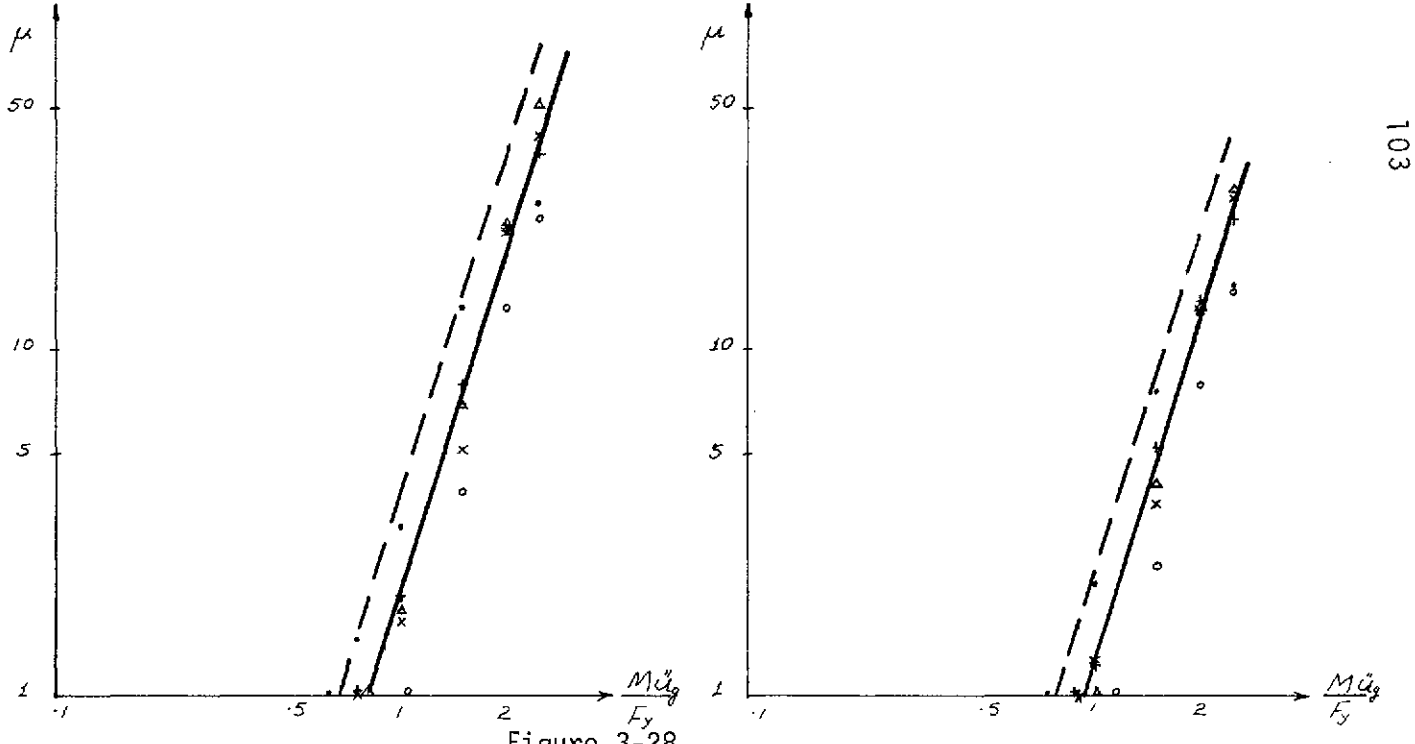

Figure 3-28

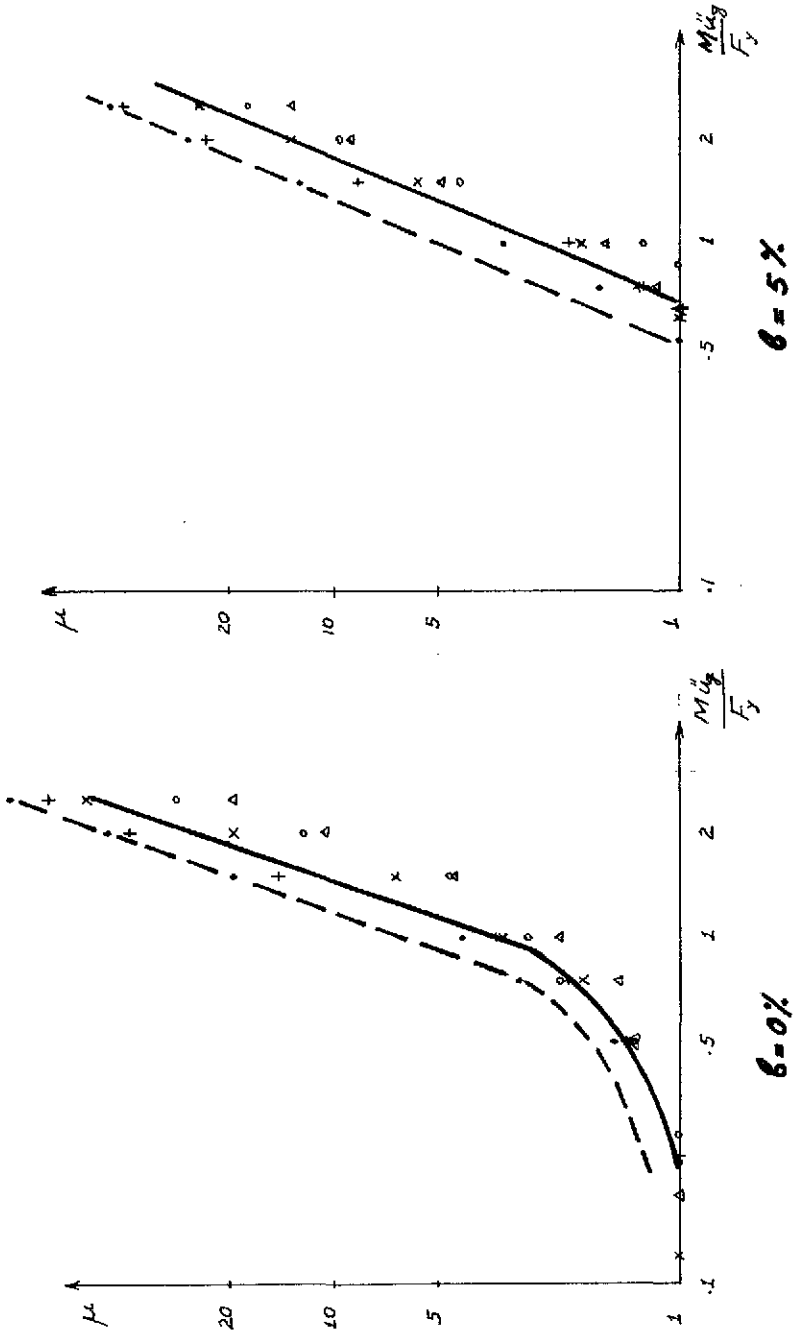

Figure 3-29

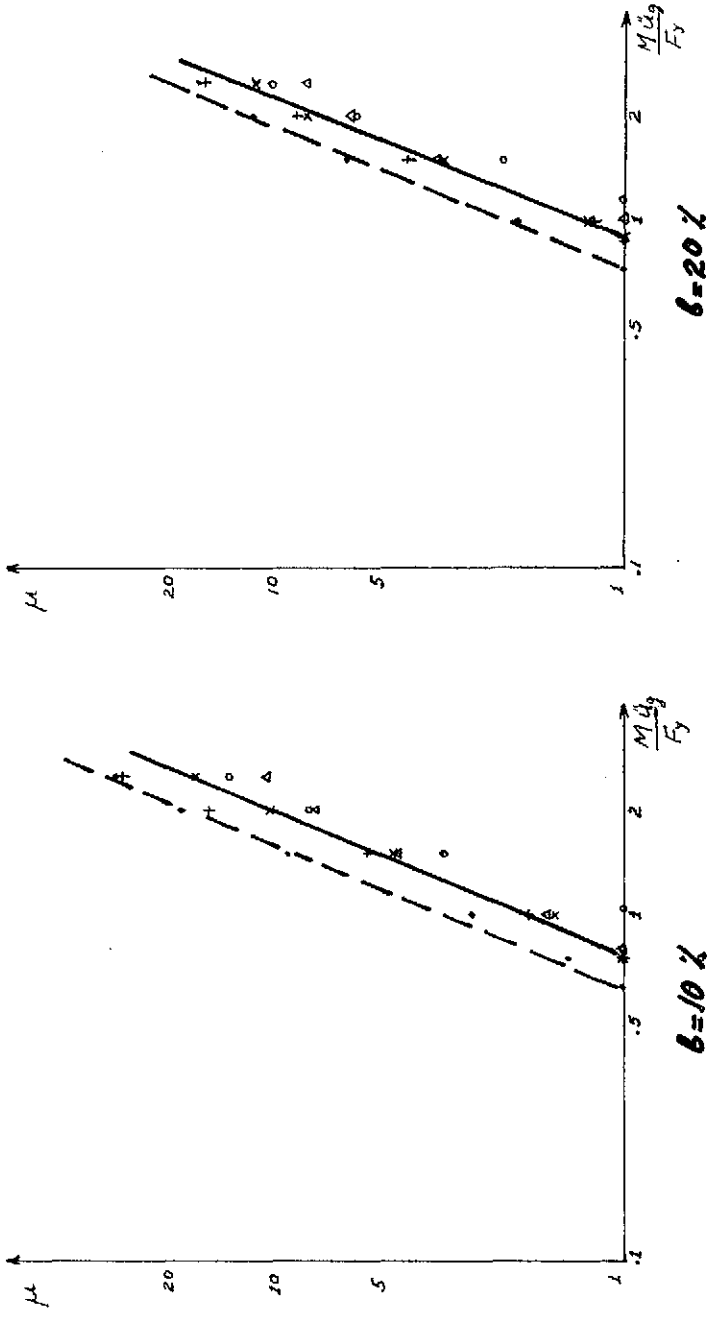

Figure 3-30

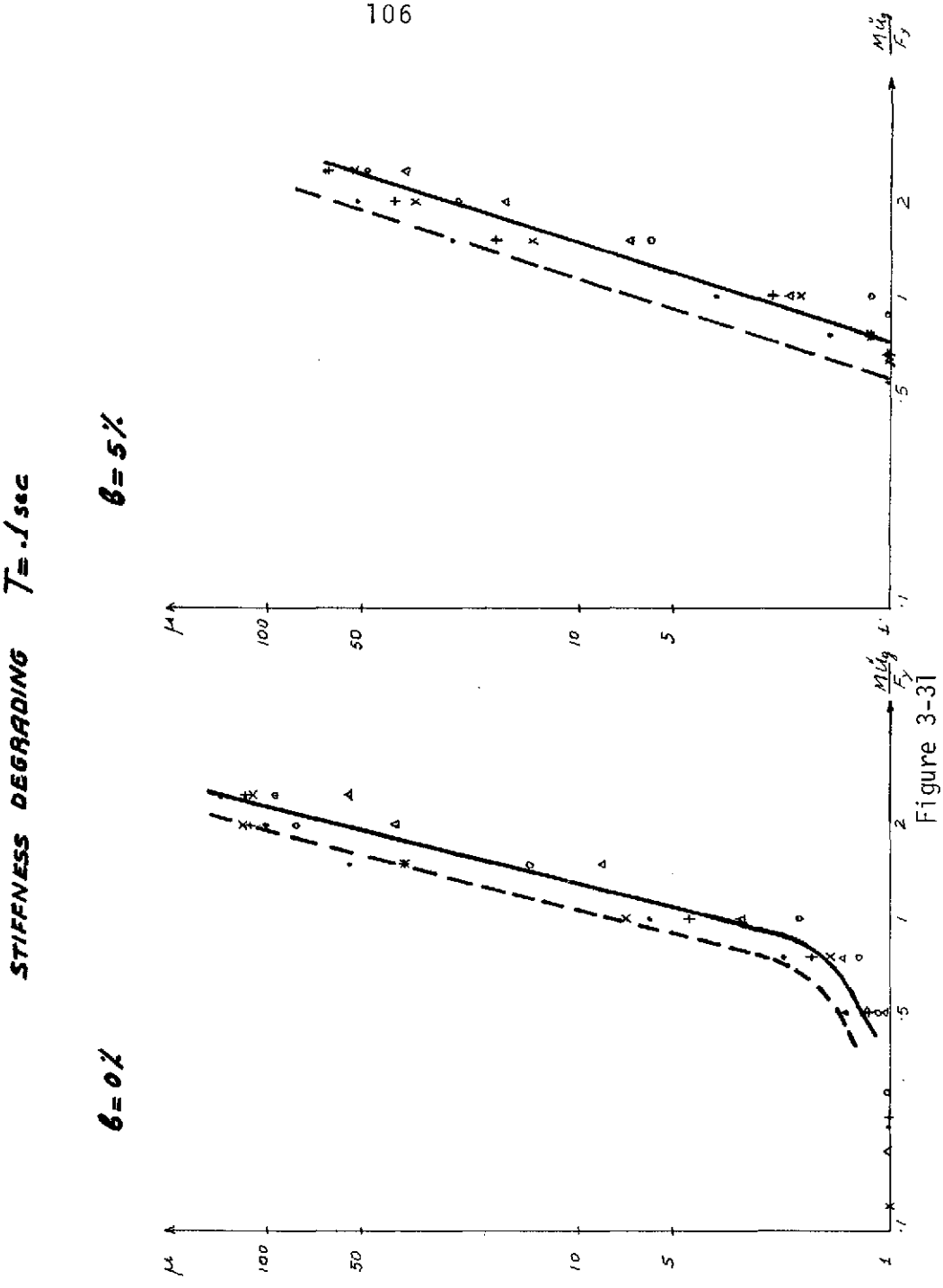
STIFFNESS DEGRADING T=.1 sec
β=0%
β=5%
μ
100
50
10
5
1
.1
.5
1
2
$\frac{M_{Ud}}{F_y}$

Figure 3-31

STIFFNESS DEGRADING $T = .1$ sec

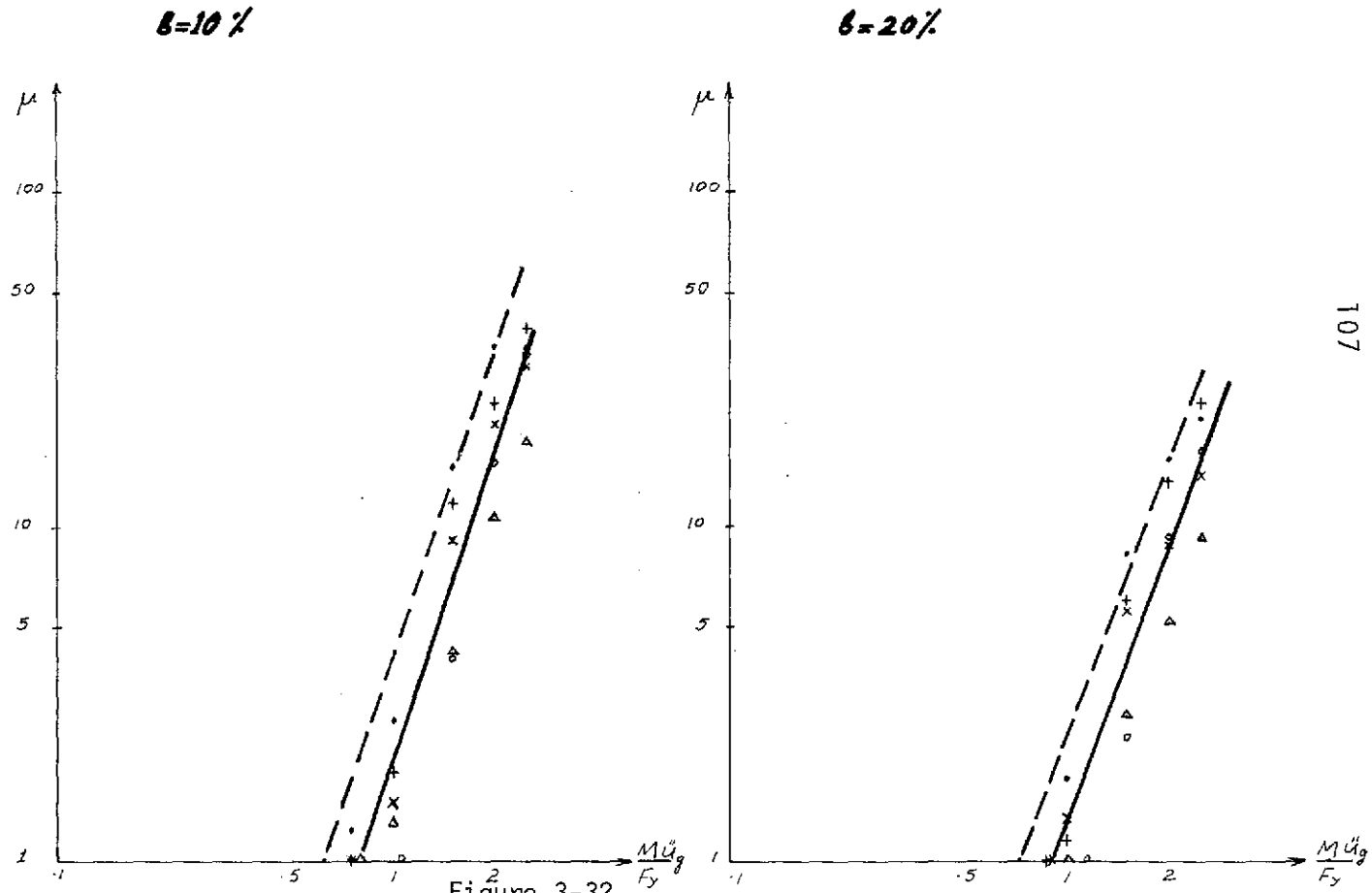

Figure 3-32

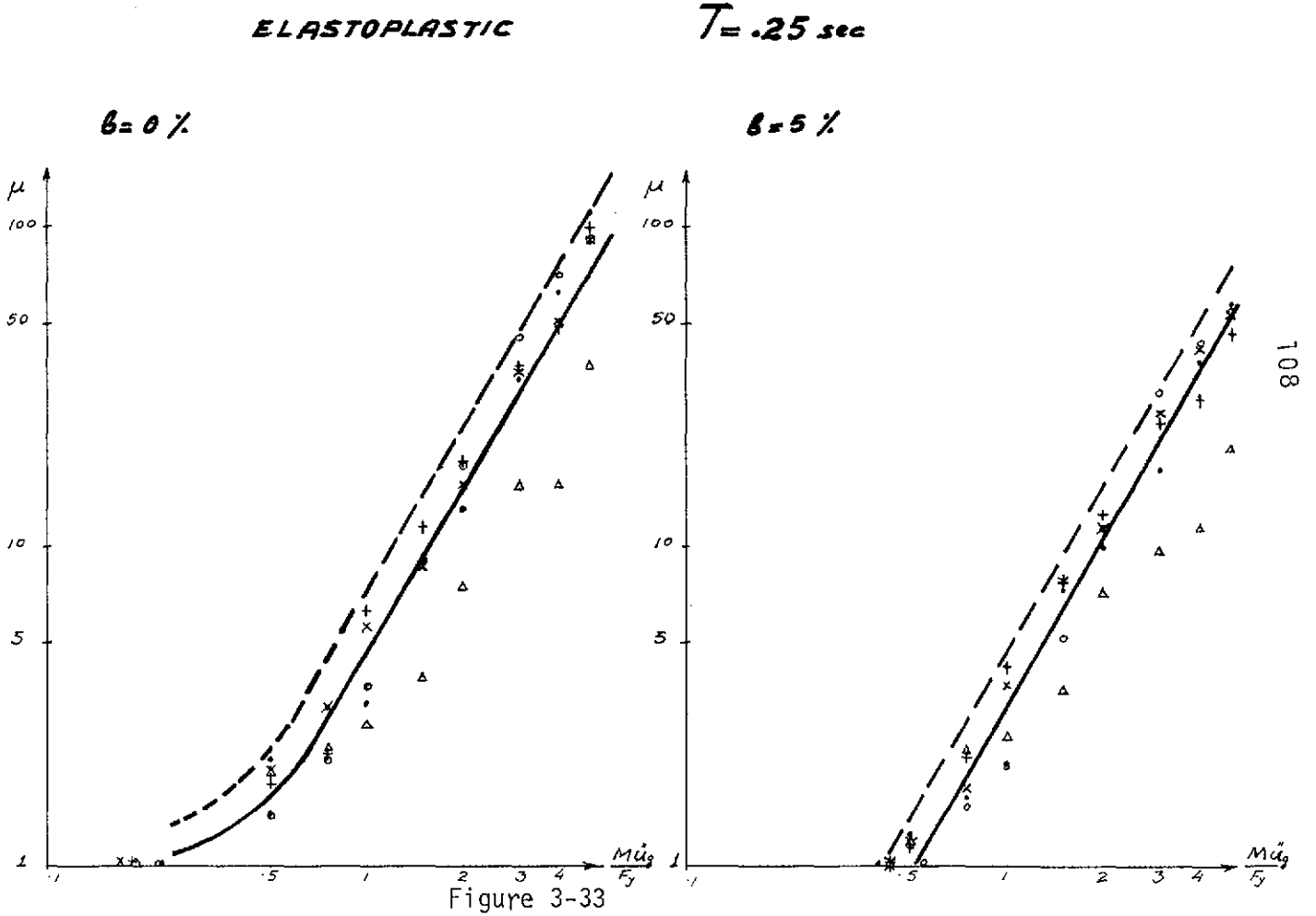

Figure 3-33

ELASTOPLASTIC $T = .25$ sec

$\beta = 10\%$ $\beta = 20\%$

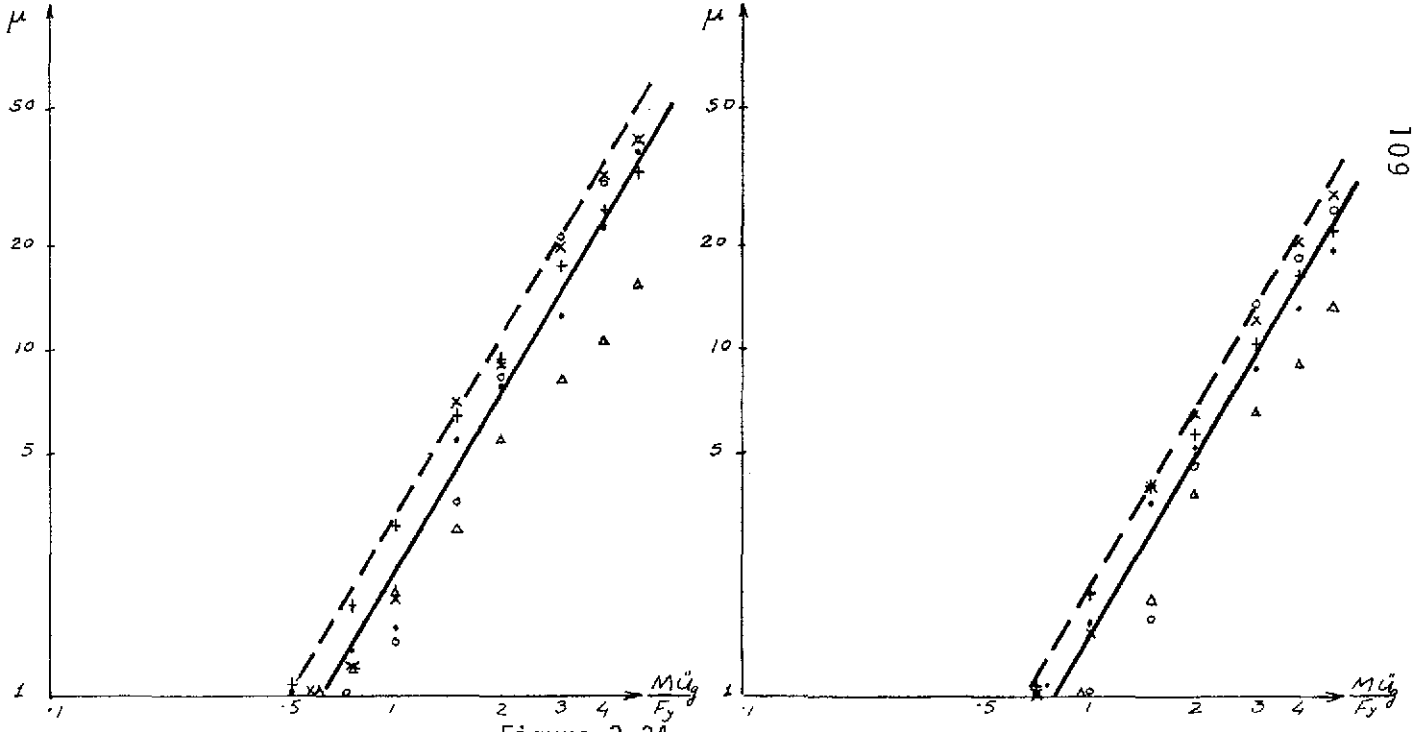

Figure 3-34

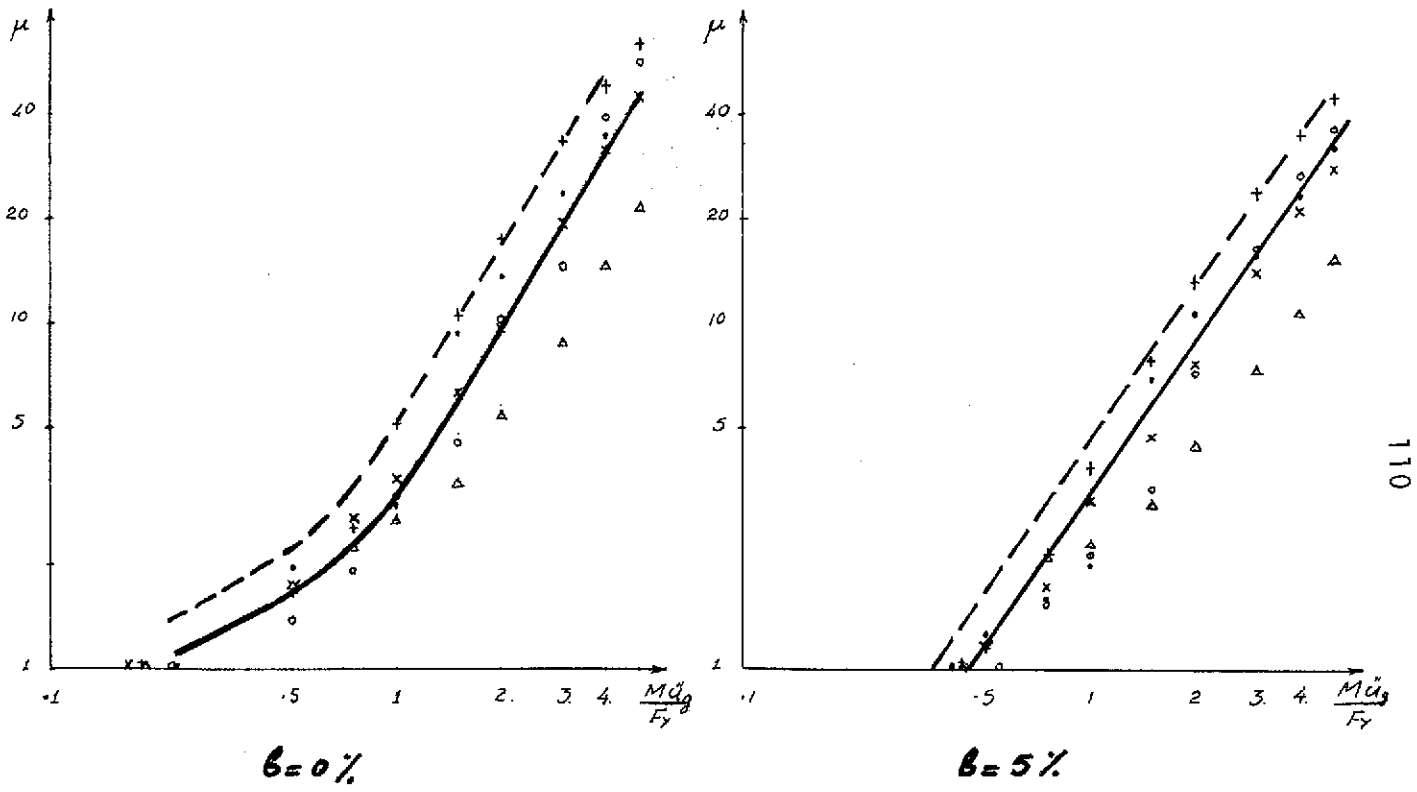

Figure 3-35

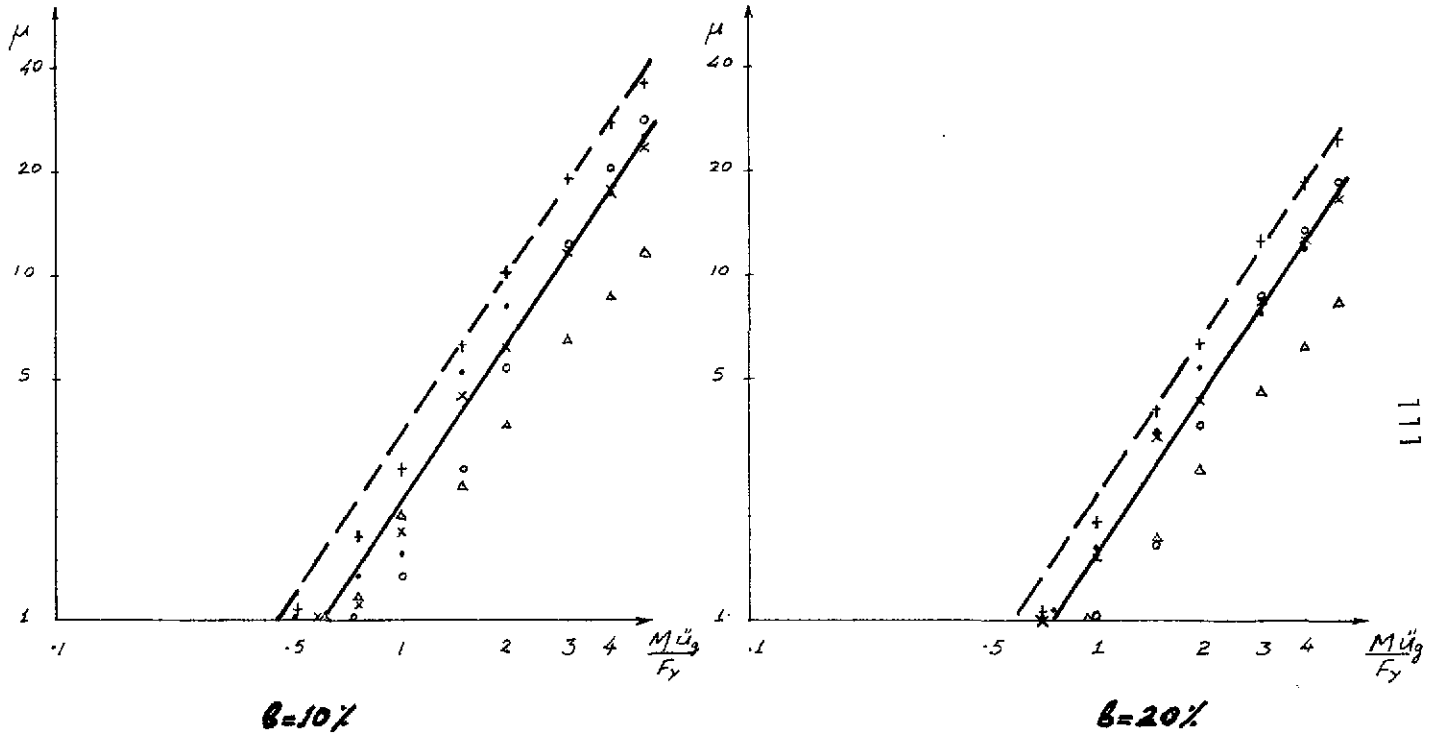
μ
40
20
10
5
1
.1
.5
1
2
3
4
MÜg/Fy
β=10%
μ
40
20
10
5
1
.1
.5
1
2
3
4
MÜg/Fy
β=20%
BILINEAR
T=.25 sec

Figure 3-36

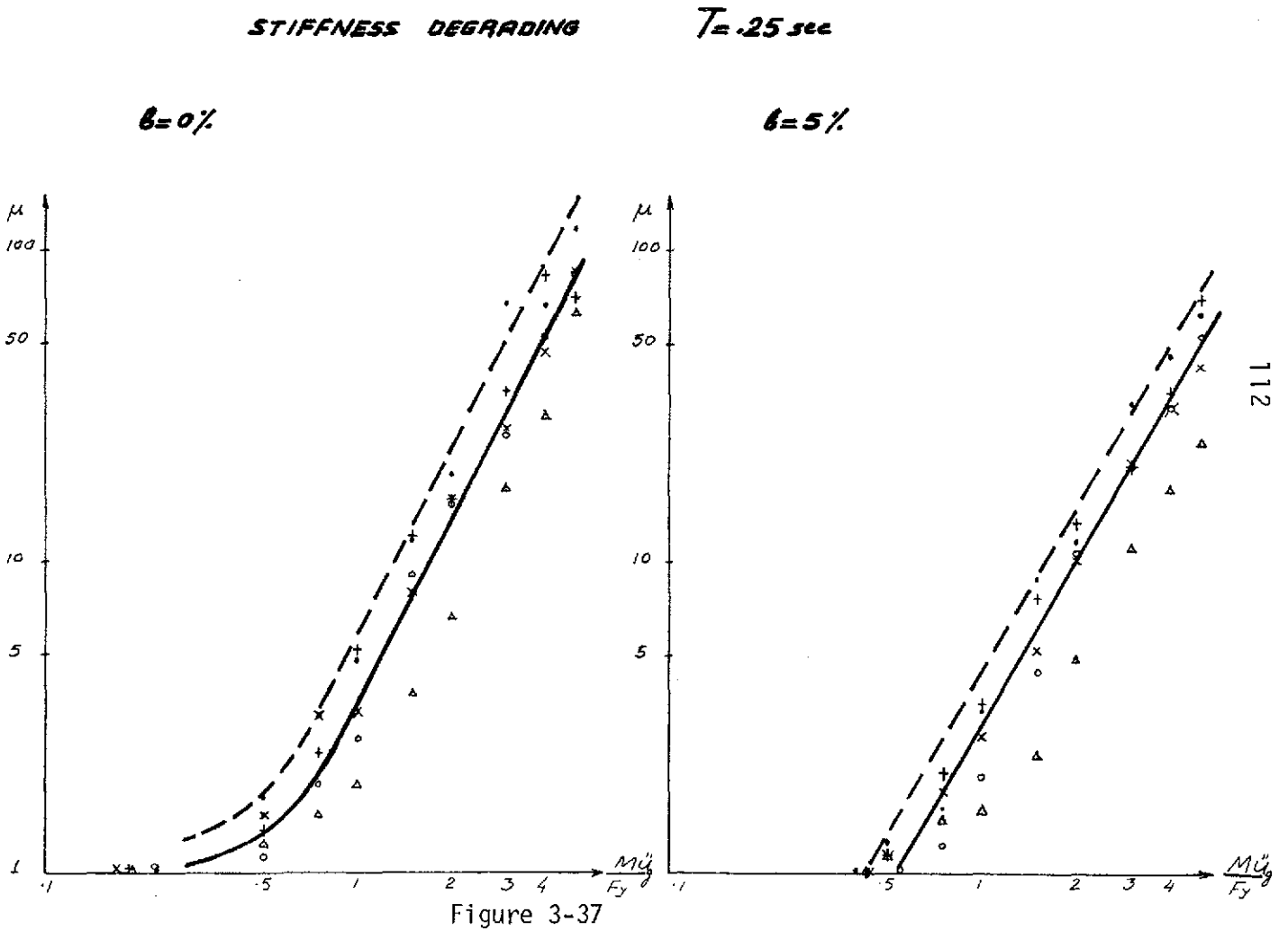

Figure 3-37

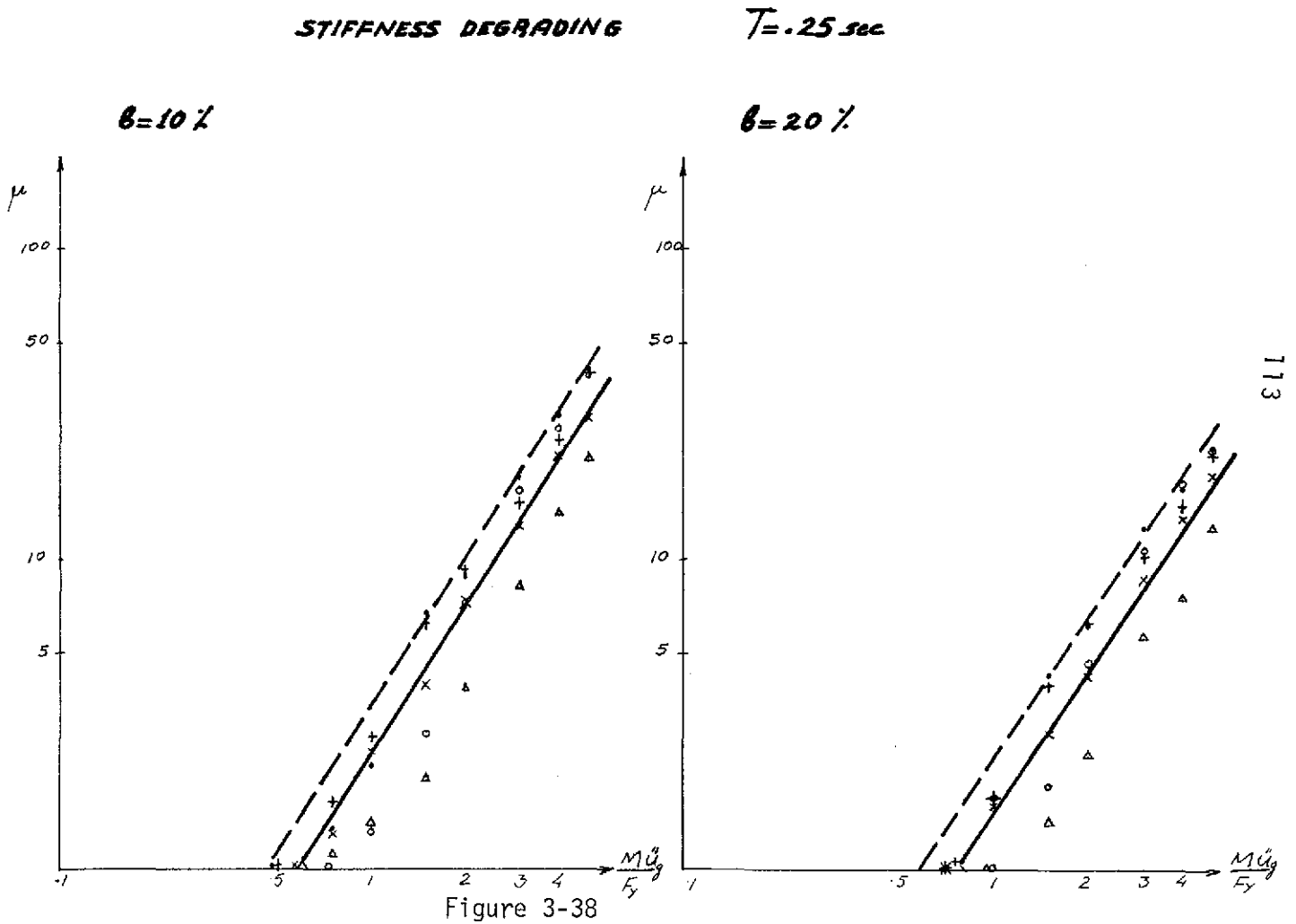
STIFFNESS DEGRADING
T=.25 sec
β=10 %
β=20 %
μ
100
50
10
5
1
.5
.1
MÜg/Fy
1
2
3
4
Figure 3-38

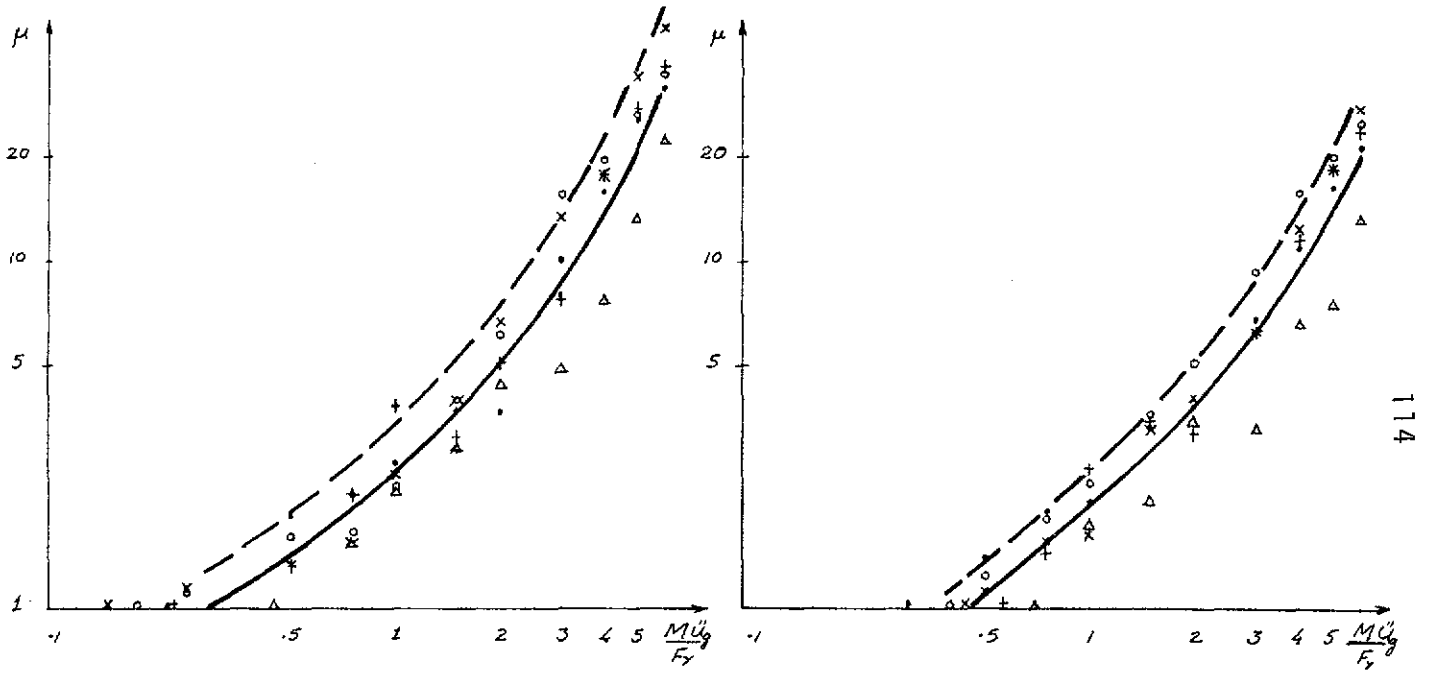
μ
20
10
5
1
-1
.5
1
2
3
4
5
MÜg/Fy
μ
20
10
5
-1
.5
1
2
3
4
5
MÜg/Fy
β=0 %
β=5 %
ELASTOPLASTIC
T=.5 sec

Figure 3-39

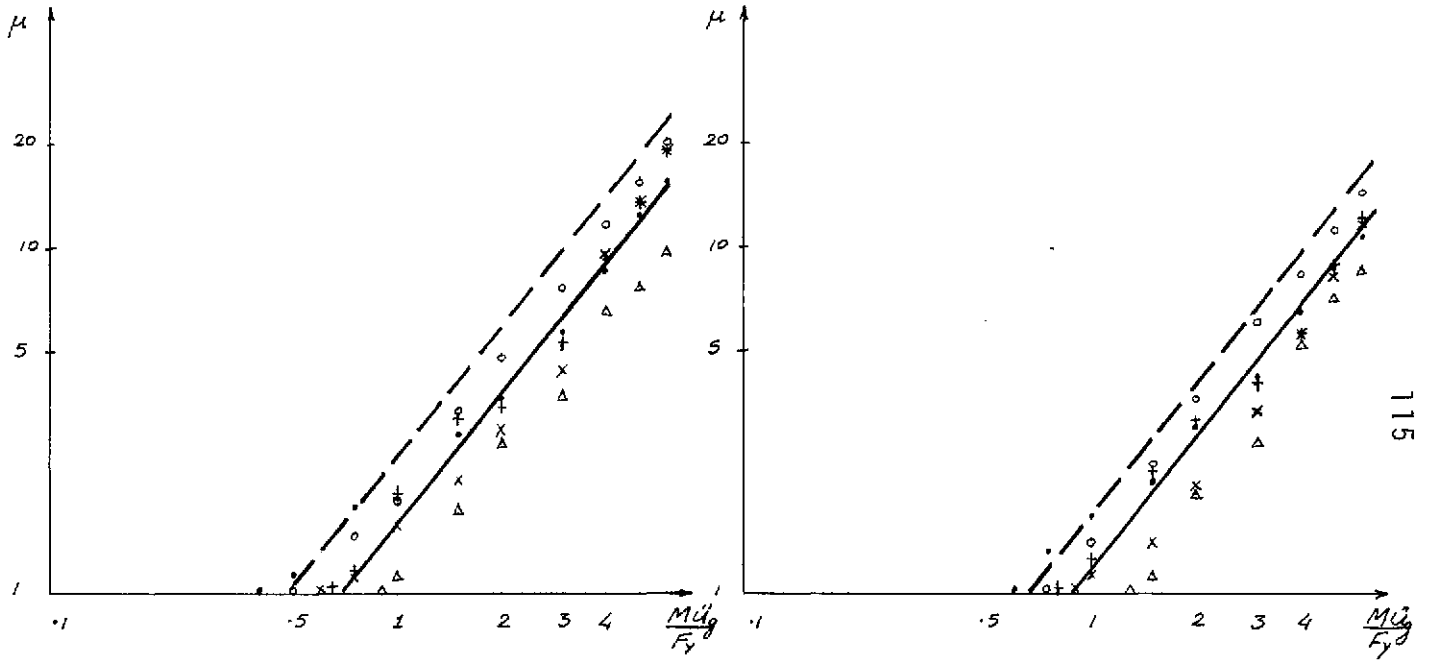

B=10 %

B=20 %

ELASTOPLASTIC T=.5 sec

Figure 3-40

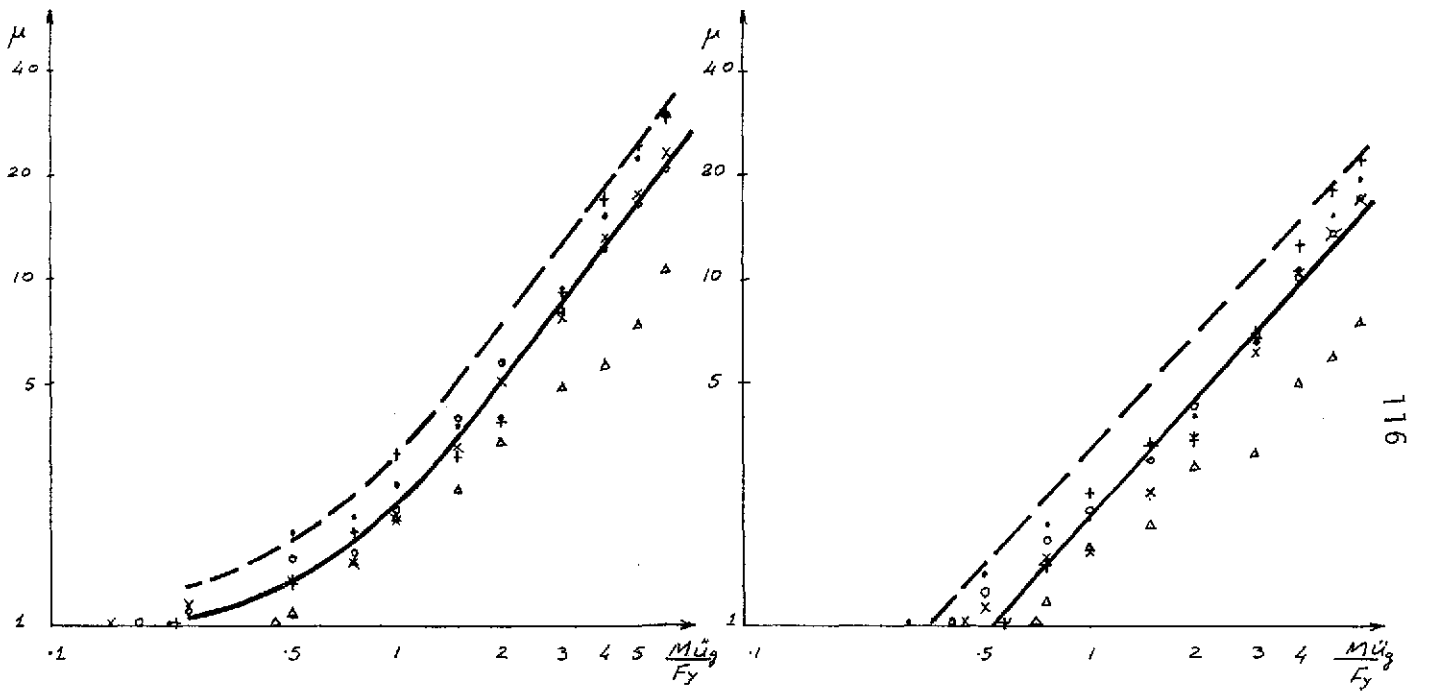
μ
40
20
10
5
1
·1
·5
1
2
3
4
5
MÜg/Fy
μ
40
20
10
5
1
·1
·5
1
2
3
4
MÜg/Fy
116
B=0%
B=5%
BILINEAR
T= .5 sec

Figure 3-41

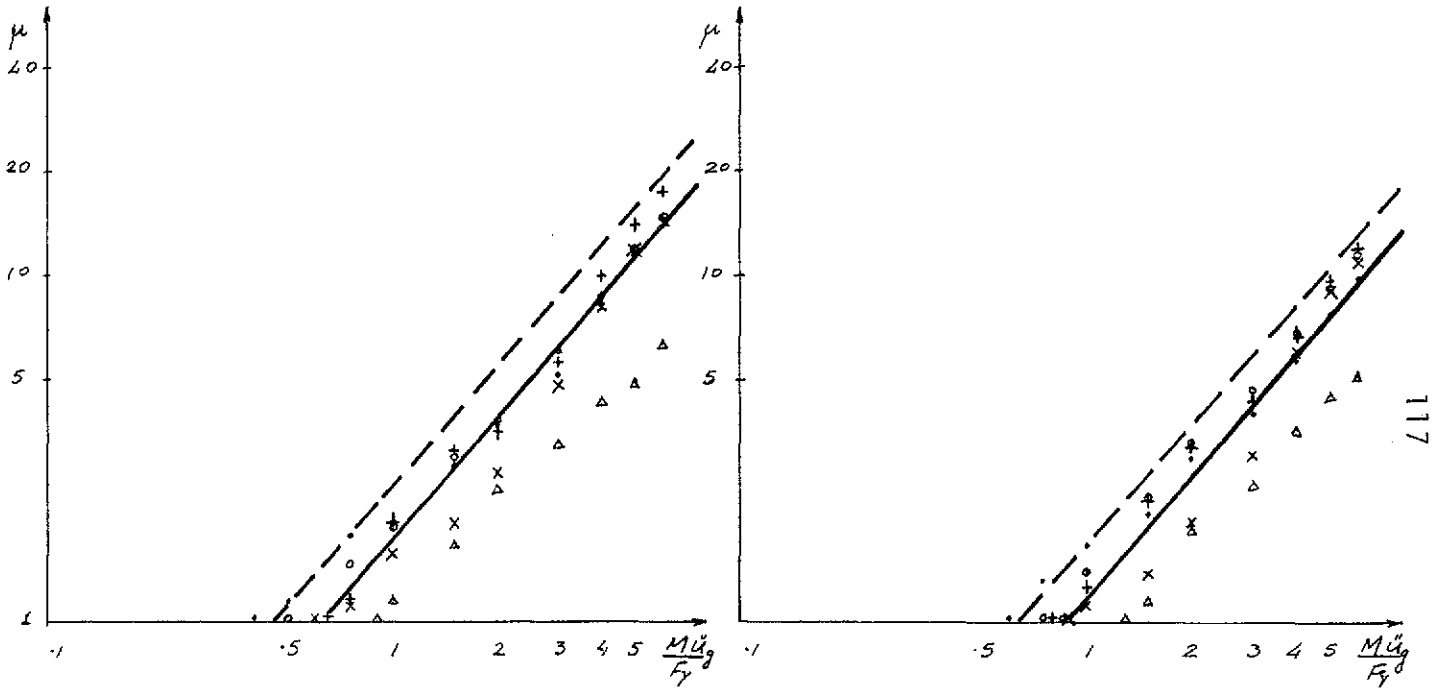

β=10%

β=20%

BILINEAR

T=.5 sec

Figure 3-42

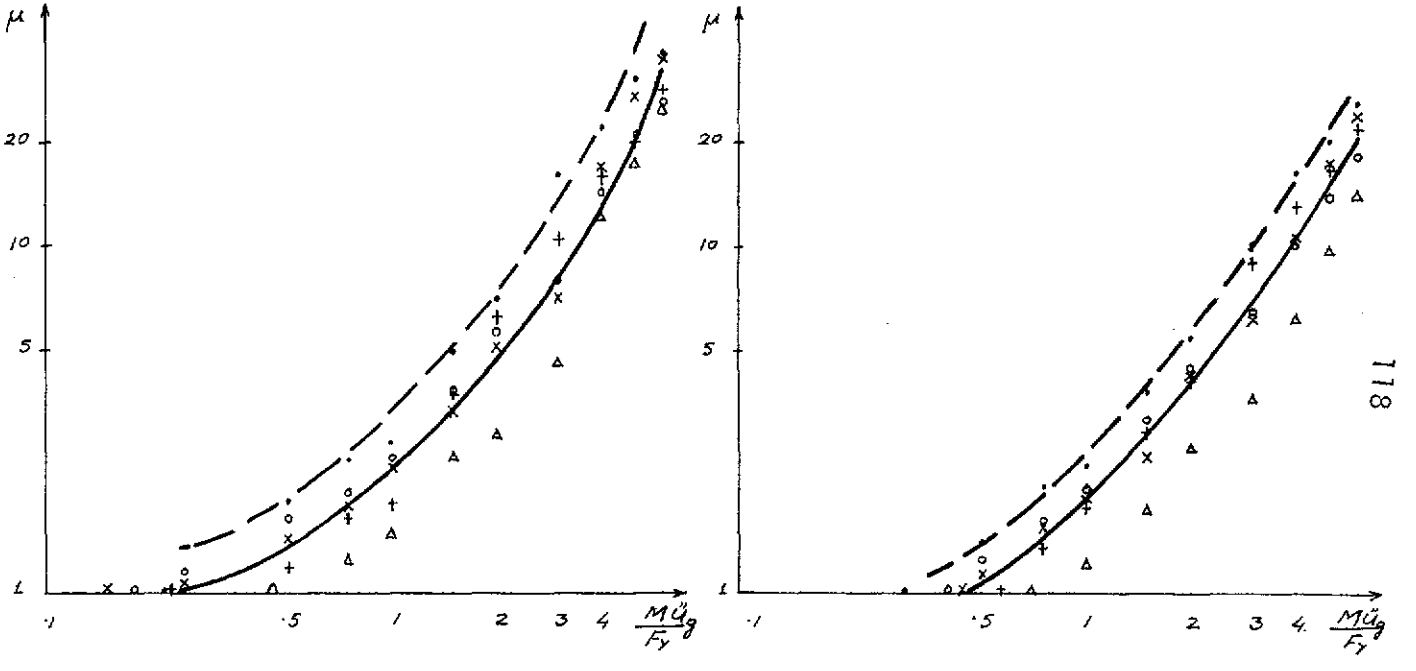

Figure 3-43

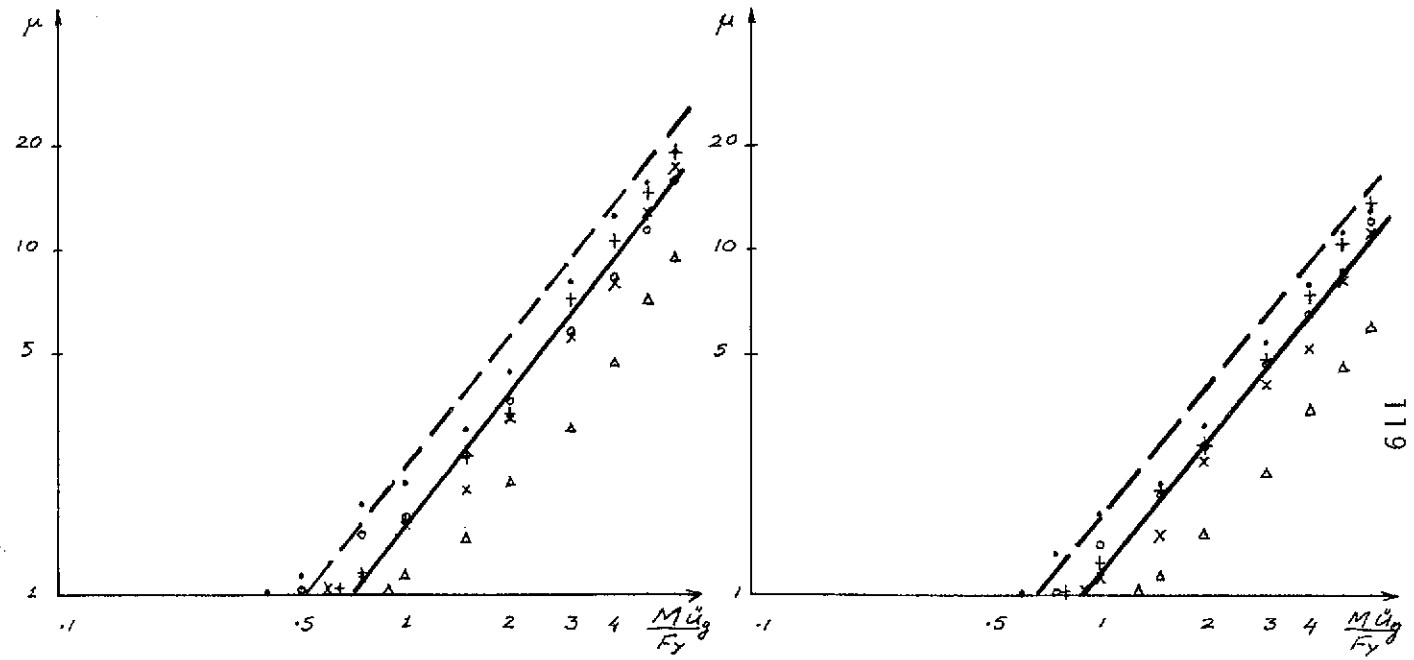

ζ=10%

ζ=20%

STIFFNESS DEGRADING $T = .5$ sec

Figure 3-44

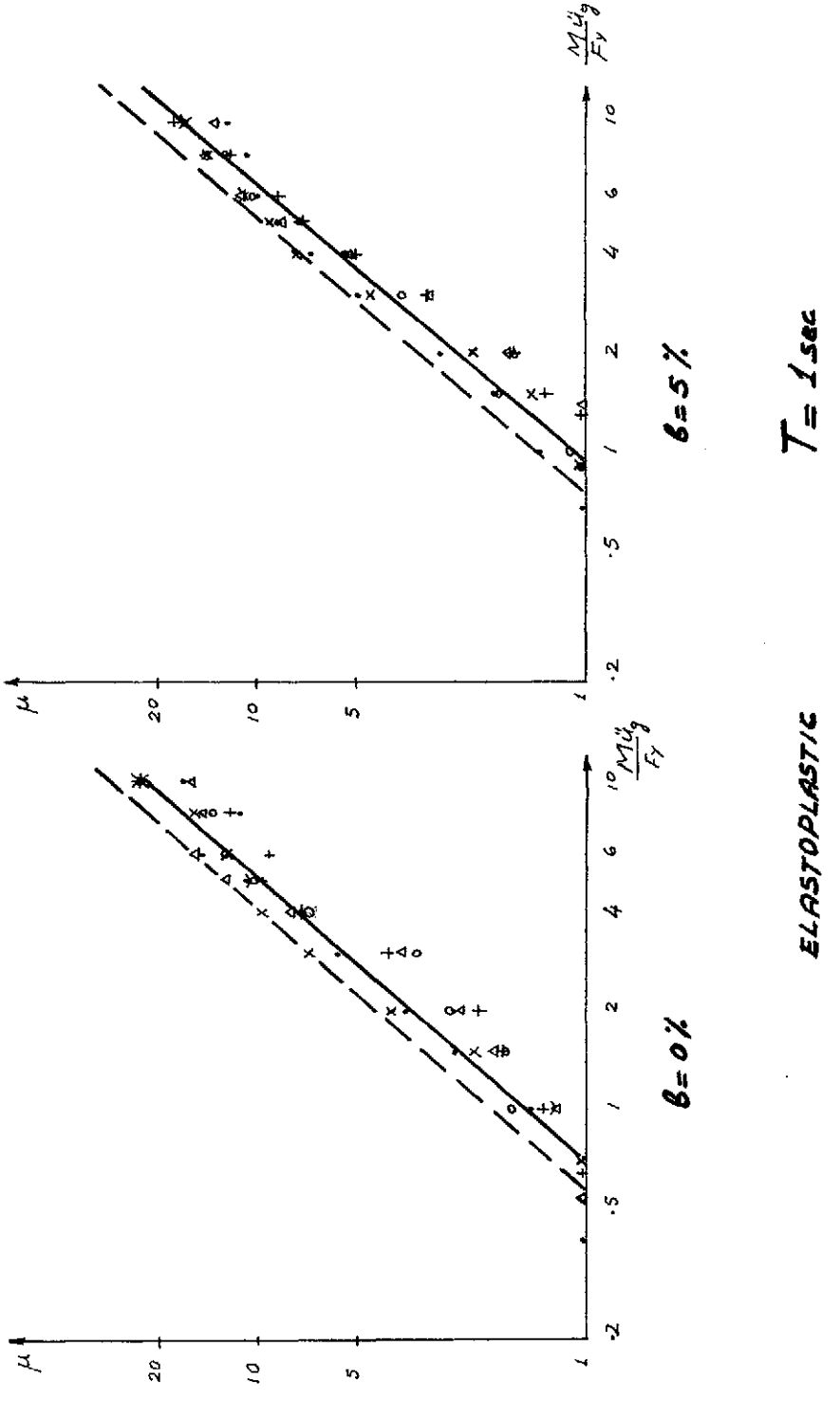

Figure 3-45

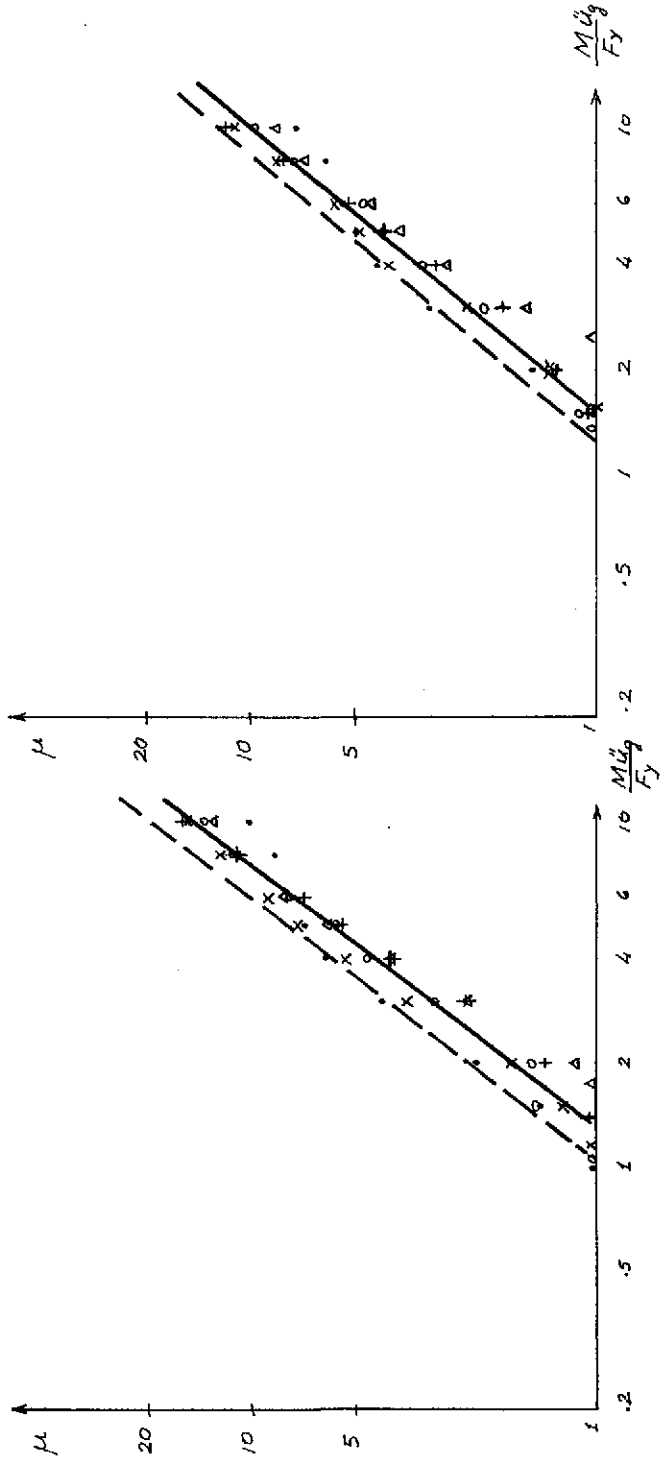
μ
20
10
5
1
.5
.2
1
2
4
6
10
$\frac{M\ddot{U}_g}{F_y}$
β=20%
β=10%
ELASTOPLASTIC
T= 1sec

Figure 3-46

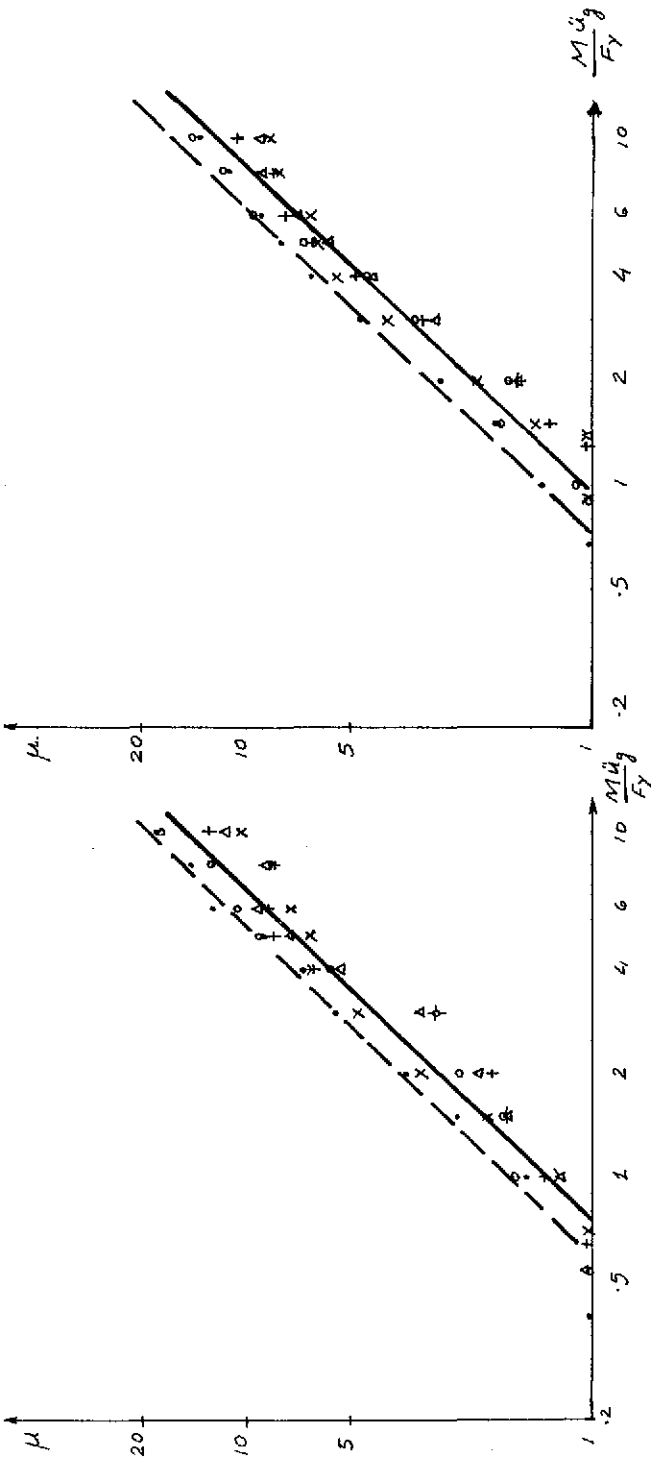

Figure 3-47

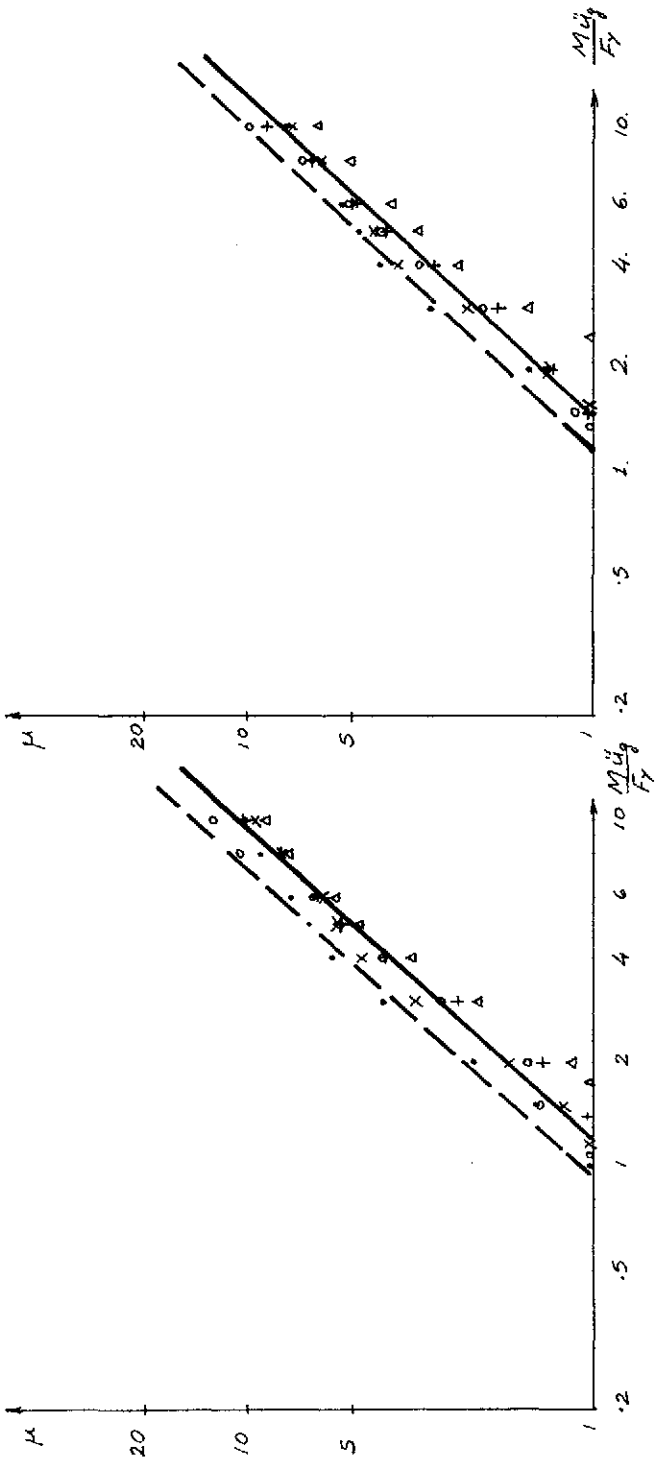

Figure 3-48

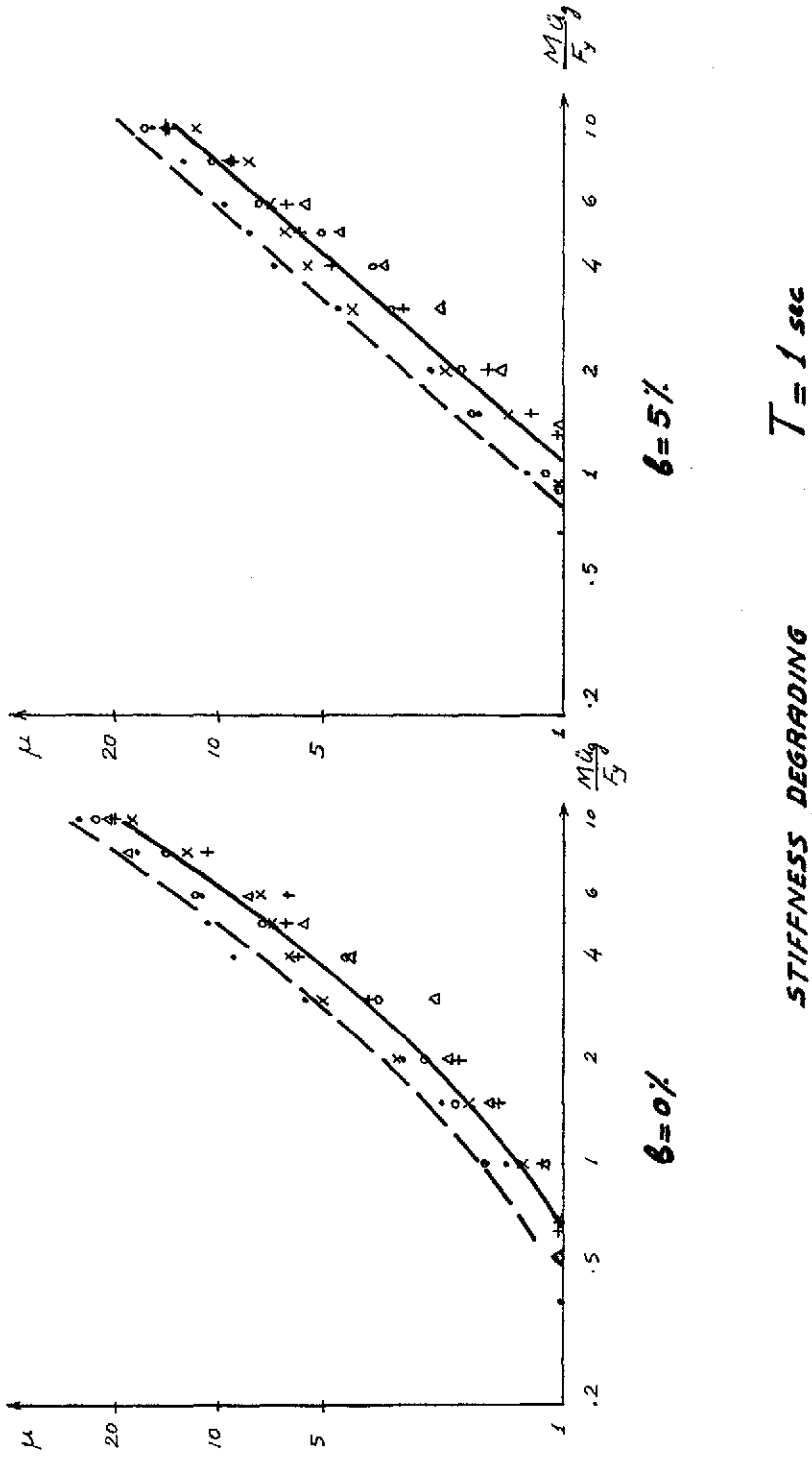

Figure 3-49

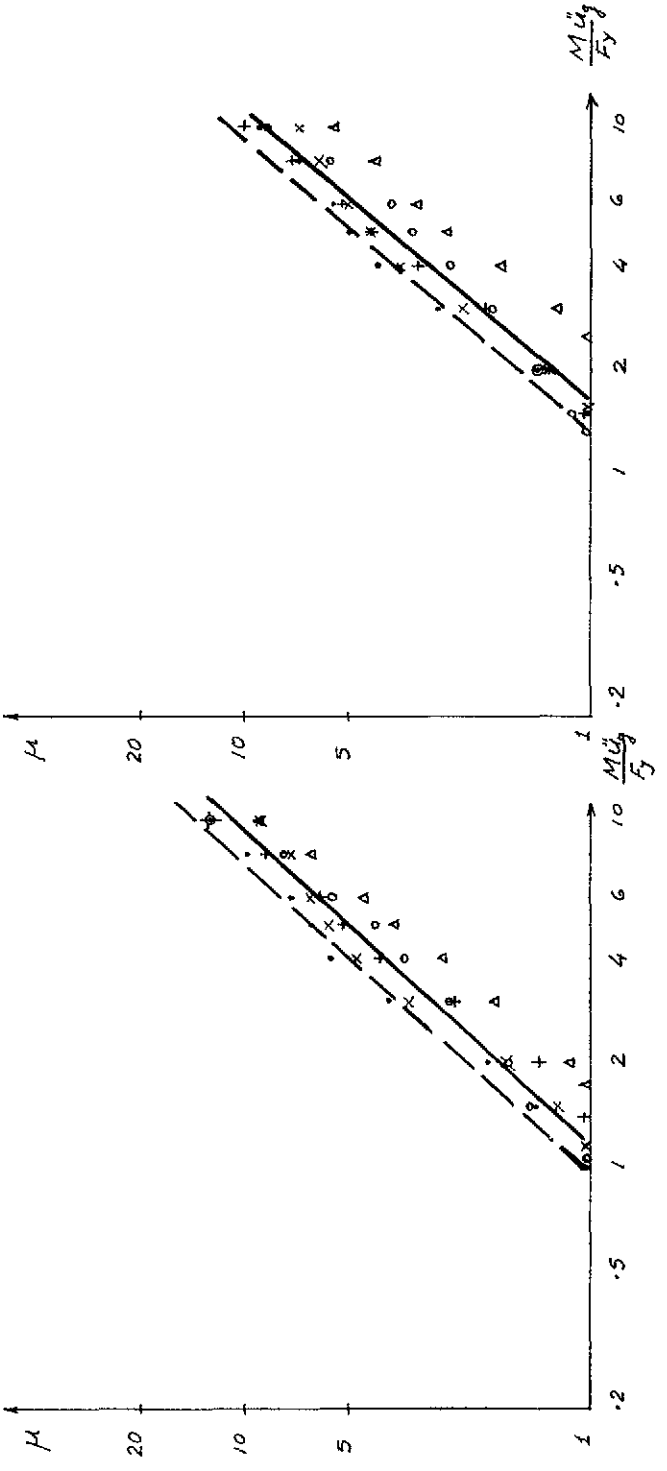
μ
20
10
5
1
.2
.5
1
2
4
6
10
$\frac{M\ddot{u}_g}{F_y}$
β=10%
β=20%
STIFFNESS DEGRADING
T= 1sec

Figure 3-50

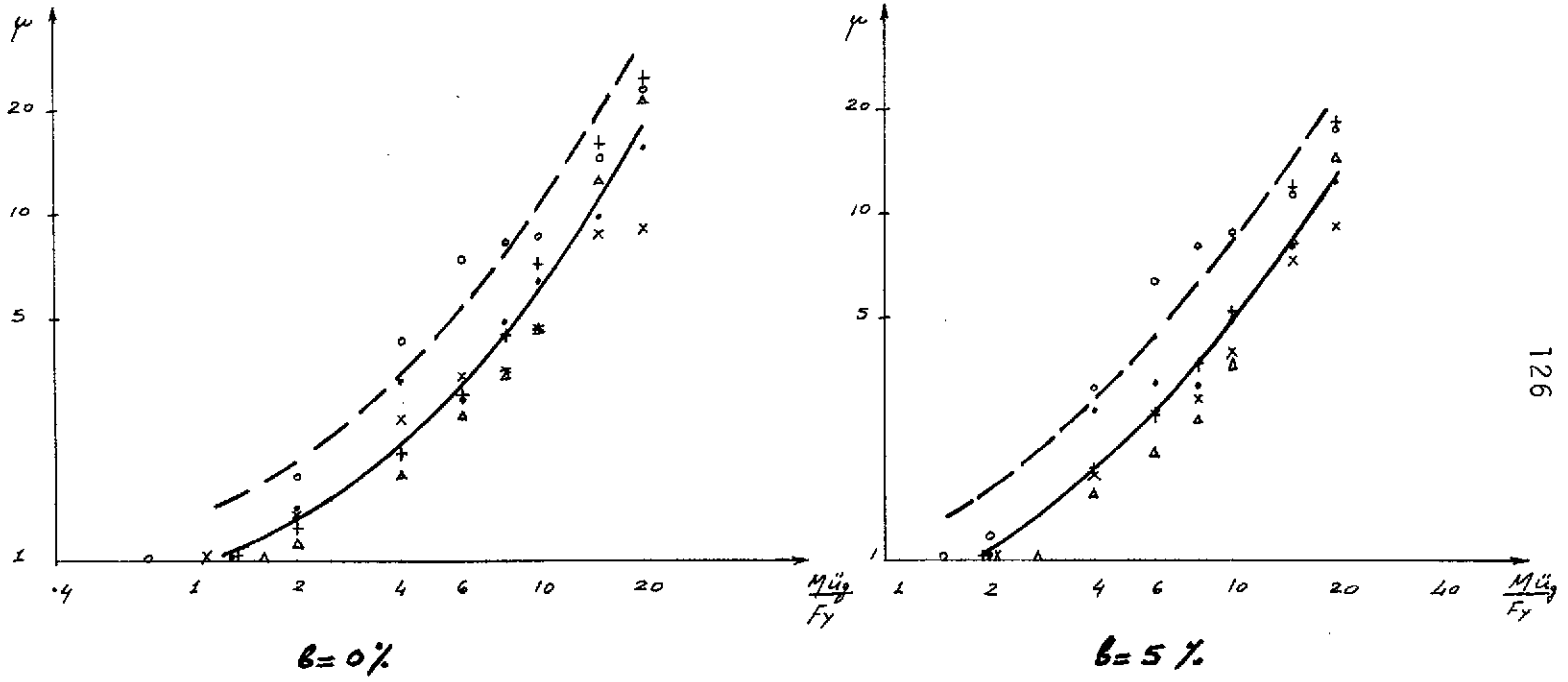
μ
20
10
5
1
.4
1
2
4
6
10
20
Müg/Fy
b= 0%
μ
20
10
5
1
1
2
4
6
10
20
40
Müg/Fy
b= 5 %
ELASTOPLASTIC
T= 2 sec

Figure 3-51

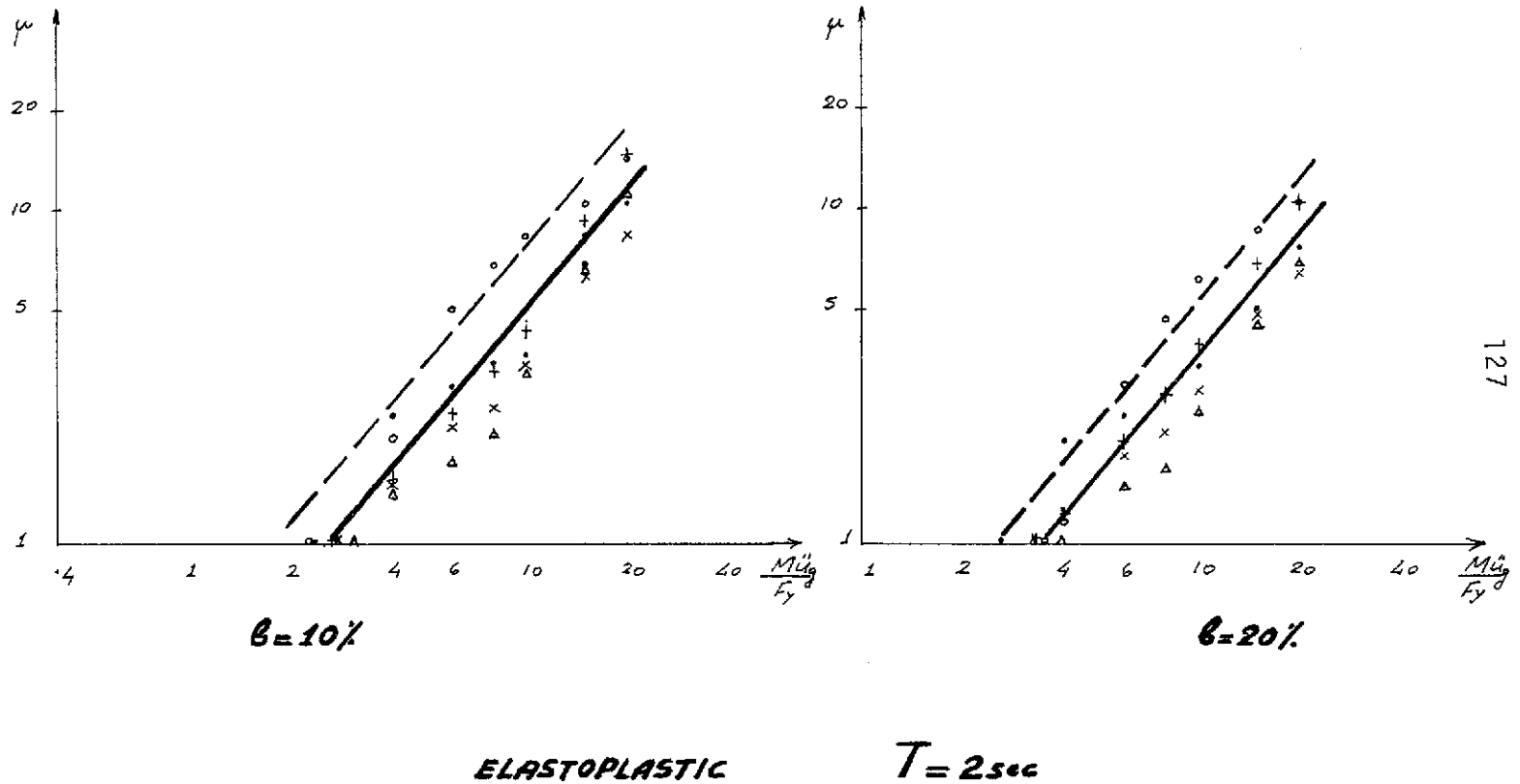

ELASTOPLASTIC $T = 2$ sec

Figure 3-52

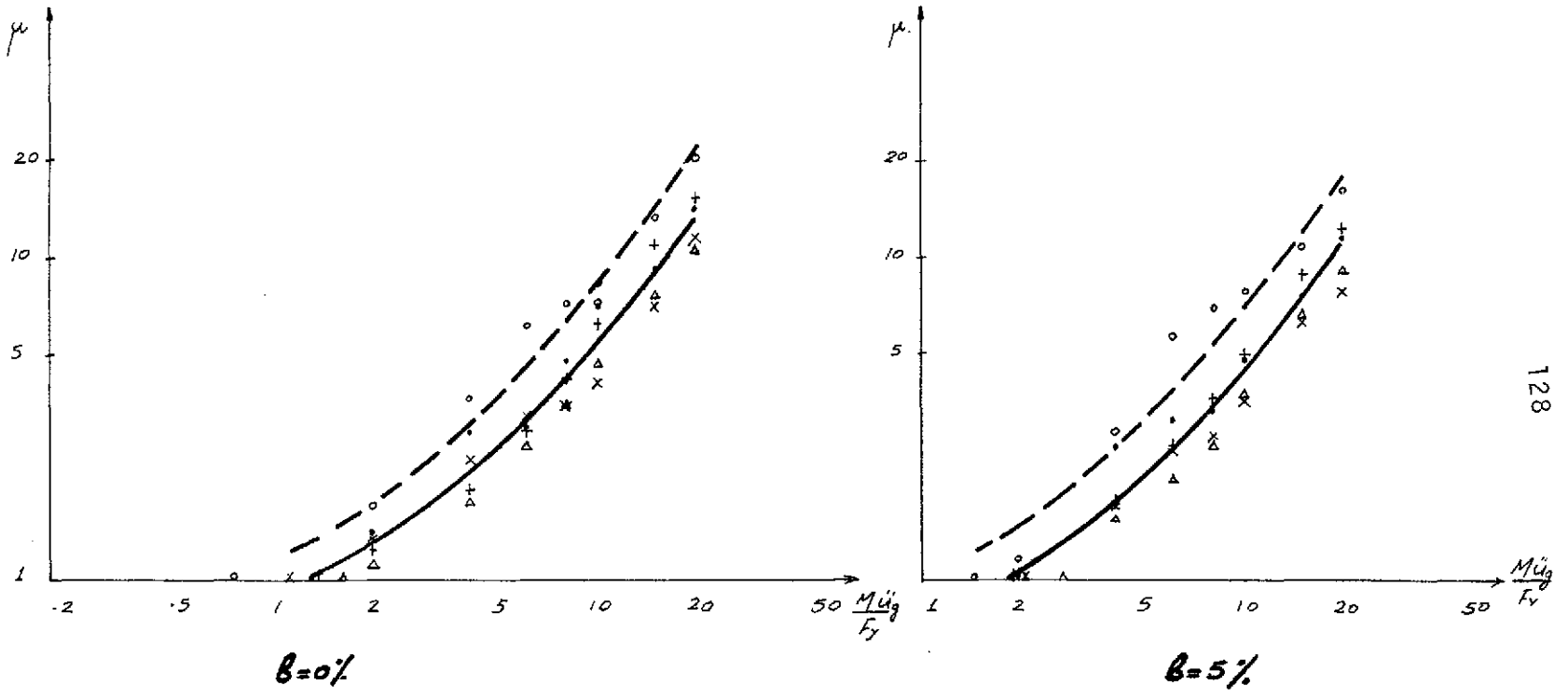

BILINEAR $T = 2\,sec$

Figure 3-53

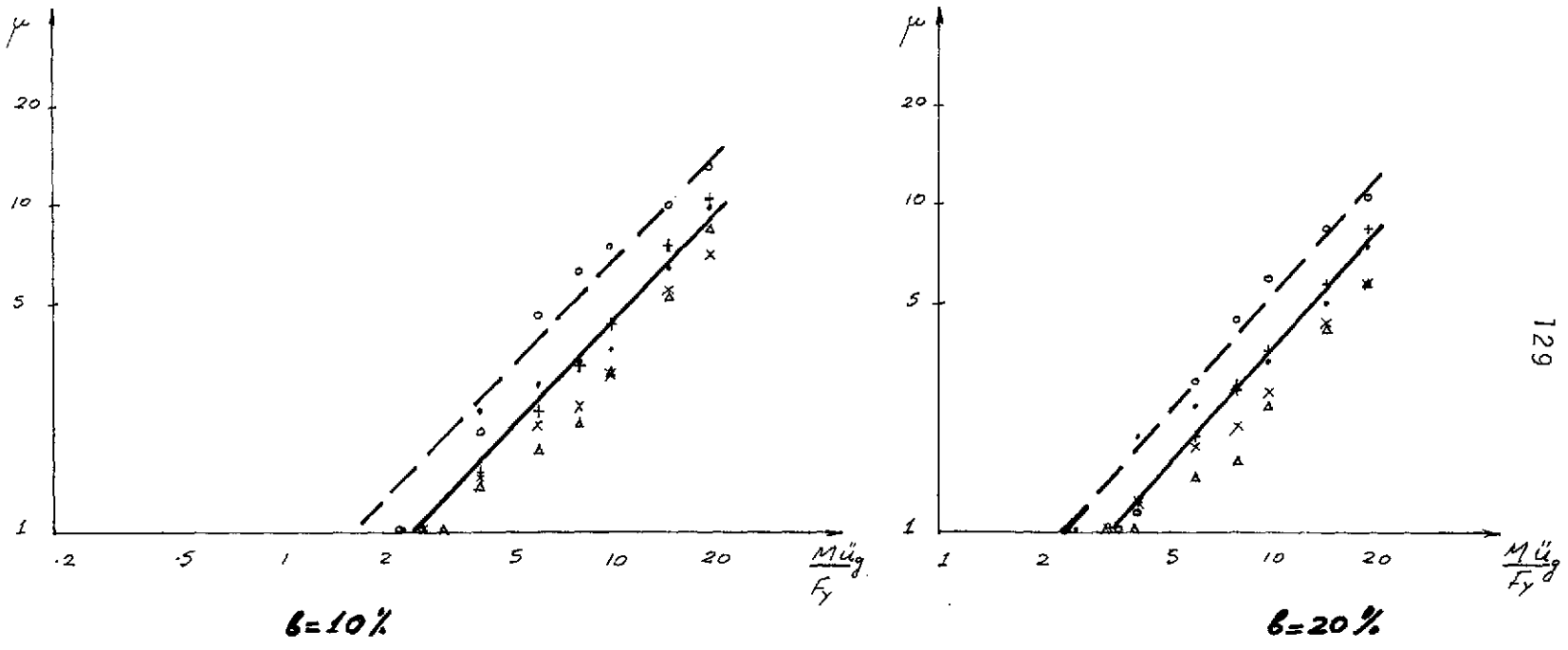

BILINEAR $T = 2$ sec

Figure 3-54

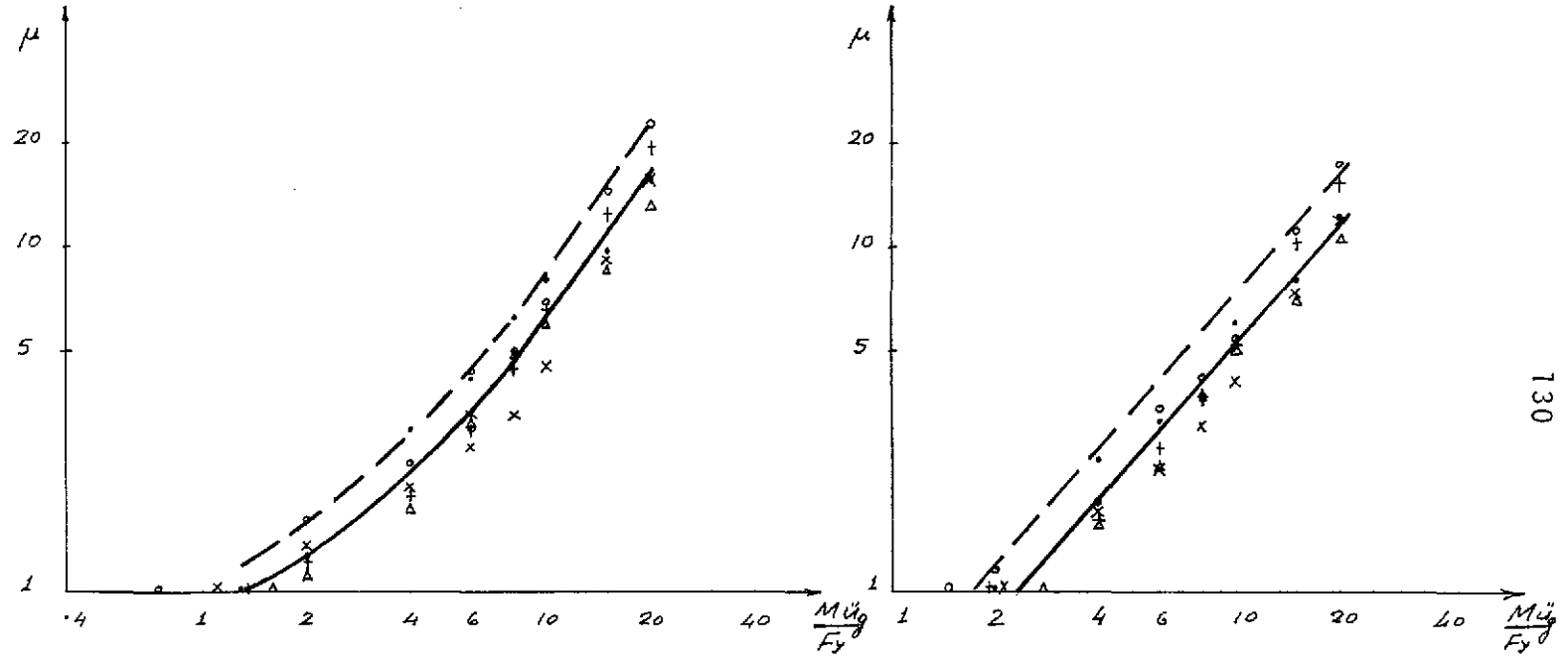
μ
20
10
5
1
·4
1
2
4
6
10
20
40
Müg/Fy
β = 0%
μ
20
10
5
1
1
2
4
6
10
20
40
Müg/Fy
β = 5%
STIFFNESS DEGRADING
T = 2 sec

Figure 3-55

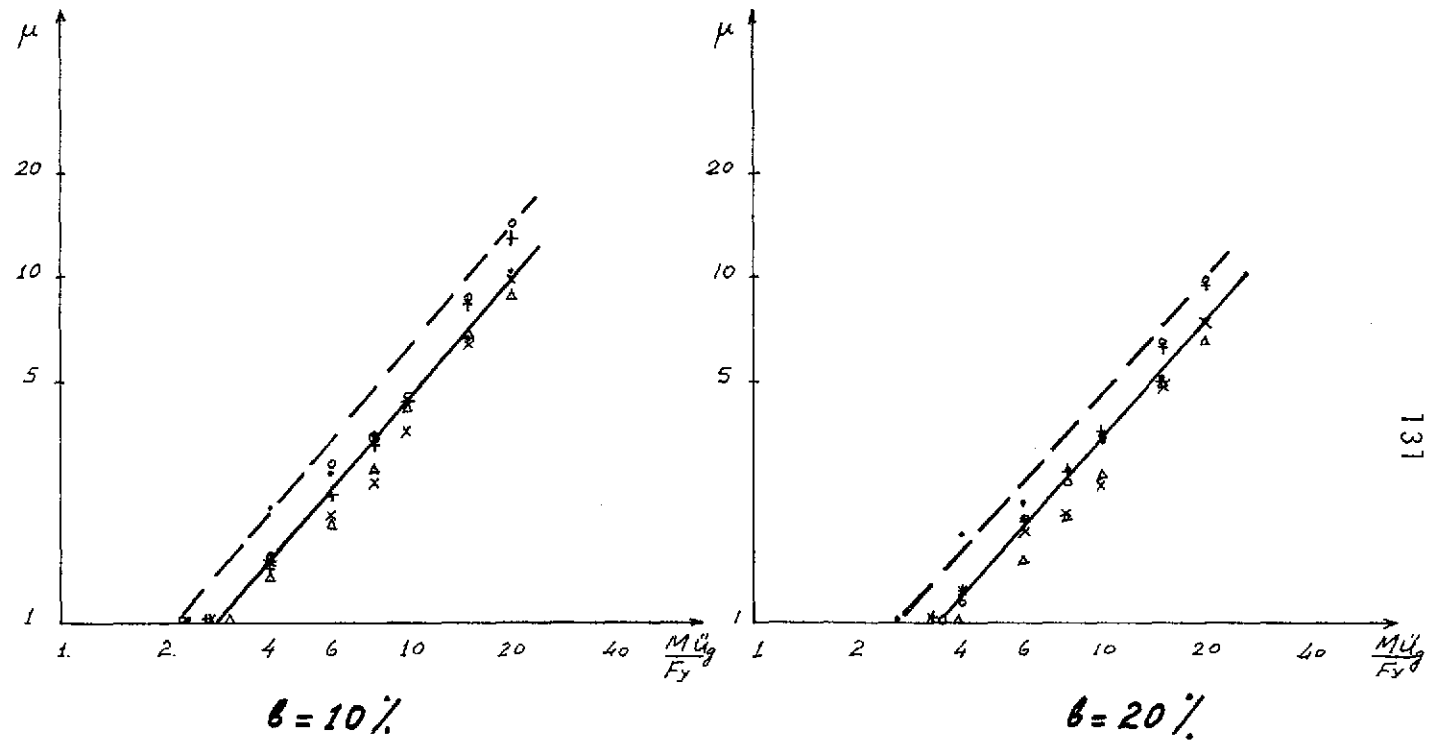
μ
20
10
5
1
1.
2.
4
6
10
20
40
Mü_g / Fy
β = 10 %
μ
20
10
5
1
1
2
4
6
10
20
40
Mü_g / Fy
β = 20 %
STIFFNESS DEGRADING
T = 2 sec

Figure 3-56

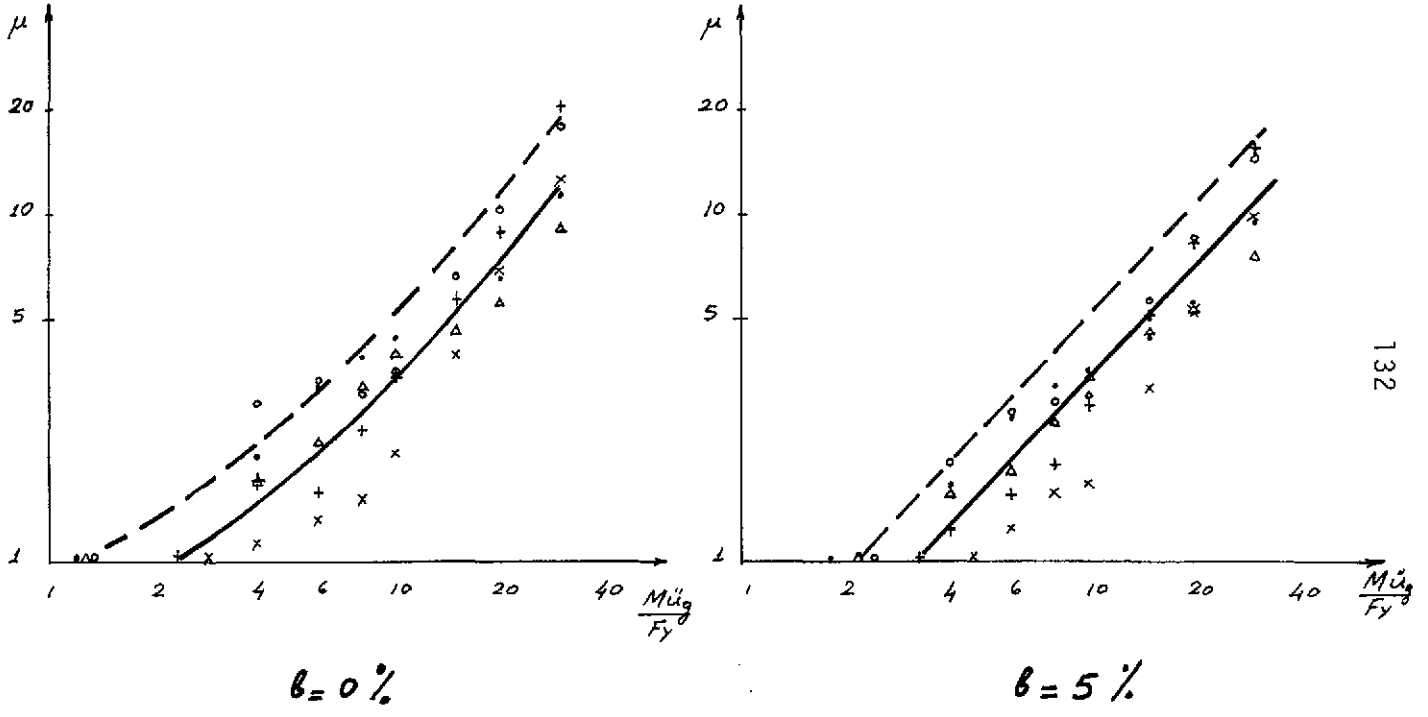

Figure 3-57

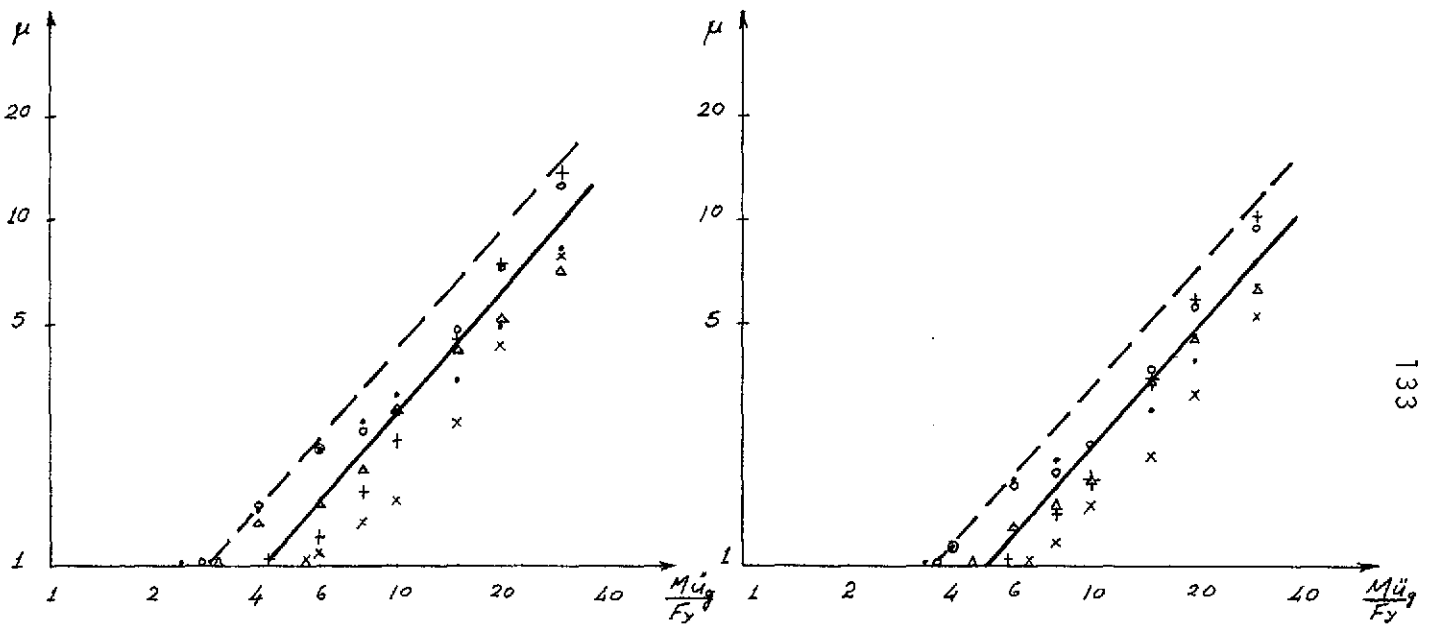

Figure 3-58

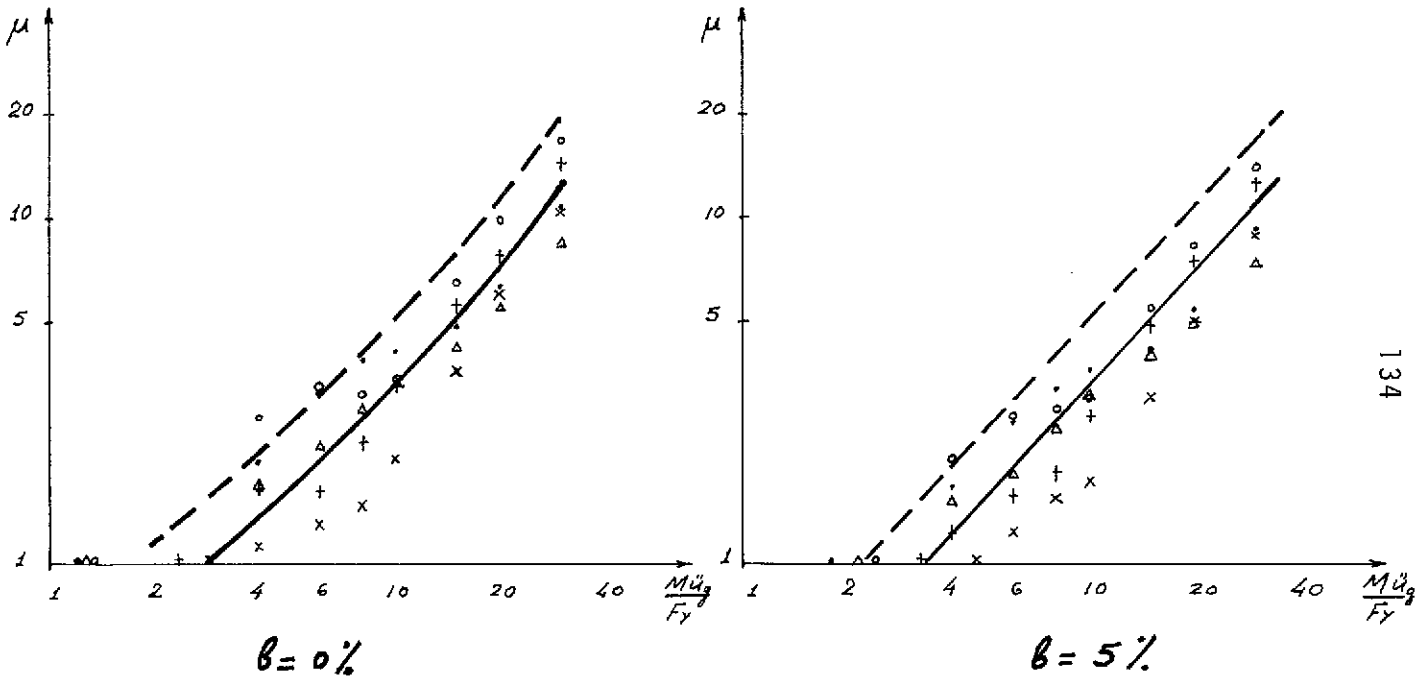

BILINEAR $T = 3$ sec

Figure 3-59

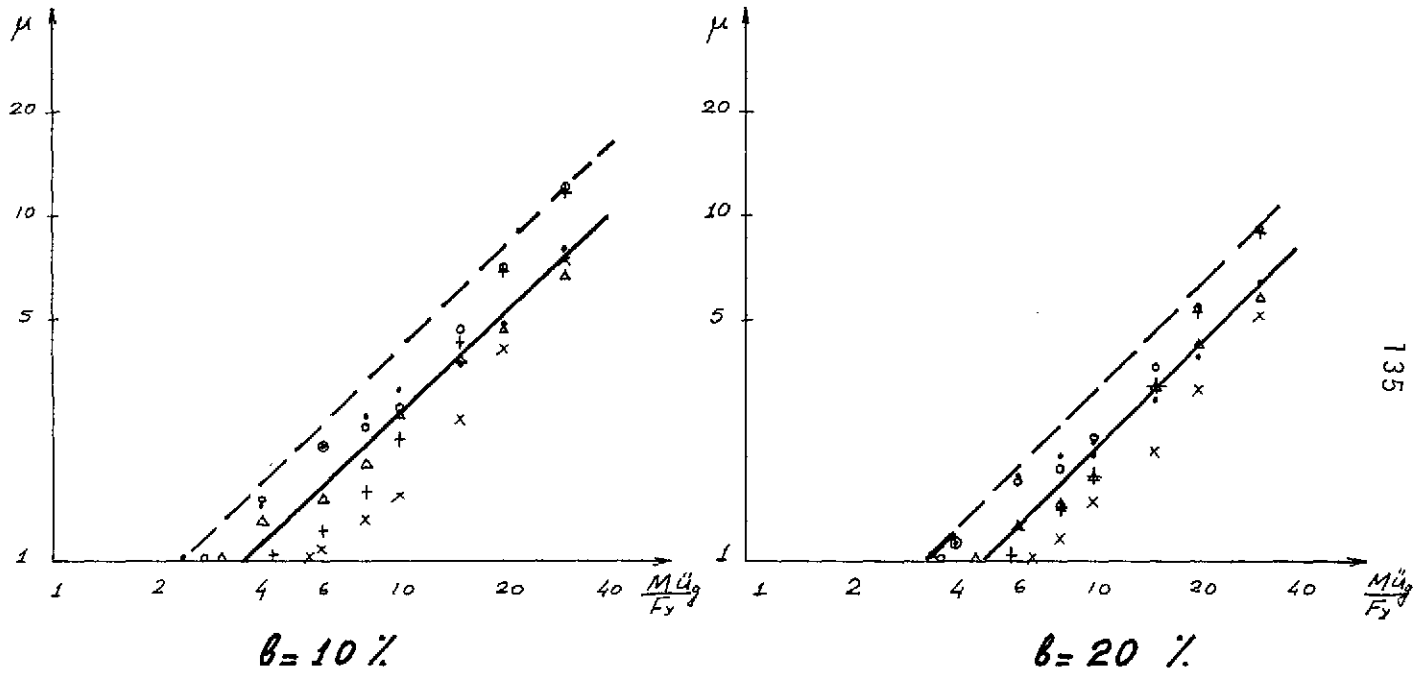

BILINEAR T=3 sec

Figure 3-60

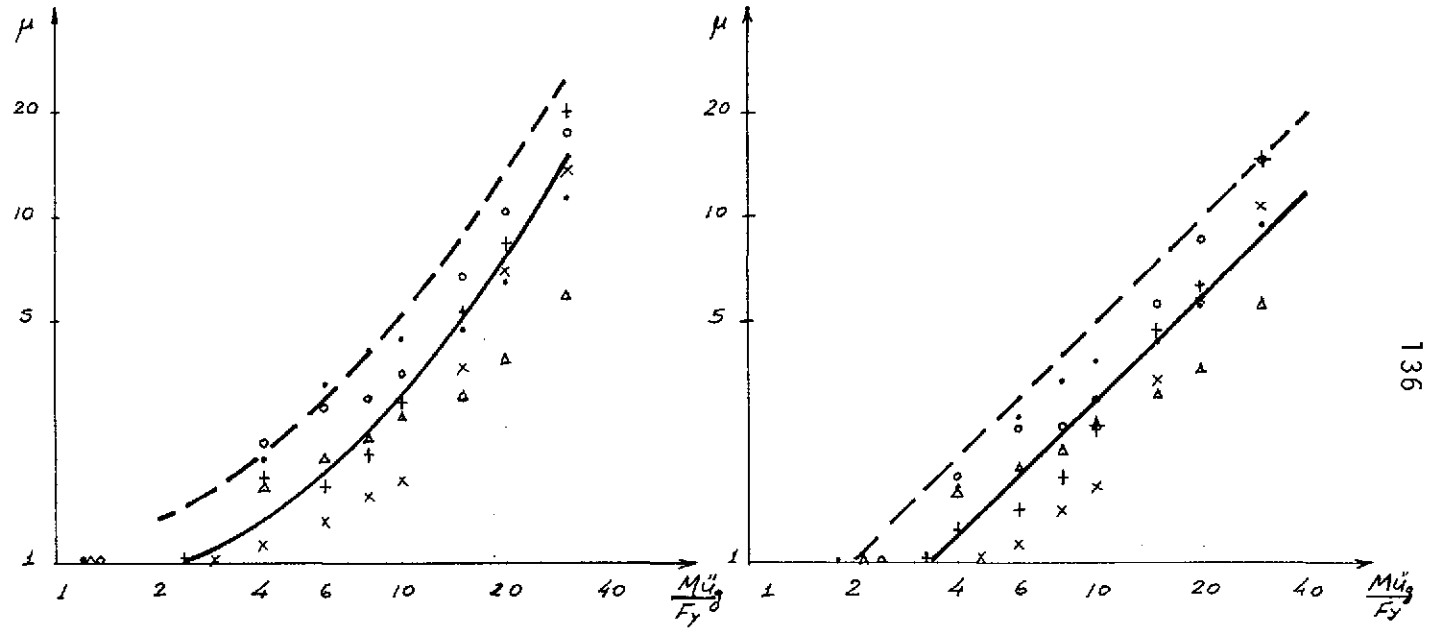

Figure 3-61

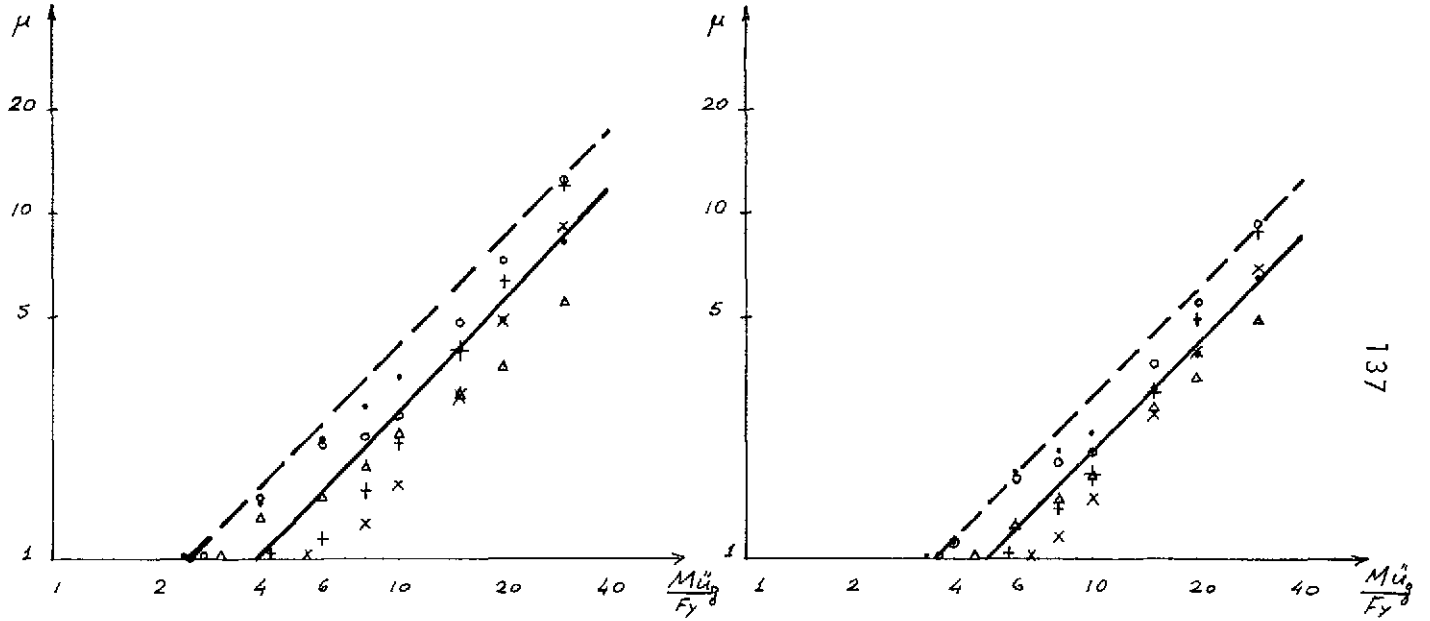

β = 10 %

β = 20 %

STIFFNESS DEGRADING

T = 3 sec

Figure 3-62

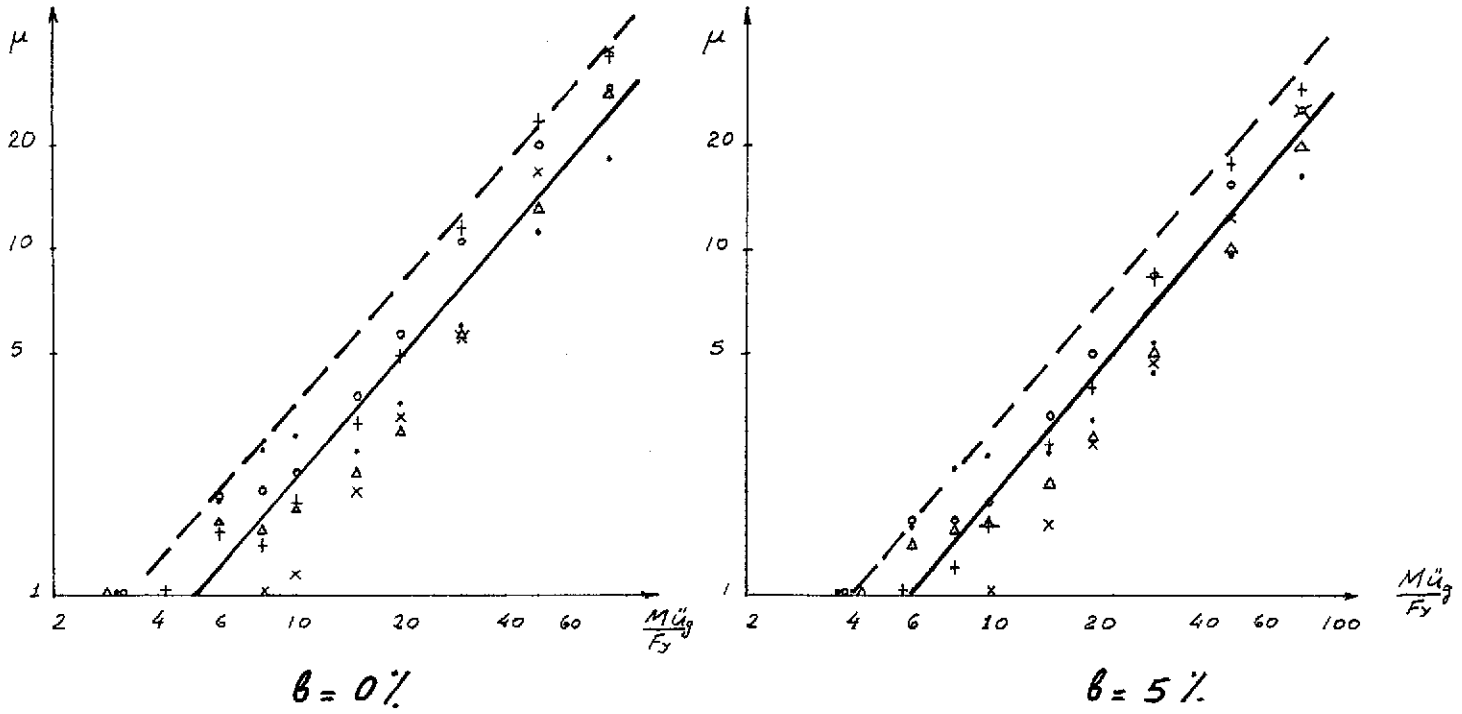

Figure 3-63

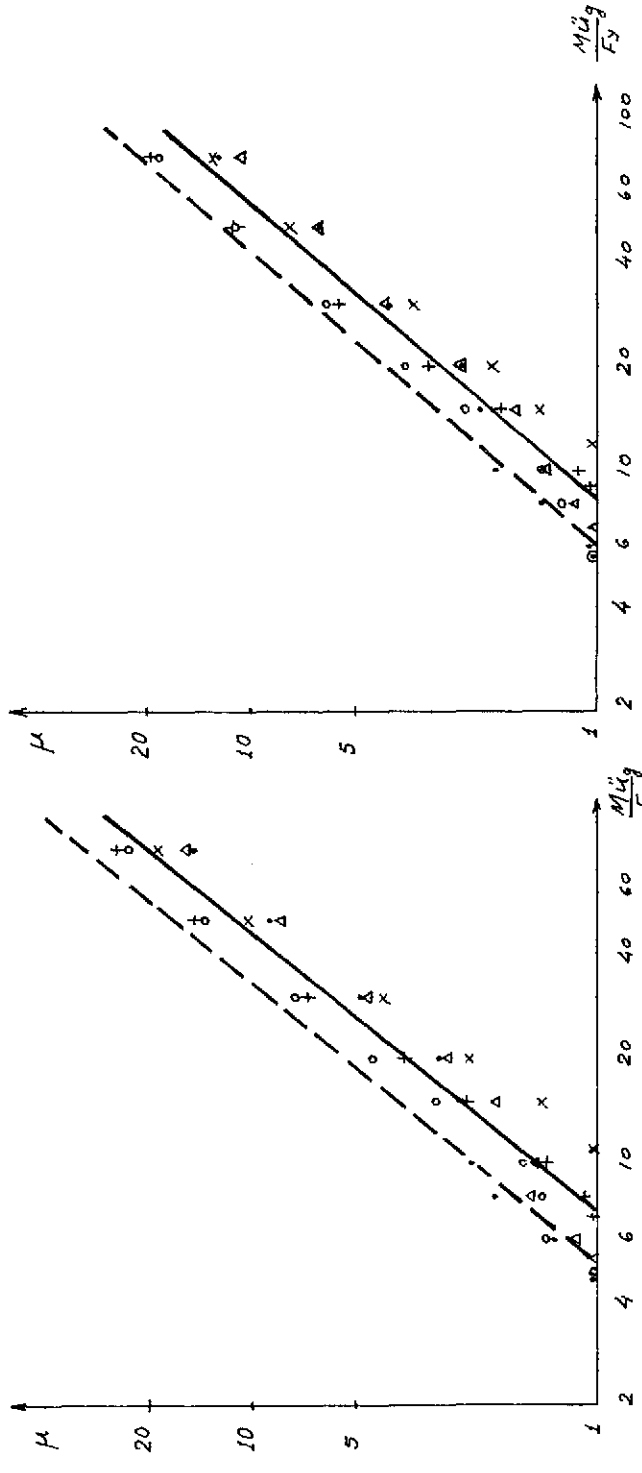
μ
20
10
5
1
2
4
6
10
20
40
60
100
$\frac{M\ddot{u}_g}{F_y}$
β=10%
β=20%
ELASTOPLASTIC
T=4 sec

Figure 3-64

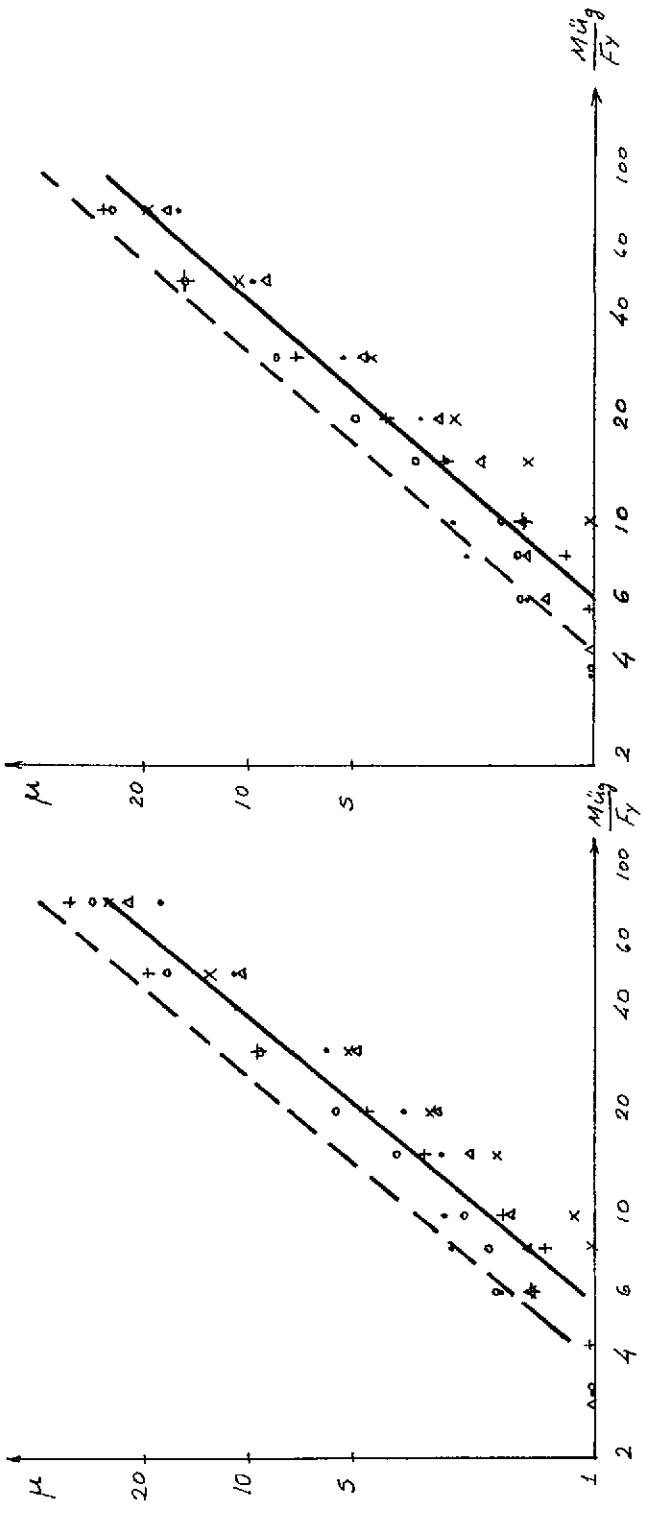
μ
20
10
5
1
2
4
6
10
20
40
60
100
$\frac{M\ddot{u}_g}{F_y}$
θ= 0%
θ= 5%
BILINEAR
T=4 sec

Figure 3-65

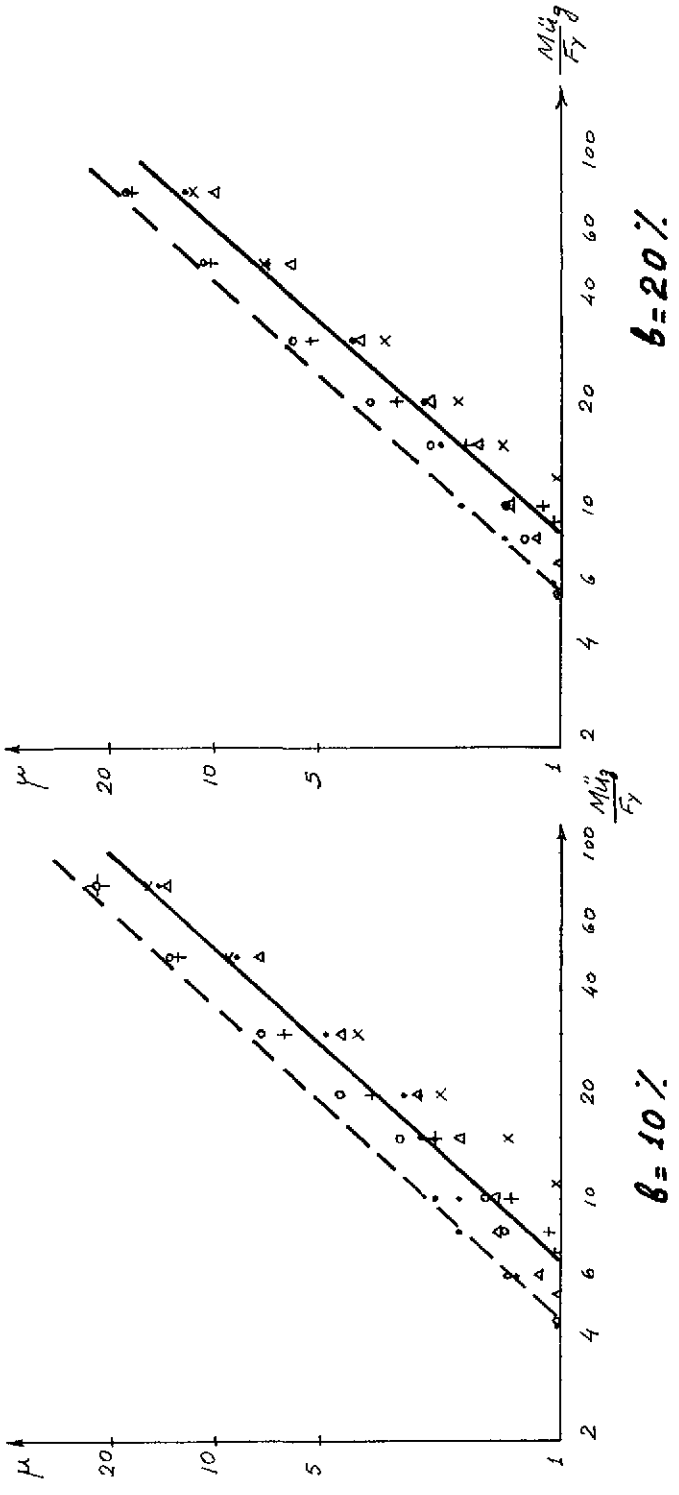
μ
20
10
5
1
2
4
6
10
20
40
60
100
$\frac{M_{UB}}{F_Y}$
$\frac{M_{UB}}{F_Y g}$
B=10%
B=20%
BILINEAR
T=4 SEC

Figure 3-66

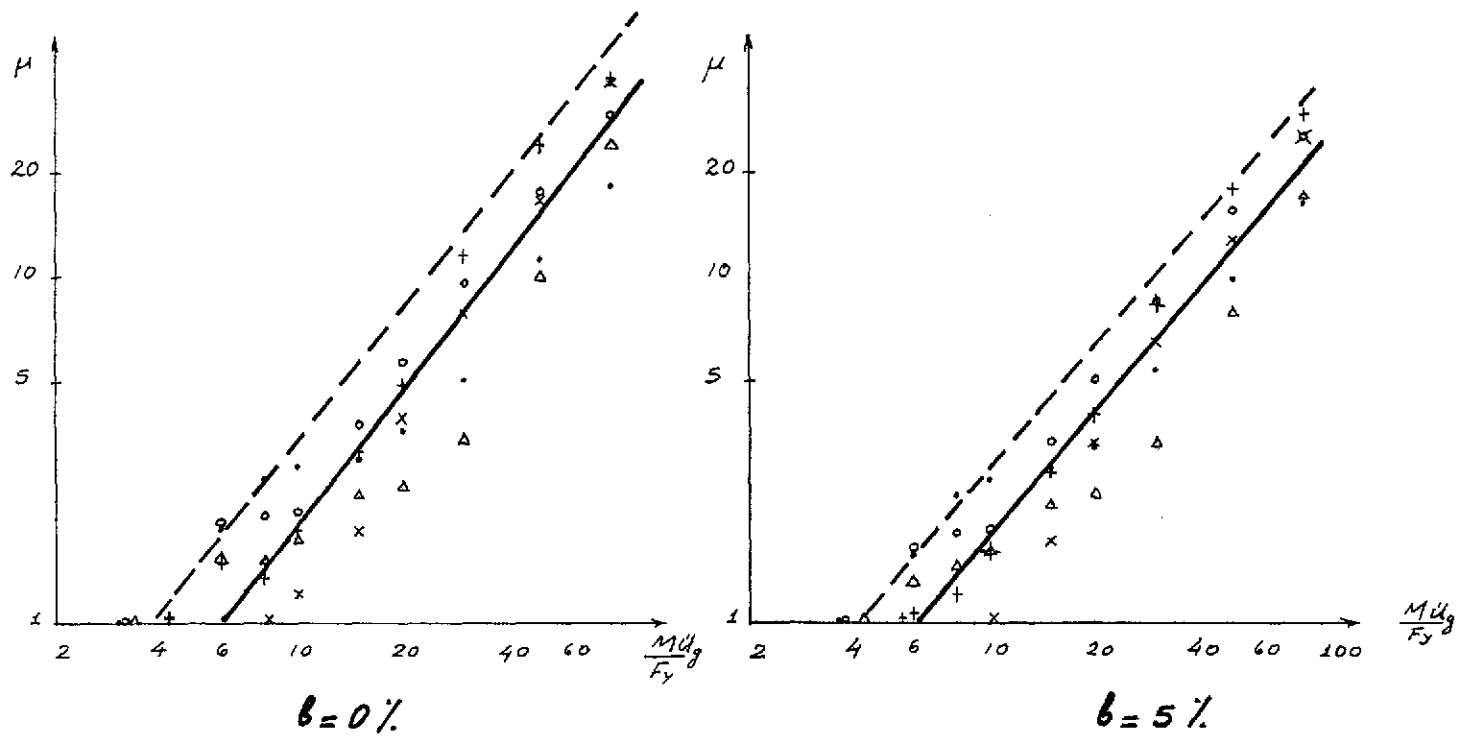

STIFFNESS DEGRADING T = 4 sec

Figure 3-67

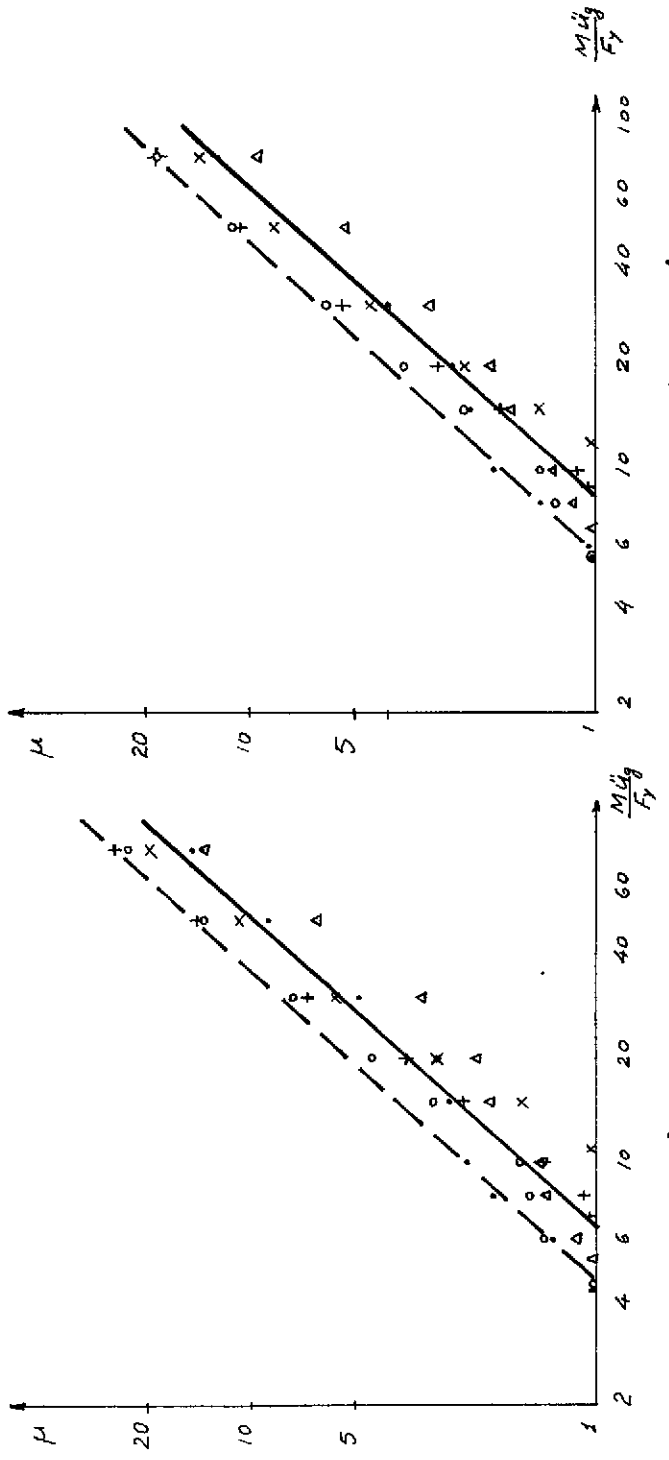
STIFFNESS DEGRADING
T = 4 sec
β = 20 %
β = 10 %
μ
20
10
5
1
2
4
6
10
20
40
60
100
$\frac{M\ddot{u}_g}{F_y}$

Figure 3-68

Table 3-4 gives a range of values for λ for various combinations of a and k.

$\lambda = .32/ak$				
k	a=1.5	a=2	a=3	a=5
.67	.320	.24	.160	.095
.80	.267	.20	.133	.080
1.00	.214	.16	.108	.064
1.33	.160	.12	.080	.048

Table 3-4 Values of λ

Selecting values of viscous damping β and ductility values μ, we can enter figures 3-27 - 3-68 and determine corresponding values of $m\ddot{u}_g/F_t$ for any set of natural periods. Then by using 3.7 with some appropriate λ, we can compute c and plot it as a function of T. This was done for the case that a = 2, k = .67, .80, 1, 1.33, β = 5% and an elastoplastic system. Values of $F_y/m\ddot{u}_g$ are tabulated in Table 3-5 for 5 values of μ and 7 values of T.

	β = 5%				
	$F_y/m\ddot{u}_g$				
T	μ=1	μ=2	μ=3	μ=4	μ=5
.10	1.470	1.180	1.000	.930	.860
.25	2.000	1.300	1.000	.860	.770
.50	2.000	1.000	.625	.475	.400
1.00	1.040	.590	.417	.333	.270
2.00	.500	.222	.150	.118	.100
3.00	.285	.167	.111	.083	.068
4.00	.167	.095	.067	.053	.044

Table 3-5 Values of $F_y/m\ddot{u}_g$

The results are plotted on log-log paper in figures 3-69, 70, 71. In all the cases the code formula has also been plotted. In the case of k = .67 (ductile frames), straight-line fits were performed and the appropriate laws are summarized here:

$\mu = 1 \qquad c = \frac{.25}{T^{1.2}}, \qquad c_{max} = .5 \quad \text{for} \quad T \leq .5 \text{ sec.}$

$\mu = 2 \qquad c = \frac{.11}{T}, \qquad c_{max} = .28 \quad \text{for} \quad T \leq .4 \text{ sec.}$

$\mu = 3 \qquad c = \frac{.076}{T}, \qquad c_{max} = .24 \quad \text{for} \quad T \leq .3 \text{ sec.}$

$\mu = 4 \qquad c = \frac{.06}{T}, \qquad c_{max} = .21 \quad \text{for} \quad T \leq .28 \text{ sec.}$

$\mu = 5 \qquad c = \frac{.05}{T}, \qquad c_{max} = .2 \quad \text{for} \quad T \leq .25 \text{ sec.}$

As it was expected, the numbers show that for one-degree-of-freedom systems with a = 2, the U.B.C. would be unconservative in the short period range and conservative for long periods.

All the above shows one way by which one could obtain reasonable values of the base shear coefficient for prespecified ductility levels. This kind of study could be used to determine laws of the form 3.5, which would allow the designer for more combinations of strength and ductilities. Of course, before one adopts such a law to include it in a code, he should perform more studies: namely, for all possible values of μ and percentages of critical damping. The effect of gravity should also be investigated mainly in the long period range where the new coefficients become smaller than the ones currently in use. It is believed, however, that this is not a problem, as the following thinking suggests. As it was mentioned earlier,

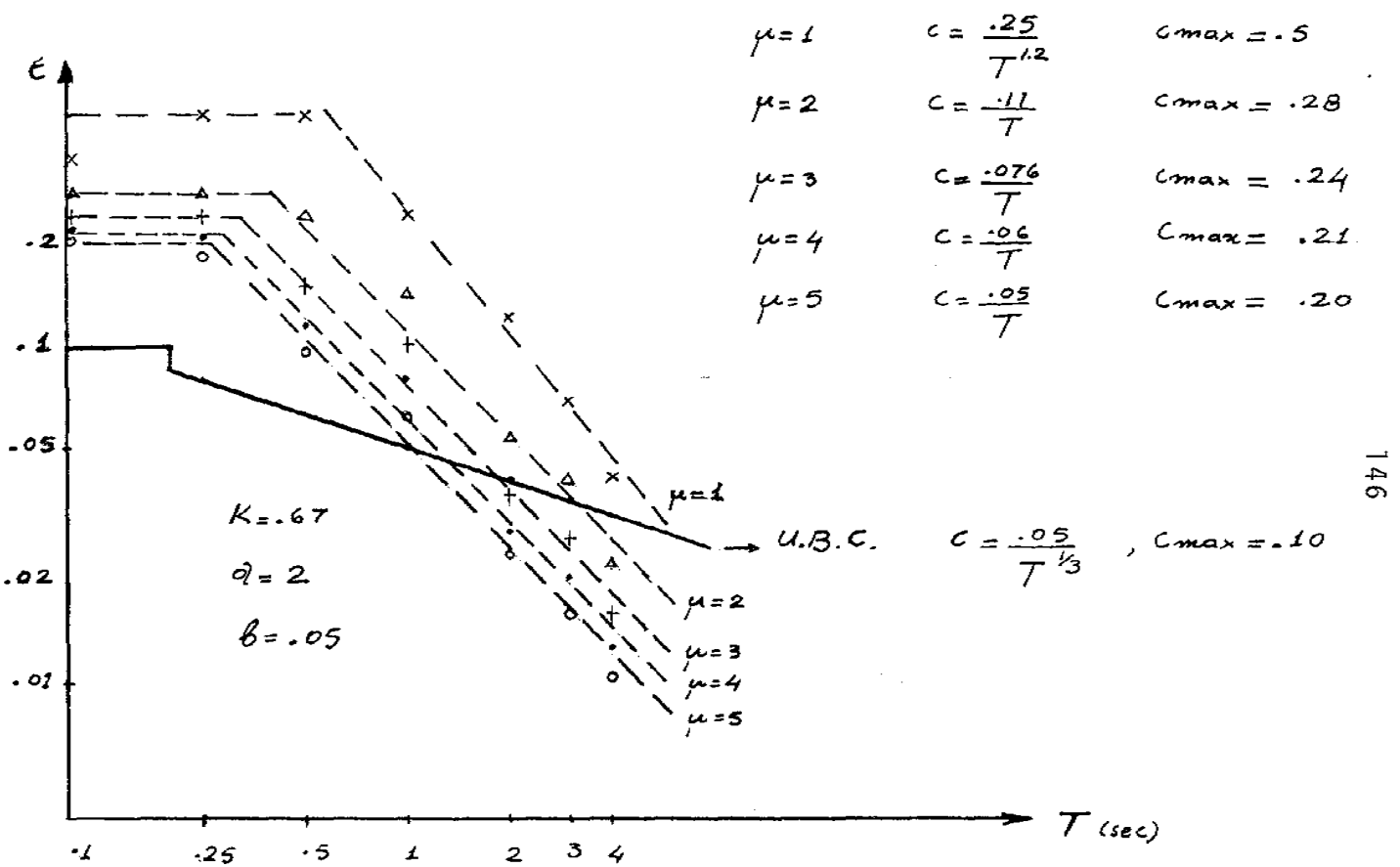
μ=1 C = .25/T^1.2 Cmax = .5
μ=2 C = .11/T Cmax = .28
μ=3 C = .076/T Cmax = .24
μ=4 C = .06/T Cmax = .21
μ=5 C = .05/T Cmax = .20
C
.2
.1
.05
.02
.01
K=.67
q=2
β=.05
μ=1
U.B.C. C = .05/T^1/3 , Cmax = .10
μ=2
μ=3
μ=4
μ=5
T (sec)
.1
.25
.5
1
2
3
4

Figure 3-69

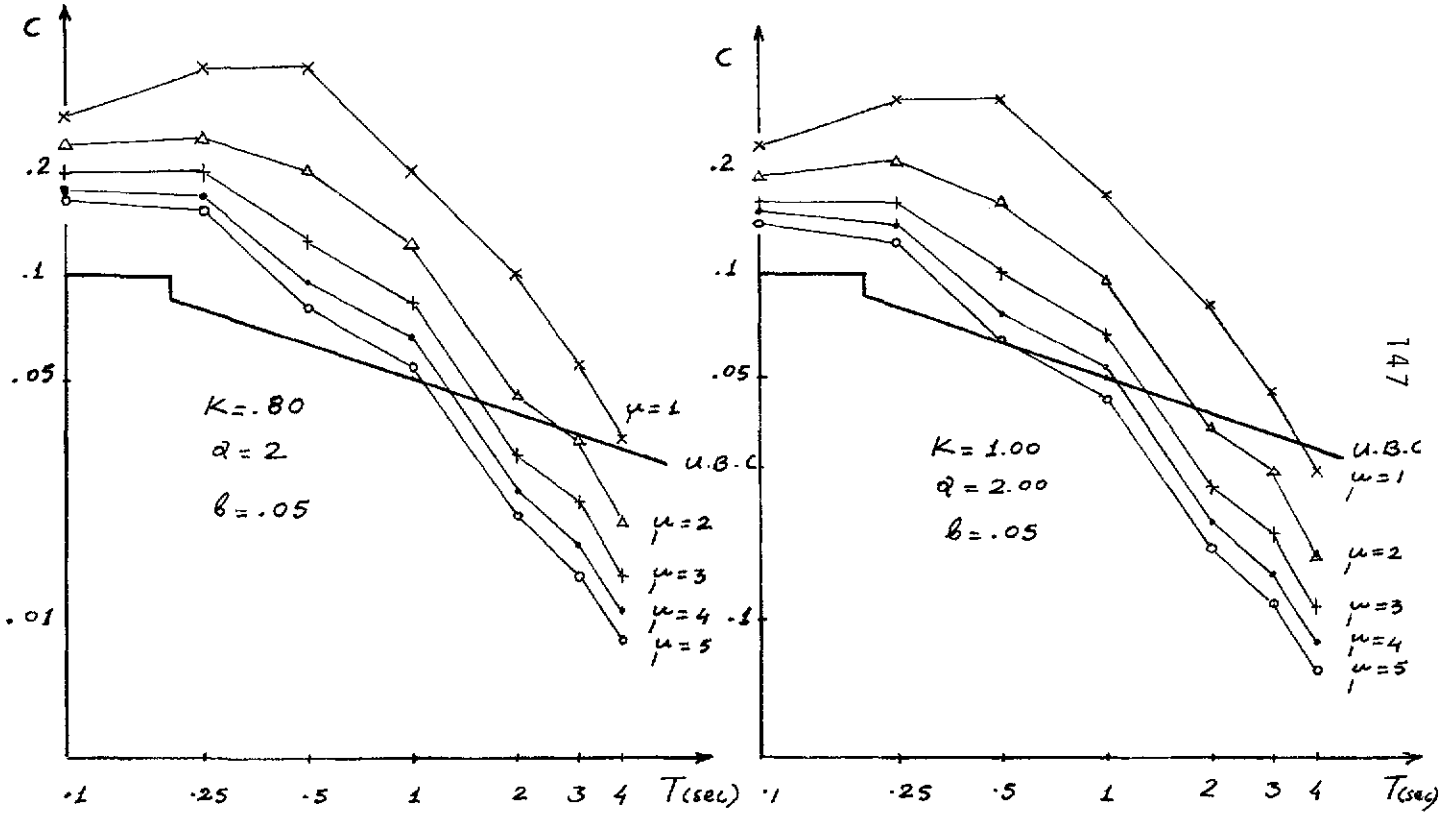
C
.2
.1
.05
.01
K=.80
Q=2
b=.05
μ=1
U.B.C
μ=2
μ=3
μ=4
μ=5
.1
.25
.5
1
2
3
4
T(sec)
C
.2
.1
.05
.1
K=1.00
Q=2.00
b=.05
U.B.C
ω=1
ω=2
ω=3
ω=4
ω=5
.1
.25
.5
1
2
3
4
T(sec)

Figure 3-70

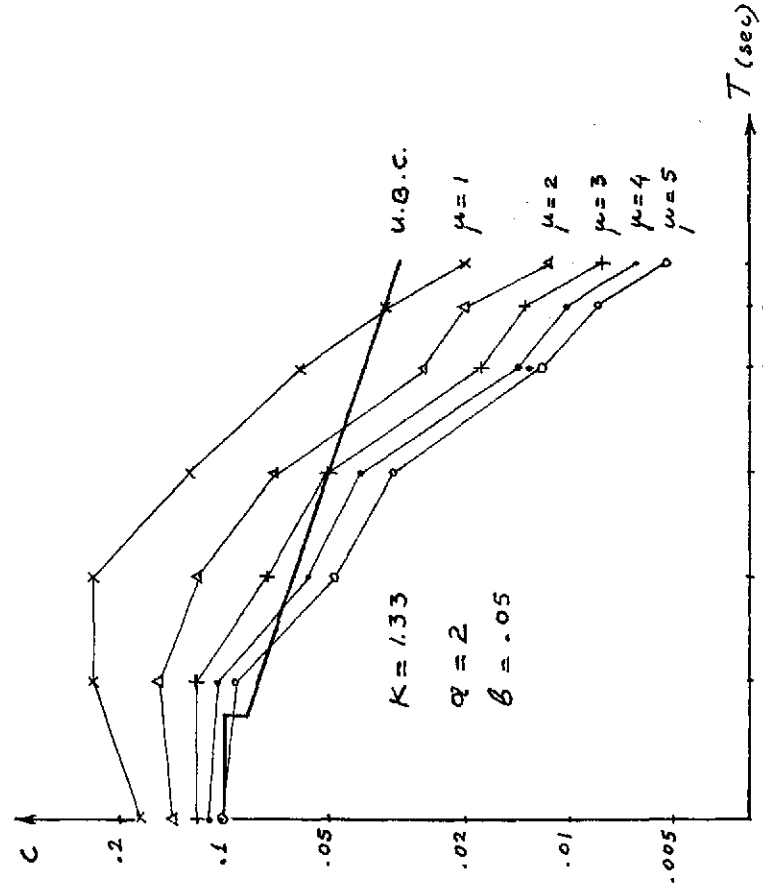

Figure 3-71

the maximum deformations of a system in the long period range remain relatively constant (approximately equal to the elastic) independent of the amount of yielding. Then even if we reduce the base shear coefficient and the structure becomes relatively weaker, the effect of gravity forces which is a function of the displacements will not change significantly.

As a final point in this paragraph, comparisons will be made between ductility factors obtained for multistory frames and numbers obtained by using the curves of the previous pages. Clough and Benuska (7) obtained ductility factors for frames of different periods. They have designed these frames following a code approach similar to the one used to derive the curves of the previous pages. One of their conclusions is that the columns remain elastic except for the ones in the top one or two stories. The girders yield and their ductility factors vary with the height. The variation is irregular and has a shape as shown below (figure 3-72).

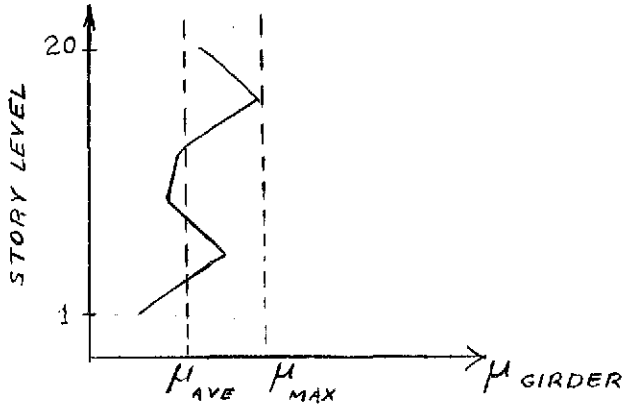

Figure 3-72 Ductility in Story Level

Values of $\mu_{ave.}$ and μ_{max} were estimated by drawing two vertical lines as shown in figure 3-72. These two values are compared with values obtained from figures 3-18 through 3-23 of this chapter. The comparisons are summarized below.

β = 0%				
	Clough (7) Fig. 2-22		Present Work Fig. 3-20	
T	$\mu_{ave.}$	$\mu_{max.}$	$\mu_{ave.}$	$\mu_{max.}$
1.6	4	7	4	6
2.2	3	6	3	4.8
2.8	2.5	5.5	2.4	3.7

*β_1=.10, β_2=.041, β_3=.025			β = .10		β = .05	
Clough(7) Fig. 2-78			Fig. 3-21		Fig. 3-20	
T	$\mu_{ave.}$	$\mu_{max.}$	$\mu_{ave.}$	$\mu_{max.}$	$\mu_{ave.}$	$\mu_{max.}$
.6	7-8	11.0	6.8	10.0	7.5	11.5
1.0	~ 5.0	7.5	4.5	6.5	5.0	7.7
1.6	~ 3.0	5.6	3.0	4.4	3.5	5.5
2.2	2.4	5.0	2.2	3.5	2.8	4.4
2.8	2.0	4.0	1.8	2.7	3.3	3.5

Average for the Two Values Of Damping	
$\mu_{ave.}$	$\mu_{max.}$
7.15	10.75
4.75	7.10
3.25	5.00
2.50	4.00
2.05	3.10

* These are the values of damping in the first three modes.

Newmark (72) estimated the required ductility for a building with a period of 2.3 seconds to be about 2. Our figures for β = 10% give 2.1.

A 13-story building, whose analysis will be described in Chapter 5, had for β = 0.02: $\mu_{ave.}$ = 1.3 and $\mu_{max.}$ = 2.87. The

natural period of the building is 4.2 sec. The corresponding numbers from the curves are: $\mu_{ave.} = 1.3$; $\mu_{max.} = 2.85$.

As a final comparison we take figure 2.47 from (7), where Clough studies the effect of intensity on ductility. To obtain corresponding numbers we must make use of both sets of curves given in this chapter.

Clough $\beta = .10$ $T = 2.2$		Present Work $T = 2.2$		
		$\beta = .05$	$\beta = .10$	Average $\beta = .05$ & $.10$
Intens.	$\mu_{ave.}$	$\mu_{ave.}$	$\mu_{ave.}$	$\mu_{ave.}$
.7	1.8	2.0	1.6	1.8
1.0	2.4	2.8	2.3	2.5
1.3	3.2	3.8	3.2	3.5

From Fig. 3-20: $\beta = 5\%$ $T = 2.2 \rightarrow \mu_{ave.} = 2.8$

From Fig. 3.21: $\beta = 10\%$ $T = 2.2 \rightarrow \mu_{ave.} = 2.3$

$\beta = 5\%$

Fig. 3-53 $T = 2$ $\mu_{ave.} = 2.8 \rightarrow \frac{M\ddot{u}_g}{F_y} = 6.6$

Fig. 3-59 $T = 3$ $\mu_{ave.} = 2.8 \rightarrow \frac{M\ddot{u}_g}{F_y} = 8.6$

Interpolate for $T = 2.2$ and get: $\frac{M\ddot{u}_g}{F_y} = 7$

$\beta = 10\%$

$.7\ (\frac{M\ddot{u}_g}{F_y}) = 4.9$ $T=2$ $\rightarrow \mu_{ave.} = 2.1$ | $T = 3$ $\mu_{ave.} = 1.55$

$1.3\ (\frac{M\ddot{u}_g}{F_y}) = 9.2$ $T=2$ $\rightarrow \mu_{ave.} = 4.0$ | $T = 3$ $\mu_{ave.} = 3.00$

Interpolate for $T = 2.2$

and find for $T = 2.2$ and $\beta = 5\%$ and Intensity $\begin{cases} .7 \rightarrow \mu_{ave.} = 2 \\ 1.3 \rightarrow \mu_{ave.} = 3.8 \end{cases}$

$$\beta = 10\% \begin{cases} \text{Fig. 3-54} \quad T = 2 \quad \mu_{ave.} = 2.3 \rightarrow \frac{M\ddot{u}_g}{F_y} = 5.5 \\ \text{Fig. 3-60} \quad T = 3 \quad \mu_{ave.} = 2.3 \rightarrow \frac{M\ddot{u}_g}{F_y} = 8.5 \end{cases} \text{ Interpolate for } T = 2.2 \text{ and get: } \frac{M\ddot{u}_g}{F_y} = 6.10$$

$$\beta = 10\% \begin{cases} .7\left(\frac{M\ddot{u}_g}{F_y}\right) = 4.3 \\ 1.3\left(\frac{M\ddot{u}_g}{F_y}\right) = 8 \end{cases} \begin{matrix} T=2 \\ \end{matrix} \begin{cases} \rightarrow \mu_{ave.} = 1.70 \\ \rightarrow \mu_{ave.} = 3.5 \end{cases} \Bigg| \Bigg| \begin{matrix} T=3 \\ \end{matrix} \begin{cases} \rightarrow \mu_{ave.} = 1.2 \\ \rightarrow \mu_{ave.} = 2.2 \end{cases} \Bigg| \Bigg| \text{Interpolate for } T = 2.2$$

and find for $T = 2.2$, $\beta = 10\%$ and intensity $\begin{cases} .7 \rightarrow \mu_{ave.} = 1.6 \\ 1.3 \rightarrow \mu_{ave.} = 3.20 \end{cases}$

The above comparisons indicate very good agreement between the numbers obtained from inelastic analysis of actual multistory frames and the curves derived in this chapter for 1 D.O.F. systems. This suggests that the curves could possibly be used for multistory frames to give average and maximum levels of required ductility. More studies and comparisons are needed, however, to substantiate this claim. As a final comment, it should always be kept in mind that the nature of the problem is such that one should be satisfied with levels of ductilities and average numbers, rather than with exact values carrying several digits after the decimal.

3.4 Effect of Gravity Loads

As of this time, our studies on the effect of gravity loads were inconclusive. As far as simple structures that can be modelled as

1 D.O.F. systems are concerned, one will have to assume natural periods between say 0.5 and 0.1 seconds. In this region it was found that even for ductility factors of the order of 10, gravity loads presented no problem. If we try, however, to extrapolate conclusions to more complicated actual structures, the main problem that we encounter is the problem of height: i.e., what is an appropriate height to use for the 1 D.O.F. In a multistory frame, the way gravity load acts is by introducing additional shears at each story level. In that respect it is the interstory height that becomes important. As far as overturning moments are concerned, however, these additional shears are multiplied with their distances from the ground. While Husid (68) makes it clear that his studies are not aimed towards actual 1 D.O.F. structures, it is not apparent to what kind of structure the heights of 5, 10, 20 and 30 feet he selected may correspond. If his studies were for 1 D.O.F. actual systems, then his parameter a_y should have been much greater than the one he used. It is our feeling that the effect of gravity loads should be studied only with an exact analysis of the multi-degree-of-freedom system rather than with the simpler 1 D.O.F.

CHAPTER 4

ANALYSIS OF MULTIDEGREE-OF-FREEDOM SYSTEMS

4.1 Introduction

One of the main purposes of this work was to develop a convenient mathematical model for the inelastic dynamic analysis of a certain class of buildings. On one hand, it was desired to include such effects as torsion, nonstructural elements, stiffness and/or strength degradation, etc., while on the other, considering mainly computational costs, it was decided to avoid the sophistication of treating each member in the structure individually as it is done in a regular stiffness analysis.

Clough and Benuska (7), Goel (8), Anderson (9), Latona (10) and Hanson and Fan (81) describe formulations for the inelastic dynamic analysis of plain frames. Vitielo (78) gives a formulation for the in-plane combination of bending elements (shear walls) with shear elements (frames). Velcov (79) performed inelastic analysis of a shear-type, symmetric building using elastoplastic and bilinear models for the resistances between floors. Jurukovski and Bickovski (80) give a formulation for the elastic dynamic response of shear buildings, accounting for torsion. Odaka et al. (84) have included rocking and swaying of the foundation in their formulation for the dynamics of shear buildings. Nigam and Housner (83) studied the elastic and inelastic response of simple structures for directions of the motion other than the principal ones, Shiga (97) dealt with elastic torsional vibrations, and Tadaki et al. (96) considered the

problem of inelastic torsional response.

In this chapter we will present the mathematical model, we will discuss the underlying assumptions and the method of solution, and we will describe the capabilities of the computer program developed for the analysis. Faced with the problem of choosing an appropriate numerical method for the step-by-step solution of the equations of motion, we compared several numerical methods and results of these comparisons will be given here. Finally, we will present a general formulation of the problem, extending it for the cases where gravity loads and soil flexibility are to be included in the analysis.

4.2 The Mathematical Model

The mathematical model used for this investigation is a combination of shear and bending springs, in any of the x, y directions, with masses lumped at the floor levels. The shear springs are intended for frames, in which axial deformation of the columns is not important (shear behavior) and the bending springs are intended for shear walls. We can have any number of shear and bending springs linked together in any direction on the floor plan.

The force-deformation characteristics of the shear springs could be any of those discussed in chapter 2, depending on the particular characteristics of the structure (elastoplastic, bilinear, trilinear, stiffness, and/or strength degrading). The bending springs (shear walls) are treated as an assembly of simple members

between floor slabs, with moment-curvature relation for each joint (at the slab level) given by a bilinear or stiffness degrading model. The floor slabs are considered rigid in their planes, so we have three degrees of freedom per floor: two translations and one rotation (Figure 4-1).

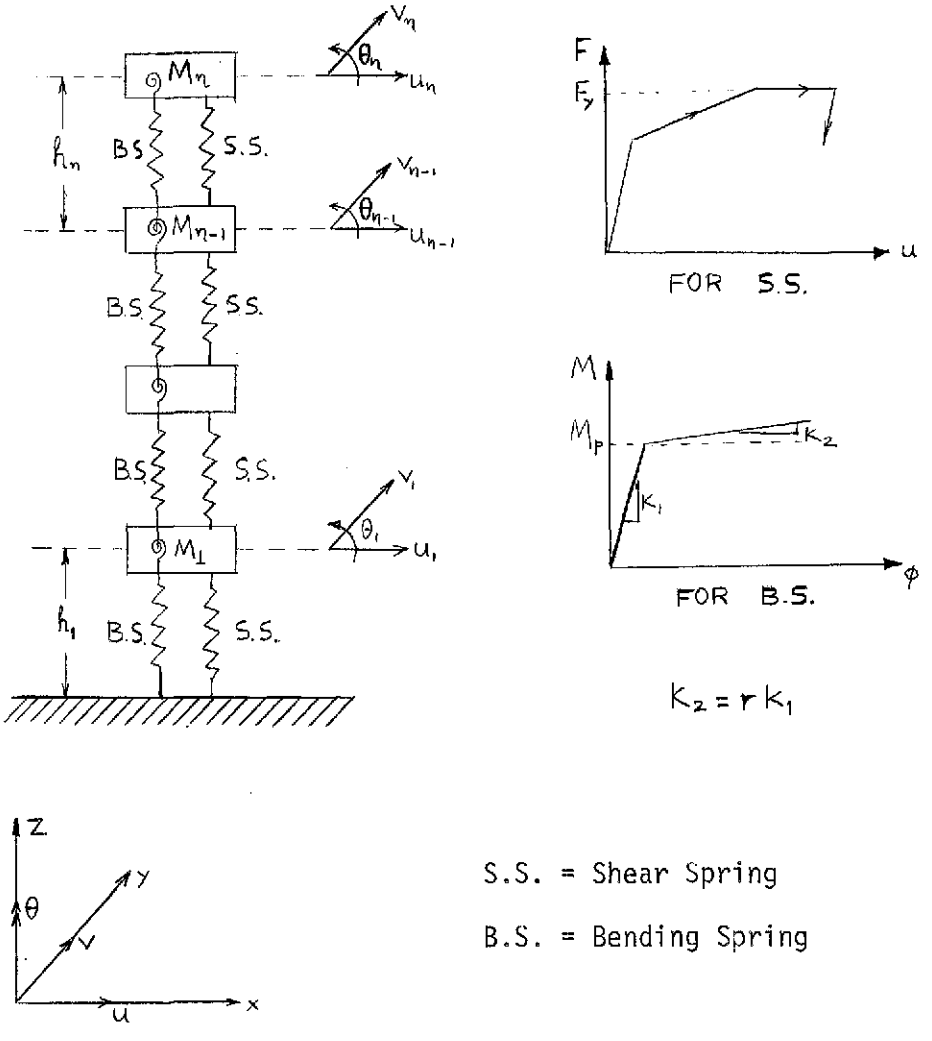

Figure 4-1 Mathematical Model for the Multi-Degree of Freedom System

Since we consider motion along three directions simultaneously, symmetry in the layout is not a problem, so we can deal with unsymmetric and eccentric-mass situations (Figure 4-2).

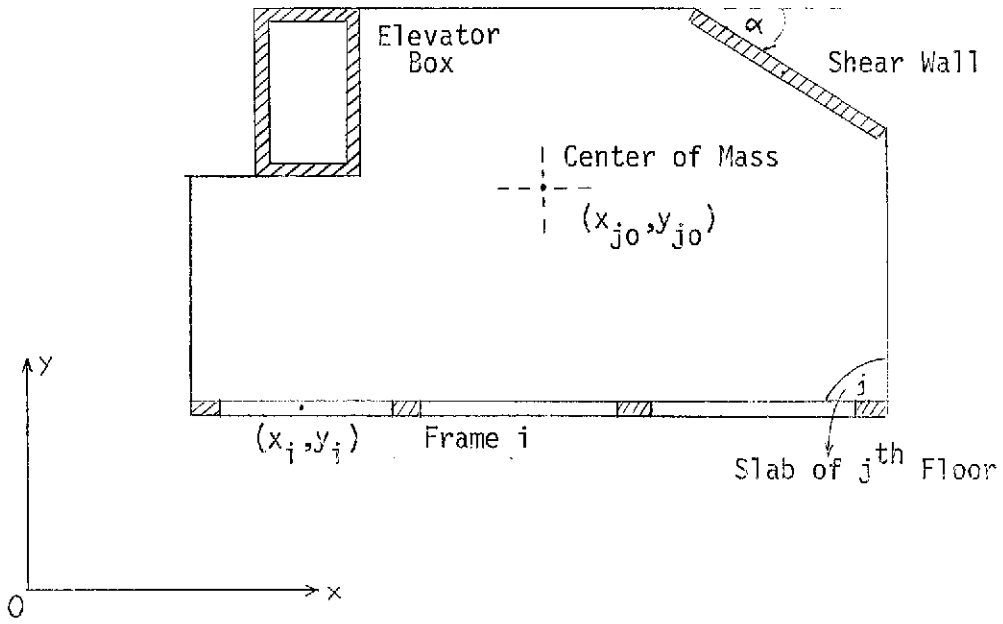

Figure 4-2 Floor Plan

The basic assumptions for our analysis are:

1. Slabs are rigid in their planes.
2. There are 3 degrees of freedom per floor.
3. Height-to-width ratio for frames such that effect of axial shortening of columns is insignificant.
4. Frames act as shear springs with properties computed as described in chapter 2.
5. Walls have a bilinear moment curvature relation.

6. If at any time during the analysis the shear capacity of an element is exceeded, a shear failure is assumed, and the element is eliminated. In the case of shear walls, the wall in the floors below the level in which failure occurred is still active, while in the floors above it is considered as block-partition type element.

Assumptions number 3 and 4 mean that in cases of tall slender frames the method would not give good results.

As a first step in the analysis we compute the dynamic characteristics of the structure in the elastic range (small vibrations), i.e., natural frequencies and modal shapes. The formulation used is outlined below and is given in terms of lateral stiffness matrices, so in this sense it is general, and it could be applied to cases where all the degrees of freedom of a frame had been considered. Consider the dynamic equilibrium of slab j (Figure 4-3):

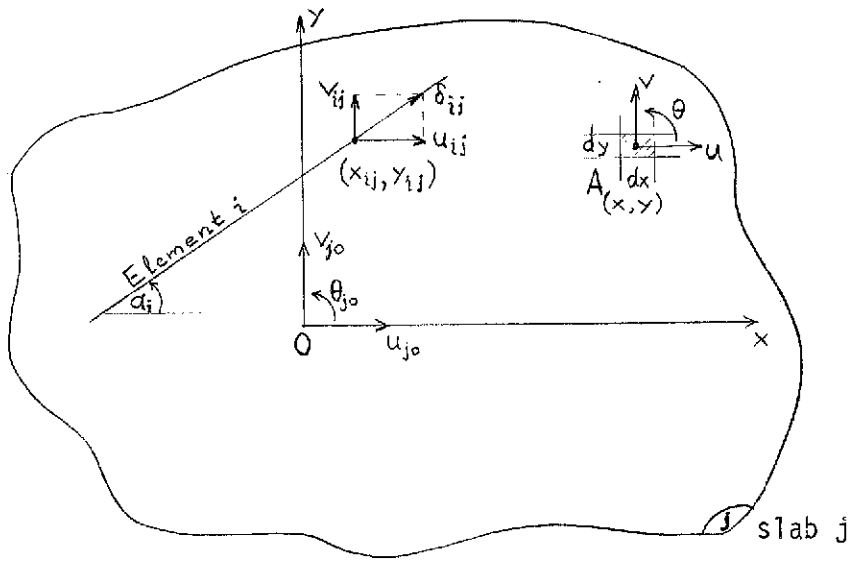

Figure 4-3 Notation for Slab j

Let A be a point in the slab with coordinates x, y and displacements u, v, θ(θ rotation). Since the slab is assumed rigid in its plane, we can write:

$$\left.\begin{aligned} u &= u_{jo} - y\,\theta_{jo} \\ v &= v_{jo} + x\,\theta_{jo} \\ \theta &= \theta_{jo} \end{aligned}\right\} \tag{4.1}$$

The differential inertial forces at A are given from:

$$\left.\begin{aligned} df_x &= -\,pdA\ddot{u} \\ df_y &= -\,pdA\ddot{V} \\ df_z &= +\,pdAy\ddot{u} - pdAx\ddot{V} \end{aligned}\right\} \tag{4.2}$$

where p is the density of the slab at A.

To find the total inertia forces of the slab, we must integrate 4.2. Doing so and utilizing 4.1, we obtain:

$$\left.\begin{aligned} f_x &= -\,m\,\ddot{u}_{jo} + \ddot{\theta}_{jo}\,S_y \\ f_y &= -\,m\,\ddot{V}_{jo} - \ddot{\theta}_{jo}\,S_x \\ f_z &= -\,I\,\ddot{\theta}_{jo} + \ddot{u}_{jo}\,S_y - \ddot{V}_{jo}\,S_x \end{aligned}\right\} \tag{4.3}$$

where: m = total mass, I = moment of inertia

$$S_x = \iint pxdA, \qquad S_y = \iint pydA$$

If we choose O as the center of mass, then $S_x = S_y = 0$, and hence

$$\left.\begin{aligned} f_x &= -\,m\,\ddot{u}_{jo} \\ f_y &= -\,m\,\ddot{V}_{jo} \\ f_z &= -\,I\,\ddot{\theta}_{jo} \end{aligned}\right\} \quad \text{Inertia forces applied to slab (j)} \tag{4.4}$$

The forces that resist the inertia forces come from the different elements(frames, shear walls, etc). Let i be such an element whose lateral stiffness matrix is K. Then the force exerted by element i on slab j is given by:

$$f_{ij} = \sum_{\ell=1}^{n} k^i_{j\ell} \delta^i_\ell$$

and its x component:

$$f_{ijx} = \cos \alpha_i \sum_{\ell=1}^{n} k^i_{j\ell} \delta^i_\ell \qquad (4.5)$$

where: n = number of stories

$k^i_{j\ell}$ = element of the j^{th} row of K

δ^i_ℓ = ℓ^{th} component of the displacement vector (relative to the ground) for element i.

To simplify notation, we drop the index i, but we still refer to element i. It is:

$$\delta_j = u_j \cos\alpha + v_j \sin\alpha$$

and from assumption 1:

$$\left.\begin{aligned} u_j &= u_{jo} - y_j \theta_{jo} \\ v_j &= v_{jo} + x_j \theta_{jo} \end{aligned}\right\} \qquad (4.6)$$

$$\delta_j = (u_{jo} - y_j \theta_{jo})\cos\alpha + (v_{jo} + x_j \theta_{jo})\sin\alpha \qquad (4.7)$$

and replacing to 4.5, we obtain (dropping the index i)

$$f_{jx} = \cos^2\alpha \sum_{\ell=1}^{n} k_{j\ell}\, u_{\ell o} + \cos\alpha \sin\alpha \sum_{\ell=1}^{n} k_{j\ell}\, v_{\ell o} + d_j \cos\alpha \sum_{\ell=1}^{n} k_{j\ell}\, \theta_{\ell o} \quad (4.8)$$

where: $$d_j = x_j \sin\alpha - y_j \cos\alpha \quad (4.9)$$

Similarly:

$$f_{jy} = \cos\alpha \sin\alpha \sum_{\ell=1}^{n} k_{j\ell}\, u_{\ell o} + \sin^2\alpha \sum_{\ell=1}^{n} k_{j\ell}\, v_{\ell o} + d_j \sin\alpha \sum_{\ell=1}^{n} k_{j\ell}\theta_{\ell o} \quad (4.10)$$

and writing:

$f_{jz} = - f_{jx}\, y_j + f_{jy}\, x_j$ we obtain:

$$f_{jz} = d_j \cos\alpha \sum_{\ell=1}^{n} k_{j\ell}\, u_{\ell o} + d_j \sin\alpha \sum_{\ell=1}^{n} k_{j\ell}\, v_{\ell o} + d_j^2 \sum_{\ell=1}^{n} k_{j\ell}\, \theta_{\ell o} \quad (4.11)$$

for equilibrium:

$$\left.\begin{aligned} f_x &= \sum_i f_{jx} \\ f_y &= \sum_i f_{jy} \\ f_z &= \sum_i f_{jz} \end{aligned}\right\} \quad \text{or}$$

$$\left.\begin{aligned} \sum_i f_{jx} + m\, \ddot{u}_{jo} &= 0 \\ \sum_i f_{jx} + m\, \ddot{v}_{jo} &= 0 \\ \sum_i f_{jz} + I\, \ddot{\theta}_{jo} &= 0 \end{aligned}\right\} \quad (4.12)$$

Equations 4.12 describe the dynamic equilibrium of floor j. For each floor we have three such equations, so for n floors the number of equations is 3 x n. Written in matrix form these equations become:

$$\begin{bmatrix} K_{xx} & K_{xy} & K_{xz} \\ K_{yx} & K_{yy} & K_{yz} \\ K_{zx} & K_{zy} & K_{zz} \end{bmatrix} \begin{bmatrix} u \\ v \\ \theta \end{bmatrix} + \begin{bmatrix} M_x & & 0 \\ & M_y & \\ 0 & & I \end{bmatrix} \begin{bmatrix} \ddot{u} \\ \ddot{v} \\ \ddot{\theta} \end{bmatrix} = 0 \qquad (4.13)$$

The submatrices of the stiffness matrix are given by the following expressions:

$$K_{xx} = \sum_{i=1}^{m} K_i \cos^2\alpha_i, \quad K_{xy} = \sum_{i=1}^{m} K_i \cos\alpha_i \sin\alpha_i, \quad K_{xz} = \sum_{i=1}^{m} D_i K_i \cos\alpha_i$$

$$K_{yx} = K_{xy}^T, \quad K_{yy} = \sum_{i=1}^{m} K_i \sin^2\alpha_i, \quad K_{yz} = \sum_{i=1}^{m} D_i K_i \sin\alpha_i$$

$$K_{zx} = K_{xz}^T, \quad K_{zy} = K_{yz}^T, \quad K_{zz} = \sum_{i=1}^{M} D_i K_i D_i$$

$$M_x = \begin{bmatrix} m_{x_1} & & & \\ & m_{x_2} & & \\ & & \ddots & \\ & & & m_{x_n} \end{bmatrix}, \qquad M_y = \begin{bmatrix} m_{y_1} & & & \\ & m_{y_2} & & \\ & & \ddots & \\ & & & m_{y_n} \end{bmatrix}$$

$$I = \begin{bmatrix} I_1 & & & \\ & I_2 & & \\ & & \ddots & \\ & & & I_n \end{bmatrix}, \qquad D_i = \begin{bmatrix} d_{i1} & & & \\ & d_{i2} & & \\ & & \ddots & \\ & & & d_{in} \end{bmatrix}$$

In the above expressions the summations are over the resisting elements.

K_i = lateral stiffness matrix of element i

α_i = angle that the centerline of element i forms with the x axis

D_i = diagonal matrix for element i, containing d_j (eq. 4.9) which are the distances of the element's centerline from the centroids of the slabs at the different levels

M_x, M_y = diagonal mass matrices in x, y directions

I = diagonal matrix containing the moments of inertias of the different slabs about a perpendicular axis through their centroid

u, v, θ = vectors containing the x, y translations and the rotations of the centroids of the slabs with respect to the ground

T - stands for "transposed"

. - indicates differentiation with respect to time

It should be noted here that M_x may be different from M_y because in some cases where the building has several similar frames in both directions we may want to model only part of it.

Equation 4.13 can be written in a more compact form as:

$$Ku + M\ddot{u} = 0 \qquad (4.14)$$

This is the general eigenvalue problem, which when solved will give the natural frequencies and modal shapes.

For the system sketched in figure 4-1, the eigenvalue problem is somewhat easier, because we can form the lateral stiffness matrix of the shear springs (which in this case is tridiagonal) directly from the spring constants. For the bending springs, how-

ever, we must perform a condensation on the total stiffness matrix to obtain the lateral one by eliminating the rotational degrees of freedom at the joints. This is done by treating the bending springs as a beam with supports at the floor levels and accounting for the shear deformation.

The contribution of each frame or wall can be assembled directly into the total stiffness matrix as soon as its lateral stiffness matrix is computed. Note also that this procedure is general and is not restricted to the assumption of shear behavior for the frames (that assumption was made for the nonlinear part of the analysis). It only requires a computer routine that will read the properties of the frame, form its total stiffness matrix and condense it to obtain the lateral one.

This formulation is not accurate for tall buildings designed to act as a tube. In that case it is necessary to consider all the 6 degrees of freedom per joint of the space frame, form the total stiffness matrix (which in this case will be of a much bigger size) and then condense it using the assumption of the rigid diaphragms for the slabs.

For the solution of the eigenvalue problem, we used the standard IBM routine, with a slight modification, which utilizes Jacobi's method. This routine is efficient for the size of problems this program was designed to handle.

After having computed the dynamic properties of the building in the elastic range, we proceed with the time-history analysis.

If we call: $\ddot{u}_g$, $\ddot{v}_g$ the time histories of the ground acceleration in the x and y directions and set:

$$\left.\begin{aligned} u_{abs} &= u_{jo} + u_g \\ v_{abs} &= v_{jo} + v_g \\ \theta_{abs} &= \theta_{jo} \end{aligned}\right\} \tag{4.15}$$

equation 4.14 becomes:

$$Ku + M\ddot{u} = R$$

where:

$$R = - \begin{bmatrix} M_x \ddot{u}_g \\ M_y \ddot{v}_g \\ 0 \end{bmatrix}$$

If we are to include viscous damping which is described by a damping matrix C, then these equations take the form:

$$M\ddot{u} + C\dot{u} + Ku = R \tag{4.16}$$

These are the differential equations of motion in matrix form, for the multidegree of freedom system described earlier, excited by a ground acceleration in the x and y directions. These equations, however, are only good for the elastic range. When the structure starts yielding, its stiffness matrix changes. In other words, the coefficients of the displacements in the above equations, which in the elastic case are constant, in the inelastic are not, but depend on the displacements. Hence it is appropriate to write 4.16 as:

$$M\ddot{u} + C\dot{u} + F(u) = R \tag{4.17}$$

where now F(u) is a vector of forces, function of the displacement vector u. Before describing the numerical procedure used for the solution of 4.17, we will discuss briefly the selection of the damping matrix C. There are several ways by which the damping matrix can be selected. The most commonly used are the following:

$$\left.\begin{array}{ll} \text{(i)} & C = aM \\ \text{(ii)} & C = bK \\ \text{(iii)} & C = aM + bK \end{array}\right\} \quad a, b \text{ constants}$$

In the first case the C matrix is proportional to the mass matrix, and the modal damping decreases continuously for increasing number of modes. The parameter a can be selected such that we have a prespecified percentage of critical damping in one particular mode (usually the first).

In the second case, where C is proportional to the stiffness matrix, the modal damping increases for increasing number of modes. Again b can be selected so as to have a prespecified percentage of critical damping in one particular mode.

Case (iii) is a combination of the first two, and the resulting viscous damping is sometimes called "Raleigh damping." In this case we can have more flexibility in the variation of modal damping over the system's modes, but ultimately the damping will start increasing for high frequencies, since the term aM will give modal dampings tending to zero. In this work we used a method known as Kuzak's method (6), which produces a C matrix that gives any desired

percentage of critical damping in any mode. This matrix is given as the product:

$$C = MQBQ^{T}M$$

where: M = mass matrix

B = diagonal matrix with elements $2\beta_i\omega_i$

β_i = percentage of critical damping in the i^{th} mode

ω_i = circular frequency of the i^{th} mode

Q = matrix whose columns are the eigenvectors of the system (normalized with respect to M)

Since in our work we solve first the eigenvalue problem, Kuzak's method is as easy to use as any of the others described earlier and in addition gives us the flexibility of having any desired amount of viscous damping in any of the modes. In all our studies we used constant percentage of critical damping for all the modes.

Equation 4.17 was solved numerically using a step-by-step integration procedure. This procedure, sometimes called "constant velocity method," assumes that the velocities of the system are constant within the time step. (See for example (1)). Under this assumption the recurrence formulas for velocities and accelerations are:

$$\left.\begin{aligned} \dot{u}_n &= \frac{1}{2\Delta t}\,(u_{n+1} - u_{n-1}) \\ \ddot{u}_n &= \frac{1}{\Delta t^2}\,(u_{n+1} - 2u_n + u_{n-1}) \end{aligned}\right\} \qquad (4.18)$$

Replacing these two expressions in 4.17, we obtain:

$$\frac{1}{\Delta t^2} M(u_{n+1}-2u_n+u_{n-1})+\frac{1}{2\Delta t} C(u_{n+1} - u_{n-1}) + F_n = R_n \qquad \text{or}$$

$$\left(\frac{1}{\Delta t^2} M + \frac{1}{2\Delta t} C \right) u_{n+1} = R_n - F_n + \frac{2}{\Delta t^2} M u_n - \left(\frac{1}{\Delta t^2} M - \frac{1}{2\Delta t} C \right) u_{n-1}$$

and:

$$u_{n+1}=\left(\frac{1}{\Delta t^2}M+ \frac{1}{2\Delta t} C\right)^{-1} \cdot \left(R_n- F_n + \frac{2}{\Delta t^2} M u_n - (\frac{1}{\Delta t^2} M - \frac{1}{2\Delta t} C)u_{n-1}\right) \quad (4.19)$$

Matrix equation 4.19 can be used for the calculation of the displacement vector at time step n+1, in terms of the displacement vectors at steps n and n-1, and the force vector F_n at n.

The force vector at time step n is computed easily for the shear springs. From the displacements of the center of mass u_n, v_n, θ_n, using the geometrical relation 4.7, we can compute the distortions of the various shear springs at time step n. Having the distortions and the forces in these springs at time step n-1, it is simple to compute the incremental forces and hence the total forces. The computation of the incremental forces depends on the particular type of force-deflection curve assumed for each spring, and special routines were written for each type of spring used. These forces then are used to form the total force vector F_n. F_n consists of three subvectors:

$$F_n = \begin{bmatrix} F_x \\ F_y \\ F_z \end{bmatrix}$$

F_x is the summation of all resisting forces on the x direction

F_y is the summation of all resisting forces on the y direction

F_z is the summation of all resisting torsional moments about the centroids of the slabs.

The determination of the contribution of the bending springs in the force vector F_n is a more difficult task. For this case we must work with increments of displacements and rotations rather than with total values. Since the numerical procedure produces total displacements, the incremental ones are found by subtracting the values of two consecutive steps. The equilibrium equations for the shear wall are in this case:

$$\left[\begin{array}{c|c} K_{t\phi\phi} & K_{t\phi\delta} \\ \hline K_{t\delta\phi} & K_{t\delta\delta} \end{array}\right]_{n-1} \begin{bmatrix} \Delta\phi_n \\ \Delta\delta_n \end{bmatrix} = \begin{bmatrix} 0 \\ \Delta F_{bn} \end{bmatrix} \qquad (4.20)$$

where:

$$\left[\begin{array}{c|c} K_{t\phi\phi} & K_{t\phi\delta} \\ \hline K_{t\delta\phi} & K_{t\delta\delta} \end{array}\right]_{n-1} =$$ Tangent stiffness matrix for the wall, partitioned for the bending rotations and the displacements (figure 4-4), at time step n-1.

$\Delta\phi_n = \phi_n - \phi_{n-1}$ = vector of incremental joint rotations at step n

$\Delta\delta_n = \delta_n - \delta_{n-1}$ = vector of incremental joint displacements at step n

$\Delta F_{bn} = F_{bn} - F_{b,n-1}$ = vector of incremental joint forces at step n.

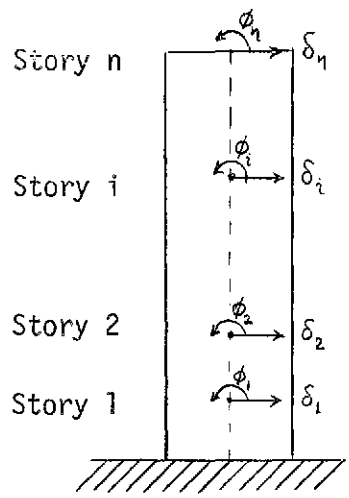

Figure 4-4 Degrees of Freedom for the Bending Springs (Shear Walls)

Again the δ's can be computed from the displacements u_n, v_n, θ_n of the center of mass at each story level, using equation 4.7. From equation 4.20 we have:

$$\Delta\phi_n = - \left(K^{-1}_{t\phi\phi} \; K_{t\phi\delta} \right)_{n-1} \Delta\delta_n$$

and

$$\Delta F_{bn} = \left(K_{t\delta\delta} - K_{t\delta\phi} \; K^{-1}_{t\phi\phi} \; K_{t\phi\delta} \right)_{n-1} \Delta\delta_n \qquad (4.21)$$

and

$$F_{bn} = F_{b,n-1} + \Delta F_{bn} \qquad (4.22)$$

This is the contribution of the bending springs (shear walls) to the total force vector F_n, required for the determination of u_{n+1} from 4.19.

The bending moments in the shear walls are computed from the incremental shears obtained from 4.21, by multiplying them with the

appropriate heights. These bending moments are checked at each time step against the ultimate moments of the section and if larger, a plastic hinge is assumed with moment at that section equal to the plastic moment. The total tangent stiffness matrix for the wall is assembled then, by using the appropriate stiffness matrices for each segment, as determined by the conditions of its end. The stiffness matrices for the various states of a segment and for the degrees of freedom shown in figure 4-5 are given below. (Axial deformations have been neglected.)

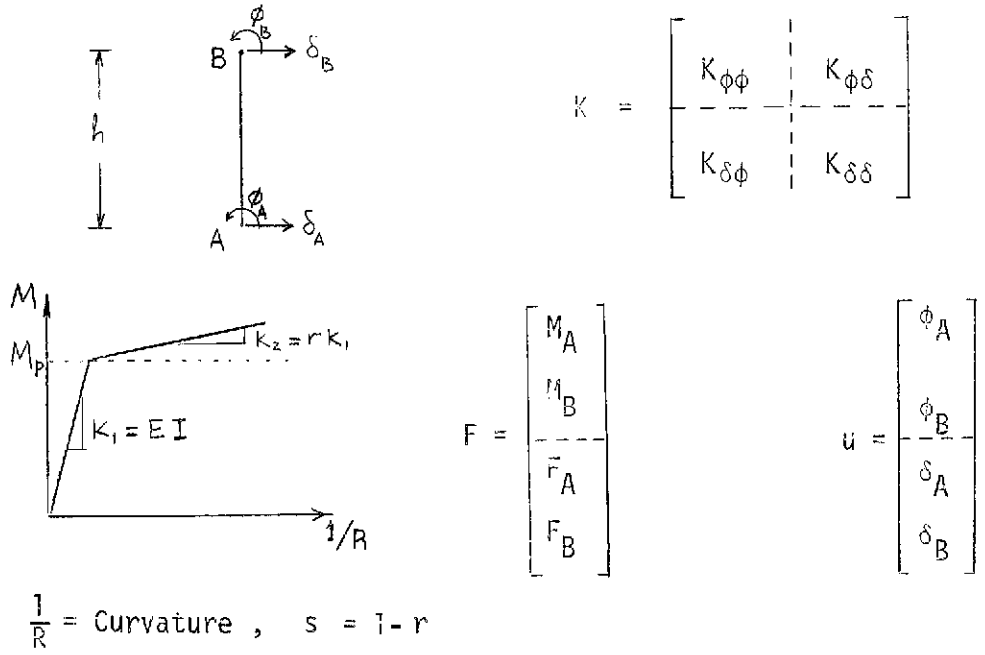

Figure 4-5 Stiffness Notation for Bending Spring (Shear Wall Segment)

1. $|M_A|, |M_B| < M_p$ — No hinges

$$K_{\phi\phi} = \begin{bmatrix} a & b \\ b & a \end{bmatrix} \qquad a = \frac{2EI(2 + B)}{h(1 + 2B)}$$

$$K_{\phi\delta} = \begin{bmatrix} -c & c \\ -c & c \end{bmatrix} \qquad b = \frac{2EI(1 - B)}{h(1 + 2B)}$$

$$K_{\delta\phi} = K_{\phi\delta}^T \qquad c = \frac{6EI}{h^2(1 + 2B)}$$

$$K_{\delta\delta} = \begin{bmatrix} d & -d \\ -d & d \end{bmatrix} \qquad d = \frac{12EI}{h^3(1 + 2B)}$$

$$B = \frac{6EI}{h^2 G A_s}$$

I = moment of inertia of the section

A_s = shear area

T = stands for "transpose"

2. $|M_A| < M_P \leq M_B$ — Hinge at top

$$K_{\phi\phi} = r\begin{bmatrix} a & b \\ b & a \end{bmatrix} + s\begin{bmatrix} e_1 & 0 \\ 0 & 0 \end{bmatrix} \qquad e_1 = a - \frac{b^2}{a}$$

$$e_2 = c\left(1 - \frac{b}{a}\right)$$

$$K_{\phi\delta} = r\begin{bmatrix} -c & c \\ -c & c \end{bmatrix} + s\begin{bmatrix} -e_2 & e_2 \\ 0 & 0 \end{bmatrix} \qquad e_3 = d - \frac{c^2}{a}$$

$$K_{\delta\phi} = K_{\phi\delta}^T$$

$$K_{\phi\phi} = r\begin{bmatrix} d & -d \\ -d & d \end{bmatrix} + s\begin{bmatrix} e_3 & -e_3 \\ -e_3 & e_3 \end{bmatrix}$$

3. $|M_B| < M_P \leq M_A$ Hinge at bottom

$$K_{\phi\phi} = r\begin{bmatrix} a & b \\ b & a \end{bmatrix} + s\begin{bmatrix} 0 & 0 \\ 0 & e_1 \end{bmatrix}$$

$$K_{\phi\delta} = r\begin{bmatrix} -c & c \\ -c & c \end{bmatrix} + s\begin{bmatrix} 0 & 0 \\ -e_2 & e_2 \end{bmatrix}$$

$$K_{\delta\phi} = K_{\phi\delta}^T$$

$$K_{\delta\delta} = r\begin{bmatrix} d & -d \\ -d & d \end{bmatrix} + s\begin{bmatrix} e_3 & -e_3 \\ -e_3 & e_3 \end{bmatrix}$$

4. $|M_A|, |M_B| \geq M_P$ Hinges at both ends

$$K_{\phi\phi} = r\begin{bmatrix} a & b \\ b & a \end{bmatrix}$$

$$K_{\phi\delta} = r\begin{bmatrix} -c & c \\ -c & c \end{bmatrix}$$

$$K_{\delta\phi} = K_{\phi\delta}^T$$

$$K_{\delta\delta} = r\begin{bmatrix} d & -d \\ -d & d \end{bmatrix}$$

The factor r which is the ratio of the two slopes of the moment-curvature diagram was chosen for most of our studies as 0.03.

From equation 4.19 we see that at any particular time step we need the displacements of the two previous steps. This means that in order to start using the method we must have the displacements of the system at the end of the first step. This was done by using a 4^{th} order Runge-Kutta method which is self sufficient. After computing the displacements, velocities and accelerations can be computed from 4.18.

Ductility factors are computed for the shear springs by dividing the maximum deformation induced in the spring by the yield deformation and for the bending springs by dividing the maximum moment at the joints by the yield moment.

For all our analyses we used: $\Delta t = 0.01$ sec. The numerical method just described was selected, among others, because it is very simple and hence less time consuming, and because its accuracy for the size of problems considered here compares well with that obtained by using more sophisticated methods. In the next section we will present results obtained from comparisons of different numerical methods.

4.3 Comparisons of Numerical Methods

For a multidegree-of-freedom system most numerical integration

schemes require a time step in the order of 1/5 to 1/10 of the smallest natural period, provided that this step reproduces well the loading. In some cases, where the higher modes correspond to very stiff configurations, this implies an extremely small Δt if the method is to be stable. The purpose of this comparison was two-fold. First we wanted to check whether a method described by Farhoomand and Wilson (98), which filters out higher frequencies, was really stable and accurate for the situations mentioned above. If that was the case, it was anticipated that the size of Δt could be determined only from the smallest significant period. Second we wanted to see whether the rule of choosing Δt as 1/5 to 1/10 of the smallest natural period would give equally good results for the simple and fast "constant velocity" method, as for a more sophisticated one like the 4^{th} order Runge-Kutta or Wilson's.

In all our comparisons we used 4 different numerical methods: 1) The 4^{th} order Runge-Kutta, 2) Wilson's method, 3) "Constant velocity method," 4) "Modified constant velocity" method. We also programmed the exact solution (using modal analysis) for all the cases. The modified "constant velocity" method is essentially the same as the one described earlier (eq. 4.19), except for the fact that it works with incremental displacements and forces rather than with total values. Since the results obtained from it were almost identical to those obtained from the "constant velocity," it will not be discussed any further.

The basic idea of Wilson's method is the following: The accel-

eration of each point of the system is assumed to vary linearly within a small time interval $2\Delta t$. With this assumption the accelerations at time steps $t - \Delta t$ and $t + \Delta t$ can be computed. The average of these two values then, is taken as the acceleration at time step t. Using this and equation 4.17, the following recurrence formulas were derived:

$$\left.\begin{aligned}
\ddot{u}_n &= \frac{3}{4\Delta t^2} A^{-1} P - \frac{3}{2\Delta t} \dot{u}_{n-1} - \frac{1}{2} \ddot{u}_{n-1} \\
\dot{u}_n &= \dot{u}_{n-1} + \frac{1}{2} \Delta t (\ddot{u}_{n-1} + \ddot{u}_n) \\
u_n &= u_{n-1} + \Delta t \dot{u}_{n-1} + \frac{1}{3} \Delta t^2 \ddot{u}_{n-1} + \frac{1}{6} \Delta t^2 \ddot{u}_n \\
A &= K_{t,n-1} + \frac{3}{2\Delta t} C + \frac{3}{2\Delta t^2} M \\
P &= R_{n+1} - F_{n-1} + (2C + \frac{3}{\Delta t} M) \dot{u}_{n-1} + (\Delta t C + 2M) \ddot{u}_{n-1}
\end{aligned}\right\} \quad (4.23)$$

where:

M = mass matrix
C = damping matrix
K_t = tangent stiffness matrix
R = load vector
F = force vector

The case selected to test Wilson's method is shown in figure 4.6. It is a portal frame whose dynamic degrees of freedom are the lateral displacements of the two joints, 1,2. It has two modes of vibration, one corresponding to the simultaneous motion of the two joints in the same direction (influenced mainly by the bending stiffness of the members) and the other corresponding to the motion of the two joints

in opposite directions (influenced mainly by the axial stiffness of the girder). The stiffness matrix, masses, natural periods and excitation are shown in the same figure.

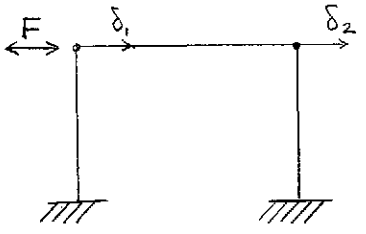

$$K = \begin{bmatrix} 6774.46 & -6650.54 \\ -6650.54 & 6774.46 \end{bmatrix}$$

$M_1 = M_2 = 0.126$

$T_1 = 0.2$ sec

$F = 80 \sin\Omega(n\Delta t)$

$T_2 = 0.0192$ sec.

Figure 4-6 Portal Frame to Test Wilson's Method

Results for three different cases are tabulated in table 4-1, 4-2. From the results in the upper part of table 4.1 we see that a time step $\Delta t = 0.01$, which is 20 times less than the significant mode, is inadequate for the Runge-Kutta and constant velocity methods. Wilson's method, on the other hand, is stable, but it gives results that are not correct or at least are far away from the exact answers. When a value of $\Delta t = 0.002$ was used, which is approximately one-tenth of the smallest period of the system, all methods gave good results. The numbers from Wilson's method are slightly smaller than the correct ones. Table 4.2 gives results for $\Delta t = 0.002$, but $\Omega = 10\pi$. Again the same conclusions are valid. A more careful look at the numbers obtained

$\Omega = 20\pi$ $\Delta t = 0.01$ sec							
EXACT		RUNGE-KUTTA		WILSON		CONST. VELOCITY	
Time Step	$\delta_{1,max}$	Time Step	δ_1	Time Step	$\delta_{1,max}$	Time Step	δ_1
7	.034			6	.0360		
13	-.034			14	-.0260		
107	.035			108	.0230		
113	-.033			122	-.0270		
307	.037	Blows up		306	.0019	Blows up	
314	-.032			312	-.0168		
507	.038			507	.0130		
514	-.030			513	-.0050		
707	.039			707	.0060		
714	-.028			72	-.0100		
907	.039			907	.0100		
914	-.026			912	-.0080		
$\Omega = 20\pi$ $\Delta t = 0.002$ sec							
34	.0340	34	.0340	33	.0348	32	.0346
66	-.0340	66	-.0340	67	-.0344	66	-.0346
533	.0350	533	.0350	534	.0362	533	.0353
566	-.0330	566	-.0336	568	-.0325	566	-.0339
766	-.0329	766	-.0333	768	-.0317	766	-.0337
833	.0358	833	.0357	834	.0369	833	.0356
866	-.0326	866	-.0332	868	-.0313	866	-.0334
933	.0358	933	.0359	934	.0371	933	.0358
966	-.0326	966	-.0331	968	-.0390	966	-.0335

Table 4-1 Results for Portal Frame to Check Stability of the Methods. $\Omega = 20\pi$.

by Wilson's method will reveal that they keep decreasing constantly as the time increases. This leads to the conclusion that the method introduces artificial damping into the system which confirms the same observation made in reference (98).

$\Omega = 10\pi$			$\Delta t = 0.002$ sec			
EXACT	RUNGE-KUTTA		WILSON		CONST. VELOCITY	
	Time Step	$\delta_{1,max}$	Time Step	$\delta_{1,max}$	Time Step	$\delta_{1,max}$
Was not Computed	49	.0637	50	.0635	49	.0638
	99	-.1276	100	-.1269	99	-.1276
	199	-.2550	200	-.2530	199	-.2550
	249	.3190	250	.3170	249	.3190
	349	.4460	351	.5530	349	.4470
	399	-.5100	401	-.5070	399	-.5110
	750	.956	751	.9470	750	.9570
	800	-.1020	802	-1.010	800	-1.0200
	950	1.211	952	1.198	950	1.2120
	999	-1.273	999	-1.240	999	-1.2740

Table 4-2 Results for Portal Frame to Check Stability of the Methods. $\Omega = 10\pi$

For the case at hand, however, when only the lateral displacements of the floors of a building are maintained as dynamic degrees of freedom (with girders assumed infinitely rigid in axial deformations) the smallest natural period is essentially constant independent of the height of the building. For a shear beam the natural frequencies are:

$$\omega_n = \frac{(2n - 1)\pi}{2H} \sqrt{\frac{G}{p}} \tag{4.24}$$

H = total height
p = density

If we take n stories and n modes and write: H = nh, then:

$$\omega_n = (1 - \frac{1}{2n}) \frac{\pi}{h} \sqrt{\frac{G}{p}}$$

and for relatively large n

$$\omega_n \approx \frac{\pi}{h} \sqrt{\frac{G}{p}} \tag{4.25}$$

which is twice the frequency of one story. A time step Δt of 0.01 seconds (used to reproduce the earthquake) should then be adequate for all buildings that behave in a shear manner, independently of the number of stories. To check this and at the same time compare the accuracy of the various methods, a 30-degree-of-freedom close-coupled system was analyzed for various inputs. The first three natural periods of the system are 3 sec, 1 sec, .6 sec, and the smallest 0.078 sec. The system was with uniform mass and stiffness over the height. Results for various loading cases and various Δt are shown in tables 4-3, 4-4, and 4.5.

From tables 4-3 and 4-4 we can see that the time step chosen was inadequate for Runge-Kutta and constant velocity methods. Wilson's method, although stable, gave erroneous results. From both these tables we can see that the response is predominantly 1^{st} mode response and the response obtained from the first three modes (table 4-4) is for all practical purposes identical to the exact. The time step

for this case is 0.05 sec, more than ten times smaller than the third natural period, which is 0.6 secs. When the time step, however, was decreased to $\Delta t = 0.01$ sec, all methods gave good results for both sinusoidal and earthquake motion.

SINUSOIDAL GROUND MOTION			$\ddot{u}_g = 100 \sin\pi(n\Delta t)$, $\Delta t = 0.12$ sec			
EXACT (30 modes)			1st MODE SOLUTION		WILSON	
Time Step	$\delta_{top,max}$		Time Step	$\delta_{top,mas}$	Time Step	$\delta_{top,max}$
12	-34.62		12	-33.15	12	-34.81
24	54.44		24	53.82	24	52.48
36	-54.81		36	-54.01	36	-48.86
48	35.11	Runge-Kutta and Constant Velocity blow up	48	33.65	48	24.13
72	-34.31		72	-32.85	73	-39.36
84	54.27		84	53.70	85	52.19
96	-54.93		96	-54.12	97	-43.06
108	35.40		108	33.94	121	17.60
132	-34.04		132	-32.55	133	-43.36
144	54.13		144	53.58	145	50.71
156	-55.04		156	-54.22	157	-36.76
168	35.69		168	34.23	182	24.47
192	-33.78		192	-32.25	194	-45.71
204	53.98		204	53.45	206	47.66
216	-55.16		216	-54.32	218	-29.64

Table 4-3 Comparison of Wilson's Method for $\Delta t = .1$ sec.

SINUSOIDAL GROUND MOTION $\ddot{u}_g = 100 \sin\pi(n\Delta t)$, $\Delta t = 0.05$ sec.						
EXACT (30 modes)		3 Modes	2 Modes	1 Mode	WILSON	
Time Step	$\delta_{top,max}$	$\delta_{top,max}$	$\delta_{top,max}$	$\delta_{top,max}$	Time Step	$\delta_{top,max}$
24	-35.27	-35.26	-35.40	-33.86	24	-35.12
48	55.60	55.52	55.77	54.85	48	54.85
72	-55.76	-55.68	-55.91	-54.98	72	-54.66
96	35.60	35.57	35.74	34.19	96	32.60
144	-34.97	-34.96	-35.09	-33.55	145	-36.00
168	55.43	55.38	55.64	54.73	168	55.65
192	-55.89	-55.81	-56.03	-55.09	192	-53.73
216	35.89	35.86	36.04	34.49	216	29.98
264	-34.66	-34.65	-34.78	-33.24	265	-37.60
288	55.27	55.23	55.51	54.61	289	56.23
312	-56.01	-55.93	-56.14	-55.19	313	-52.21
336	36.19	36.15	36.33	34.78	336	28.08
384	-34.38	-34.35	-34.46	-32.93	385	-39.47
408	55.12	55.08	55.37	54.48	409	56.30
432	-56.13	-56.05	-56.25	-55.29	433	-51.02
456	36.47	36.44	36.64	35.08	457	26.16
504	-34.09	-34.05	-34.15	-32.62	505	-40.87
528	54.97	54.95	55.23	54.34	529	56.27
Runge-Kutta and Constant Velocity blow up.						

Table 4.4 Comparison of Wilson's Method for $\Delta t = .05$ sec.

SINUSOIDAL GROUND MOTION $\ddot{u}_g = 100 \sin\pi(n\Delta t)$, $\Delta t = .01$							
EXACT (30 modes)		RUNGE-KUTTA		WILSON		CONST. VELOCITY	
Time Step	$\delta_{top,max}$	Time Step	$\delta_{top,max}$	Time Step	$\delta_{top,max}$	Time Step	$\delta_{top,max}$
120	-35.49	120	-35.51	121	-35.49	120	-35.49
241	55.99	241	56.00	242	55.91	241	56.00
357	-56.13	357	-56.09	358	-56.05	357	-56.15
477	35.80	477	35.70	479	35.58	477	35.81
720	-35.18	720	-35.31	721	-35.37	720	-35.17
840	55.81	840	55.87	841	55.72	840	55.83
957	-56.23	957	-56.19	958	-56.13	957	-56.27
SAME SYSTEM FOR 10 sec. OF EL CENTRO, Δt = 0.01 sec.							
177	7.29	177	7.29	178	7.28	177	7.30
329	-17.51	329	-17.51	330	-17.61	329	-17.51
489	25.10	489	25.12	488	25.29	489	25.12
622	-28.44	622	-28.44	616	-28.49	622	-28.54
770	29.09	771	29.10	768	29.30	773	29.10
925	-31.16	925	-31.18	921	-31.37	925	-31.19

Table 4-5 Comparisons of All Methods for Δt = 0.01 sec.

For all the above cases the value of viscous damping was zero. To test our routines with damping a 10-degree-of-freedom system was analyzed for the first 10 seconds of El Centro. Its largest natural period was 1.42 sec, and its smallest 0.111 sec. The time step used Δt = 0.01 sec and the percentage of critical damping B = 3%.

The results obtained are listed here:

EXACT	$\delta_{top,max} = 6.2644"$	at t = 6.13 sec.
RUNGE-KUTTA	$\delta_{top,max} = 6.2649"$	at t = 6.12 sec.
CONSTANT VELOCITY	$\delta_{top,max} = 6.2570$	at t = 6.12 sec.

From all these comparisons, and others that are not reported here, the following conclusions were reached:

1. A time step $\Delta t = 0.01$ is sufficient for all the methods examined here and for the range of structures to be considered in this thesis.
2. The accuracy of the results obtained by the constant velocity method were comparable with those obtained from the 4^{th} order Runge-Kutta and slightly better from those obtained by Wilson's.
3. Wilson's method was always stable for all the Δt's examined in contrast to the other two.
4. Results obtained by Wilson's method are not correct if the time step is not sufficiently small.
5. It is not enough for Wilson's method to select the appropriate Δt from the natural period corresponding to the last significant mode. It is very probably the smallest natural period that determines the size of Δt (for the results to be correct), as in the other methods.
6. Wilson's method introduces damping into the system.

Based on the above, the constant velocity method, being the simplest and the fastest of all, was selected with a $\Delta t = 0.01$ sec., for all our analyses.

4.4 Brief Description of the Computer Program

A computer program was developed for this analysis, written in FORTRAN IV, that uses 350k of primary memory on an I.B.M. 370/155 computer. No secondary storage is required. The program is designed for buildings having a maximum of 30 stories, 30 different structural elements (in plan) and 3000 points of ground acceleration in each direction.

Since it was intended primarily for research, no special effort was put into adding special features, desirable in a program for commercial use (such as free input, problem-oriented language, unit conversion, etc.). The geometry of the building is specified through the number of stories, the heights, the number of elements, and a plan. The information given for a plan is the coordinates of some point along the centerline of each element and the orientation of this centerline with respect to the x axis. The masses are given for each floor level separately, together with the coordinates of the centroid and the corresponding moments of inertia. For bending springs (shear walls) the required properties are given floor by floor. For shear springs there is the option of either specifying the spring characteristics (and spring type) floor by floor directly or in the case of frames to specify its geometry and the member properties at each level, and then the program will compute the spring properties by using the approximate formulas presented in chapter 2. Information for identical elements or floors need not be repeated. A single number is required for the viscous damping, the percentage of critical to

be used in each mode. The user has the option to specify the number of modes he wants for the elastic part of the analysis, together with the coordinates of a "geometrical center" with respect to which the modal shapes will be computed. The next set of information needed by the program is about the earthquake ground motions. It can read and store two different earthquake records (up to 3000 points each), one for the x and the other for the y direction, and it can combine them with appropriate direction cosines, so that directions of the motion other than x and y can be considered. The user can also specify a number of scales by which the originally read accelerograms will be multiplied and new analyses will be performed. The information given with each earthquake record is a scale factor, a time interval Δt and the values of the acceleration. Finally, the last piece of information required concerns plotting of various time-histories for relative displacements, absolute accelerations, inter-story displacements and force versus deformation, at any level and for any direction. If the required number of plots exceeds the capacity of the program, the analysis will automatically be repeated until all the requested plots have been produced. This particular feature was a product of trade-off between increasing core requirements, possibility of using secondary storage and computational costs, arising from the fact that at each step of the numerical analysis previous information is lost, unless stored.

The program will print the following results:

1. Natural periods and modal shapes. (two for x and y and one for torsion).

2. For each element and for each floor it will print maximum interstory displacements, maximum ductility factors and permanent sets.

3. For each floor level:

   a) Maximum floor acceleration, direction and time of occurrence.

   b) Maximum floor displacement (with respect to the ground) direction and time of occurrence.

   c) Maximum interstory displacement (of the centroids), direction and time of occurrence.

   d) Maximum x acceleration, displacement and interstory displacement, corresponding y and rotational values and times of occurrence.

   e) Maximum y acceleration, displacement and interstory displacement, corresponding x and rotational values and times of occurrence.

   f) Maximum torsional acceleration, rotation and interstory rotation, corresponding x and y values and times of occurrence.

4. For each floor level:

   Root mean square of the maximum accelerations and interstory displacements of all the elements for the x and y directions.

5. For each floor level:

   Root mean square of the time histories of the global accelerations and interstory displacemtns for the x and y directions and for the torsion.

6. For each floor level:

   Average root mean square of accelerations and interstory

displacements for the x and y directions computed from time histories of each of the elements.

7. Maximum base shears and overturning moments in the x and y directions.

Output 4, 5, 6 is intended for later use of the program to estimate economic damage to the building due to earthquakes of different intensities. The program has also the capability of producing plots on an SC4020 plotter. The user can request and obtain any number of plots for the following:

1. For any floor level and for any of the three directions:
   a) Time histories of absolute accelerations.
   b) Time histories of displacements (and rotation) relative to ground.
   c) Time histories of interstory displacements (and rotations).
   d) Plot of total floor shear (torsional moment) vs. corresponding displacement (rotation) for all the duration of the earthquake.
2. For any element and for any floor:
   a) Time histories of accelerations.
   b) Time histories of displacements relative to ground.
   c) Time histories of interstory displacements.
   d) Plot of spring force vs. deformation for all the duration of the earthquake.

The user can specify the starting and finishing time for the time history plots.

The maximum number of points that can be plotted in one analysis is 4500. If the user specifies plots that need N points in

total where N > 4500, the program will repeat the analysis$(\frac{N}{4500} + 1)$ times untill it produces all the requested plots. For each earthquake scale that the user requests, he must specify what plots he wants. These plots can be different from one scale to another.

4.5 Some Comparisons of Results with Exact Solutions in the Elastic Range

The analytical model described in 4.2 approximates multistory-multibay frames as close-coupled systems, determining their lateral stiffness story by story, using formulas from chapter 2. It is anticipated that this approximation would give good results for buildings whose ratio of height to width is not excessively high. If this is not the case, then axial deformations of the columns become important and reduce significantly the lateral stiffness of the building. Under these conditions the method used is not valid any more, and the results obtained can be erroneous. In order to see to what extent the above is true, we determined the natural periods and modal shapes of three different structures first with this program and then with another one that solves the problem exactly, accounting for all the degrees of freedom of a frame. The first structure analyzed is a three-story building. The geometry and the properties of the structure are shown in figure 4-7. The areas of the columns were assumed very large and similarly the moments of inertia for the girders. The properties of the structure were so chosen in order to see the accuracy of the new program under "ideal conditions." The results obtained

are shown in table 4-6. We see that the agreement is perfect, as expected. Modal shapes were for all practical purposes identical.

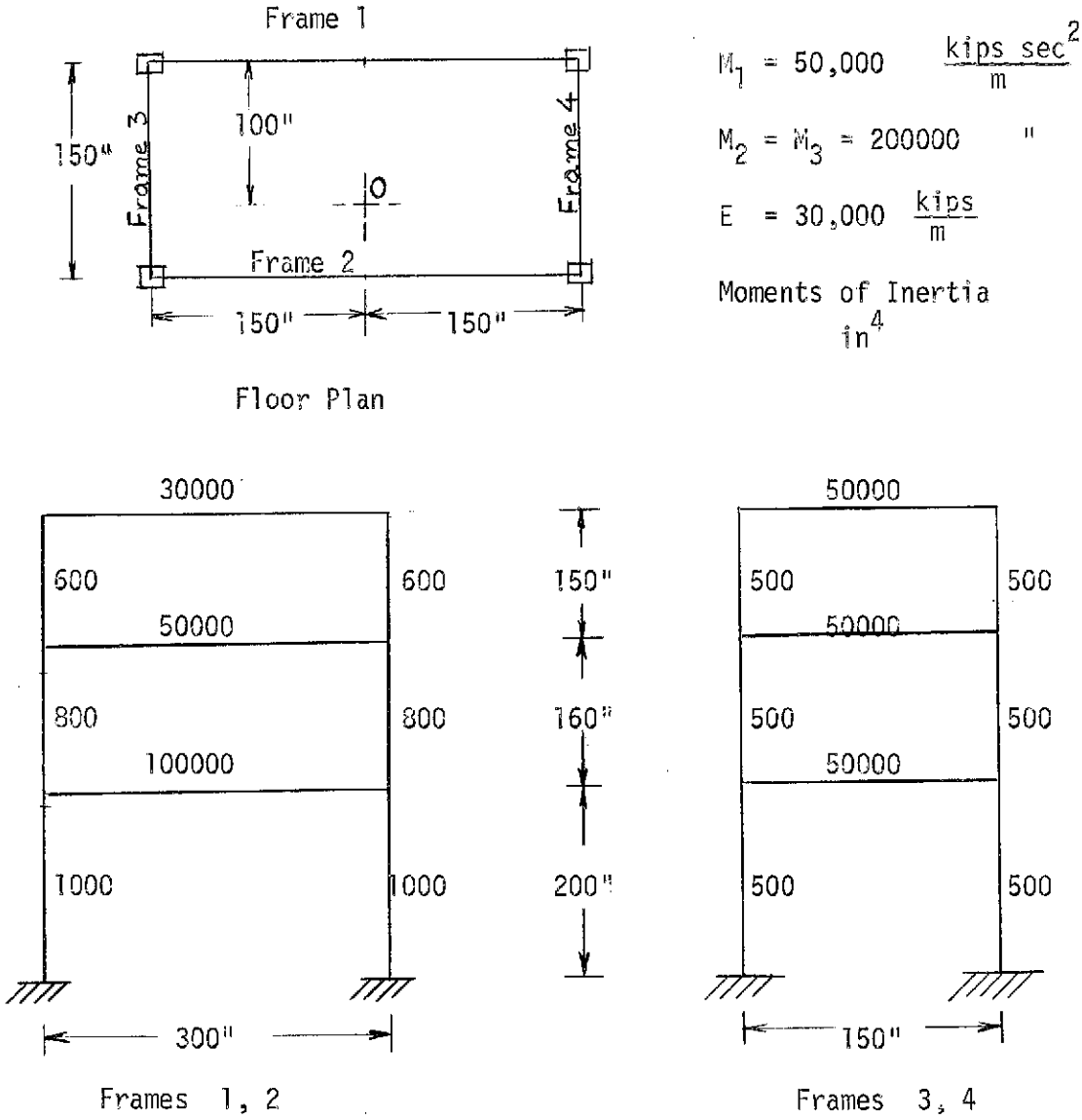

Figure 4-7 3-Story - 1-Bay Building with Eccentricity
Very Stiff Girders, No Column Shortening

Mode	1	2	3	4	5	6	7	8	9
T_{approx}	3.058	1.78	1.331	.811	.475	.459	.415	.327	.260
T_{exact}	3.056	1.78	1.328	.806	.473	.455	.409	.324	.256

Table 4-6 Exact and Approximate Periods in Seconds for a Three-Story Space Structure

The second structure analyzed was a 13-story steel frame. It is identical to the frame SFY1 whose properties are given in chapter 5, except for the first story which here is 25% stiffer. The axial deformations of the columns were taken into account for the exact solution. Periods for the first 4 modes are given in table 4-7.

Mode	1	2	3	4
T_{approx}	4.447	1.561	.931	.717
T_{exact}	4.410	1.470	.818	.565

Table 4-7 Exact and Approximate Periods in Seconds for SFY1 Frame

Again the agreement for the first mode at least is very good. It is a little surprising, however, that the approximate periods are slightly larger than the exact, while the opposite should be expected. The explanation to this is that the particular frame analyzed has 4 spans and very flexible girders. So the effect of the axial shorten-

ing of the columns is really negligible in this case. The above difference is due to the other approximations involved in the formula used to estimate the story stiffness. The effect of the column shortening, however, is apparent in the next case. The frame shown in figure 4-8, which was taken from reference (76) is a frame designed by Clough and Benuska (7) and used for their analyses reported in reference (7). We ran this frame first with the program developed for this thesis, and second with an exact program that performs dynamic analyses of multistory frames, accounting for all the degrees of freedom. The exact analysis was done for three cases. The only difference between them was the axial deformations of the columns. For the first case we assumed very large areas of the columns. For the second case we used numbers reported in reference (70) for an early version of this frame that assumes square columns, and in the third we used 1/10 the areas of the columns used in the second. The results for the first 4 modes are summarized in table 4.8.

Mode		1	2	3	4
Approximate		1.577	0.653	0.398	0.290
Exact	Case 1	1.563	0.642	0.387	0.278
	Case 2	1.862	0.702	0.404	0.288
	Case 3	3.521	1.018	0.528	0.362

Table 4-8 Exact and Approximate Periods in Seconds for Clough's Frame

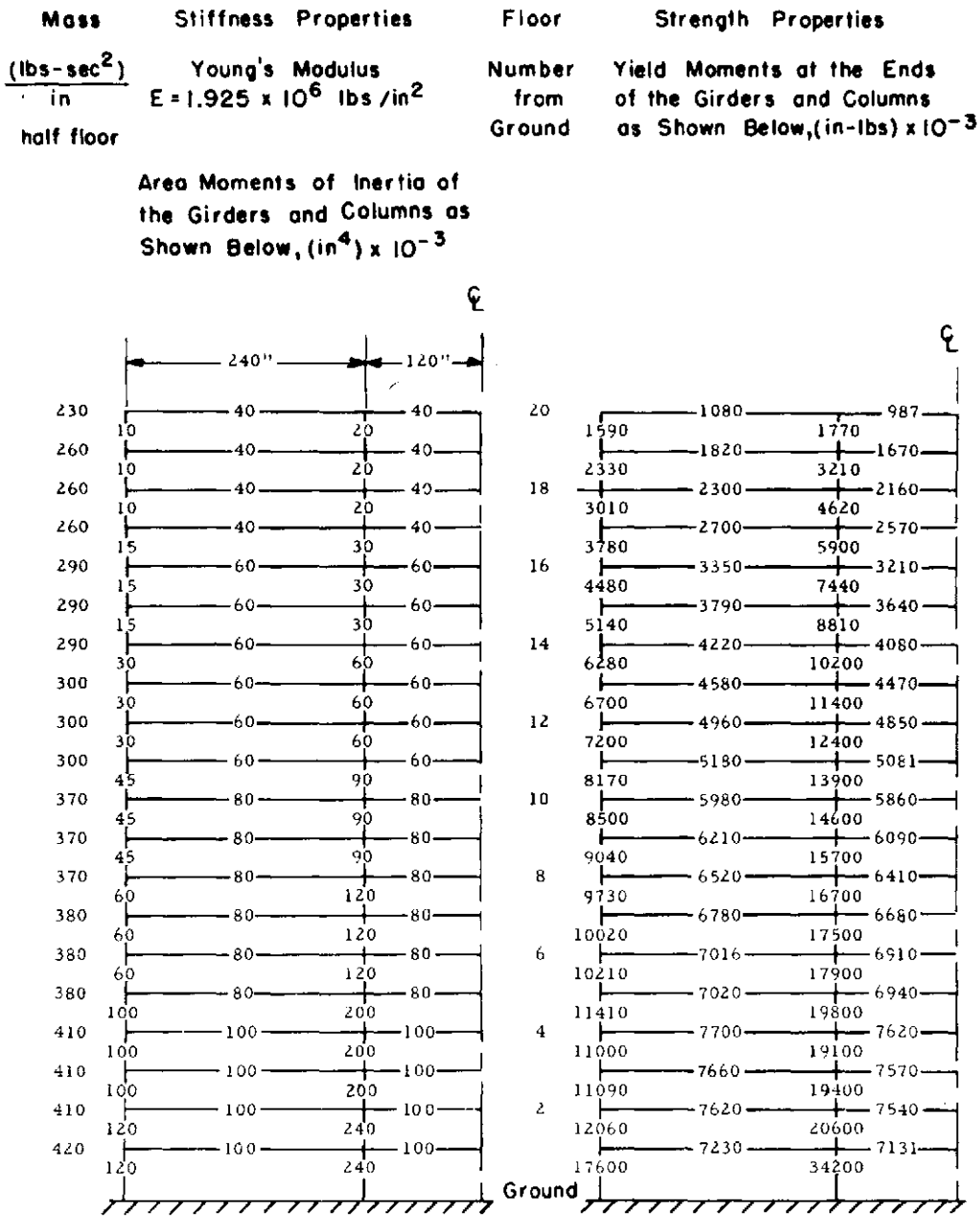

The structural parameters of the frame. Only half of the frame is shown since it is symmetric with respect to the center line . The height between floors is 144 inches except between ground and the first floor where it is 180 inches.

Figure 4-8 20-Story, 3-Bay Frame
(Adapted from Reference (76))

It is obvious from Table 4-8 that the effect of axial deformations of the columns for which the approximate method used here doesn't account, is important in this case. Clough and Benuska (7) and Giberson (76) report a first natural period for this frame of 2.2 seconds. Apparently then the areas of the columns used must be somewhere between those of cases 2 and 3. These areas were not available when this thesis was written.

The conclusion from all these comparisons is that the program gives good results in cases where the axial shortening of the columns is not important. If this is not the case, however, the frame cannot be properly considered as a close-coupled system.

4.6 Some Additional Considerations

A formulation that accounts for gravity loads and flexibility of the soil will be presented here. Due to time constraints, however, this formulation has not been implemented into the version of the program reported in this thesis.

4.6.1 Gravity loads.

The way in which gravity loads affect the deformations of structural members is by introducing secondary moments that are proportional to the displacements at any point. Assume that member AB in figure 4-9 is in equilibrium under the action of the lateral force F and the gravity load Mg. Also assume that the boundary conditions at A and B are such that the member has the general deflected shape

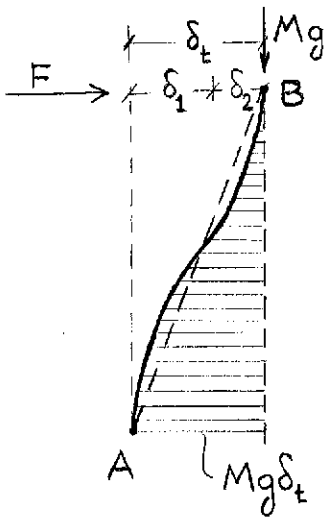

Figure 4-9 Effect of Gravity Loads

as shown in the figure. Let δ_1 be the displacement at B due to the action of F alone and δ_2 the additional displacement due to Mg. The additional moments introduced by the gravity load Mg are proportional to the shaded area with a maximum at A that is equal to $Mg\delta_t$. A straight line approximation to this moment diagram is also shown. This can be produced by a horizontal force $F' = Mg\delta_t/h$ acting at B. It can be immediately seen then, that the effect of gravity on the lateral stiffness is its reduction by a factor Mg/h, i.e.:

$$k_t = k - \frac{Mg}{h} \tag{4.26}$$

where $k = \frac{F}{\delta_1}$ is the lateral stiffness without including gravity load effects.

This can seen more rigorously as follows. Let us call:

$$f = \frac{\delta_1}{F} = \text{flexibility without gravity loads}$$

$$f_t = \frac{\delta_t}{F} = \text{flexibility with gravity loads.}$$

Then with the straight line approximation mentioned above we can write:

$$\delta_2 = f\,F' = f\,\frac{Mg\delta_t}{h} = f\,\frac{Mg}{h}\,(\delta_1 + \delta_2)$$

or

$$\delta_2 = \frac{\dfrac{Mg\delta_1^2}{hF}}{1 - \dfrac{Mg\delta_1}{hF}}$$

So

$$f_t = \frac{\delta_t}{F} = \frac{\delta_1 + \delta_2}{F}$$

and replacing δ_2 we obtain:

$$f_t = \frac{1}{\dfrac{1}{f} - \dfrac{Mg}{h}}$$

By definition, however:

$$k = \frac{1}{f}$$

So in terms of stiffnesses we have:

$$\frac{1}{k_t} = \frac{1}{k - \dfrac{Mg}{h}}$$

or

$$k_t = k - \frac{Mg}{h}$$

For a multidegree-of-freedom system, then, it is only necessary to add to the inertia forces of each level a force:

$$F_{jg} = - \sum_{\ell=j+1}^{n} M_\ell g \frac{\delta_{j+1}}{h_{j+1}} + \sum_{\ell=j}^{n} M_\ell g \frac{\delta_j}{h_j}$$

where:

F_{jg} = Additional force at level j

M_ℓ = Mass of floor ℓ

g = Acceleration of gravity

h_j, h_{j+1} = Heights of floors j, j+1

$\delta_j = u_j - u_{j-1}$

$\delta_{j+1} = u_{j+1} - u_j$

u_j, u_{j+1} = Displacements of floors j, j+1 relative to the ground.

4.6.2 Effect of soil flexibility

Soil flexibility can be incorporated in the analysis by adding appropriate springs and effective masses, whose properties will be determined from those of the soil (see for example Whitman and Richart (99)). In the general case we will have to consider six springs corresponding to the six degrees of freedom of the foundation. In this formulation, however, we will not consider vertical accelerations, but only swaying, rocking and torsion. In order to make the formulation easier to understnad, a two-degree-of-freedom system having rocking and swaying of the foundation will first be considered, and then we will generalize it for multidegree-of-freedom systems in two directions, including torsion as well. Figure 4-10 shows the system considered.

The structural properties are described by k_L, the lateral stiffness matrix of the structure for rigid foundation. Thus the formulation is valid for both close-coupled and far-coupled systems.

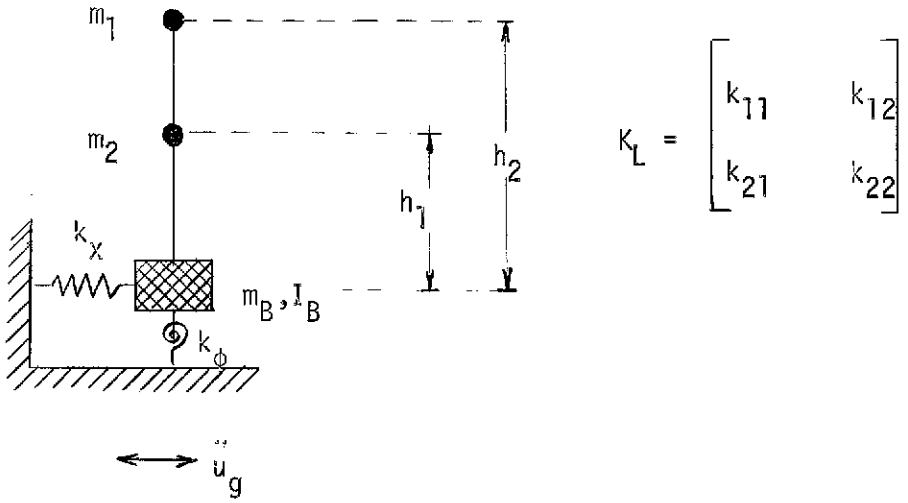

Figure 4-10 2-D.O.F. System with Flexible Foundation

The expressions for the absolute displacements of the three masses are:

$$\left.\begin{aligned} u_{1t} &= u_1 + u_g = \delta_1 + u_B + h_1 \phi_B + u_g \\ u_{2t} &= u_2 + u_g = \delta_2 + u_B + h_2 \phi_B + u_g \\ u_{BT} &= u_B + u_g \end{aligned}\right\} \qquad (4.27)$$

where:

$$\left.\begin{aligned} \delta_1 &= u_1 - u_B - h_1 \phi_B \\ \delta_2 &= u_2 - u_B - h_2 \phi_B \end{aligned}\right\} \quad \text{Structural deformation} \qquad (4.28)$$

u_B, ϕ_B : displacement and rotation of the foundation.

The equations of motion can then be written as follows:

$$
\left.
\begin{aligned}
& m_1\ddot{u}_{1T} + k_{11}\,\delta_1 + k_{12}\,\delta_2 = 0 \\
& m_2\ddot{u}_{2T} + k_{21}\,\delta_1 + k_{22}\,\delta_2 = 0 \\
& m_B\ddot{u}_{BT} + k_x u_B - (k_{11} + k_{21})\,\delta_1 - (k_{12} + k_{22})\,\delta_2 = 0 \\
& I_B\ddot{\phi}_B + k_\phi\phi_B - (k_{21}\,h_2 + k_{11}\,h_1)\,\delta_1 - (k_{22}\,h_2 + k_{12}\,h_1)\,\delta_2 = 0
\end{aligned}
\right\}
$$

and replacing δ_1, δ_2 obtained from 4.28:

$$
\left.
\begin{aligned}
& m_1\ddot{u}_1 + k_{11}u_1 + k_{12}u_2 - (k_{11} + k_{12})u_B - (k_{11}h_1 + k_{12}h_2)\phi_B = -\,m_1\ddot{u}_g \\
& m_2\ddot{u}_2 + k_{21}u_1 + k_{22}u_2 - (k_{21} + k_{22})u_B - (k_{21}h_1 + k_{22}h_2)\phi_B = -\,m_2\ddot{u}_g \\
& m_B\ddot{u}_B - (k_{11} + k_{12})u_1 - (k_{12} + k_{22})u_2 + \\
& \qquad (k_x + k_{11} + k_{12} + k_{21} + k_{22})u_B + \\
& \qquad (k_{11}h_1 + k_{21}h_1 + k_{12}h_2 + k_{22}h_2)\phi_B = -\,m_B\ddot{u}_g \\
& I_B\ddot{\phi}_B - (k_{11}h_1 + k_{21}h_2)u_1 - (k_{21}h_1 + k_{22}h_2)\,u_2 + \\
& \qquad (k_{11}h_1 + k_{21}h_2 + k_{12}h_1 + k_{22}h_2)u_B + \\
& \qquad (k_{11}h_1^2 + k_{21}h_1h_2 + k_{12}h_1h_2 + k_{22}h_2^2 + k_\phi)\phi_B = 0
\end{aligned}
\right\} \quad (4.29)
$$

These are the differential equations of motion for the system of figure 4.10. The unknowns are defined by equations 4.27 and 4.28. In matrix form these equations can be written as:

$$
\begin{array}{c}
\overset{\longleftarrow 2 \longrightarrow}{} \quad \overset{\longleftarrow 1 \longrightarrow}{} \quad \overset{\longleftarrow 1 \longrightarrow}{} \\
\begin{matrix} 2 \\ 1 \\ 1 \end{matrix}
\begin{bmatrix}
K_1 & -K_L I & -K_L H \\
-I^T K_L & k_x + I^T K_L I & I^T K_L H \\
-H^T K_L & H^T K_L I & k_\phi + H^T K_L H
\end{bmatrix}
\begin{bmatrix} u_1 \\ u_2 \\ u_B \\ \phi_B \end{bmatrix}
+
\begin{bmatrix}
m_1 & & & 0 \\
& m_2 & & \\
& & m_3 & \\
0 & & & I_B
\end{bmatrix}
\begin{bmatrix} \ddot{u}_1 \\ \ddot{u}_2 \\ \ddot{u}_B \\ \ddot{\phi}_B \end{bmatrix}
=
\end{array}
$$

$$
= - \begin{bmatrix} m_1 \\ m_2 \\ m_B \\ 0 \end{bmatrix} \ddot{u}_g \qquad (4.30)
$$

where: $I = \begin{bmatrix} 1 \\ 1 \end{bmatrix}$, $H = \begin{bmatrix} h_1 \\ h_2 \end{bmatrix}$

The numbers around the stiffness matrix define the dimensions of the corresponding submatrices.

The part of the total displacements of the structure needed for the determination of forces is computed from 4.28 after u_1, u_2, u_B, ϕ_B have been determined from 4.30. The generalization of the above procedure to a system with 3n degrees of freedom is done as follows. First we write in vector notation the equations for the displacements corresponding to 4.27 and 4.28, but including torsion as well.

$$
\left.
\begin{aligned}
U_t &= U + I\, u_g = \delta_x + I\, u_B + H\, \phi_{BY} - Y_m\, \theta_B \\
V_T &= V + I\, v_g = \delta_y + I\, v_B - H\, \phi_{BX} + X_m\, \theta_B \\
\theta_T &= \theta \qquad\quad = \theta_s + I\, \theta_B
\end{aligned}
\right\} \qquad (4.31)
$$

where

$$\left.\begin{aligned} \delta_x &= U - I\, u_B - H\, \phi_{BY} + Y_m\, \theta_B \\ \delta_y &= V - I\, v_B + H\, \phi_{BX} - X\, \theta_B \\ \theta_s &= \theta - I\, \theta_B \end{aligned}\right\} \qquad (4.32)$$

Figure 4-11 shows the coordinate system used.

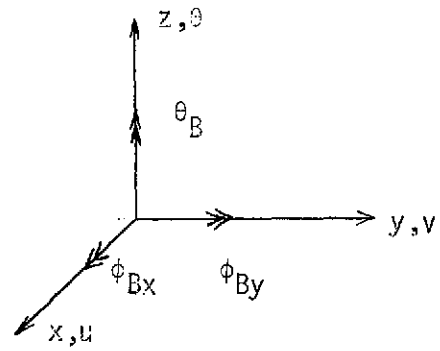

Figure 4-11 Coordinate System Used

If we replace u,v,θ in equation 4.13 by the above expressions for δ_x, δ_y, θ_s and in the right-hand side we put the vector of inertial forces, we have the equations of motion for the masses in the structure. Since the stiffness matrix is symmetric, the equations for the foundation can be easily written. Diagonal terms are of the form of the ones in equation 4.30. The upper part of the stiffness matrix, the mass matrix, the displacement vector and the load vector are given in the following pages. Also given are the sizes of the various submatrices.

$$
\begin{array}{c}
\begin{array}{c} \\ n \\ n \\ n \\ 1 \\ 1 \\ 1 \\ 1 \\ 1 \end{array}
\begin{array}{c}
\begin{array}{cccccccc} n & n & n & 1 & 1 & 1 & 1 & 1 \end{array} \\
\begin{bmatrix}
M_x & & & & & & & \\
 & M_y & & & & & & \\
 & & I & & & & & \\
 & & & m_{bx} & & & & \\
 & & & & m_{by} & & & \\
 & & & & & I_{By} & & \\
 & & & & & & I_{Bx} & \\
 & & & & & & & I_{Bz}
\end{bmatrix}
\end{array}
\end{array}
$$

Augmented Mass Matrix

$$
\begin{bmatrix} U \\ V \\ \theta \\ u_B \\ v_B \\ \phi_{BY} \\ \phi_{BX} \\ \theta_B \end{bmatrix}
\begin{array}{c} n \\ n \\ n \\ 1 \\ 1 \\ 1 \\ 1 \\ 1 \end{array}
-
\begin{bmatrix} M_x\ddot{u}_g \\ M_y\ddot{v}_g \\ 0 \\ m_{bx}\ddot{u}_g \\ m_{by}\ddot{v}_g \\ 0 \\ 0 \\ 0 \end{bmatrix}
$$

Displacement Vector

Load Vector

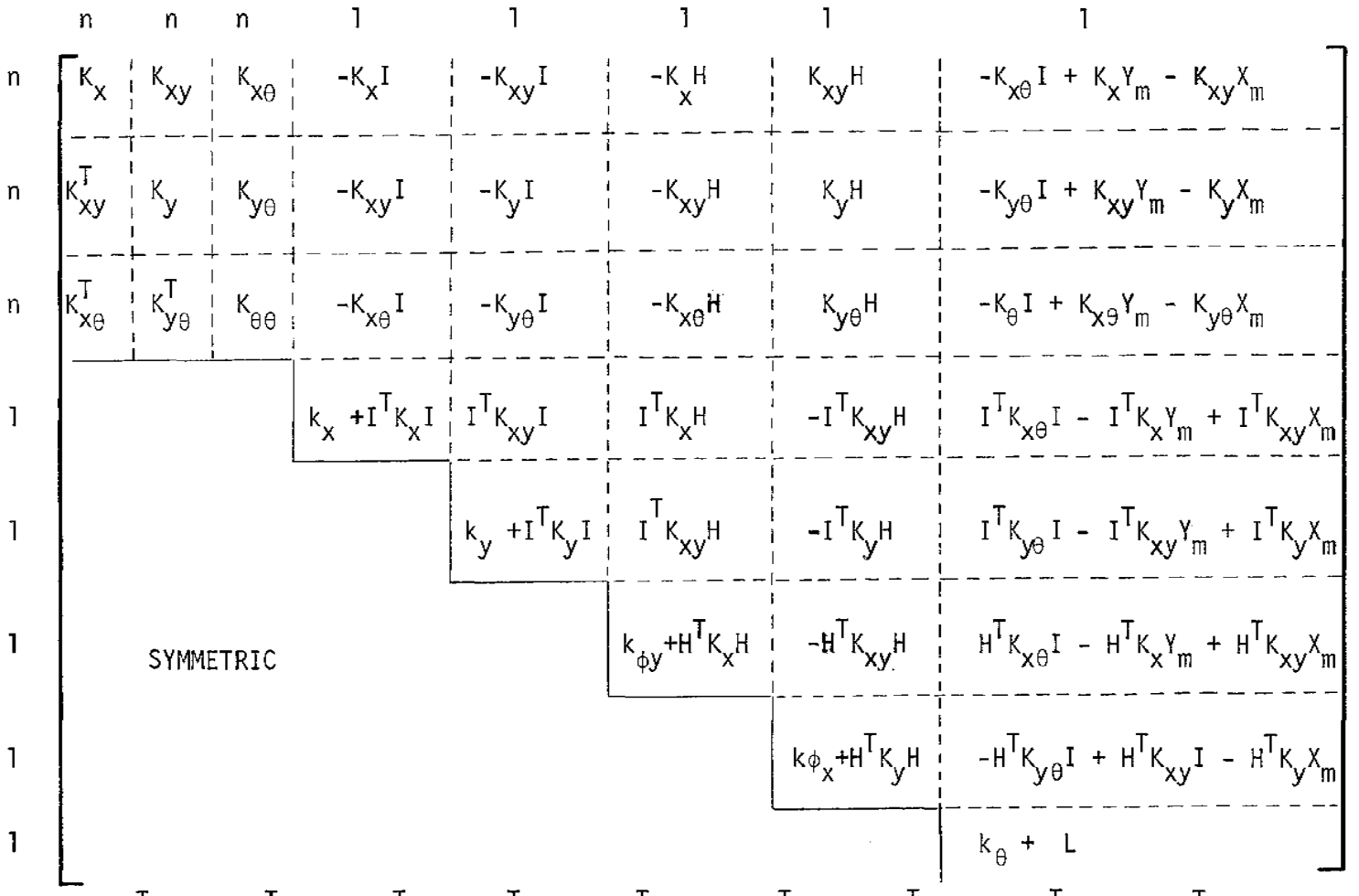

$$L = Y_m^TK_xY_m + X_m^TK_yX_m + I^TK_\theta I - Y_m^TK_{x\theta}I - I^TK_{x\theta}Y_m + X_m^TK_{y\theta}I + I^TK_{y\theta}X_m - X_m^TK_{xy}Y_m - Y_m^TK_{xy}X_m$$

Augmented Stiffness Matrix

The stiffnesses of the soil springs are in the diagonal terms, k_x, k_y for swaying, $k_{\phi x}$, $k_{\phi y}$ for rocking and k_θ for torsion.

I is a unit vector.

H is a vector with the heights measured from the level of the horizontal springs.

X_m, Y_m, vectors containing the x and y coordinates of the centers of masses.

m_{bx}, m_{by} = effective masses of the foundation.

I_{bx}, I_{by}, I_{Bz} = effective moments of inertia of the foundation.

Thus we have (3n + 5) equations witn (3n + 5) unknowns.

CHAPTER 5

RESPONSE OF MULTIDEGREE-OF-FREEDOM SYSTEMS UNDER EARTHQUAKE EXCITATION

5.1 Introduction

The computer program described in the previous chapter was used for the analysis of several buildings and the results obtained are reported here. Three typical frames with 5, 10 and 20 stories were designed and analyzed in an attempt to investigate to what extent the conclusions reached in chapter 3 for 1-DOF systems apply to multi-degree-of-freedom systems (M-DOF) as well. Torsion was introduced in one case by assuming eccentric masses and ductility factors are compared with those when there is no torsion. Next, results from the analysis of three different buildings are presented. The first one is a 13-story steel frame building, the second is a 17-story concrete shear wall building, and the third one is an 11-story concrete frame building. They were all designed by an engineering firm according to the Uniform Building Code (U.B.C.). Each of them was actually designed for 5 (0,1,2,3,4) earthquake zones (4 being an extra one added), so for each building several designs were produced. Each of these designs was analyzed for an artificial earthquake scaled to seven different intensities. The results of these studies are intended for damage prediction during an earthquake; not all of them, however, will be reported here.

Clough and Benuska (7), Goel (8), and Anderson (9) have done the most systematic studies on inelastic response. Clough's studies

are the most reliable source of information on inelastic response of plane frames. The basic frame that he used is the one shown in figure 4-8 and his main conclusion is that yielding occurs mainly in the girders, while the columns remain elastic except for the ones of the top few floors. For the El Centro earthquake, ductility factors up to 5 should be expected in the girders. He has used bilinear moment curvature relations and has neglected the effect of axial loads on the plastic moment capacity of the members. He also studied buildings consisting of shear walls and moment-resisting frames. Goel's main frame has 1 bay, 25 stories, and he analyzed it for three different records, all scaled to the same intensity (1.5 x El Centro). He has used moment-curvature relationships of the Ramberg-Osgood type, and he assumed that the columns remain elastic. The rest of his assumptions are the same as Clough's. His conclusions are in general similar to Clough's, except that the ductility factors he obtained are always much smaller. He also concludes that the effect of gravity loads on the ductility requirements is insignificant, while the frequency contents of the accelerogram are very important. Anderson used a 1-bay 10-story and a 1-bay 20-story frame to compare the effect of the design philosophy on the inelastic seismic response. He compared minimum weight design, allowable stress, and strong column-weak girder design. He used bilinear moment-curvature laws, he included gravity loads, and he allowed for hinge formation in the span of the girders. He also included the reduction of the plastic moment capacity of the columns due to the axial loads. His main findings are

that minimum weight design produces frames unacceptable for effective seismic resistance and that strong-column weak-girder frames are superior to those produced by the allowable stress method. The ductility factors he obtains are about similar to those of Clough, except for the columns of the frame that were designed according to allowable stresses, where he obtains much larger numbers. This is due to the reduction in effective yield moment caused by axial-flexural interaction.

While the above conclusions are valid for the particular frames and models used, extrapolation of these conclusions to other cases is questionable. The main reason for this is due to the geometry of the frames analyzed. It was pointed out in chapter 4 that axial shortening of the columns of Clough's frame produces an increase in the period of vibration from 1.577 sec. to 2.2 sec. This effect is even more pronounced for the frames in references (8) and (9), since these frames have only 1 bay and 10 to 40 stories. Results for 20-story, 1-bay frames may not be applicable to cases where axial shortening of the columns is negligible.

5.2 Effect of Natural Period on Ductility Requirements of MDOF-Close-Coupled Systems

One of the conclusions from the studies in chapter 3 of this thesis was that the ductility requirements of 1-DOF non-linear systems, whose strength was based on base shears computed by code procedures, depend on the natural period of the system, increasing as the natural

period decreases. In order to see whether the same conclusions can be extended to MDOF-systems as well, three basic frames with 5, 10 and 20 stories were analyzed. The 20-story frames are variations of the basic frame used in references (7) and (76). The properties of the frames analyzed and the ductility factors obtained are shown in figures 5-1 through 5-5. The stiffness variation with height for all the cases is linear, with a slope similar to that of the basic frame in reference (7), but the numerical values were adjusted to give periods of 0.5, 1.0 and 2.2 seconds. The frames were designed according to the U.B.C. for gravity loads and zone-3 earthquakes. The plastic moments were then assumed to be twice the design moments for the girders and six times for the columns. Ultimate strength was then estimated as described in chapter 2. The force deflection model used was trilinear with first breaking point at one-half the ultimate strength and ductility factors were computed with yield displacements corresponding to this point. The excitation was the first 10 seconds of the NS component of the El Centro 1940 record. 10% of viscous damping was assumed in all the cases.

Two 5-story frames were analyzed (Figure 5-1), the difference between them being that B has its 1^{st} story 12% stronger than A and also has stronger strength taper. This was achieved by varying the relative stiffnesses of columns and girders. We see that frame A has a very large ductility factor (~ 10.3) at the bottom story, while for B it is the second story that has the biggest. In both frames, however, the ductility factors are largest at the lower stories, decreas-

STORY	STIFFNESS	MASS	STRENGTH	
			FRAME A	FRAME B
1	372.	.190	62.	70.
2	324.	.190	60.	59.
3	276.	.167	48.	48.
4	228.	.167	46.	44.
5	180.	.136	34.	30.
PERIOD			.5 sec	
3 BAYS @ 20'		5 STORIES @ 12'		

* UNITS : Kips, inches

PROPERTIES OF 5 STORY FRAMES

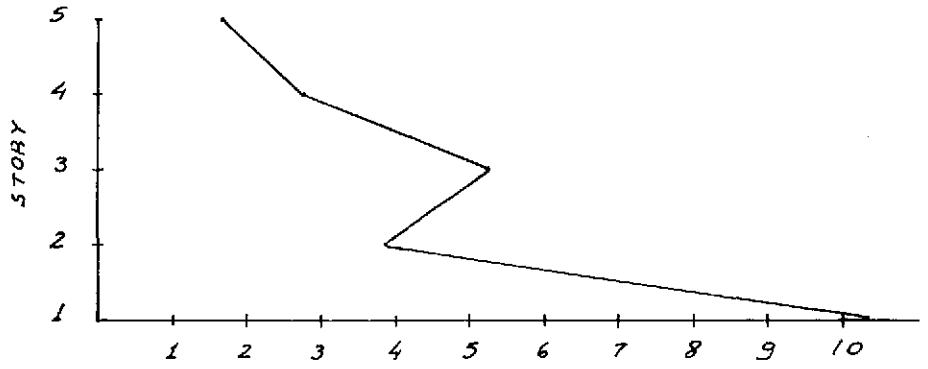

DUCTILITY FACTOR FRAME A

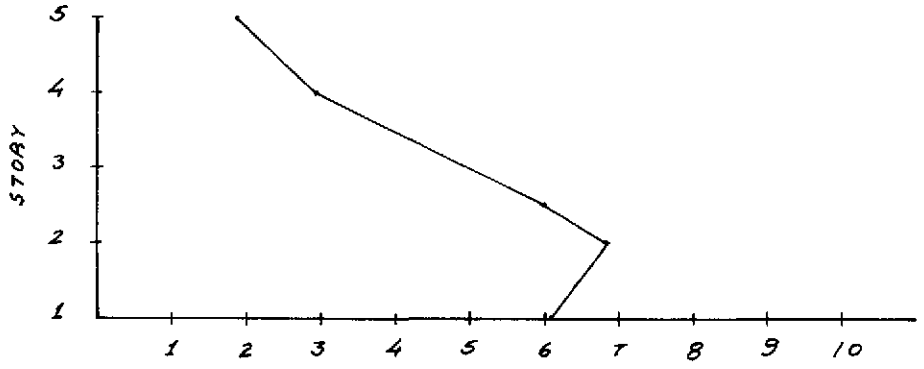

DUCTILITY FACTOR FRAME B

Figure 5-1 PROPERTIES AND RESULTS FOR 5-STORY FRAMES

ing continuously from bottom to top. The average ductility for all stories is 4.8 for frame A and 4.7 for B. The same behavior is observed in Figure 5-2 for the 10-story frames. The maximum ductility for A is about 5 and for B about 6, while the average for all stories is 3.2 and 3.35 respectively.

Figure 5-3 shows the properties of the three 20-story frames analyzed. The only significant difference between A and B is the strength of the first story, which for B was again made larger. Both frames have a natural period of 2.2 sec. Frame C is identical to that of Figure 4-8 and has a natural period of 1.577 sec. All three frames have the same masses and the same variation of stiffness from top to bottom. The numerical values for the stiffnesses of A, B were chosen so as to match the natural period of the frame reported in references (7) and (76). Strengths for these two frames were computed as described above, while for frame C the properties of Figure 4-8 were used. At this point it must be recalled from the previous chapter that the difference between the natural period 2.2 reported for frame C and 1.577 obtained here is due to the axial shortening of the columns which is not accounted for in our model. Ductility factors for frames A and B are very similar except from the first story, the difference being due to the strength increase of this story for frame B. The behavior of frame C (Figure 5-5) is very similar to that of A, except that its ductility factors are slightly higher. The average ductility for all the 20 stories are 1.94, 1.9 and 2 for A, B and C respectively. It is interesting to observe

STORY	STIFFNESS	MASS	STRENGTH	
			FRAME A	FRAME B
1	564.	.292	126.	126.
2	564.	.292	118.	113.
3	516.	.292	116.	112.
4	468.	.272	105.	104.
5	420.	.272	101.	99.
6	372.	.272	97.	94.
7	324.	.252	82.	82.
8	276.	.252	77.	74.
9	228.	.252	70.	68.
10	180.	.233	60.	50.
PERIOD			1.0 sec	
3 BAYS @ 20' 1st STORY 15', REST @ 12'				

* UNITS kips, inches

PROPERTIES OF 10 STORY FRAMES

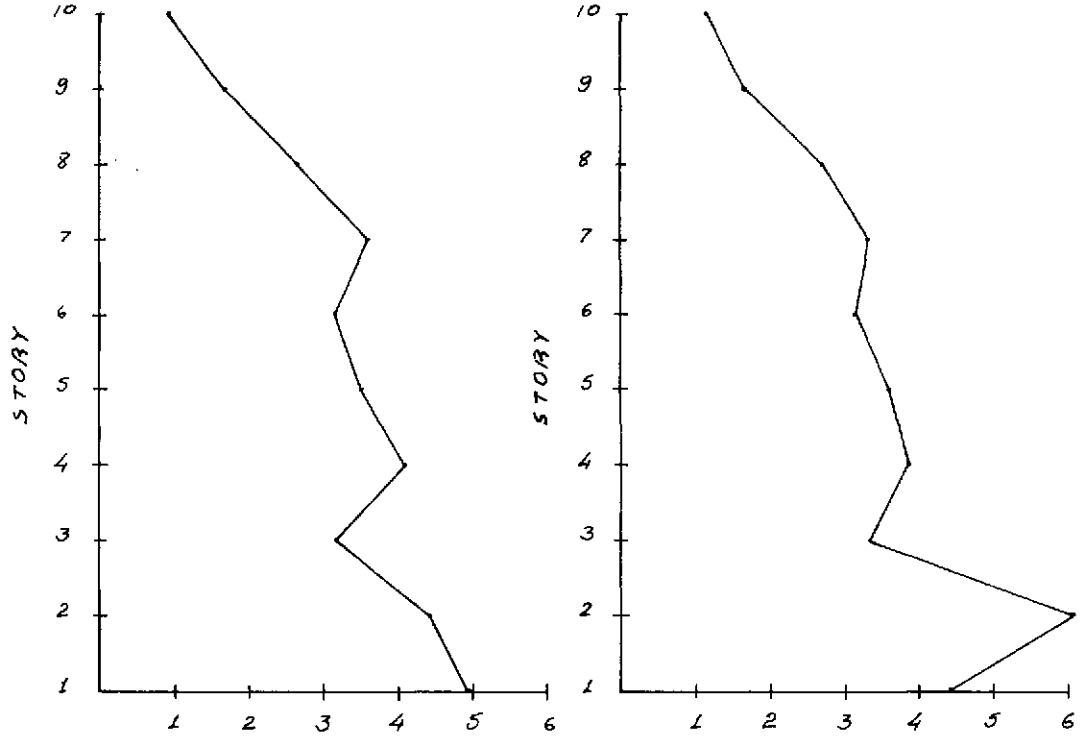

DUCTILITY FACTOR FRAME A DUCTILITY FACTOR FRAME B

Figure 5-2 PROPERTIES AND RESULTS FOR 10-STORY FRAMES

STORY	MASS	FRAME A		FRAME B		FRAME C	
		STIFFN.	STRENG.	STIFFN.	STRENG.	STIFFN.	STRENG.
1	.420	558.	240.	564.	320.	1096.	240.
2	.410	567.	316.	564.	316.	1114.	316.
3	.410	545.	318.	545.	316.	1071.	318.
4	.410	545.	319.	545.	316.	1071.	319.
5	.380	497.	291.	497.	290.	977.	291.
6	.380	405.	291.	405.	290.	796.	291.
7	.380	405.	281.	405.	280.	796.	281.
8	.370	405.	270.	405.	270.	796.	270.
9	.370	370.	257.	370.	256.	726.	257.
10	.370	370.	247.	370.	246.	726.	247.
11	.300	334.	214.	334.	214.	655.	214.
12	.300	266.	205.	266.	204.	522.	205.
13	.300	266.	189.	266.	188.	522.	189.
14	.290	266.	174.	266.	172.	522.	174.
15	.290	193.	156.	193.	154.	380.	156.
16	.290	193.	138.	193.	136.	380.	138.
17	.260	174.	111.	174.	110.	341.	111.
18	.260	128.	94.	128.	92.	253.	94.
19	.260	128.	74.	128.	72.	253.	74.
20	.230	128.	44.	128.	48.	253.	74.
PERIOD		2.21 sec				1.577 sec	
3 BAYS @ 20'		1st STORY 15', REST @ 12'					

PROPERTIES OF 20 STORY FRAMES

* UNITS kips, inches

Figure 5-3 PROPERTIES OF 20-STORY FRAMES

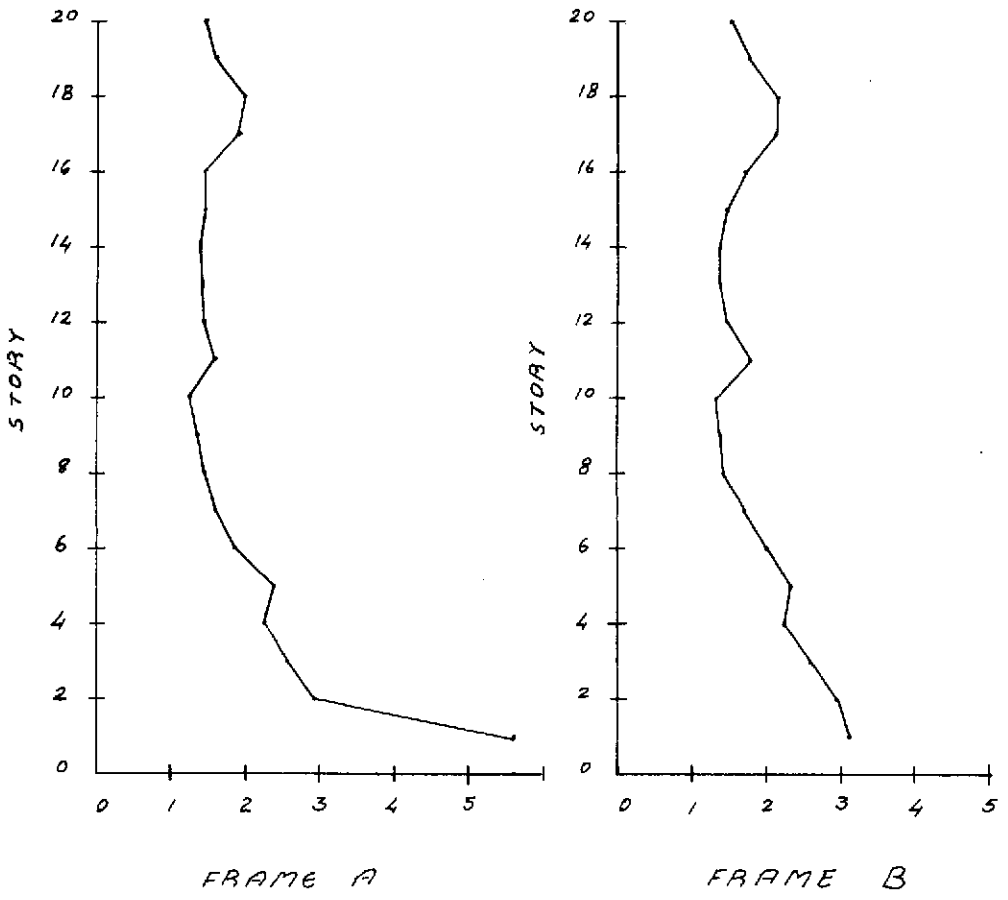

Figure 5-4

MAXIMUM DUCTILITY REQUIREMENTS FOR 20-STORY FRAMES A AND B

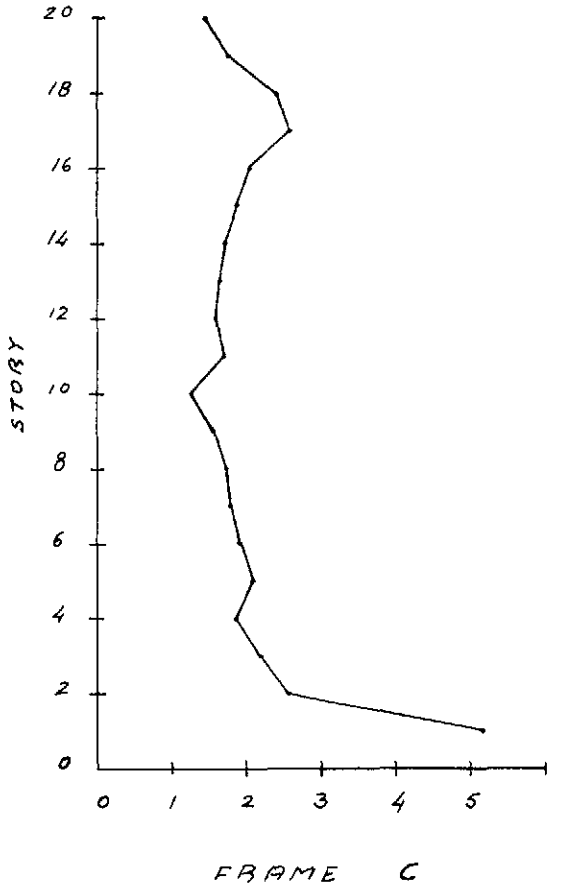

Figure 5-5

MAXIMUM DUCTILITY REQUIREMENTS FOR 20-STORY FRAME C

that the variation of the ductility factors with height is similar to that reported for the girders of the same frame in reference (7), except for the lower stories. The explanation for this is that for this particular frame most of the inelastic action takes place in the girders, while the columns remain elastic. On the other hand, since our model cannot account for axial deformations of the columns, it is bound to have a first modal shape close to that of a shear beam, which has the largest interstory distortions at the lower stories. This is very clearly shown in Figure 5-6, in which the maximum relative displacements for frame A are compared to those from reference (7). We see that our model predicts larger displacements at the lower stories, while for the rest there is reasonable agreement. Concentration of yielding in one story creates "soft story" action which reduces the response of the stories above. It is partly for this reason that the average ductility for all stories here is slightly less than that of Clough as reported in chapter 3.

All the above suggest that ductility requirements for frames designed by the U.B.C. increase as the period of the structure decreases. This is in agreement with the conclusions reached in chapter 3 for 1-DOF systems. They also suggest that for buildings which deflect essentially like a shear beam (axial shortening of the columns negligible), the first story should be made either stronger than what usual design practice produces, or more ductile. In cases, however, where axial deformation of the columns is important, the simplified model of this thesis will overestimate ductilities at the

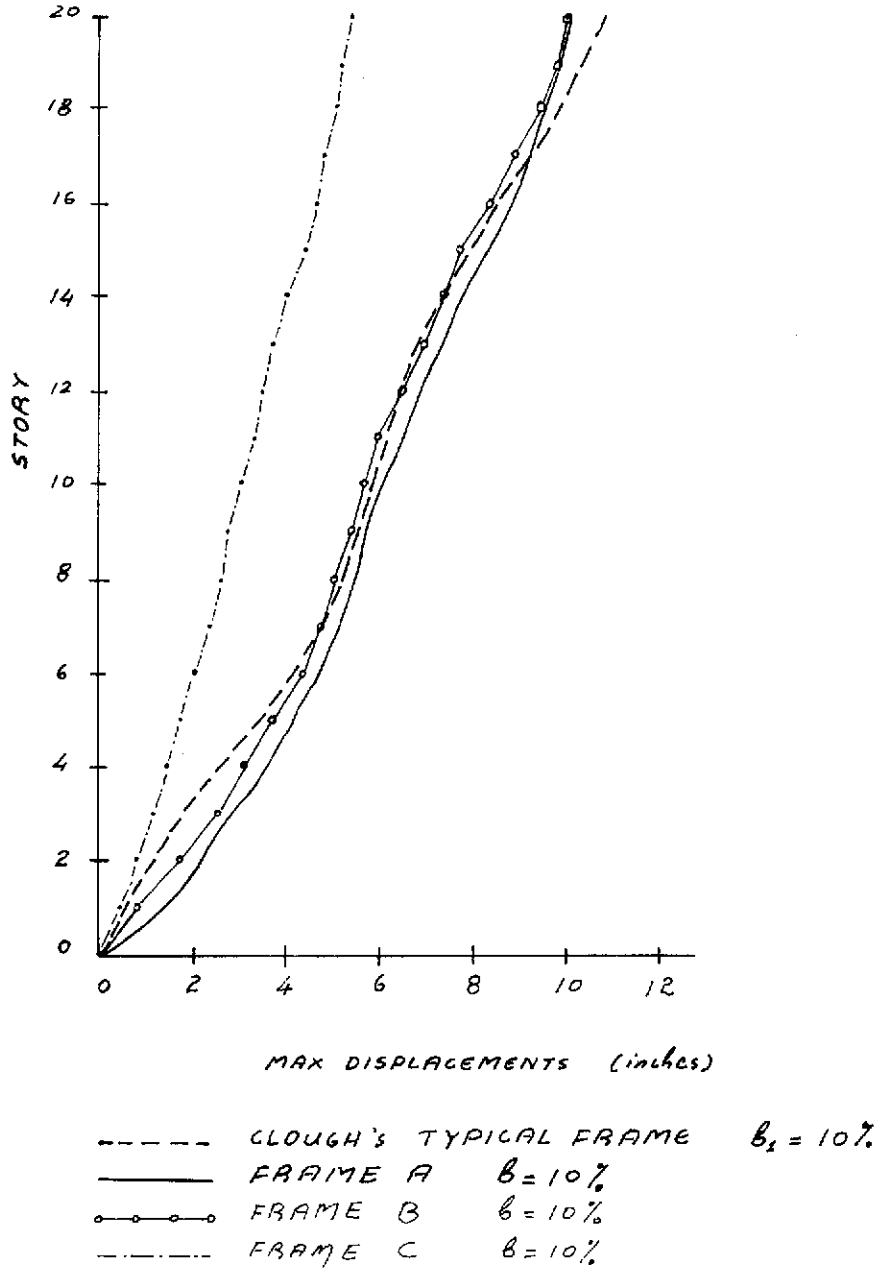

Figure 5-6 COMPARISON WITH CLOUGH'S FRAME

lower stories and underestimate them at the top.

5.3 Effect of Torsion on Ductility Requirements

Almost all of the studies on inelastic response of MDOF-systems are for planar frames, the main reason for this being the rapid increase of computational requirements for increasing numbers of degrees of freedom. With our model, however, in which we have reduced the total number of degrees of freedom to three per floor, it is possible to study non-symmetric structures with mass eccentricities and to investigate the effect of torsion on the inelastic response. Torsion is always undesirable in earthquake resistant design, because it introduces additional shears and moments to the various structural components. When the structure starts going inelastic, torsional effects may be aggravated due to possible unsymmetric yielding and shift of the original torsional center.

In order to illustrate the capability of the computer program to deal with unsymmetric situations in space and at the same time see the effect of torsion on the ductility requirements, two 5-story structures (Figure 5-7) were analyzed for 10 sec. of the NS El Centro 1940 record. All the frames are identical to frame A of Figure 5-1 and for case A the mass eccentricity is zero, while for B it is constant for all the floors and equal to d/6. The masses, mass-moments of inertia, and natural periods for cases A and B are summarized on the following page (Table 5-1). 10% of viscous damping was assumed for all the modes.

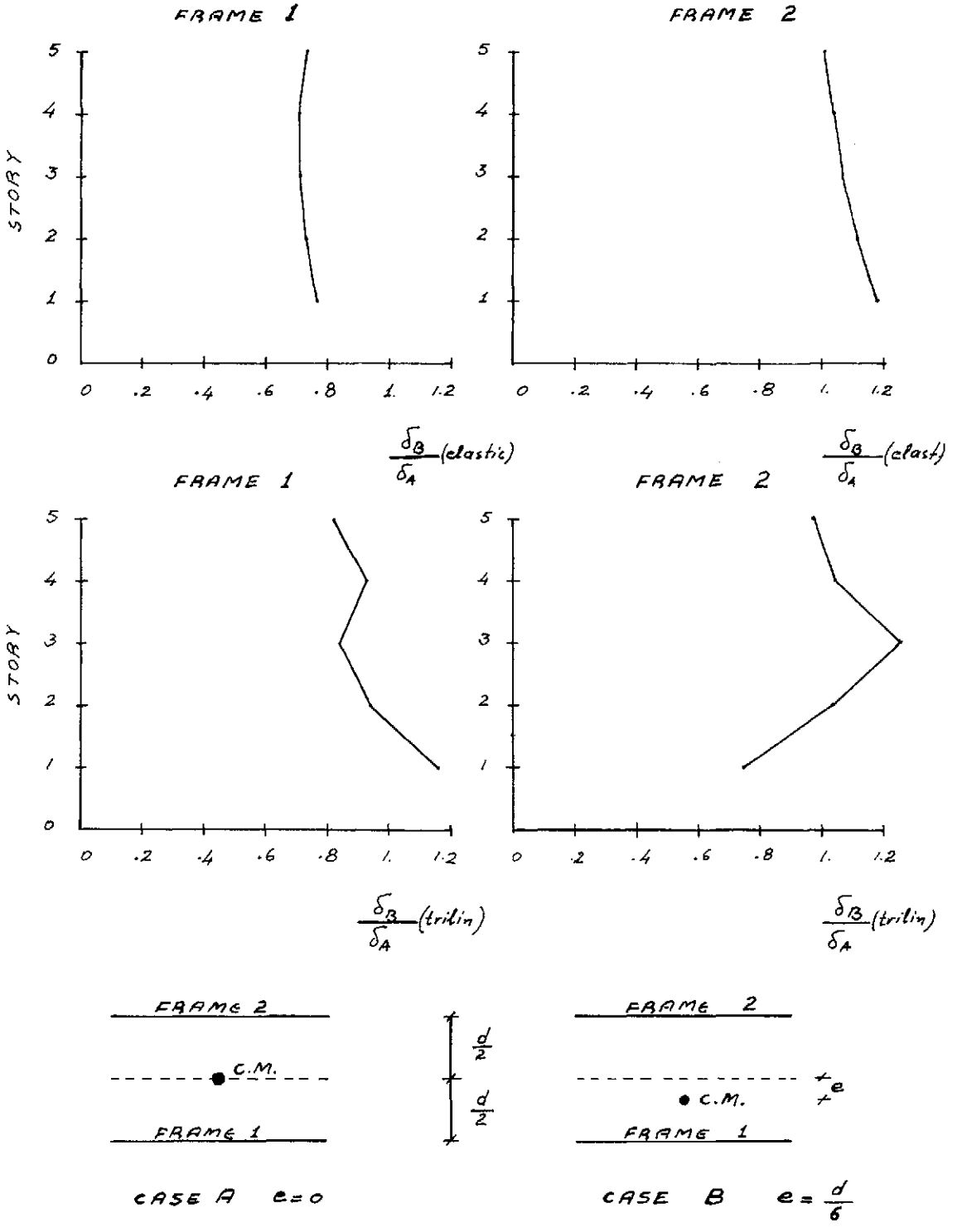

Figure 5-7 EFFECT OF TORSION

	CASE A				CASE B			
Floor	Mass	Inertia	Mode	Period	Mass	Inertia	Mode	Period
1	.380	20500.	1	.646	.380	20500.	1	.690
2	.380	20500.	2	.501	.380	20500.	2	.469
3	.334	18000.	3	.250	.334	18000.	3	.267
4	.334	18000.	4	.193	.334	18000.	4	.181
5	.272	14700.	5	.161	.272	14700.	5	.172

Table 5-1 Properties for Torsion

The first mode of both structures is torsional and the second translational. The translational period in case A is identical to that of the 5-story frame alone, while in case B it has been reduced to .469 due to the coupling with torsion. The results are presented in terms of the ratio of the maximum interstory displacements for case B (eccentric masses), to the maximum interstory displacements for case A (no eccentricity). For the inelastic case, this ratio is equal to the ratio of the ductility factors for the two cases. The top part of Figure 5-7 is for elastic behavior which was achieved by setting very high strengths so that yielding never took place. In the elastic case we see that frame 1 has reduced distortions, while for frame 2 they have increased. The increase is larger for the lower stories and becomes less for the top ones. In the inelastic case, however, the behavior becomes irregular, and for both frames there are stories where the ductility requirements have increased. For case B the maximum increase is 26% and occurs at the 3^{rd} floor, while for A it is 16% and occurs at the 1^{st}. This increase of ductility

requirements, when torsion is introduced into the structure, can be explained with the reasoning given at the beginning of this paragraph. At this point it seems that more cases should be investigated by varying the amount and the distribution of mass eccentricities at the different levels and by using a wider range of structures (to include also shear walls), before quantitative suggestions can be made.

5.4 Response of 3 Symmetric Buildings to an Artificial Earthquake

The three buildings for which results will be presented here were designed by an engineering firm for gravity and earthquake loads, according to standard design procedures. They were selected so as to represent typical apartment or office buildings in the Boston area, as part of ongoing research for optimum seismic protection. Although they have been claimed as typical, they are somewhat flexible, especially the steel building.

The motion for which these buildings were analyzed is an artificial earthquake with duration of 10 seconds. The input modulating time function has a rise time of 2 seconds, is constant between 2 and 7 seconds, and decreases linearly to zero between 7 and 10 seconds. The response spectra of this particular motion for $\ddot{u}_{g_{max}} = .11g$ and for several values of viscous damping are shown in Figure 5-8. This motion was scaled to several peak ground accelerations with a maximum $\ddot{u}_{g_{max}} = .27g$ and all the results presented here are for this value.

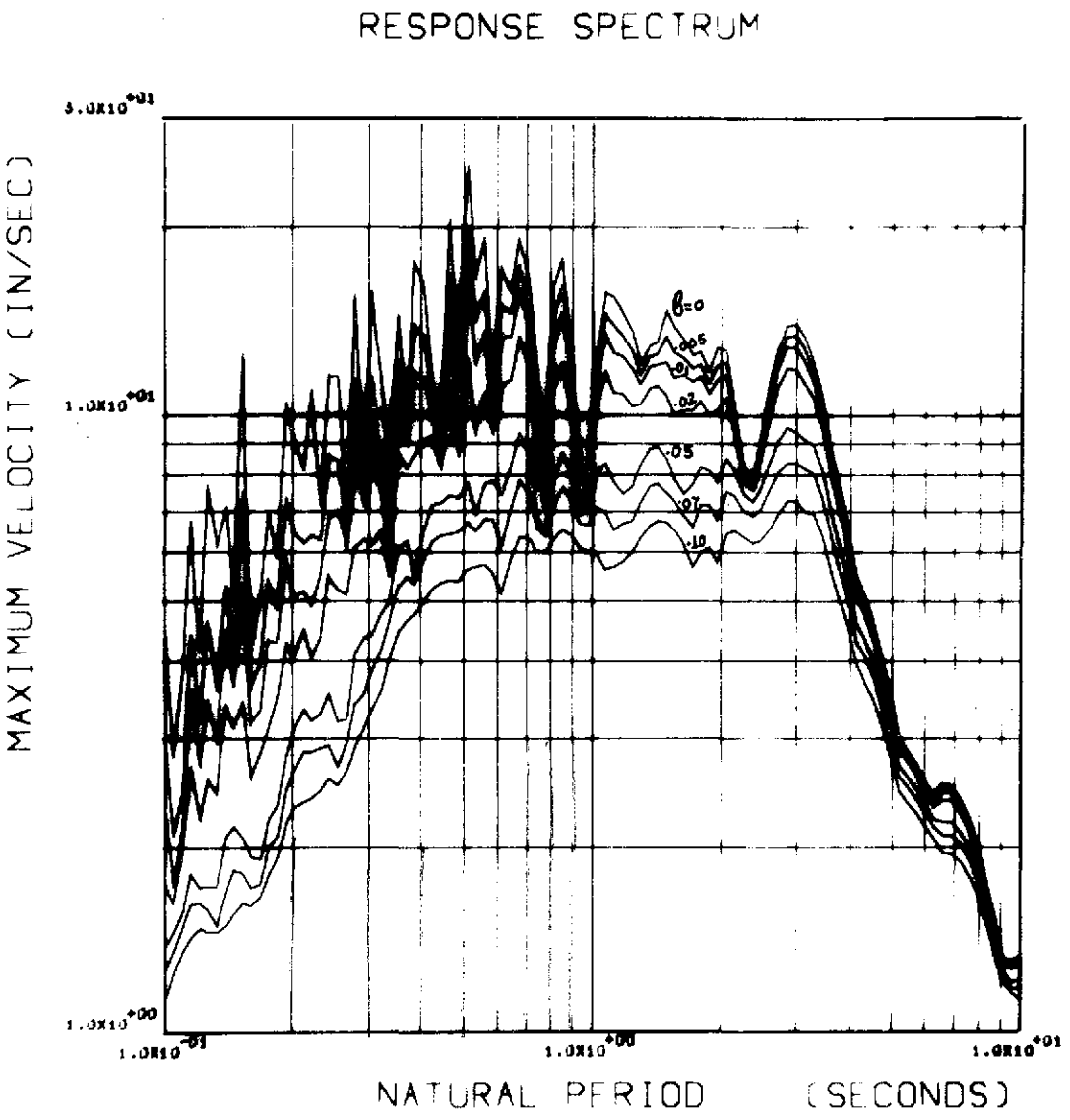

Figure 5-8 Response Spectra of the Artificial Earthquake

5.4.1 13-Story Steel-Frame Building

The steel-frame building has the layout shown in Figure 5-9, with 3 moment resisting frames in the X-direction and 4 in the Y. The elevations of these frames are shown in Figures 5-10 and 5-11. Between the ground and the 1^{st} floor there is another story, which does not extend over the whole area, but leaves a large portion open. This story was eliminated from the mathematical model, by increasing the stiffness and strength of the 1^{st} story appropriately. The various frames are almost identical in each direction, except for the first story, which, however, was made identical by uniform distribution of the additional stiffness and strength of the mezzanine level that was eliminated. Three different designs, for earthquake zones 2, 3 and 4, were analyzed. The Z factor for zone 4 was taken as 2. The notation used is SFX1, SFY1 for zone 2, SFX2, SFY2 for zone 3, and SFX3, SFY3 for zone 4, X being for the X-direction and Y for the Y. The properties of SFX2, SFY2 are tabulated in Table 5-2, while the masses and the natural periods of the structural frame alone have been included in Figure 5-9. The lightweight partitions of this building have been detailed so as not to interfere with the response of the structural frame. On the other hand, a set of block-masonry walls that forms the elevator area was included in the analysis, as a limited-elastic model—i.e., with resistance varying linearly up to a certain interstory distortion and then dropping to zero when this distortion is exceeded. The properties of these walls were estimated from the architectural plans, and the limiting distortions

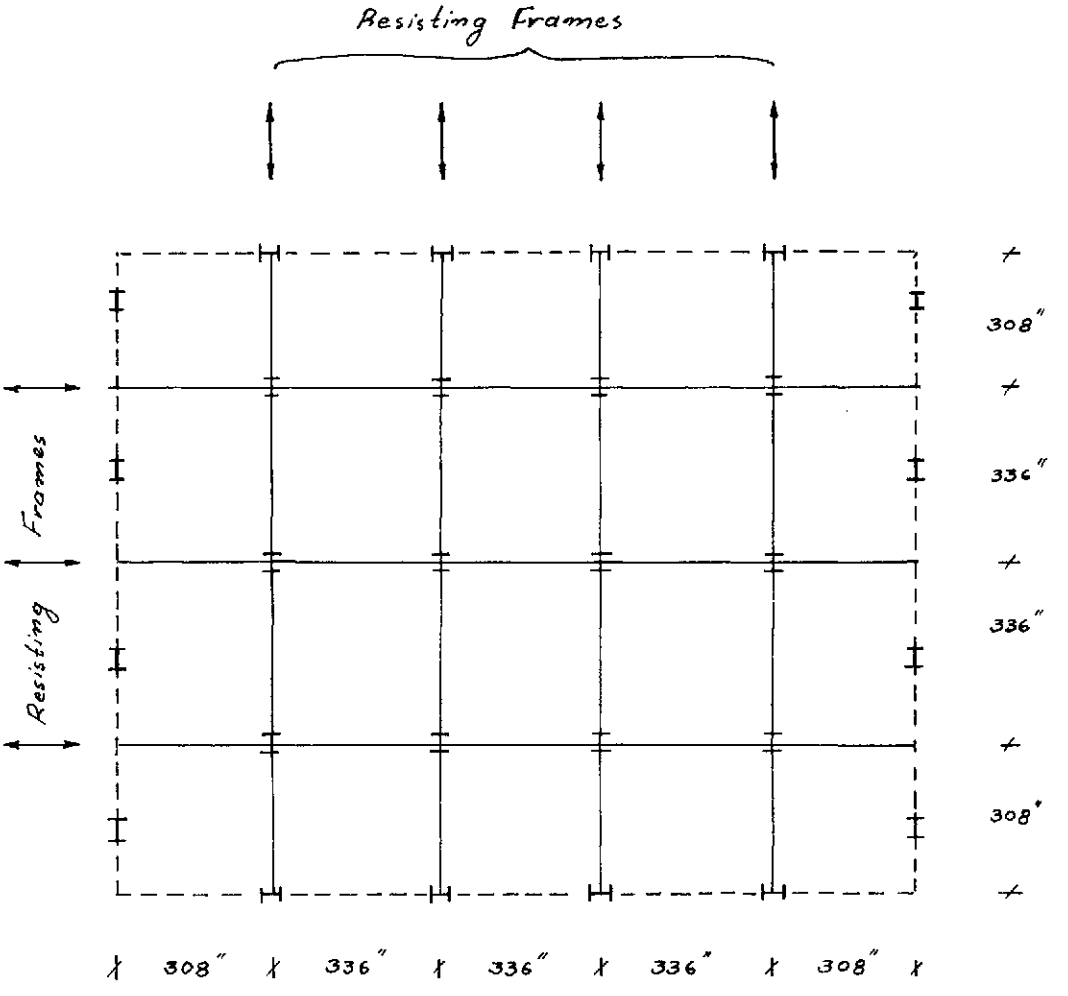

FLOOR	MASS
1	3.40
2-11	3.15
12	7.36
13	3.60

* UNITS: KIPS, INCHES

NATURAL PERIODS (sec)						
MODE	SFX1	SFX2	SFX3	SFY1	SFY2	SFY3
1	5.27	4.2	3.08	4.5	3.31	2.95
2	1.965	1.53	1.14	1.59	1.17	1.02
3	1.14	.91	.71	.95	.68	.61

Figure 5-9 FLOOR PLAN OF 13-STORY STEEL BUILDING

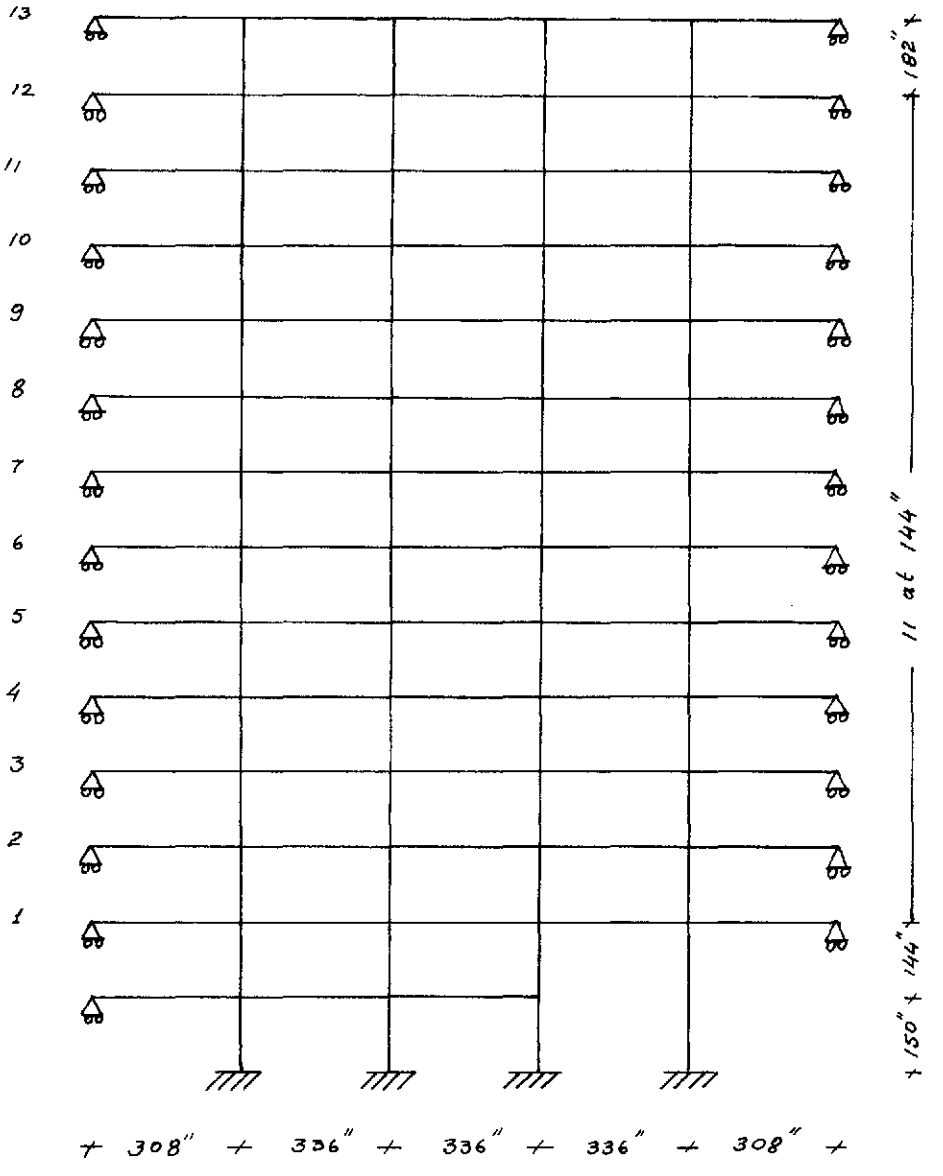

Figure 5-10

GEOMETRY OF STEEL FRAME IN THE X DIRECTION (SFX)

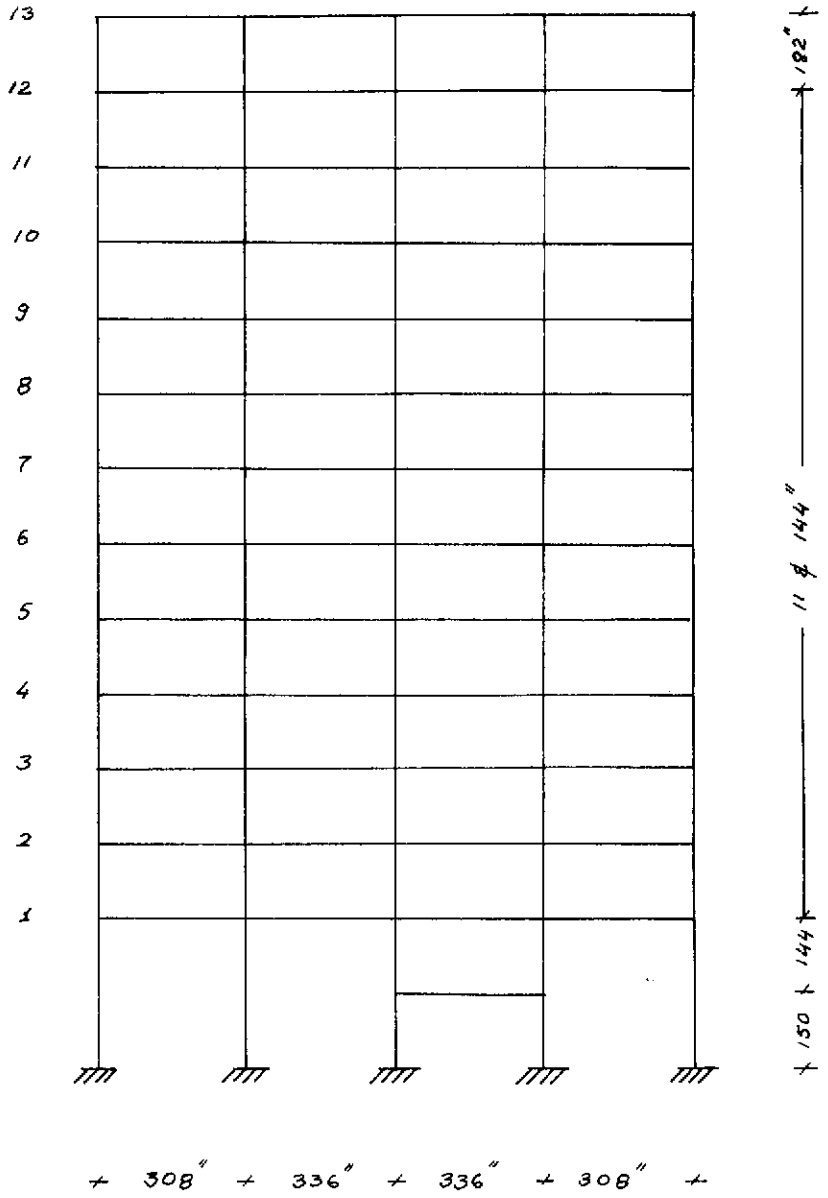

Figure 5-11

GEOMETRY OF STEEL FRAME IN THE Y DIRECTION (SFY)

PROPERTIES OF SFX2 (in^4, Kips.in)						
FLOOR	$I_{col,ext}$	$M_{p,col,ext}$	$I_{col,int}$	$M_{p,col,int}$	I_{girder}	$M_{p,girder}$
1	.1	.1	5200.	33600.	2830.	8800.
2	.1	.1	1990.	13300.	1290.	5800.
3	.1	.1	"	"	1440.	6400
4	.1	.1	1810.	12200.	"	"
5	.1	.1	"	"	1290.	5800.
6	.1	.1	1470	10030.	"	"
7	.1	.1	"	"	"	"
8	.1	.1	1330.	9140.	1050.	5250
9	.1	.1	"	"	836.	4250
10	.1	.1	930.	6480	"	"
11	.1	.1	"	"	"	"
12	.1	.1	745.	5220.	891	4040
13	.1	.1	"	"	374	1950.

PROPERTIES OF SFY2 (in^4, Kips.in)						
1	1810	12200	9450	42500	3270	10000
2	1030	7130	5450	26500	1680	7400
3	"	"	"	"	"	"
4	930	6480	4910	24250	"	"
5	"	"	"	"	"	"
6	790	5540	3910	19850	"	"
7	"	"	"	"	1310	6700
8	"	"	3530	18100	"	"
9	"	"	"	"	1050	5250
10	703	4940	2400	12800	"	"
11	"	"	"	"	"	"
12	528	3930	1900	10300	1850	8160
13	"	"	"	"	836	4240

Table 5-2

PROPERTIES OF STEEL FRAMES SFX2, SFY2

were found to be .02" in the X direction and .033" in the Y. The main effect of these walls is to increase the stiffness of the building considerably without affecting the ultimate strength, since at high levels of excitations the walls break. After including these block walls the natural periods of vibration were computed and the results are tabulated below, together with measured values from ambient vibrations (Table 5-3).

	NATURAL PERIODS	
	X	Y
COMPUTED (walls included)	1.53 sec.	1.95 sec.
COMPUTED (walls not included)	5.27 sec.	4.50 sec.
MEASURED	1.70 sec.	2.00 sec.

Table 5-3

Computed and Measured Periods of Steel Building

The agreement is more than satisfactory, given the complex arrangement of the walls and the uncertainty about their properties.

The force-displacement model used for the analysis is a trilinear one with ultimate strength twice that at first yielding. The slope of the second branch was taken as 20% of the initial and ductility factors were computed based on first yielding. 2% of viscous damping was assumed in all the modes. Results of the analysis are shown in Figures 5-12, 13, 14, 15 in terms of maximum ductility

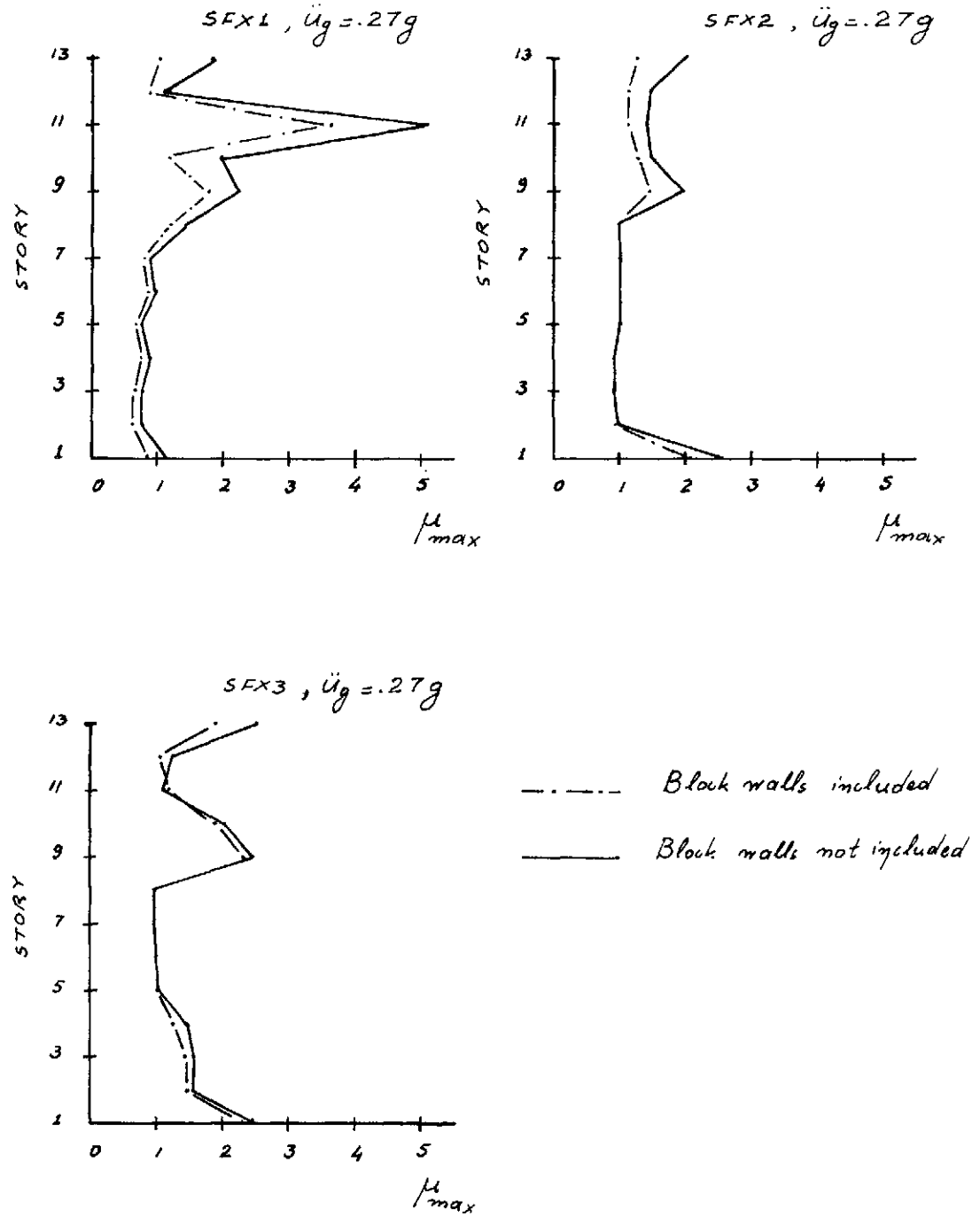

Figure 5-12 MAXIMUM DUCTILITY FACTORS FOR STEEL FRAMES , X-DIRECTION

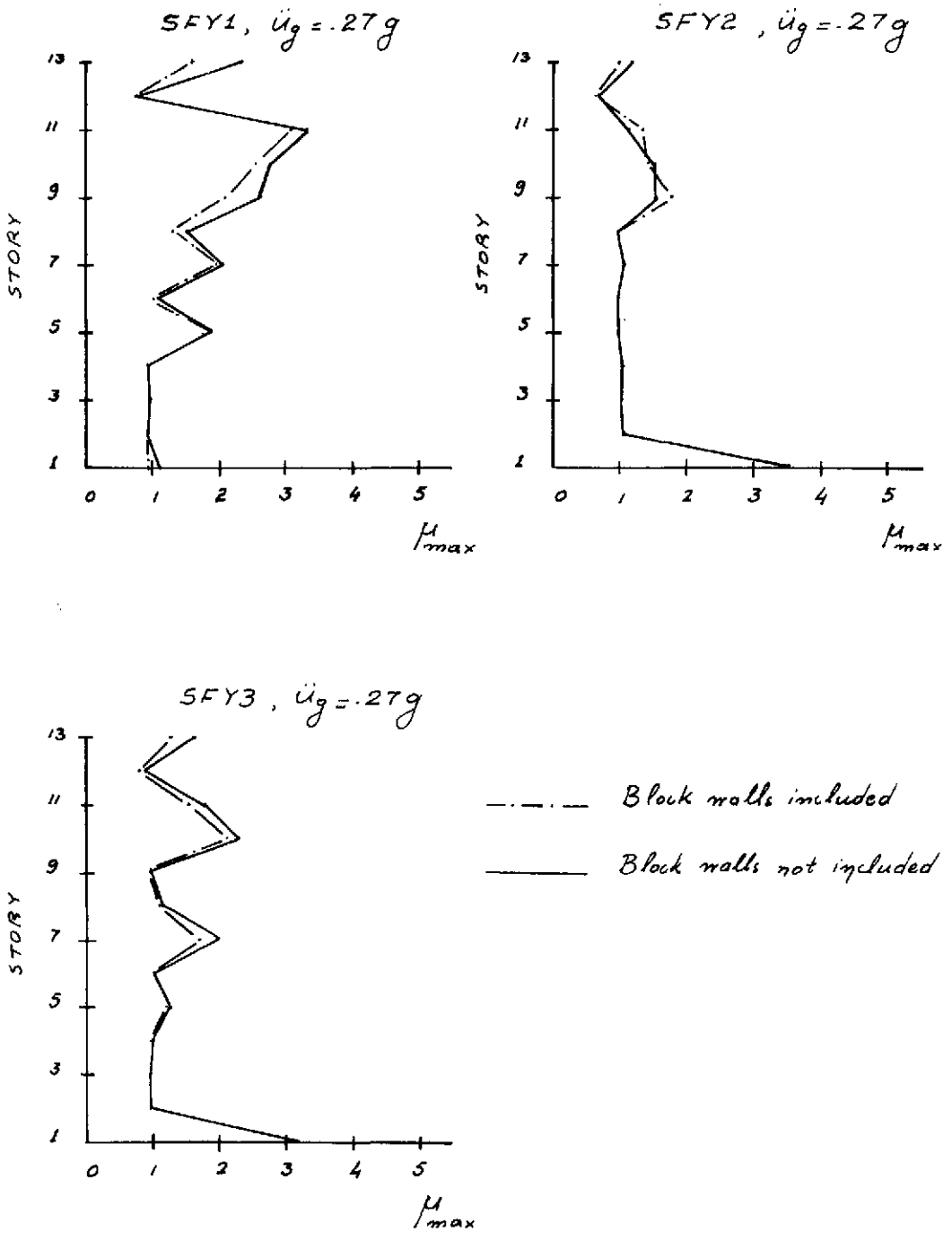

Figure 5-13 MAXIMUM DUCTILITY FACTORS FOR STEEL FRAMES, Y-DIRECTION

factors, maximum relative displacements and maximum interstory displacements. There is a considerable decrease of ductility from case 1 to case 2, but no improvement seems to occur for case 3, which was designed for a Z factor equal to 2. On the contrary, this design seems to have slightly higher ductility requirement than the second one that was designed for zone 3 (Z = 1). For the first design a maximum ductility factor of 5.2 occurs at the 11^{th} story, while for the others it occurs at the first being 2.5 in the X-direction and 3.5 in the Y. The behavior in the two directions is very similar as expected, because the variation of strength and stiffness across the height is similar. In the same figures the required ductilities when the block walls were included in the analysis have been plotted. The effect is really negligible as expected, since the walls break and are assumed not working at an early stage of the excitation. It should be realized, however, that the ductility factors computed are some kind of average numbers for the whole floor, while local ductilities corresponding to individual members may be higher.

In Figures 5-14, 5-15, maximum elastic and inelastic displacements have been plotted. Again we see that the block walls have a negligible effect. Several other interesting observations can also be made here. It is a little surprising that the maximum relative displacement of the top story increases as the earthquake design zone increases. This is consistently observed in both X and Y directions. This behavior can be explained if one looks at the spectrum of the particular input motion (Figure 5-8). The first design with

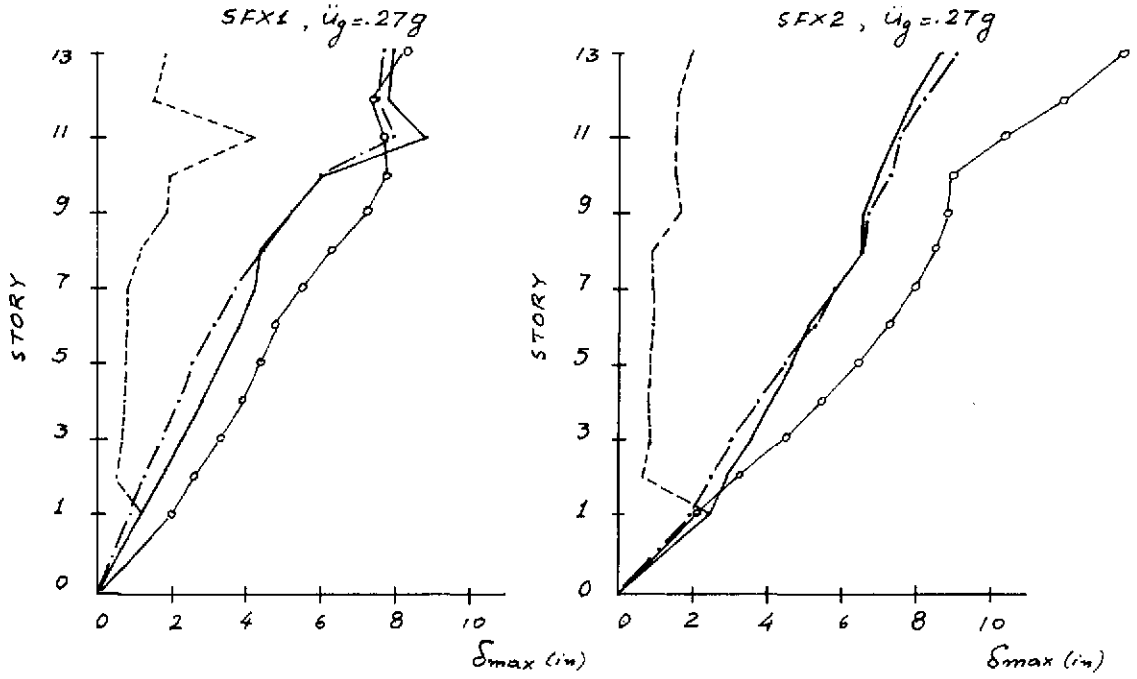

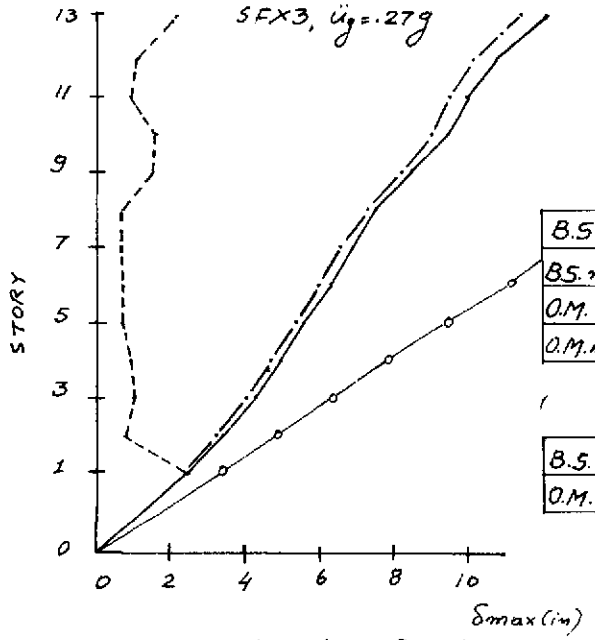

	SFX1	SFX2	SFX3
B.S. max	159. Kips	196 Kips	364 Kips
B.S. max el	265 "	350 "	890. "
O.M. max	126880 K"	257250 K"	539240. K"
O.M. max el	153500. "	352000 "	1085000. "

	SFX1+BW	SFX2+BW	SFX3+BW
B.S. max	136. Kips	188 Kips	366. Kips
O.M. max	134800. Kips"	273390 K"	538614. Kips"

B.S. = Base shear
O.M. = Overturning moment

- - - - Max Interstory Displac.
——— Max inelastic Displac. (no Block Walls)
—·—·— Max displ. with Block walls included
—o—o— Max Elastic Displac.

Figure 5-14 X-DISPLACEMENTS FOR STEEL FRAMES

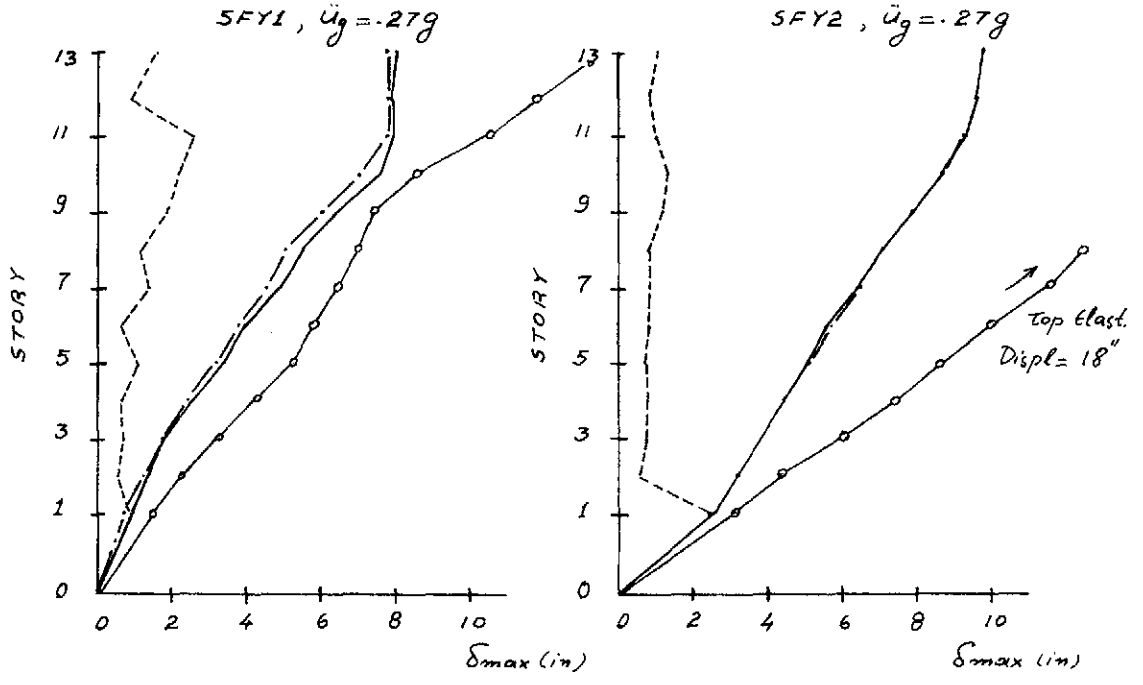

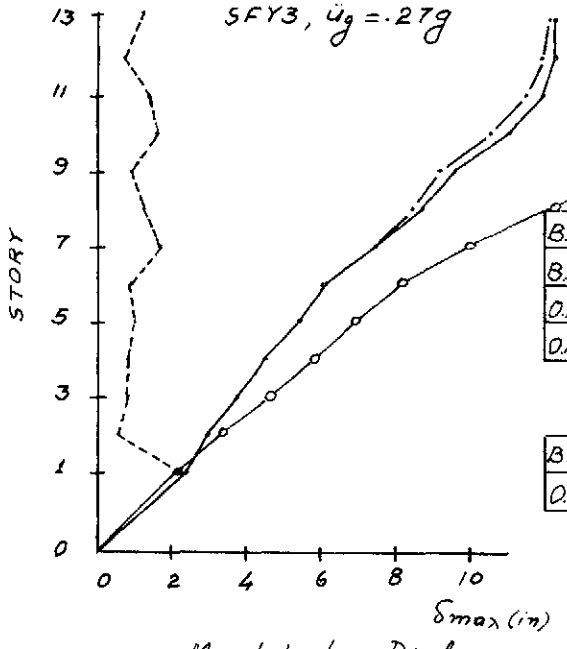

	SFY1	SFY2	SFY3
B.S. max	128. Kips	207 Kips	326 Kips
B.S. max. el.	220. "	580 "	638 "
O.M. max	127050 Kips"	311550 Kips"	474770. Kips"
O.M. max el.	174000 "	690000. "	875000. "

	SFY1+BW	SFY2+BW	SFY3+BW
B.S. max	124. Kips	210 Kips	331 Kips
O.M. max	130720. Kips"	323800. Kips"	484594 Kips"

B.S. = Base shear
O.M. = Overturning moment

------ Max Interstory Displac.

———— Max Inelastic Displacements (No Block walls)

— . — . — Max Inelastic Displ. with Block walls included

—o—o— Max Elastic Displacements

Figure 5-15 Y-DISPLACEMENTS FOR STEEL FRAMES

a natural period 5.27 sec. in the X direction lies at the very extreme of the spectrum (line of constant displacement), so when we increase the earthquake design zone, we produce a stiffer structure, shifting it to the left. The design for zone 3 lies still on the same line, while that for zone 4 is at the very peak (junction of the constant velocity with the constant displacement line). The slope of the right branch of the spectrum is different from 45°, so this line is not a "constant displacement" line. The amount of change is indicated below (Table 5-4), in which the spectral displacements for the three designs have been tabulated. They are given for the first mode only since this is the only significant one for the displacement at the top.

	SPECTRAL DISPLACEMENTS		
	Zone 2	Zone 3	Zone 4
X	2.35	3.26	5.65
Y	3.15	5.25	5.90

Table 5-4 Spectral Displacements

It is this increase of the spectral displacement as we move to shorter periods, within the long period range of the spectrum, that creates the rather strange behavior. Another interesting observation is the difference between elastic and inelastic displacements. It has been claimed (based mainly on studies for 1-DOF systems) that within the long period range of the spectrum (constant displacement

region) the maximum inelastic displacement is approximately equal to the maximum elastic. This does not seem to be the case in Figures 5-14 and 5-15 except for SFX1. The reason for this is partly what was mentioned above (when a structure starts yielding, its period increases), but mainly the yielding that takes place in the first story. If we look at the ductility curves of the previous figures, we see that when the difference between the two responses is big, we always have large amounts of plastic deformations in the first story, which acts then essentially as a "soft story" and absorbs a considerable amount of energy. The result for the upper part of the structure, then, is a considerable decrease of the response. Similar behavior was observed when the El Centro record was used. Figures 5-16, 17, 18, 19 are time histories of accelerations and displacements for the top story for $\ddot{u}_g$ = 0.007g (elastic behavior) and $\ddot{u}_g$ = .27g (inelastic). From 5-16 and 5-17 we can clearly see the effect of the block walls and the time at which they break.

5.4.2 11-Story Concrete-Frame Building

The second building that was designed and analyzed is an 11-story concrete building with moment resisting frames in both directions. The building was designed for gravity loads and a zone 3 earthquake according to the U.B.C. In the X direction only the two exterior frames were designed to carry the lateral forces, but we also included in the analysis the two interior lines of columns, by

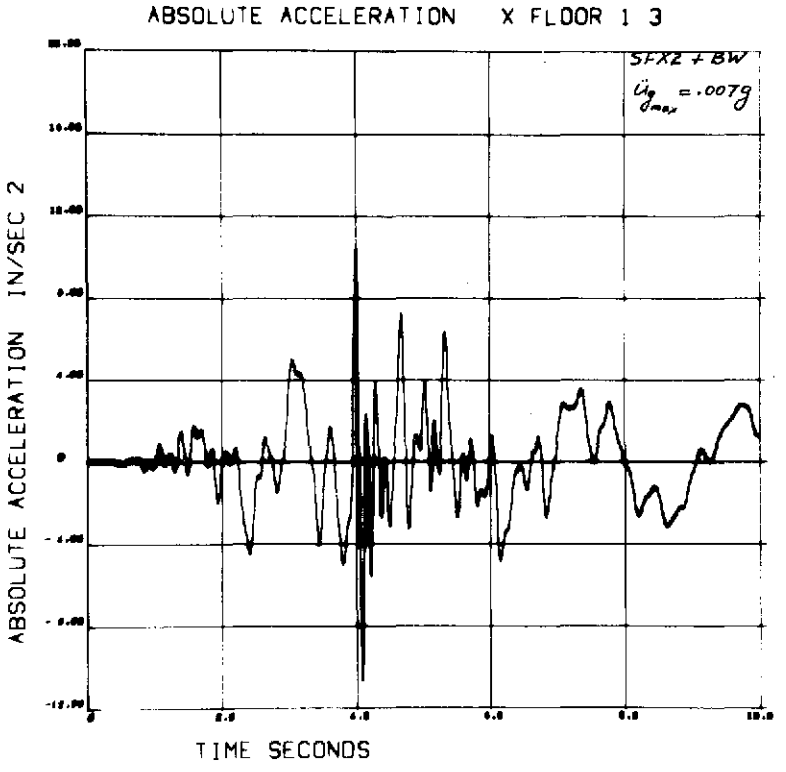

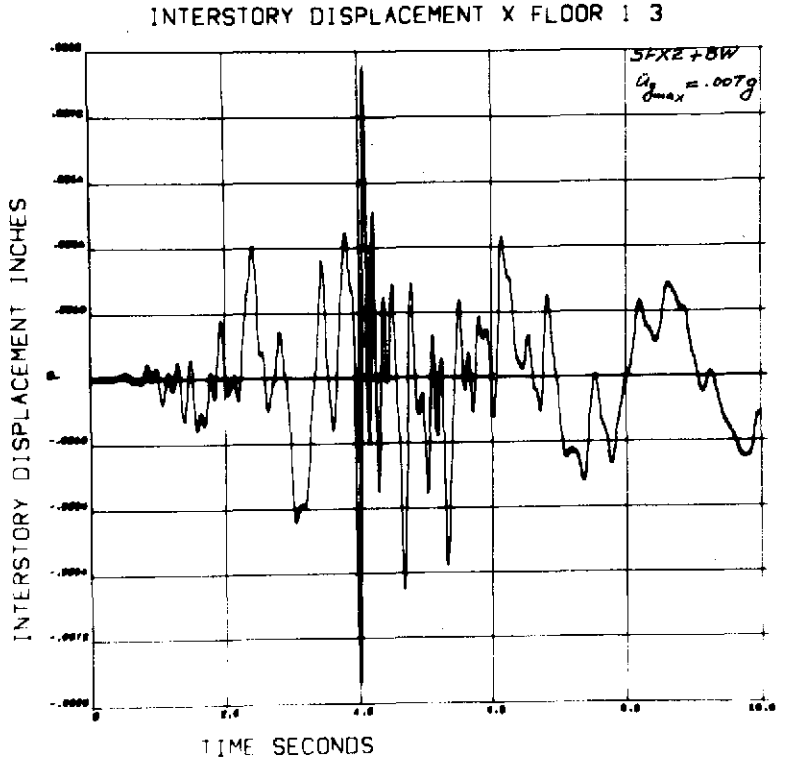

Figure 5-16 Response with Block Walls

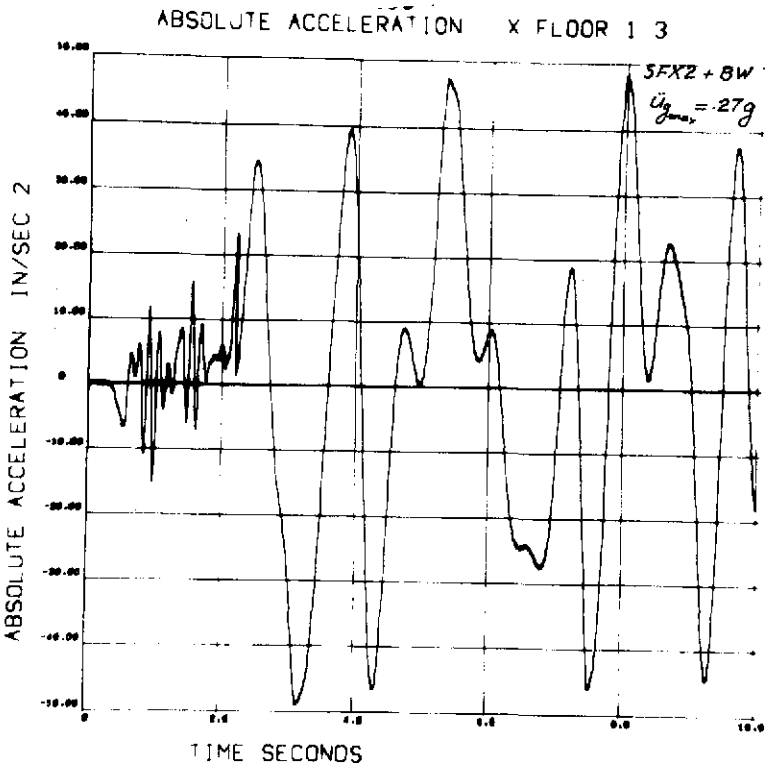

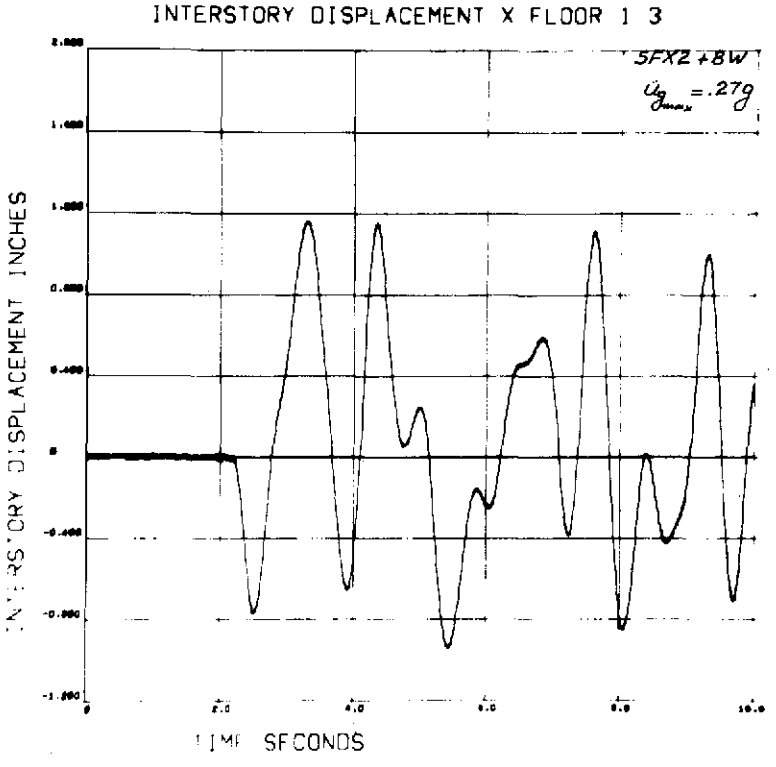

Figure 5-17 Response with Block Walls

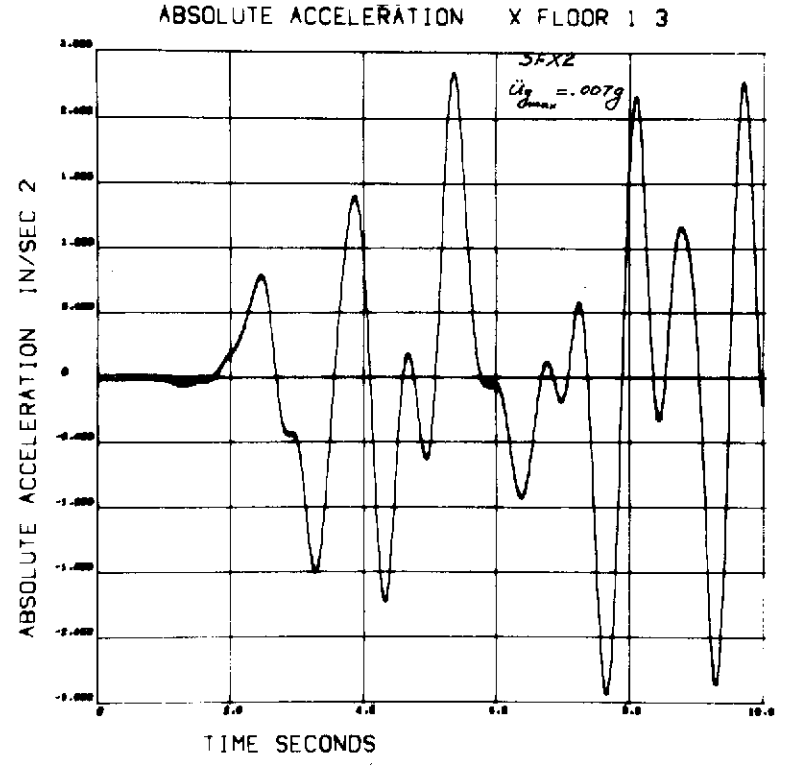

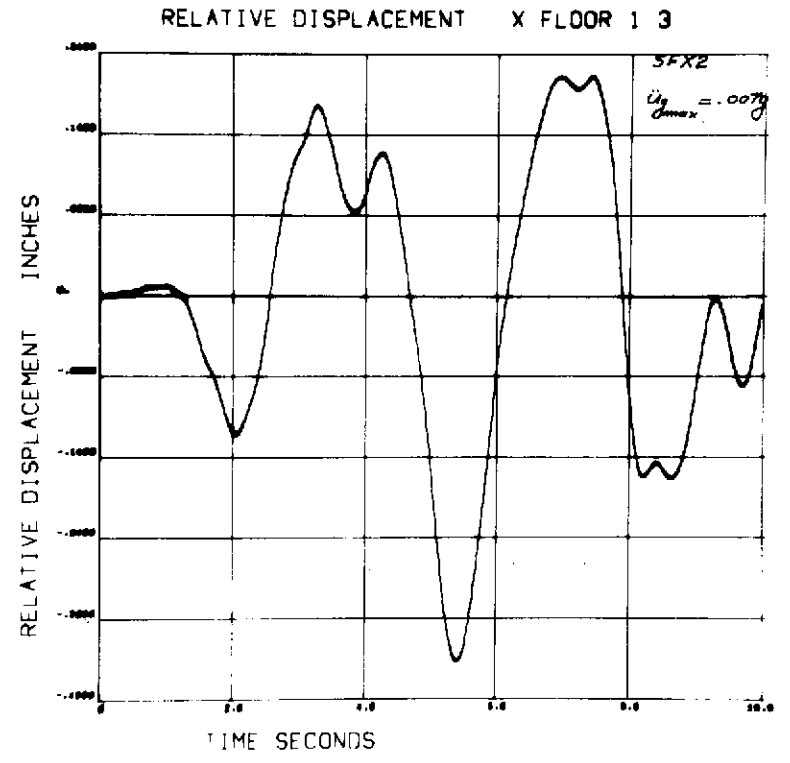

Figure 5-18 No Block Walls - Elastic Response

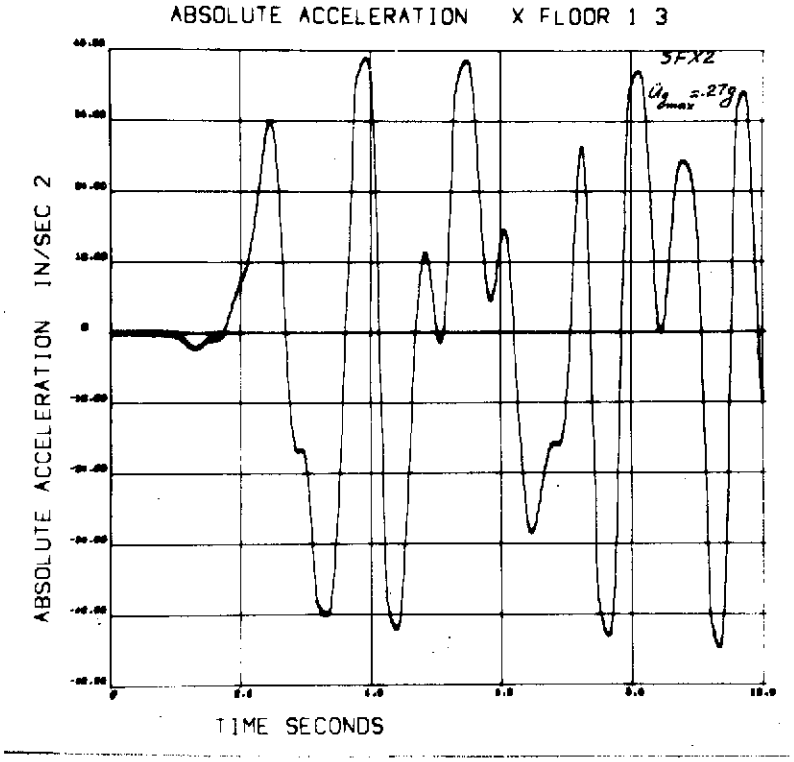

Figure 5-19 No Block Walls - Inelastic Response

using part of the slab as an effective girder. In the Y direction all the 11 frames are moment resisting frames, designed as such. The framing plan and the notation for the frames is shown in Figure 20, while the frame elevations are shown in Figure 5-21. Table 5-5 contains the properties of the frames and also the first natural periods. The moments of inertia given in this table were computed using the approximations discussed in chapter 2 of this thesis, so it should not be surprising that the periods of Table 5-5 are somewhat high, compared to those that would be obtained if uncracked sections had been used. The force-deformation model used for the analysis is a stiffness degradation with slope of the unloading branch equal to the initial one. The ductility factors were computed by using yield displacements corresponding to the maximum strength of each story as estimated by procedures described in chapter 2. It should be made clear here that this yield displacement is twice that used for the steel frame, which was based on the trilinear model. If this gradual hinge formation was to be accounted for and yield displacements to be computed as for the trilinear model, then the ductility factors reported here would be about twice as much. The amount of viscous damping was taken as 5% in all the modes. Partitions were assumed to be detailed so as not to interfere with the frame response.

Figure 5-22 shows the maximum ductility factors plotted for the different stories and corresponding to a peak ground acceleration equal to .27g. In the X direction we see that the moment resisting

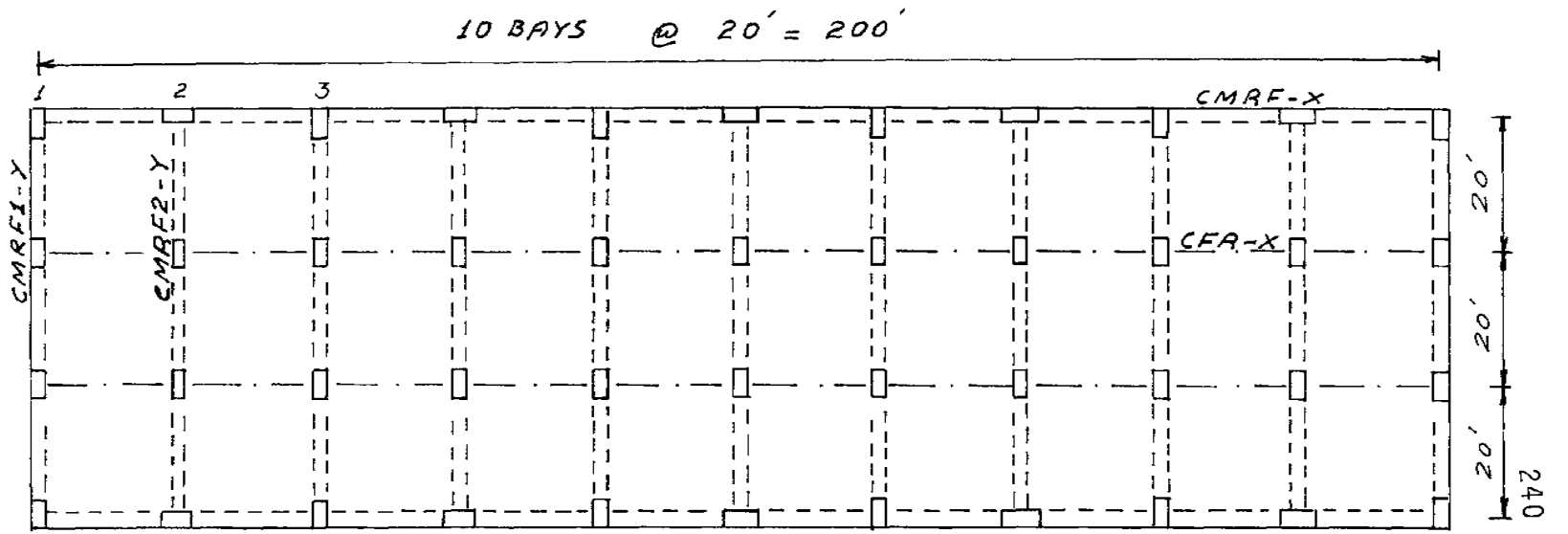

Figure 5-20

TYPICAL FLOOR FRAMING PLAN FOR 11 STORY CONCRETE BUILDING WITH MOMENT RESISTING FRAMES IN 2 DIRECTIONS DESIGN FOR ZONE-3

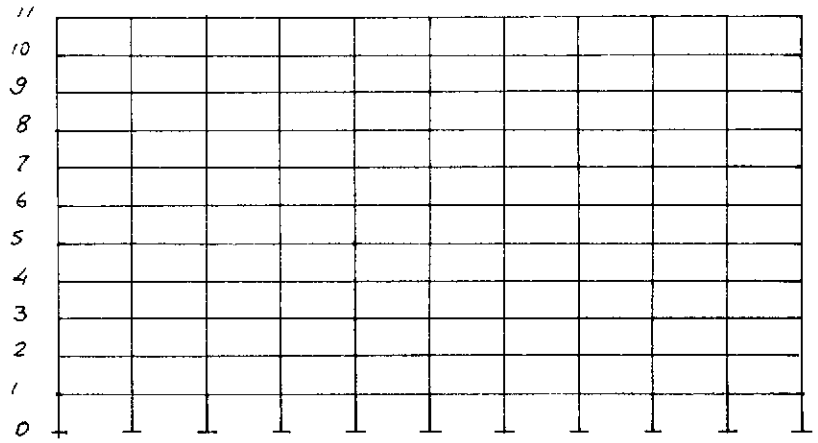

CMRF-X , CFR-X

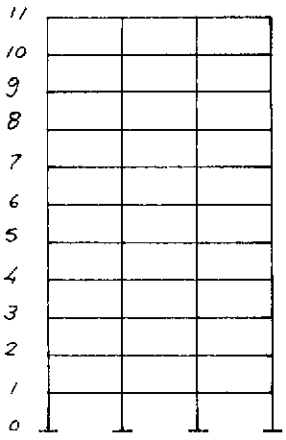

CMRF1-Y, CMRF2-Y

STORY HEIGHT : 9'.0
BAY WIDTH : 20'.0

Figure 5-21 ELEVATIONS OF FRAMES OF 11-STORY CONCRETE BUILDING

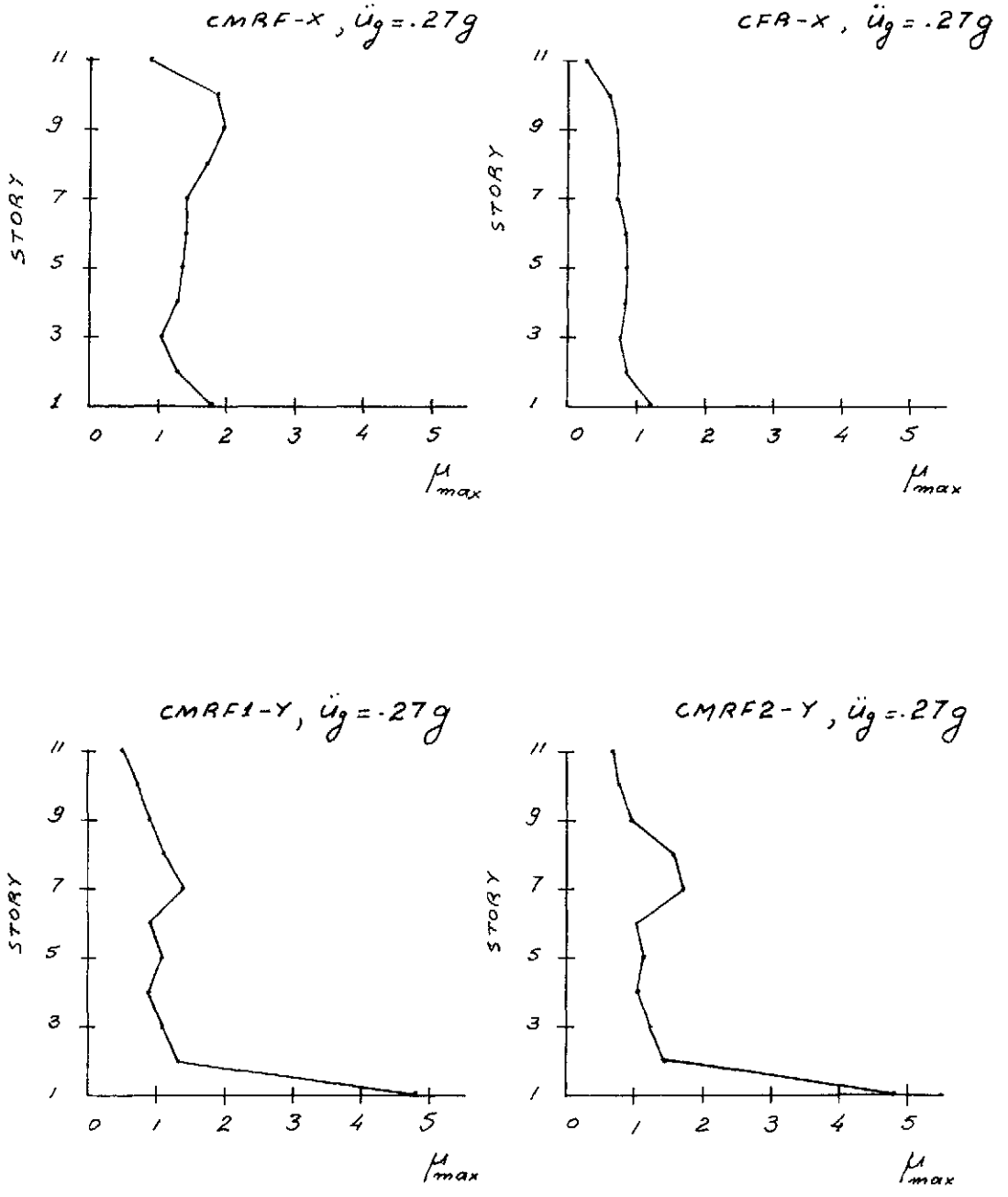

Figure 5-22

MAXIMUM DUCTILITY FACTORS FOR FRAMES OF 11-STORY CONCRETE BUILDING

	CMRF -X					CFR -X	
FLOOR	PLASTIC MOMENTS						
	COL 1	COL 2	COL 3	EXT. GIR.	INT. GIR.	COL	GIRD
1	229.	862.	278.	275.	275.	230.	137.
2	231.	600.	287.	311.5	287.5	〃	〃
3	189.	438.	258.	〃	〃	〃	〃
4	179.	367.	270.	300.	275.	200.	〃
5	166.6	339.	258.8	275.	〃	〃	〃
6	160.	311.	189.	〃	248.	〃	〃
7	153.5	291.	133.2	250.	224.	165.	〃
8	144.5	264.	120.	224.	203.	〃	〃
9	134.	236.	105.	176.	176.	〃	〃
10	125.	211.	92.3	156.	138.	120.	〃
11	115.	119.5	77.8	119.5	119.5	〃	〃
	MOMENT OF INERTIA						
1-11	.208	1.310	.208	.267	.267	.208	.088

* UNITS : KIPS, FEET

	CMRF1 -Y				CMRF2 -Y			
FLOOR	PLASTIC MOMENTS							
	EXT. COL.	INT. COL.	EXT. GIR.	INT. GIR.	EXT. COL.	INT. COL.	EXT. GIR.	INT. GIR.
1	489.	544.	197.	250.	278.	647.	197.	197.
2	475.	422.	250.	197.	228.	617.	〃	〃
3	322.	400.	〃	〃	198.	538.	〃	〃
4	300.	373.	〃	〃	174.	522.	〃	〃
5	283.	345.	〃	〃	160.	412.	〃	〃
6	267.	317.	〃	〃	147.	397.	〃	〃
7	247.	289.	〃	〃	133.	358.	156.	156.
8	228.	267.	〃	156.	120.	317.	〃	〃
9	211.	239.	〃	〃	105.	278.	197.	〃
10	194.	211.	〃	〃	92.3	239.	〃	〃
11	172.	184.	197.	〃	77.8	200.	120.	〃
	MOMENT OF INERTIA							
1-11	1.3	1.3	.266	.266	.208	1.3	.266	.266

MASS/STORY = 67 Kips sec^2/ft

STORY HEIGHT = 9.'0

T_x = 2.356 sec
T_y = 2.046 〃

Table 5-5 PROPERTIES OF 11-STORY CONCRETE BUILDING

frame has a maximum ductility of about 2 in the 9^{th} floor, while the interior frame remains almost elastic. The reason for this is that the exterior frame is much stiffer than the interior one, so it takes a bigger portion of the force. On the other hand, the interior frame has considerable strength and hence it behaves elastically. In the Y direction the ductility factors for the two types of frames are very similar, the maximum occurring at the bottom story. In Figure 5-23 maximum elastic and inelastic displacements relative to the ground were plotted, as well as interstory displacements. Again we observe that in the Y direction, in which a substantial amount of yielding takes place in the 1^{st} story, the elastic displacements in the top portion of the building are larger, while in the X direction they are about equal to the inelastic. Various time histories are shown for the top story in Figures 5-24, 25, 26, 27, in which the influence of the higher modes on the acceleration response is apparent. Figure 5-28 gives the loading and unloading loops for the 1^{st} story of the exterior frame in the X direction, and one can see the behavior of the stiffness degrading model there.

5.4.3 17-Story Concrete Shear Wall Building

The last building that was analyzed has the layout shown in Figure 5-29. It was also designed for gravity and zone 3 earthquake loads. The lateral force resisting elements are the two exterior frames in the X direction and the six shear walls in the Y direction.

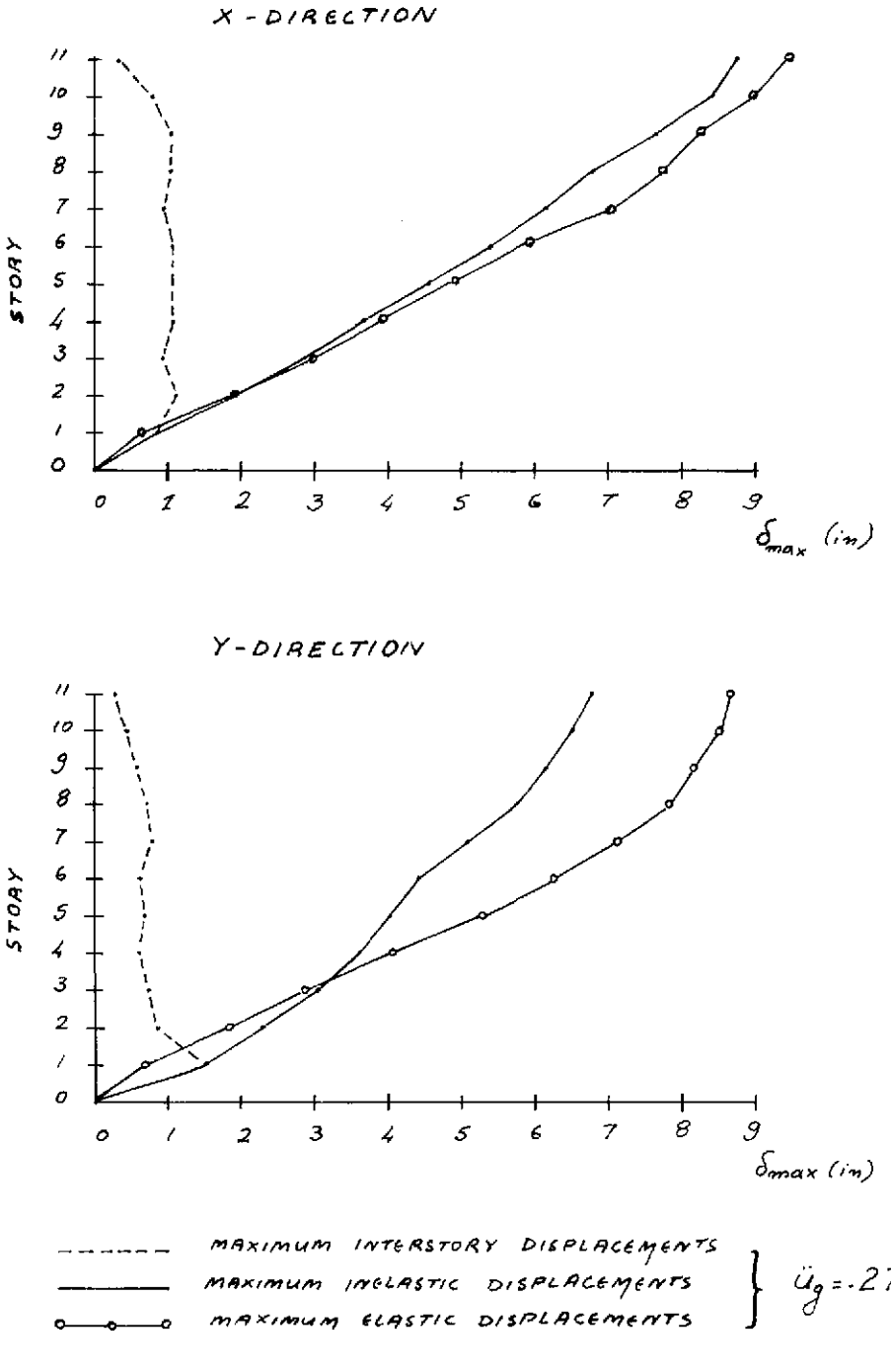

Figure 5-23

DISPLACEMENTS OF 11-STORY CONCRETE FRAME BUILDING

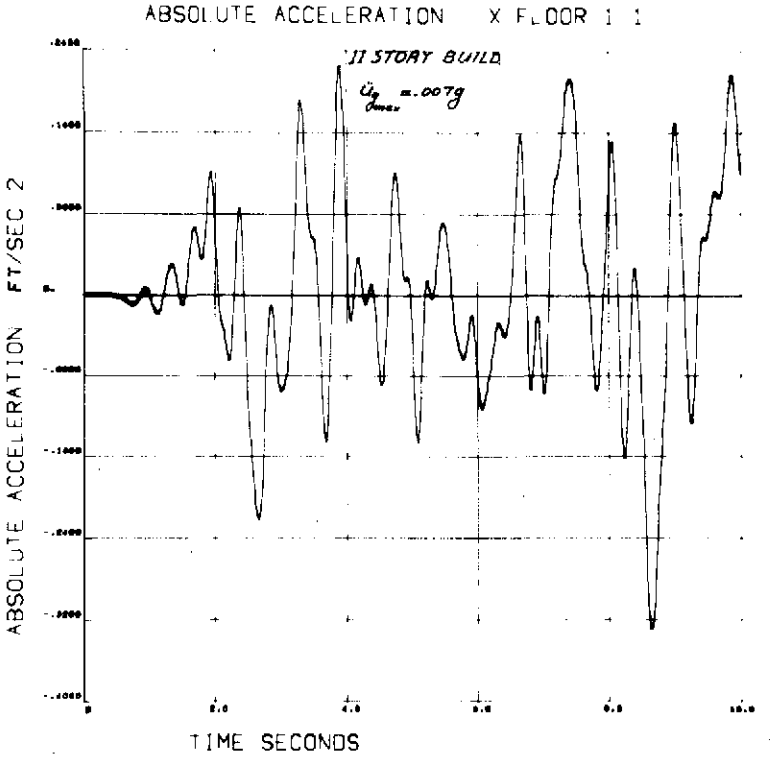

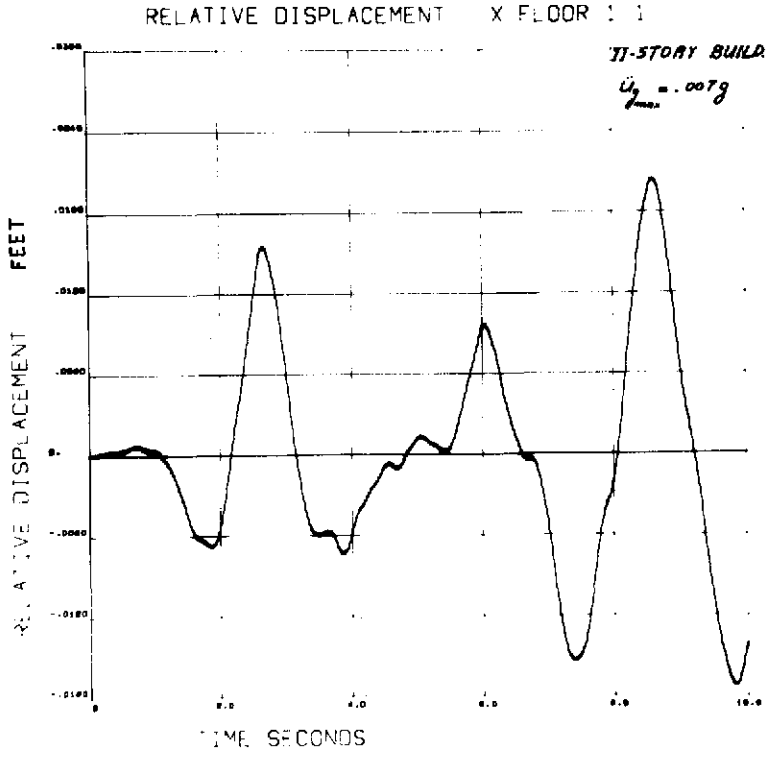

Figure 5-24 Elastic Response

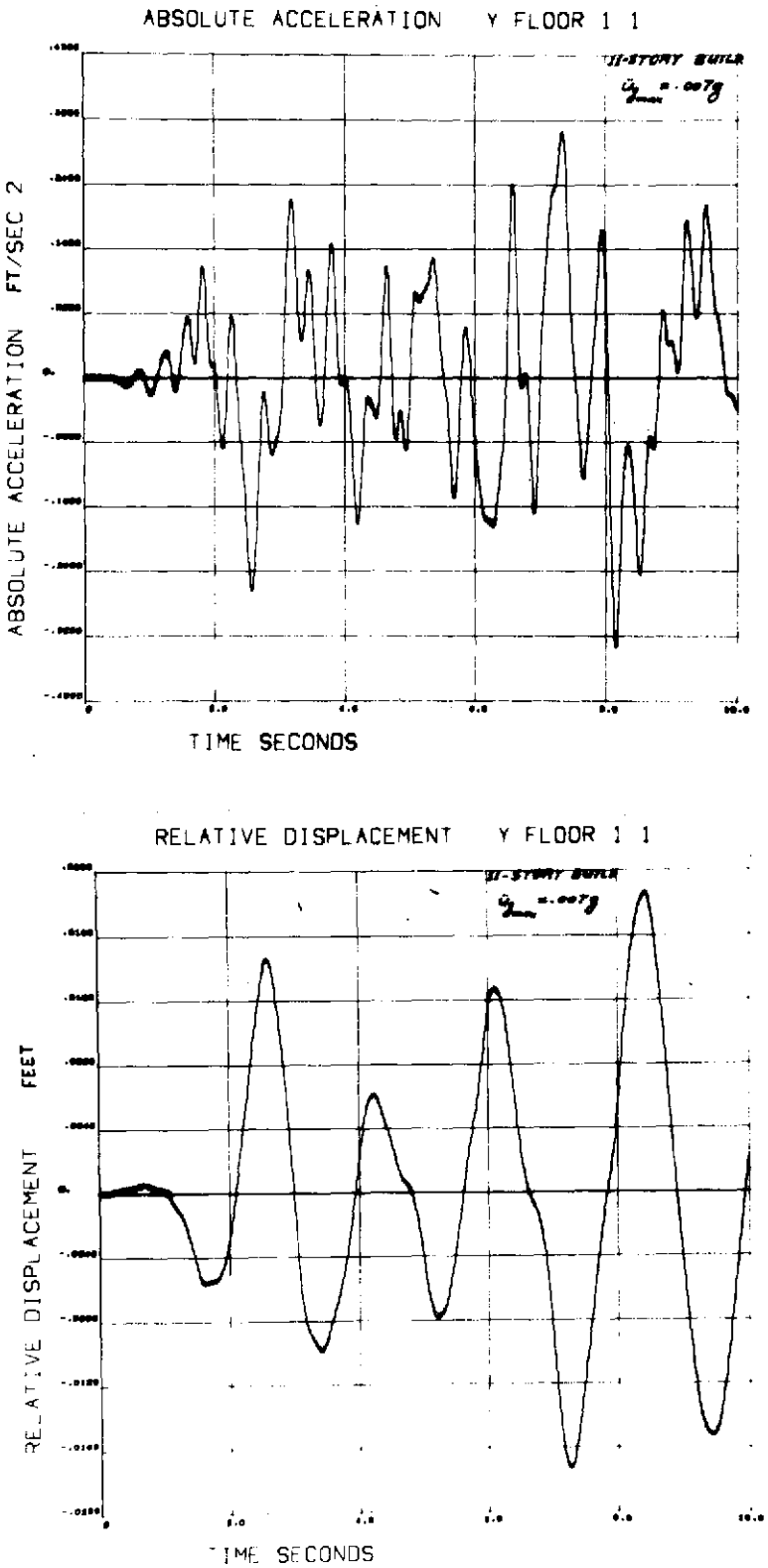

Figure 5-25 Elastic Response

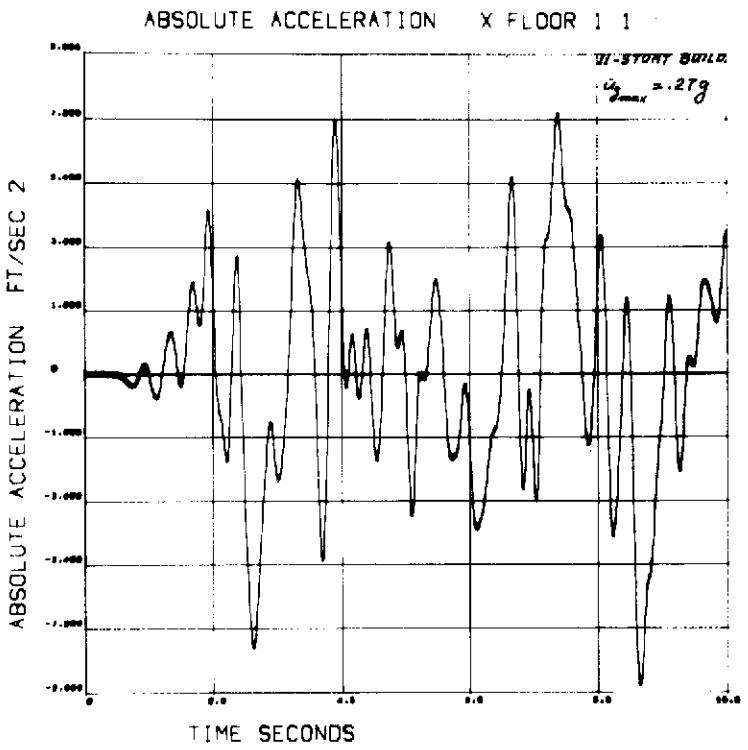

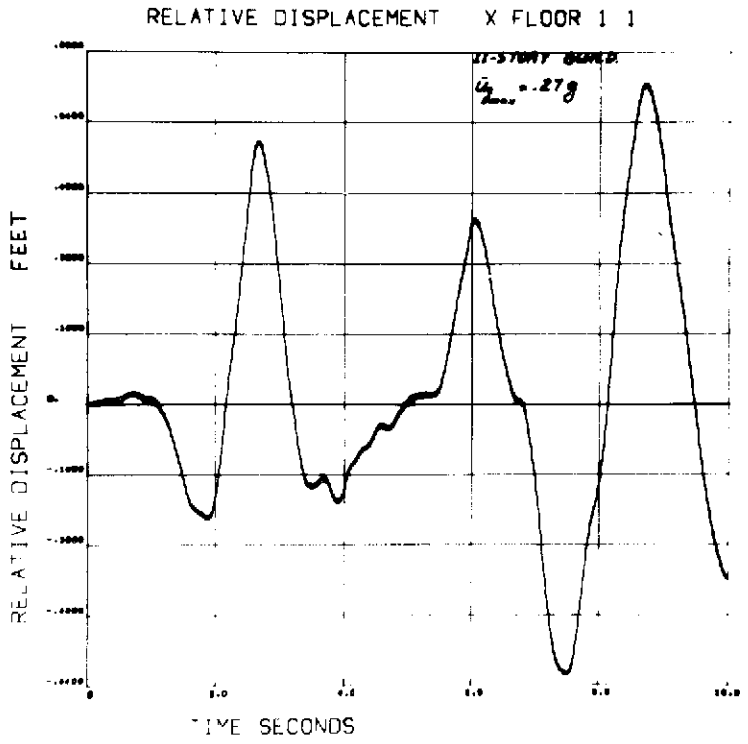

Figure 5-26 Inelastic Response

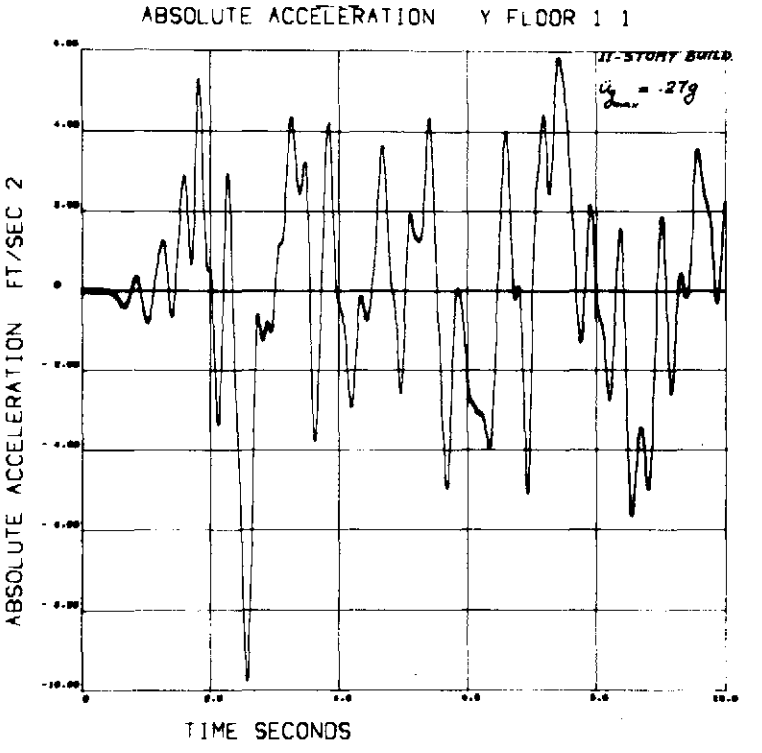

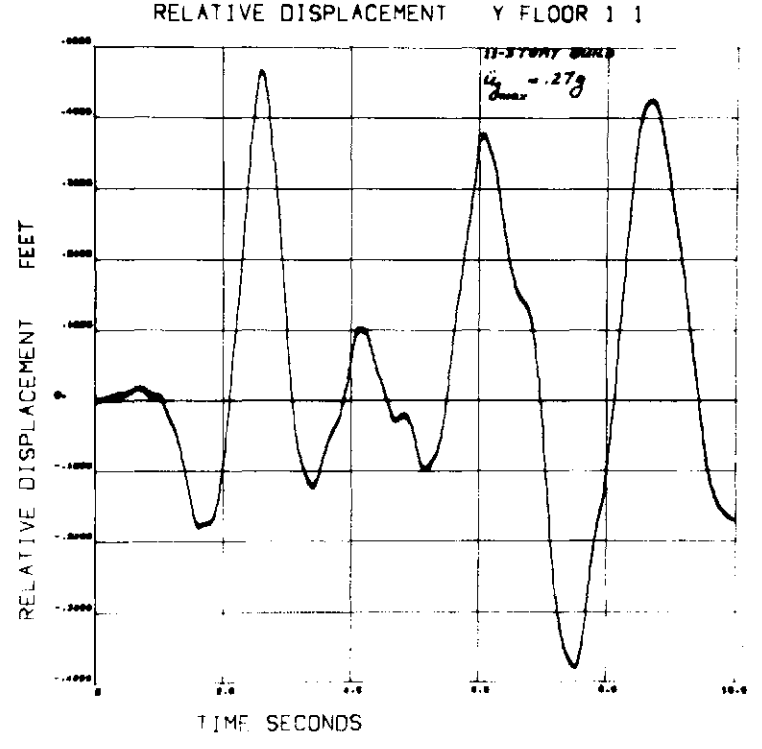

Figure 5-27 Inelastic Response

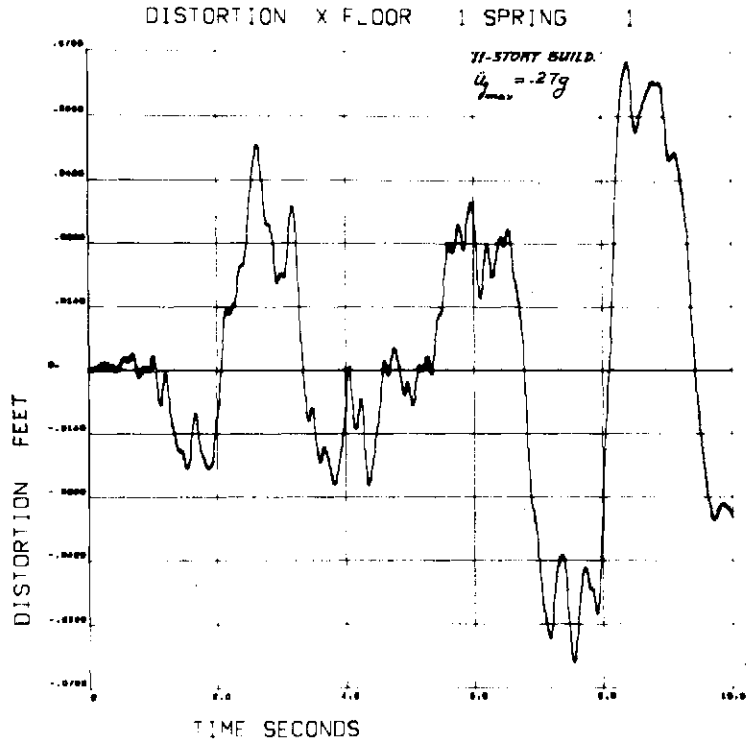

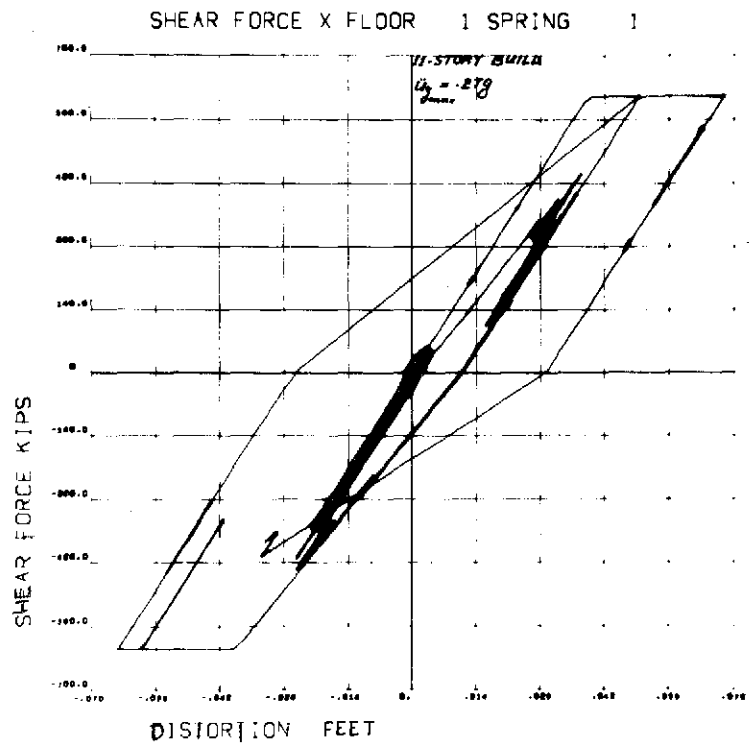

Figure 5-28 Stiffness Degradation Model for Concrete Frame

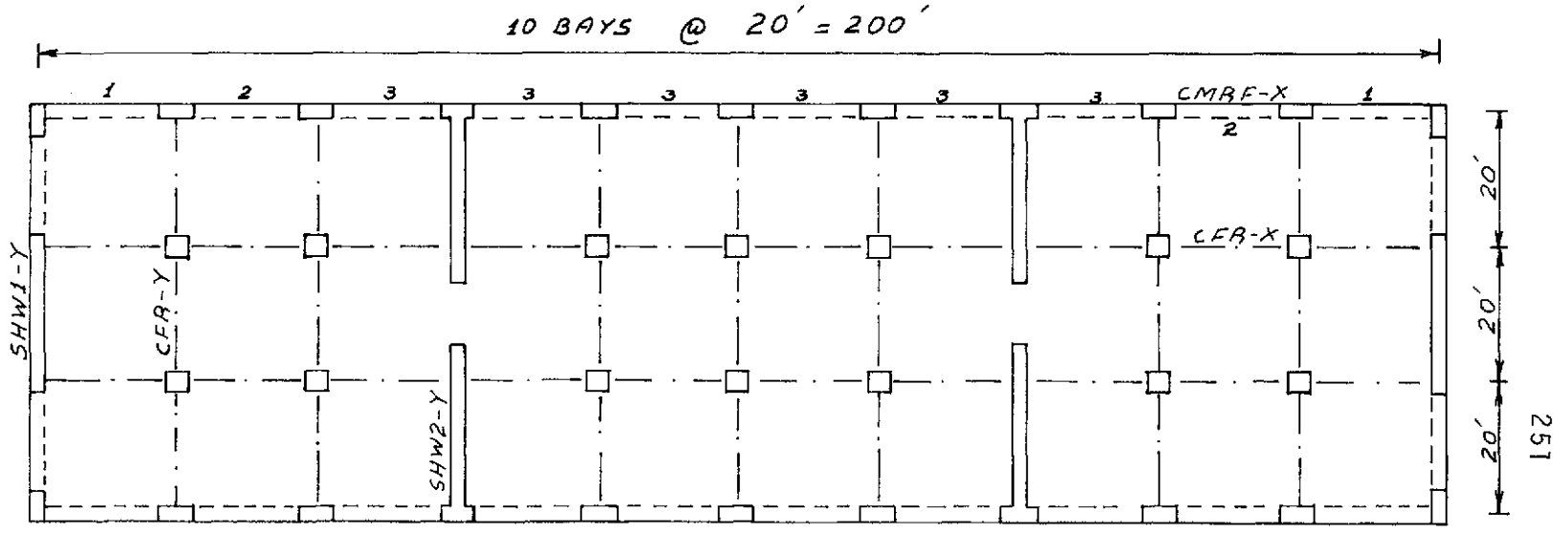

Figure 5-29

TYPICAL FLOOR FRAMING PLAN FOR 17 STORY CONCRETE SHEAR WALL BUILDING. MOMENT RESISTING FRAMES IN LONG DIRECTION
DESIGN FOR ZONE 3

Again the interior columns were assumed to form additional frames, having as girders an effective portion of the slab. The properties of the frames and walls are tabulated in Tables 5-6 and 5-7. Moments of inertias for the girders and columns were computed as for the 11-story concrete frame, while for the shear-walls they were taken as one-half the gross moment of inertia. An average ultimate shear capacity was also estimated for the shear walls. This capacity is in general a function of the wall properties and the applied moments and axial forces, but it does not change significantly with height, so it was assumed constant and is given in the last column of Table 5-7. The computer program checks at each step and for each story whether this capacity has been exceeded. If that is the case, then it assumes that the wall has a shear crack there and starts treating the portion of the wall in the floors above as partitions (limited elastic-close coupled), while for the floors below the crack the wall is still acting. Such a case was observed when we analyzed the design of this building for zone 0 (wind loads only) for the same earthquake. Again the stiffness degrading model was used for the frames and a bilinear moment-curvature diagram for the walls. Viscous damping was assumed 5% in all the modes. The comments of the previous paragraph for the frame ductilities apply to the frames here also.

Before presenting the results we will comment on the definition of ductility factor for the shear walls, since it is different from what has been used until now. So far, ductility has been de-

	CMRF - X							
FLOOR	PLASTIC MOMENTS					MOM. OF INERTIA.		
	EXT. COL.	INT. COL.	GIR. 1	GIR. 2	GIR. 3	GIR. 1	GIR. 2	GIR. 3
1	243.	913.	244.	303.	361.	.25	.31	.36
2	244.	702.	361.	377.	392.	.36	.36	.36
3	249.	733.	"	"	"	"	"	"
4	233.	761.	"	"	"	"	"	"
5	240.	673.	"	"	"	"	"	"
6	227.	629.	334.	348.	361.	.40	.38	"
7	230.	572.	"	"	"	"	"	"
8	200.	550.	"	"	"	"	"	"
9	182.	433.	361.	361.	"	.36	.36	"
10	140.	372.	246.	280.	314.	.22	.24	.25
11	129.	350.	"	"	"	"	"	"
12	120.	316.	"	246.	246.	"	.22	.22
13	111.	289.	"	"	"	.21	.21	.21
14	100.	261.	220.	220.	220.	.18	.18	.18
15	92.1	233.	"	"	"	"	"	"
16	73.3	205.	174.	174.	174.	.20	.17	.15
17	120.	177.	133.	133.	133.	.12	.12	.12
	MOMENT OF INERTIA							
1-17	.21	.13						

	CFR - X			CFR - Y		
FLOOR	PLASTIC MOMENTS					
	EXT. COL	INT. COL	GIRDERS	EXT. COL.	INT. COL.	GIRDERS
1-4	235.	640.	36.	90.	640.	36.
5-8	"	530.	"	"	530.	"
9-12	"	370.	"	135.	370.	"
13-17	"	235.	"	"	235.	"
	MOMENTS OF INERTIA					
1-17	.94	.94	.12	.208	.94	.12

MASS / FLOOR = 67 Kips sec^2/ft
STORY HEIGHT = 9.0 ft
BAY WIDTH = 20.0 ft

T_x = 3.135 sec
T_y = 2.322 sec

Table 5-6 PROPERTIES OF FRAMES FOR 17-STORY CONCRETE SHEAR-WALL BUILDING.

FLOOR	SHW1 - Y				SHW2 - Y			
	I	A_s	P.M.	SH.C.	I	A_s	P.M.	SH.C.
1	441.	18.3	37300.	980.	732.	21.7	58800.	1640.
2	"	"	33300.	"	"	"	53600.	"
3	"	"	29200.	"	"	"	48900.	"
4	"	"	28800.	"	"	"	43600.	"
5	"	"	24200.	"	"	"	38600.	"
6	"	"	21400.	"	"	"	33700.	"
7	"	"	18600.	"	"	"	32900.	"
8	"	"	16100.	"	"	"	27600.	"
9	"	"	13300.	"	"	"	22500.	"
10	"	"	10500.	"	"	"	16600.	"
11	"	"	8660.	"	"	"	15000.	"
12	"	"	6600.	"	"	"	10500.	"
13	"	"	6120.	"	"	"	9600.	"
14	"	"	5830.	"	"	"	8900.	"
15	"	"	5280.	"	"	"	8820.	"
16	"	"	4730.	"	"	"	7770.	"
17	"	"	4170.	"	"	"	7110.	"

Table 5-7

SHEAR-WALL PROPERTIES OF 17-STORY CONCRETE BUILDING

fined as the ratio of the maximum displacement to the yield displacement for an element. This was possible because of the assumption of close-coupled systems. The wall, however, is a far-coupled system, and the above definition is meaningless. Since it does not deform symmetrically, the end conditions of the member are not known, so we cannot use a definition based on angles of rotation. The definition we have adopted is similar to that of reference (9) and is based on curvature. Figure 5-30 shows the bilinear model used for the moment vs. curvature of a shear wall section.

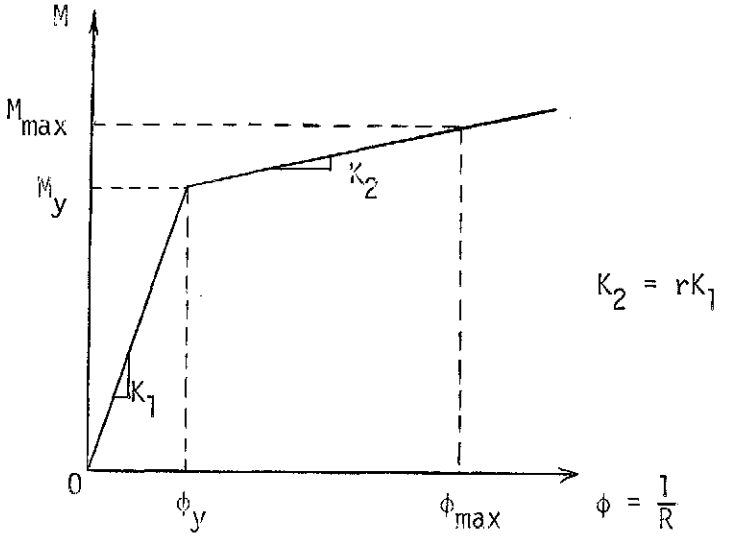

Figure 5-30

Ductility Definition for Shear Walls

We define: $$\mu = \frac{\phi_{max}}{\phi_y} = 1 + \frac{\phi_{max} - \phi_y}{\phi_y} \qquad (5.1)$$

It is $$\phi_y = \frac{M_y}{K_1}$$

and $$M_{max} = M_y + (\phi_{max} - \phi_y) \cdot K_2$$

So $$\phi_{max} - \phi_y = \frac{M_{max} - M_y}{K_2}$$

Replacing ϕ_y and $\phi_{max} - \phi_y$ in 5-1 we finally get:

$$\mu = 1 + \frac{K_1}{K_2} \cdot \left(\frac{M_{max}}{M_y} - 1 \right) \qquad (5.2)$$

where: $K_1 = EI$

$K_2 = rK_1$ $\quad (r = 0.03)$

M_y = Plastic moment of the section that includes the effect of gravity loads.

M_{max} = Maximum moment at the section computed by the program.

Ductility factors for the interior and exterior walls have been plotted in Figure 5-31. In both cases the walls remain elastic in all floors except the 10^{th}, 11^{th}, 12^{th} and 13^{th}. Maximum ductilities occur in both cases at the 12^{th} floor and their value is extremely high (about 10). Since walls are not usually reinforced for such high ductility levels, failure of the walls should be expected in that area. Clough (7) has obtained similar results

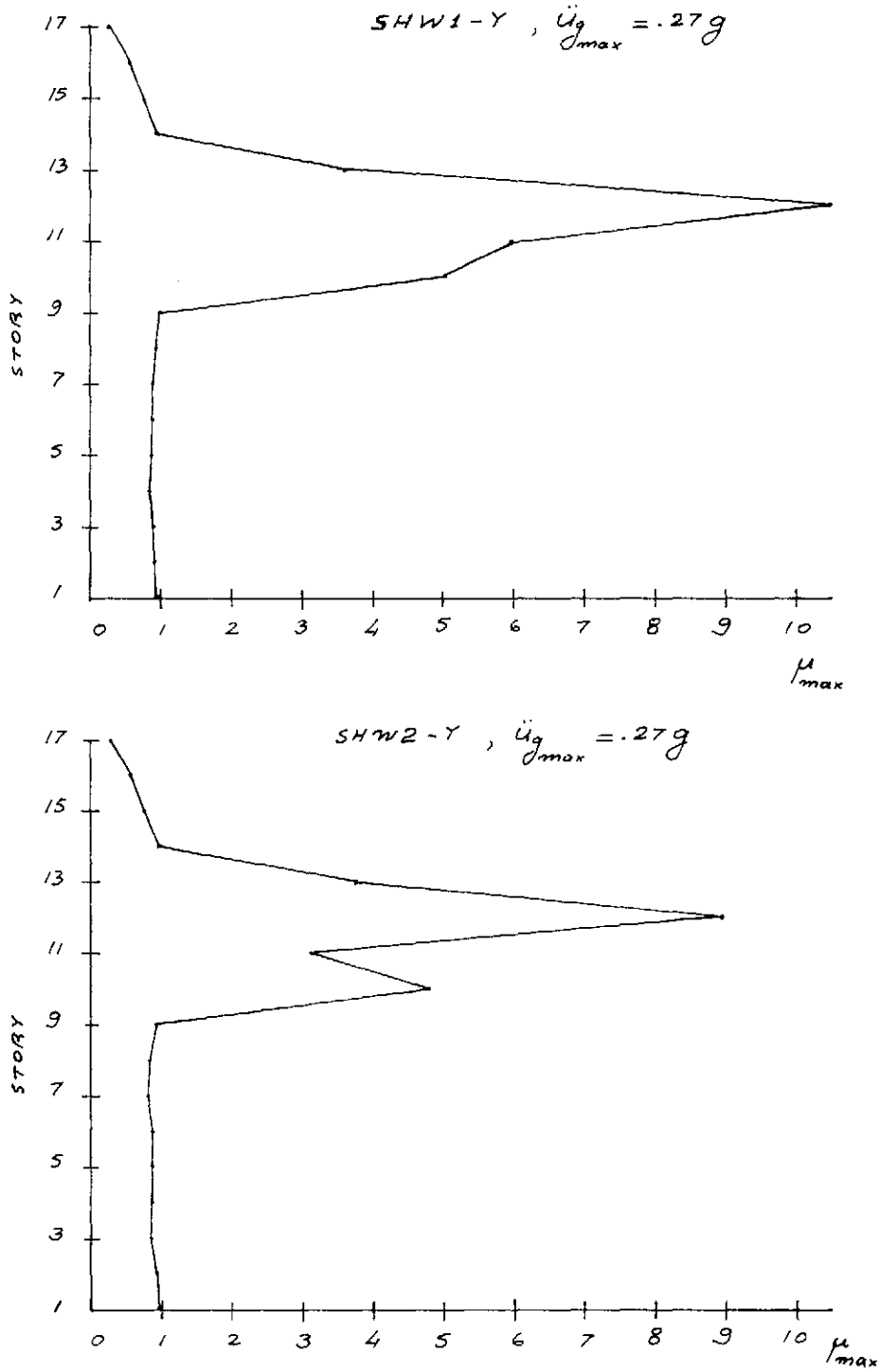

Figure 5-31 SHEAR WALL DUCTILITIES FOR 17-STORY CONCRETE SHEAR-WALL BUILDING

for the shear wall buildings he analyzed. It is interesting that these high ductilities occur in the 12^{th} floor and not at the bottom. The reason for this is the interaction of the walls with the interior frames CFR-Y, that were included in the analysis. Due to the different deformation patterns of the two elements, large forces are acting on the walls at the top levels, becoming minimum around mid-height and changing sign at the lower stories. Although the maximum moments occur at the bottom, the ratio of the applied moments to the yield moments becomes maximum a little above mid-height and hence the observed behavior. The exterior wall experienced a maximum shear of 727 kips at the bottom story and the interior 973 kips, both below the corresponding ultimate shear capacities. The shear-wall-frame interaction can also be observed in the lower part of Figure 5-32, where the ductility factors for the frames in the Y direction were plotted. These factors being minimum at the lower stories keep increasing towards the top, reaching a maximum of 4.5 at the top. The actual local ductilities will probably be twice as big if we take into account that yielding starts occurring at a story shear about half the ultimate. The same is true for the frames in the X direction. The interior frame, which was not designed as moment resisting, is controlled by the strength of the slab, which is very low (in comparison with the girder strength of the exterior frame), so its ductility factors are very large. On the other hand, the ductility factors of the moment resisting frame are relatively small, with a maximum of 2.7 at the bottom story. This indicates

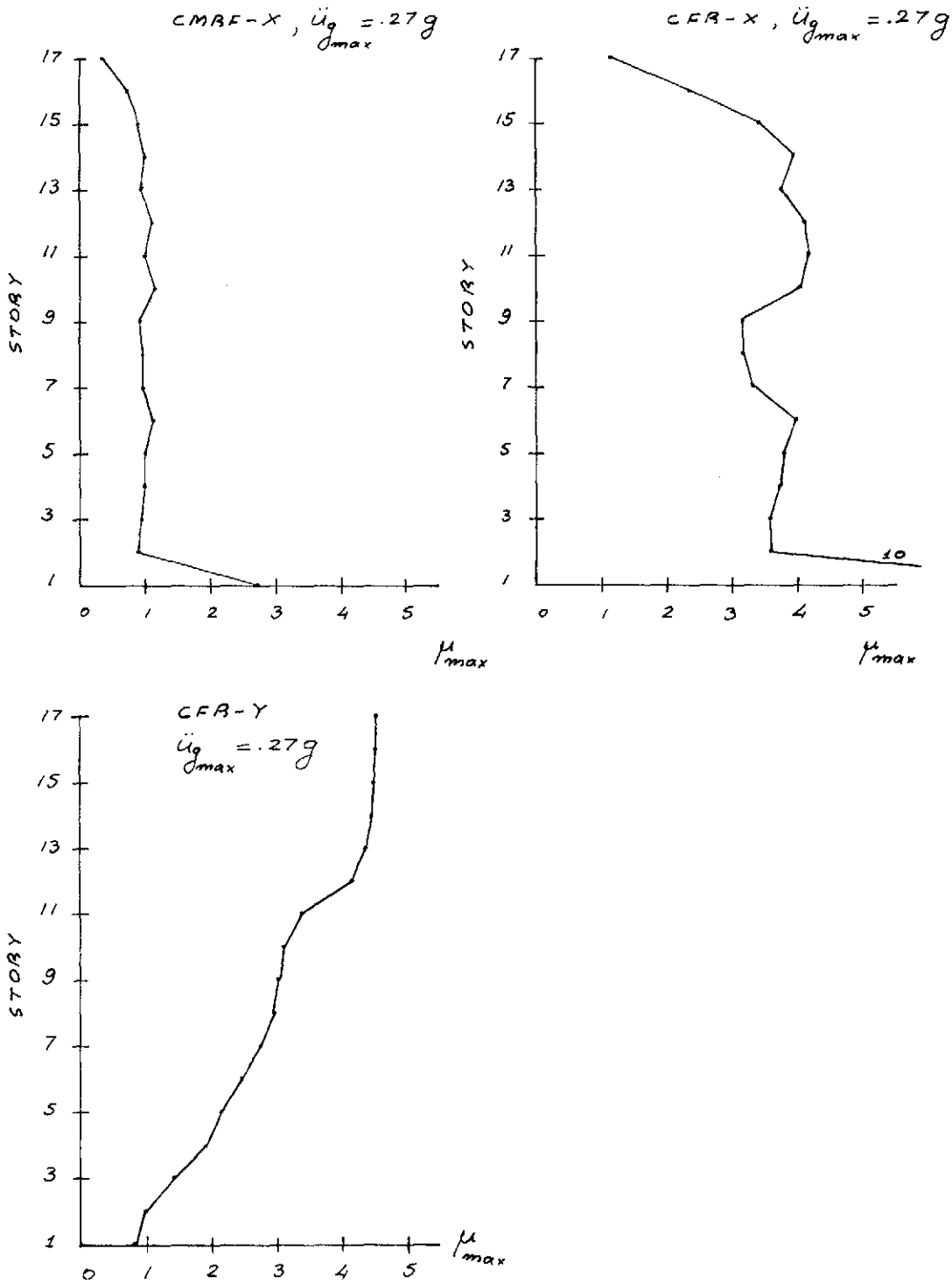

Figure 5-32 FRAME DUCTILITIES FOR 17-STORY CONCRETE SHEAR-WALL BUILDING

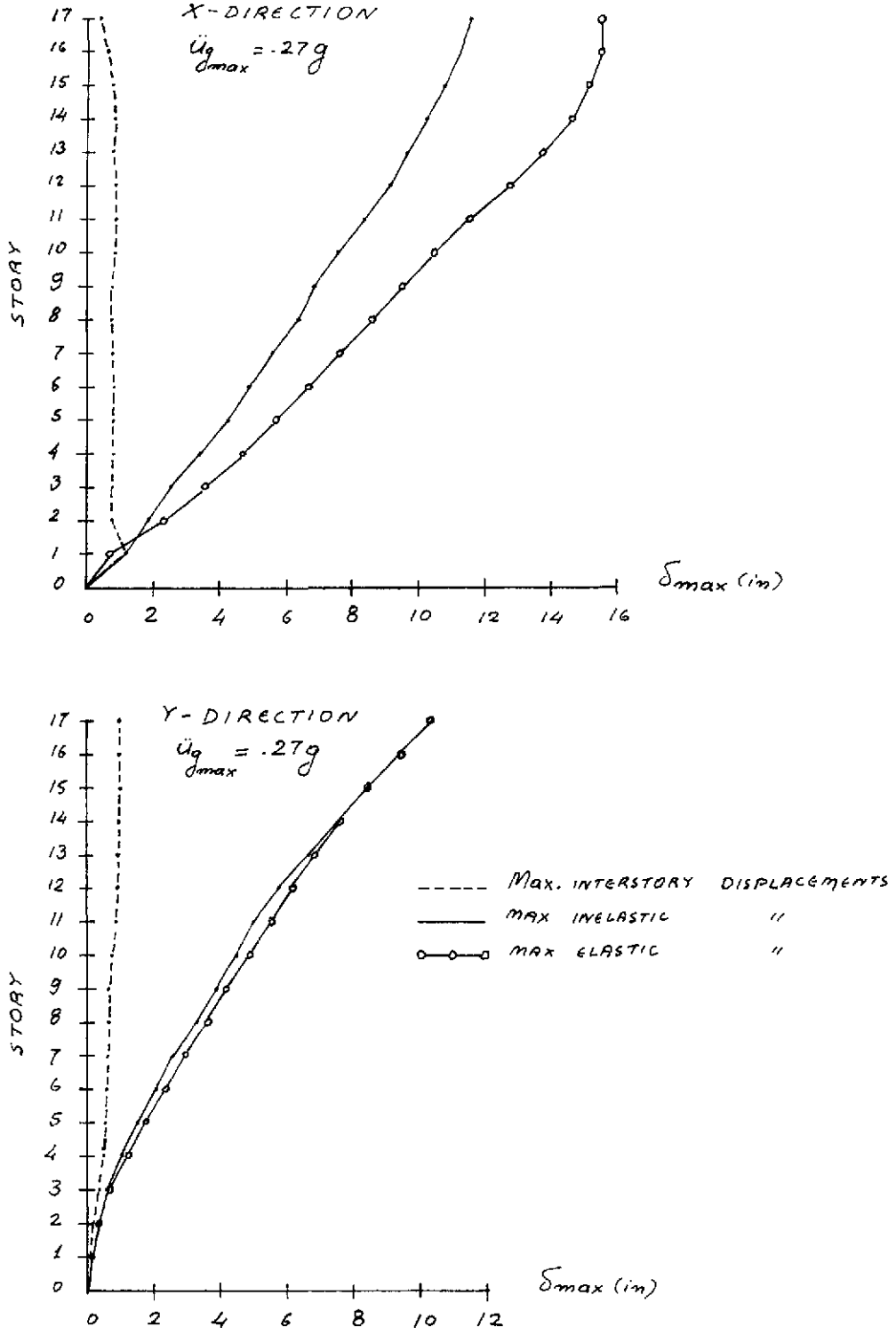

Figure 5-33

DISPLACEMENTS OF 17-STORY CONCRETE SHEAR-WALL BUILDING

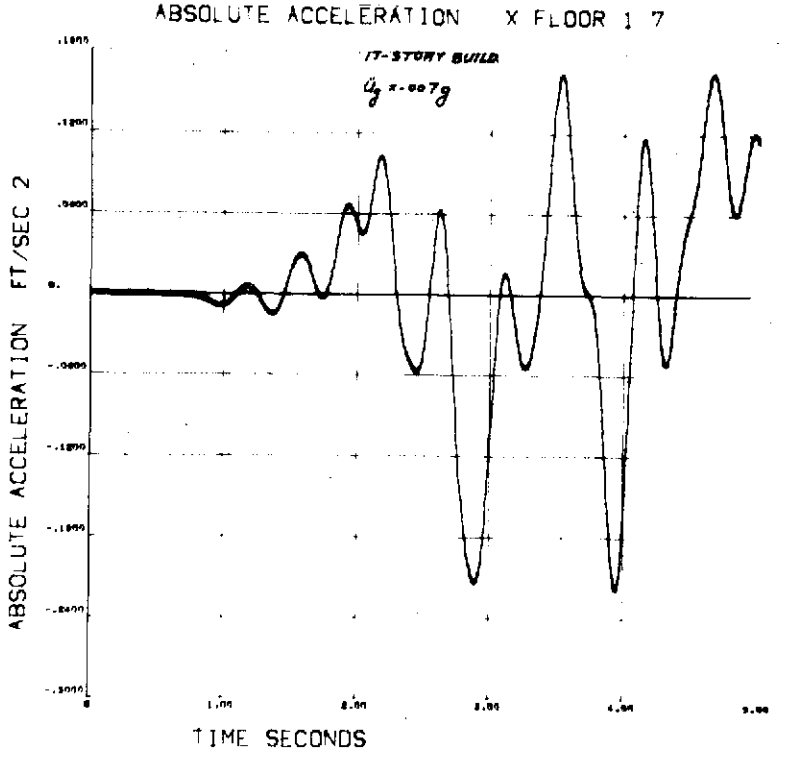

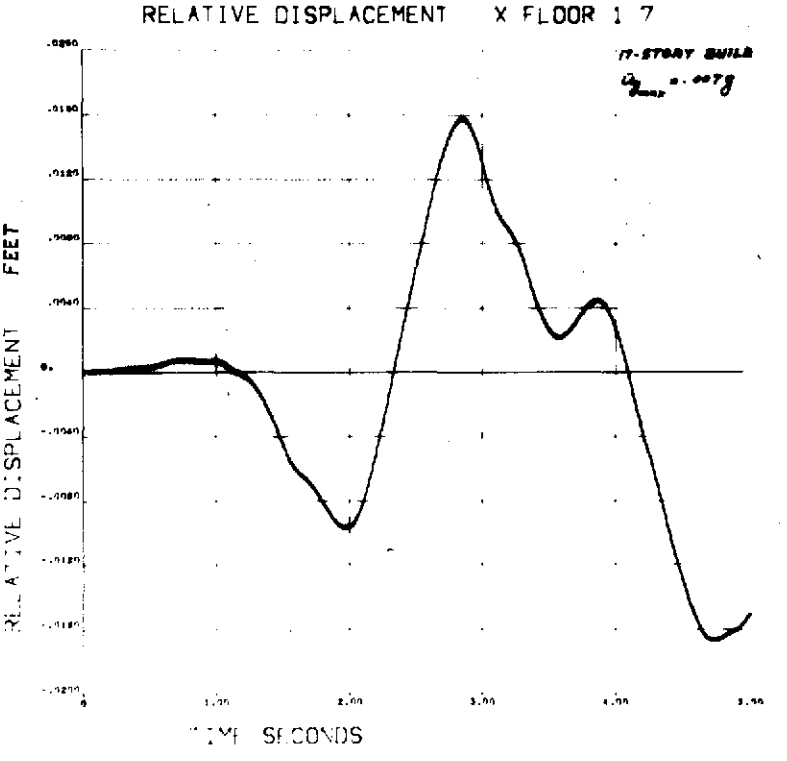

Figure 5-34 Elastic Response

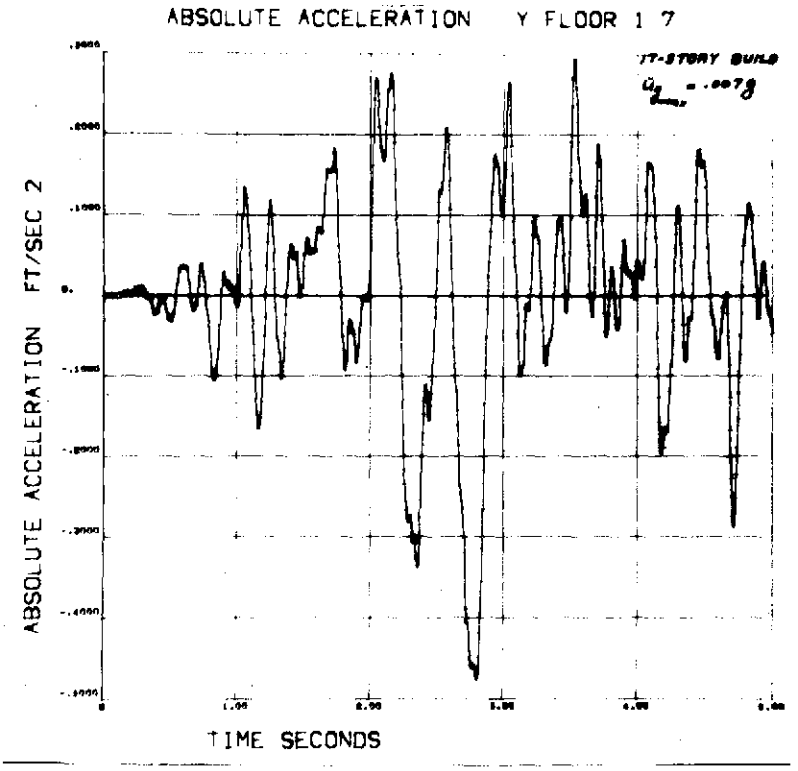

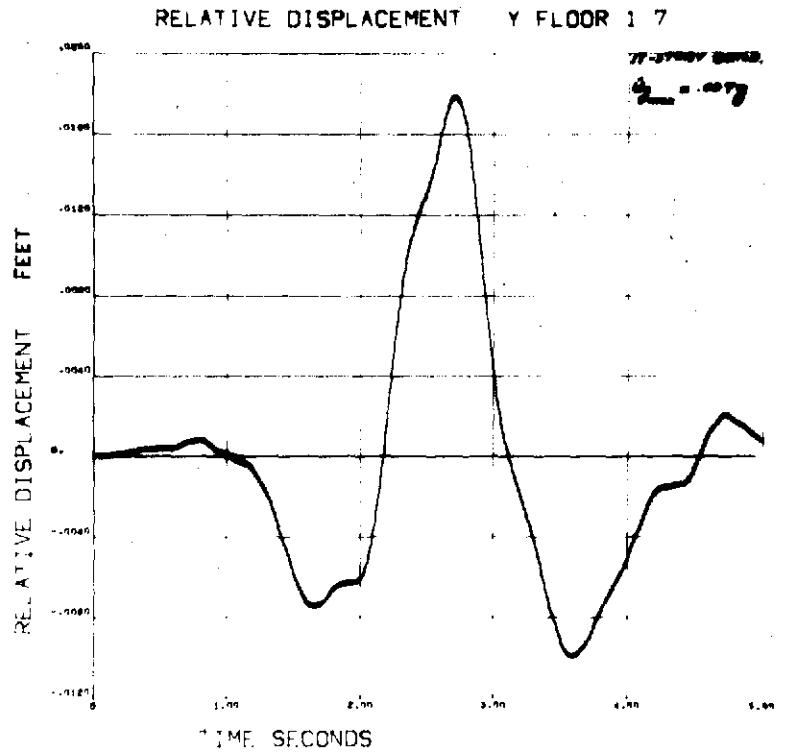

Figure 5-35 Elastic Response

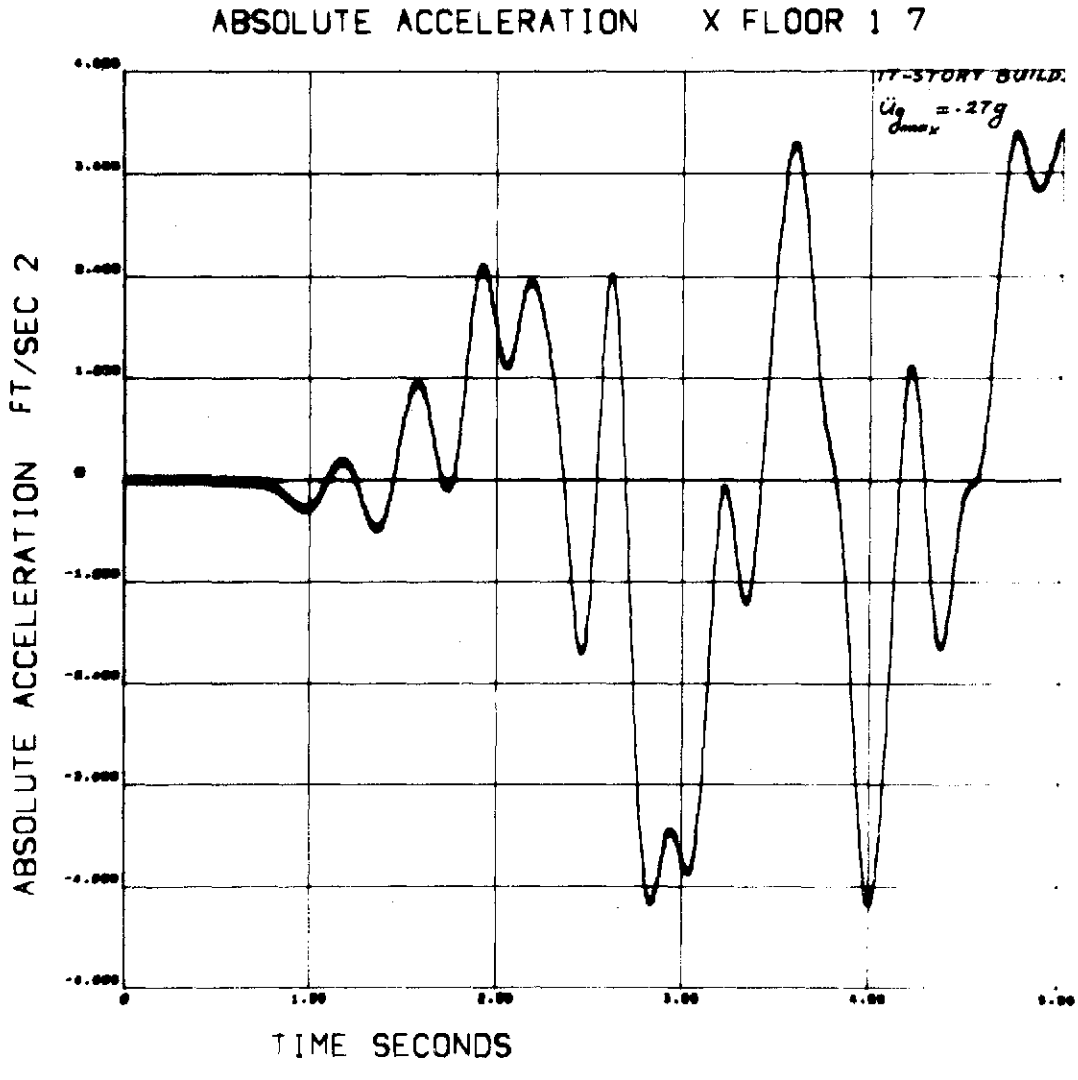

Figure 5-36 Inelastic Response

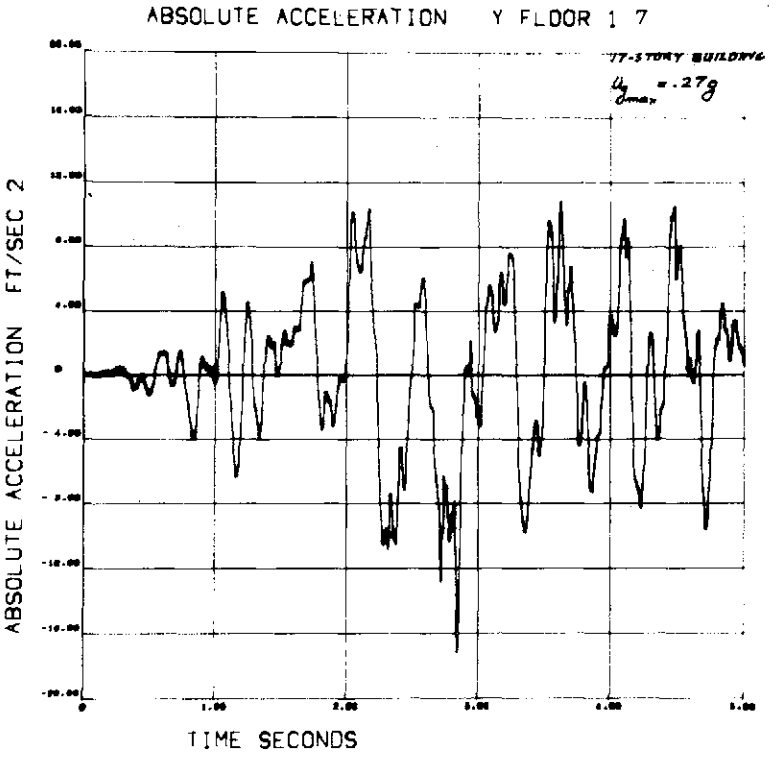

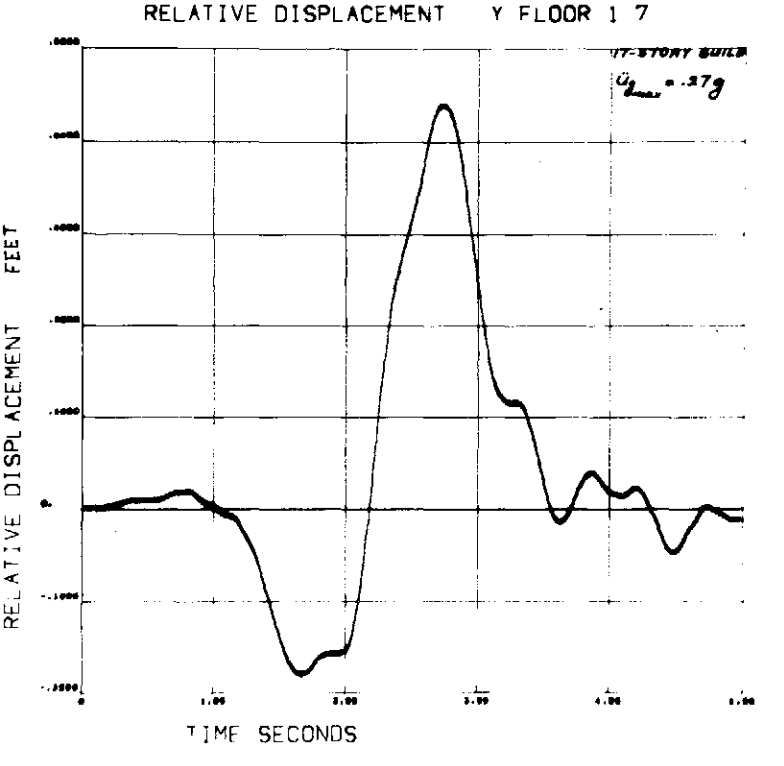

Figure 5-37 Inelastic Response

that a strong earthquake in the X direction will cause considerable damage to the interior columns and slabs, but probably not collapse. Maximum displacements were plotted in Figure 5-33. We see that in the Y direction the elastic displacements are very close to the inelastic ones, while in the X they are larger. The explanation to this, given earlier, applies here too.

Time histories for elastic and inelastic top story displacements and accelerations are given in Figures 5-34, 35, 36, 37. The difference between the responses in the two directions is first due to the different fundamental periods and second due to the different participation of the higher modes. Various other time histories have been included in Appendix C.

As a final point before closing the chapter, it is worth mentioning that the time step used for the analysis of the shear wall building was 0.005 sec, half of that used for all other cases. The discussion in chapter 4 was only for the case of shear-type buildings, for which it was pointed out that the smallest natural period does not change significantly with increasing number of stories. For cantilever type structures, however, this is not true any more, and the smallest period of a shear wall is much smaller than that of an equally stiff frame. It was for this reason that a time step $\Delta t = 0.01$ sec was causing numerical instability. The $\Delta t = 0.005$ sec used is about 1/3 of the smallest period.

CHAPTER 6

CONCLUSIONS AND RECOMMENDATIONS

6.1 Introduction

The results and conclusions reached in this study have been discussed in detail in chapters 2, 3, 4, 5. A summary of the most important ones will be given here, together with recommendations for future research.

6.2 Conclusions

The main conclusions of this work are the following:

1. It is possible to create mathematical models that simulate the behavior of a big variety of structural elements (braced frames, infilled frames, etc.) and to include such factors as stiffness and/or strength degradation.

2. Three new models are proposed here:
   (a) A stiffness and strength degradation model for infilled concrete frames.
   (b) A stiffness and strength degradation model for infilled steel frames.
   (c) A trilinear model

3. The stiffness degrading model with varying slope of the unloading branches gives very similar results with the standard degrading model.

4. Based on studies with 1-DOF systems, which were confirmed by studies on M-DOF close-coupled systems, it was concluded that the Uniform Building Code does not provide uniform safety (expressed in terms of ductilities) over the entire spectral

range, but it is unconservative for short period structures and rather conservative for flexible long period buildings.

5. It was shown that it is possible to derive base shear-coefficient laws that will provide uniform ductilities over the entire frequency range. Several such laws were derived for various prespecified values of the required ductility factor.

6. It is possible to predict the overall inelastic behavior of a building by using a simplified mathematical model and including additional effects that are normally neglected in a more accurate analysis.

7. The model gives good results for shear type buildings or for combination of frames and shear walls.

8. It predicts average story ductilities, but not local values, and it fails to reproduce the behavior of frames in which the axial shortening of the columns is significant.

9. The method used to estimate the strength of a story in a frame probably underestimates the strength of the first story.

10. Shear walls should be designed to remain elastic under the strongest earthquake, since if the yield moment is slightly exceeded, large ductilities will be required.

11. Frames that have a first mode similar to that of a shear beam should have either increased strength of the bottom story or increased ductility.

12. Torsional effects increase the ductility requirements.

6.3 Recommendations for Future Research

At this point it seems appropriate that further research is needed in the following areas:

1. In the area of modelling behavior of structural components more experimental work is needed for infilled frames.

2. Least square fits of the curves obtained in chapter 3 and additional computer runs with artificial earthquakes that produce smooth response spectra seem desirable.

3. For 1-DOF systems additional studies for various values of the parameter λ, defined in chapter 3, should be done, and base-shear-coefficient laws that include the ductility factor and the percentage of viscous damping should be sought.

4. For moment resisting frames, a more accurate method to predict the ultimate strength and the first yield level of a story should be sought.

5. More studies on the effect of gravity for 1-DOF are desirable.

6. More studies on the effect of torsion seem appropriate.

7. Implementation of the formulation for gravity loads and soil flexibility for M-DOF systems.

8. More research is needed to correlate ductilities for M-DOF systems to those of equivalent 1-DOF's.

References

1. Biggs, J.M., Introduction to Structural Dynamics, McGraw-Hill, New York, 1964.

2. Hurty, W.C. and Rubinstein, M.F., Dynamics of Structures, Prentice-Hall, New Jersey, 1964.

3. Newmark, N.M. and Rosenblueth, Fundamentals of Earthquake Engineering, Prentice-Hall, New Jersey, 1971.

4. Wiegel, R.L., Earthquake Engineering, Prentice-Hall, New Jersey, 1970.

5. Blume, J.A. et al., Design of Multistory Reinforced Concrete Buildings for Earthquake Motions, Portland Cement Association, Illinois, 1961.

6. Roesset, J.M.V., Unpublished course notes for Structural Dynamics, M.I.T. 1969.

7. Clough, R.W. and Benuska, K.L., FHA Study of Seismic Design Criteria for High-Rise Buildings, HUD TS-3, August 1966.

8. Goel, S.C., Response of Multistory Steel Frames to Earthquake Forces, Steel Research for Construction, Bulletin 12, November 1968.

9. Anderson, J.C., Seismic Behavior of Multistory Frames, Designed by Different Philosophies, Ph.D. Thesis, University of California, Berkeley, Civil Engineering, 1969.

10. Latona, R.W., Non-Linear Analysis of Building Frames for Earthquake Loading, M.I.T. Department of Civil Engineering Research Report R70-65, 1970.

11. Shiga et al., "The Dynanic Properties of Reinforced Concrete Frames," Proceedings of the U.S. - Japan Seminar on Earthquake Engineering, with Emphasis on Safety of School Buildings, Sept. 1970, pp. 346-363, Japan.

12. Higashi, Y. and Ohkubo, Y., "Statical and Dynamic Loading Tests of Reinforced Concrete Frames with Thin Spandrel or Wing Walls," Proceedings of the U.S. - Japan Seminar on Earthquake Engineering, with Emphasis on the Safety of School Buildings, Sept. 1970, pp. 225-239, Japan.

13. Shah, S.P. and Winter, G., "Response of Concrete to Repeated Loading," International Symposium on the Effect of Repeated Loading of Materials and Structures, Rilem Instituto de Ingenieria, Vol. III, September 1966, Mexico.

14. Burns and Siess, "Plastic Hinging in Concrete," Journal of The Structural Division, A.S.C.E., Oct. 1966, pp. 65-78.

15. Burns and Siess, "Repeated and Reversed Loading in Reinforced Concrete," Journal of the Structural Division, A.S.C.E., Oct. 1966, pp. 45-64.

16. Hanson, N.W., "Seismic Resistance of Concrete Frames with Grade 60 Reinforcement," Journal of the Structural Division, A.S.C.E., June 1971, pp. 1685-1700.

17. Bertero, V. and McClure, G., "Behavior of Reinforced Concrete Frames Subjected to Repeated Reversible Loads," Journal of the A.C.I., October, 1964, pp. 1305-1328.

18. Kusho, S.K. and Hayashi, S., "Strength Reduction of Reinforced Concrete Members due to Alternately Cyclic Loading," ASCE-IABSE: 3rd Regional Conference, Proceedings, Tokyo, Japan, September 1971.

19. Hanson, N.W. and Connor, H.W., "Seismic Resistance of R.C. Beam-Column Joints," Journal of the Structural Division, A.S.C.E., October 1967, pp. 533-560.

20. Medland, I.C. and Taylor, D.A., "Flexural Rigidity of Concrete Column Sections," Journal of The Structural Division, A.S.C.E., February 1971, pp. 573-586.

21. Poluakov et al., "Strength and Deformations of Concrete, Masonry and Joints under Rapid Once-Applied and Repeated Loadings," Rilem-Instituto de Ingenieria, Vol. III, Sept. 1966, Mexico.

22. Sinha, B.P. et al., "Response of Singly Reinforced Beams to Cyclic Loading," Journal of the ACI, August 1964, pp. 1021-1037.

23. Agrawal, G.L. et al., "Response of Doubly Reinforced Concrete Beams to Cyclic Loading," Journal of the ACI, July 1965, pp. 823-834.

24. Sinha et al., "Stress-Strain Relations for Concrete under Cyclic Loading," Journal of the ACI, February 1964, pp. 195-212.

25. Takeda, T. et al., "Reinforced Concrete Response to Simulated Earthquakes," Proceedings of the 3rd Japan Earthquake Engineering Symposium, 1970, pp. 357-364.

26. Otani, S. et al., "Response of Reinforced Concrete Frames Subjected to Simulated Earthquakes," Proceedings of the 3rd Japan Earthquake Engineering Symposium, 1970, pp. 365-372.

27. Tani, S. et al., "Study on Restoring Force Characteristics of Reinforced Concrete Structures (Static Analysis), Proceedings of the 3rd Japan Earthquake Engineering Symposium, 1970, pp. 699-698.

28. Tani, S. et al., "Study on Restoring Force Characteristics of Reinforced Concrete Structures (Nonlinear Seismic Response) Proceedings of the 3rd Japan Earthquake Engineering Symposium, 1970, pp. 699-706.

29. Nielsen, N.N. and Imbeault, F.A., "Validity of Various Hysteretic Systems," Proceedings of the 3rd Japan Earthquake Engineering Symposium, 1970, pp. 707-714.

30. Aoyama, H. et al., "A Study on the Cause of Damage to the Hachinoke Technical College due to 1968 Tokachi-Oki Earthquake (Parts 1, 2), Proceedings of the U.S. - Japan Seminar on Earthquake Engineering with Emphasis on the Safety of School Buildings, Sept. 1970, Japan, pp. 199-224.

31. Ohsaki, Y. et al., "Experimental Study on Five-Story Full-Size Apartment House of Reinforced Concrete Walled Frames," Proceedings of the U.S. - Japan Seminar on Earthquake Engineering with Emphasis on the Safety of School Buildings, Japan 1970, pp. 240-266.

32. Kokusho, S. and Ogura, K., "Shear Strength and Load Deflection Characteristics of Reinforced Concrete Members," Proceedings of the U.S. - Japan Seminar on Earthquake Engineering with Emphasis on the Safety of School Buildings, Japan, 1970, pp. 364-381.

33. Bertero, V. et al., Stiffness Degradation of Reinforced Concrete Members Subjected to Cyclic Flexural Moments, Earthquake Engineering Research Center, Report No. EERC 69-12, Berkeley, December 1969.

34. Beaufait, F. and William, R., "Experimental Study of Reinforced Concrete Frames Subjected to Alternating Sway Forces," Journal of the ACI, November 1968, pp. 980-984.

35. Bertero, V. and Bresler, B., "Seismic Behavior of Reinforced Concrete Structures," Proceedings of the 4th World Conference on Earthquake Engineering, Vol. I, B-2.

36. Neville, A.M., Properties of Concrete, Wiley, 1963.

37. Gulkan, P. and Sozen, Y., Response and Energy Dissipation of Reinforced Concrete Frames Subjected to Strong Base Motions, Civil Engineering Studies, Structural Research Series No. 377, University of Illinois, May 1971.

38. _____, Plastic Design of Multistory Frames, Lecture Notes, Vol. 2, Lehigh University, Summer 1965.

39. Hanson, R.D., "Comparison of Static and Dynamic Hysteresis Curves," Journal of the Engineering Mechanics Division, A.S.C.E. October, 1966, pp. 87-113.

40. Symonds, P.S., "Cyclic Loading Tests on Small-Scale Portal Frames," Final Report, IABSE, 4th Congress, Cambridge and London, 1953.

41. Symonds, P.S. and Neal, B.G., "Cyclic Loading of Portal Frames, Theory and Tests," Vol. 18, Publication IABSE, Zurich, 1958.

42. Naka et al., "Research on the Behavior of Steel Beam-to-Column Connections in the Seismic Resistant Structure," Proceedings of the 4th World Conference on Earthquake Engineering, Vol. II, B-3.

43. Watanabe, H., "Dynamic Characteristics of Elasto-Plastic Restoring Force of Mild Steel," Proceedings of the 3rd Japan Earthquake Engineering Symposium, 1970.

44. Popov, E.P. and Pinkney, R.B., "Cyclic Yield Reversal in Steel Building Connections," Journal of the Structural Division, A.S.C.E., March 1969, pp. 327-353.

45. Wakabayashi, M., "The Behavior of Steel Frames with Diagonal Bracings under Repeated Loadings," Proceedings of the U.S. - Japan Seminar on Earthquake Engineering with Emphasis on the Safety of School Buildings, Sept. 1970, pp. 328-345.

46. Hanson, R.D. and Almuti, A.M., "Post-Elastic Response of Mild Steel Structures," Proceedings of the 3rd Japan Earthquake Engineering Symposium, 1970, pp. 643-650.

47. Arnold, P. et al., "The Effect of Instability on the Cyclic Behavior of a Frame," Rilem - Instituto de Ingenieria, Vol. V, September 1966, Mexico.

48. Carpenter, L.D. and Le-Wu-Lu, "Repeated and Reversed Load Tests on Full-Scale Steel Frames," Proceedings of the 4th World Conference on Earthquake Engineering, Vol. I, B-2.

49. Bertero, V. et al., "Half-Scale Tests of Subassemblages of Multistory Unbraced Steel Frames under Cyclic Loading," Proceedings of the 3rd Japan Earthquake Engineering Symposium, 1970, pp. 659-666.

50. Tamura et al., "A Vibration Test of a Large Model Steel Frame with Precast Concrete Panel, untill Failure," Proceedings of the 4th World Conference on Earthquake Engineering, Vol. I, B-2.

51. Kaneta et al., "On the Strength and Ductility of Welded Joints Subjected to Low-Cycle Elasto-Plastic Deformations," Proceedings of the 3rd Japan Earthquake Engineering Symposium, 1970, pp. 667-674.

52. Williams, H.A. and Benjamin, J.R., Experimental Behavior and Empirical Results. Plain Concrete and Brick-Walled Bents under Static Shear Loading, Investigation of Shear Walls, Part 1, Stanford University, 1952.

53. Williams, H.A. and Benjamin, J.R., Prediction of the Behavior of the Plain Concrete, Reinforced Concrete and Brick-Walled Bents under Static Shear Loading, Investigation of Shear Walls, Part 5, Stanford University, 1953.

54. Benjamin, J.R. and Williams, H.A., Summary of Results of Study of Reinforced Concrete and Brick-Walled Bents, under Static Shear Loading, Investigation of Shear Walls, Part 13, Final Report, Stanford University.

55. Esteva, L., "Behavior under Alternating Loads of Masonry diaphragms Framed by Reinforced Concrete Members," Rilem - Instituto de Ingenieria, Vol. 5, September 1966.

56. Smith, B.S., "Lateral Stiffness of Infilled Frames," Journal of The Structural Division, A.S.C.E., December 1962, pp. 183-199.

57. Smith, B.S., "Behavior of Square Infilled Frames," Journal of the Structural Division, A.S.C.E., February 1966, pp. 381-403.

58. Fedorkiw, J.P. and Sozen, M.A., A Lumped Parameter Model to Simulate the Response of Reinforced Concrete Frames with Filler Walls, A Report to the Department of Defense, University of Illinois, Urbana, Illinois, June 1968.

59. Bonvalet, C. et al., "Influence des remplissages dans les bâtiments a ossature soumis aux efforts horizontaux dus au vent et aux séismes," Annales de l'Institute Technique du Batiment et des Travaux Publics, No. 276, December 1970.

60. Kaldjian, M.J. and Fan, Wm. R.S., Response of Steel Frames to Earthquake Forces, Steel Research for Construction, Bulletin No. 11, November 1968.

61. Housner, G.W., "Limit Design of Structures to Resist Earthquakes," Proceedings of the 1st World Conference on Earthquake Engineering.

62. Housner, G.W., "Behavior of Structures during Earthquakes," Journal of the Engineering Mechanics Division, A.S.C.E., October 1959, pp. 109-129.

63. Berg, G.V. and Thomaides, S.S., "Energy Consumption by Structures in Strong Motion Earthquakes," Proceedings of the 2nd World Conference on Earthquake Engineering, Vol. II.

64. Veletsos, A.S. and Newmark, N.M., "Effect of Inelastic Behavior on the Response of Simple Systems to Earthquake Motions," Proceedings of the 2nd World Conference on Earthquake Engineering, Vol. II.

65. Veletsos, A.S. et al., "Deformation Spectra for Elastic and Elastoplastic Systems, Subjected to Ground Shock and Earthquake Motions," Proceedings of the 3rd World Conference on Earthquake Engineering, Vol. II.

66. Veletsos, A.S., "Maximum Deformations of Certain Non-Linear Systems," Proceedings of the 4th World Conference on Earthquake Engineering, Vol. II.

67. Jennings, P.C., Response of Simple Yielding Structures to Earthquake Excitation, Ph.D. Thesis, California Institute of Technology, 1963.

68. Husid, R., Gravity Effects on the Earthquake Response of Yielding Structures, California Institute of Technology, Research Report, 1967.

69. Clough, R.W. and Johnston, S.B., "Effect of Stiffness Degradation on Earthquake Ductility Requirements," Proceedings of the Japan Earthquake Engineering Symposium, 1967.

70. Clough, R.W. et al., "Inelastic Earthquake Response of Tall Buildings," Proceedings of the 3rd World Conference on Earthquake Engineering, Vol. II.

71. Arias, A., "A Measure of Earthquake Intensity," Seminar on Seismic Design for Nuclear Power Plants, Department of Civil Engineering, M.I.T., 1969.

72. Newmark, N.M., "Current Trends in the Seismic Analysis and Design of High-Rise Structures," Chapter 16, in Earthquake Engineering, by Wiegel.

73. Penzien, J., "Elastoplastic Response of Idealized Multi-Story Structures, Subjected to a Strong Motion Earthquake," Proceedings of the 2nd World Conference on Earthquake Engineering, Vol. II.

74. Garcia, F.and Roesset, J.M., Influence of Damping on Response Spectra, M.I.T. Department of Civil Engineering, Research Report R70-4, January 1970.

75. Anagnostopoulos, S.A., A Computer System for Approximate Analysis of Multistory Buildings under Earthquake Loads," M.I.T. Department of Civil Engineering Research Report R70-6, January 1970.

76. Giberson, M.F., "Maximum Response Ranges of Non-Linear Multi-Story Structures Subjected to Earthquakes," Bulletin of the Seismological Society of America, Vol. 58, No. 5, October 1968, pp. 1639 - 1655.

77. Leslie, S.K.and Biggs, J.M., Earthquake Code Evolution and the Effect of Seismic Design on the Cost of Buildings, M.I.T. Department of Civil Engineering Research Report R72-20, May 1972.

78. Vitiello, E., "Seismic Elastic-Plastic Behavior of Multi-Story Buildings with 'Shear-bending Type' Resistant Structures," Proceedings of the 3rd European Symposium on Earthquake Engineering, Sofia, Bulgaria, September 1970, pp. 581-583.

79. Velkov, M., "Elastoplastic Response of a Reinforced Concrete Multi-Storied Building with Energy Absorption Elements," Proceedings of the 3rd European Symposium on Earthquake Engineering, Sofia, Bulgaria, September 1970, pp. 505-512.

80. Jurukovski, D. and Bickovski, V., "Dynamic Response to Torsional and Shear Vibrations," Proceedings of the 3rd European Symposium on Earthquake Engineering, Sofia, Bulgaria, September 1970, pp. 673-683.

81. Hanson, R.D. and Fan, W.R.S., "The Effect of Minimum Cross-Bracing on the Inelastic Response of Multi-story Buildings," Proceedings of the 4th World Conference on Earthquake Engineering, Vol, II, A4.

82. Guru, B.P. and Heidebrecht, A.C., "Factors Influencing the Inelastic Response of Multi-Story Frames, Subjected to Strong Mo-

tion Earthquakes," Proceedings of the 4th World Conference on Earthquake Engineering, Vol. II, A4.

83. Nigam, N.C. and Housner, G.W., Elastic and Inelastic Response of Framed Structures during Earthquakes," Proceedings of the 4th World Conference on Earthquake Engineering, Vol. II, A4.

84. Odaka, T. et al., "Non-Linear Response Analysis of Multi-Story Structures, Including Rocking and Swaying Vibration, Subjected to Earthquake Ground Motions," Proceedings of the 4th World Conference on Earthquake Engineering, Vol. II, A4.

85. Shibata, A. et al., "Torsional Response of Buildings to Strong Earthquake Motions," Proceedings of the 4th World Conference on Earthquake Engineering, Vol. II, A4.

86. Spencer, R.A., "The Non-Linear Response of a Multi-Story Prestressed Concrete Structure to Earthquake Excitation," Proceedings of the 4th World Conference on Earthquake Engineering, Vol. II, A4.

87. Walpole, W.R. and Shepherd, R., "The Inelastic Response of a Steel Frame," Proceedings of the 4th World Conference on Earthquake Engineering, Vol. II, A4.

88. Piceski, A. and Petrovski, D., "Response of a 16-Story Frame Structure with Bilinear Characteristics, on Recorded Earthquakes," Proceedings of the 3rd European Symposium on Earthquake Engineering, Sofia, Bulgaria, September 1970, pp. 591-597.

89. Hanson, R.D. and Degenkolb, H.J., The Venezuela Earthquake, A Report of the American Iron and Steel Institute, 1969.

90. Jennings, P.C., Engineering Features of the San Fernando Earthquake of February 9, 1971, California Institute of Technology, 1971.

91. Uniform Building Code, Section 2314, 1970 edition, ICBO, Pasadena, 1970.

92. Benjamin, J.R. and Williams, H.A., "The Behavior of One-Story Brick Shear Walls," Journal of the Structural Division, A.S.C.E., July 1958, pp. 1723-1—1723-30.

93. Benjamin, J.R. and Williams, H.A., "Behavior of Reinforced Concrete Shear Walls," Transactions, A.S.C.E., Vol. 124, 1959, pp. 669-702.

94. Blume, J.A., "A Reserve Energy Technique for the Earthquake Design and Rating of Structures in the Inelastic Range," Proceedings of the 2nd World Conference on Earthquake Engineering, Vol. II.

95. Fintel, M. and Kahn, F.R., "Shock-Absorbing Soft Story Concept for Multi-Story Earthquake Structures," Journal of the ACI, May 1969, pp. 381-390.

96. Tadaki, K. et al., "Torsional Problems in a Seismic Design of High-Rise Buildings," Proceedings of the 4th Conference on Earthquake Engineering, Vol. II, A-4.

97. Shiga, T., "Torsional Vibrations of Multi-Storied Buildings," Proceedings of the 3rd World Conference on Earthquake Engineering, Vol. II.

98. Farhoomand, I., and Wilson, E., A Nonlinear Finite Element Code for Analyzing the Blast Response of Underground Structures, U.S. Army Engineer Waterways Experiment Station, Contract Report N-70-1, January 1970.

99. Whitman, R.V. and Richart, F.E., "Design Procedures for Dynamically Loaded Foundations," Journal of the Soil Mechanics Division, A.S.C.E., June 1967.

100. Wilson, G.L., "A Method of Analysis for the Evaluation of Foundation-Structure Interaction," Proceedings of the 4th World Conference on Earthquake Engineering, Volume III, A-6.

BIOGRAPHY

The author was born in 1946 in Greece, where he graduated from the Piraeus 1st High School in June 1963.

He entered the School of Civil Engineering of the Technical University of Athens in September 1963 and graduated with a Diploma in Civil Engineering in June 1968 (5-year program).

In September 1968 he started graduate work specializing in structures at M.I.T., where he received the S.M. degree in Civil Engineering in February 1970 and the C.E. degree in June 1971. The first year after he passed his doctoral exams he worked on Building Systems and on elastic dynamic response of tall buildings. He started working on his doctoral thesis in September 1971.

During his graduate work at M.I.T. he was supported by teaching and research assistantships. He also held a 3-year N.A.T.O. fellowship.

His work experience includes design and analysis of structures and summer work for the Finnish State Railways. He is a member of Sigma Xi, a licensed Civil Engineer in Greece, and he belongs to several professional societies. He is author of one M.I.T. report, and co-author of another.

APPENDIX A

DERIVATION OF APPROXIMATE FORMULA FOR STORY STIFFNESS

Approximate determination of the story stiffness in a multi-story frame (taken from course lectures by Professor J.M. Biggs).

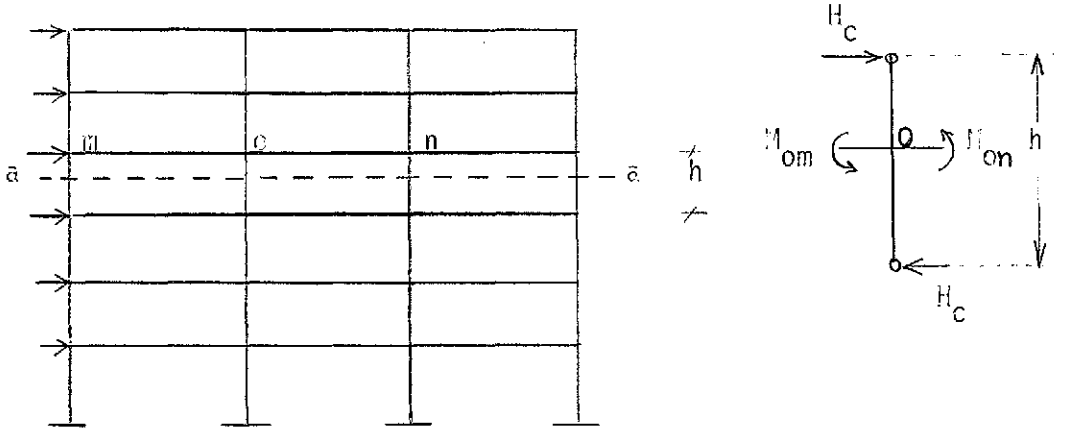

H_B = Total shear at level aa

Assume: a) Column shears above and below joint O both H_c.

b) Inflection points in columns above and below at same location.

c) Rotation of all joints in floor = θ.

Then,

$$M_{om} = 2E\ K_{om}\ (2\theta_o + \theta_m) = 6\ E\ K_{om}\ \theta$$

$$M_{on} = 2E\ K_{on}\ (2\theta_o + \theta_n) = 6\ E\ K_{on}\ \theta$$

$$M_{om} + M_{on} = 6\,E\theta\Sigma\,K_{go} = H_c.h$$

where Kgo = sum of girder stiffnesses at "o"

Adding all joints, we have for the whole floor:

$$12\,E\theta\,\overset{F}{\Sigma}K_g = \Sigma H_c.h = H_B.h$$

and $$\theta = \frac{H_B \,.\, h}{12E \,.\, \overset{F}{\Sigma}\, K_g}$$ Average joint rotation in the floor

where $\overset{F}{\Sigma}K_g$ = sum of all girder stiffnesses in floor

H_B = total story shear.

Now consider one column:

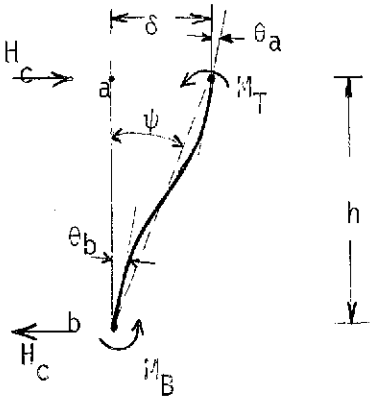

$$M_T = 2EK_c(2\theta_a + \theta_b - 3\psi)$$

$$M_B = 2EK_c(2\theta_b + \theta_a - 3\psi)$$

$$-H_c.h = M_T + M_B = 2EK_c\,(3\theta_a + 3\theta_b - 6\psi)$$

Assuming all θ's equal in each floor we obtain, for all columns:

$$\Sigma(M_T + M_B) = -H_B.h$$

or $$2E(\Sigma K_c)\,(3\theta_a + 3\theta_b - 6\psi) = -H_B.h$$

or $$\psi = \frac{H_B.h}{12E\Sigma K_c} + \frac{\theta_a}{2} + \frac{\theta_b}{2}$$ ΣK_c = sum of column stiffness

Substituting the values of θ obtained above

$$\text{i.e.} \quad \theta_a = \frac{H_B h}{12E\Sigma Kga}$$

$$\theta_b = \frac{H_B h}{12E\ \Sigma Kgb}$$

we obtain

$$\psi = \frac{H_B h}{24E}\left(\frac{2}{\Sigma K_c} + \frac{1}{\Sigma Kga} + \frac{1}{\Sigma Kgb}\right)$$

Noting that $\delta = \psi h$ and $K_o = \frac{H_B}{\delta}$ we obtain

$$K_o = \frac{24E}{h^2} \cdot \left\{ \frac{1}{\frac{2}{\Sigma K_c} + \frac{1}{\Sigma Kga} + \frac{1}{\Sigma Kgb}} \right\}$$

APPENDIX B

THE TRILINEAR SYSTEM

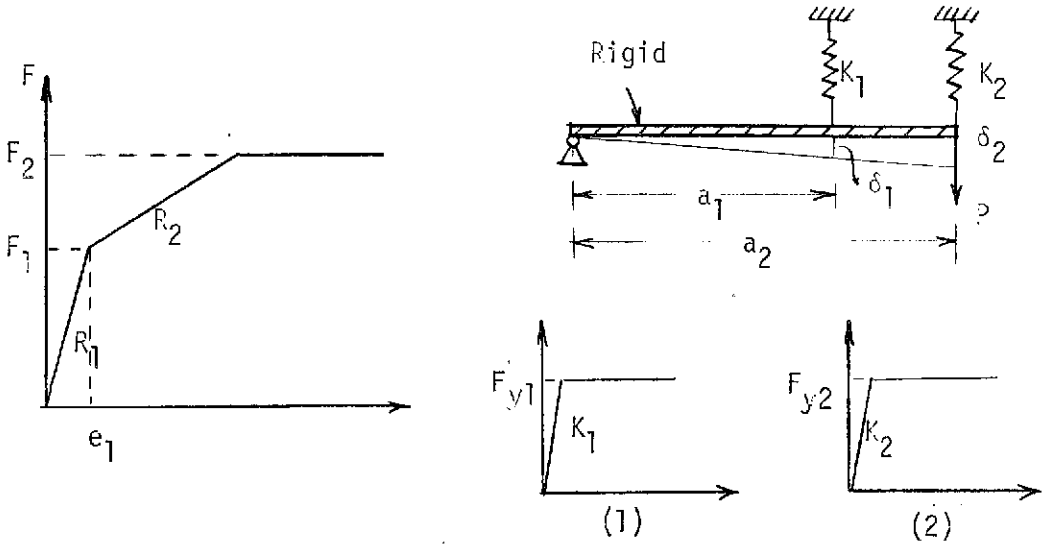

We assume that we have the properties of the trilinear spring (could be computed as described in reference (38)) and we want to find its loading and unloading laws. This could be done by considering a physical model like the one shown in the picture and determining the properties of the two elastoplastic springs so that the P vs δ_2 curve is the trilinear on the left.

Using geometry and equilibrium we have:

$$\delta_1 = \frac{a_1}{a_2}\,\delta_2$$

$$P_{max} \cdot a_2 = F_{y1} a_1 + F_{y2}\, a_2 = F_2$$

and $$F_2 = \frac{a_1}{a_2} F_{y1} + F_{y2} \qquad (1)$$

For $P < F_1$: $$Pa_2 = P_2 a_2 + P_1 a_1 = K_2 \delta_2 a_2 + K_1 \frac{a_1}{a_2} \delta_2 a_1$$

and $$\frac{P}{\delta_2} = R_1 = \left(\frac{a_1}{a_2}\right)^2 K_1 + K_2 \qquad (2)$$

Assume that spring K_2 yields first i.e. $\frac{F_{y1}}{K_1} > \left(\frac{a_1}{a_2}\right) \cdot \frac{f_{y2}}{K_2}$

Then:

$$e_1 = \frac{F_1}{R_1} = \frac{F_{y2}}{K_2} \quad \text{and}$$

$$F_1 = F_{y2} + \left(\frac{a_1}{a_2}\right)^2 \cdot K_1 e_1$$

$$= F_{y2} + \left(\frac{a_1}{a_2}\right)^2 \cdot K_1 \cdot \frac{F_{y2}}{K_2}$$

or $$F_1 = \left\{\left(\frac{a_1}{a_2}\right)^2 \cdot \frac{K_1}{K_2} + 1\right\} \cdot F_{y2} \qquad (3)$$

When we are in the second branch of the trilinear:

$$Pa_2 = F_{y2} \cdot a_2 + K_1 \cdot \frac{a_1}{a_2} \cdot \delta a_1 \rightarrow$$

$$P = F_{y2} + \left(\frac{a_1}{a_2}\right)^2 \cdot K_1 \cdot \delta$$

We want $\frac{dP}{d\delta} = R_2 \rightarrow$

$$R_2 = \left(\frac{a_1}{a_2}\right)^2 \cdot K_1 \qquad (4)$$

Calling $\frac{a_1}{a_2} = \lambda \qquad (0 < \lambda \leq 1)$ we can solve (1), (2), (3), (4) and obtain

$$K_1 = \frac{1}{\lambda^2} R_2 \qquad F_{y1} = \frac{1}{\lambda}\left(F_2 - F_1 \cdot \frac{R_1 - R_2}{R_1}\right)$$

$$K_2 = R_1 - R_2 \qquad F_{y2} = F_1 \cdot \frac{R_1 - R_2}{R_1}$$

These relations allow us to compute the properties of the two elasto-plastic springs, in terms of properties of the trilinear one and the parameter λ. λ can have any arbitrary value between 0 and 1. For different values of λ we will have different elastoplastic springs but their combination will always give the trilinear. Computationally it is advantageous to choose $\lambda = 1$ and then:

$$\begin{aligned} K_1 &= R_2 & F_{y1} &= F_2 - F_1 (R_1 - R_2)/R_1 \\ K_2 &= R_1 - R_2 & F_{y2} &= F_1 (R_1 - R_2)/R_1 \end{aligned} \qquad (5)$$

and $$P_{tril} = P_1 + P_2$$

Test of the assumption $\frac{F_{y1}}{K_1} > \left(\frac{a_1}{a_2}\right) \cdot \frac{F_{y2}}{K_2}$:

If we replace in this inequality values of F_{y1}, F_{y2}, K_1, K_2 taken from (5) and set $\frac{a_1}{a_2} = \lambda = 1$, after some algebraic manipulations, we obtain

$F_2 > F_1$ which is obviously true.

APPENDIX C

VARIOUS TIME HISTORIES

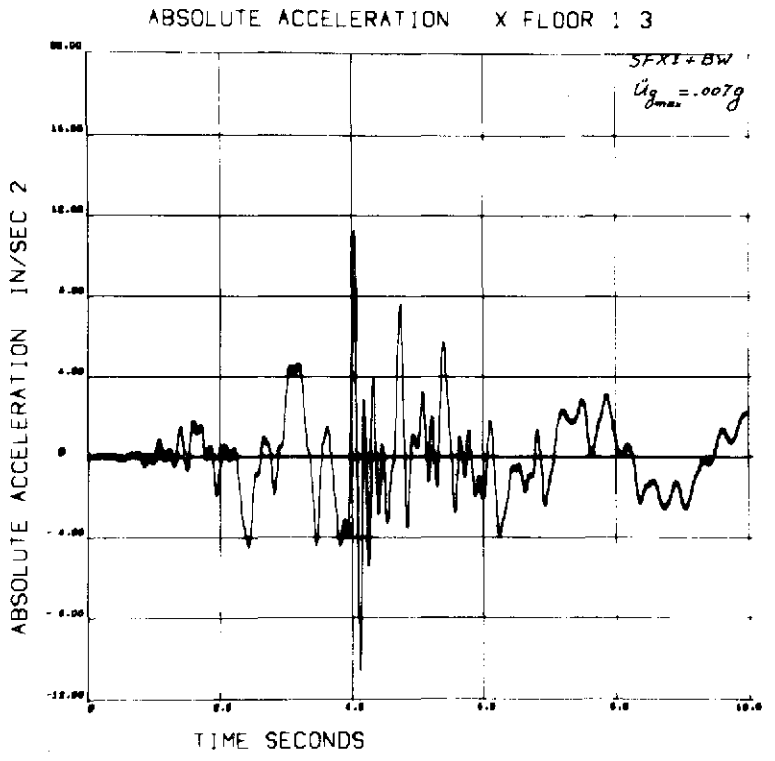
ABSOLUTE ACCELERATION X FLOOR 1 3
SFXI+BW
$\ddot{u}_{g_{max}}$ = .007g
ABSOLUTE ACCELERATION IN/SEC 2
TIME SECONDS

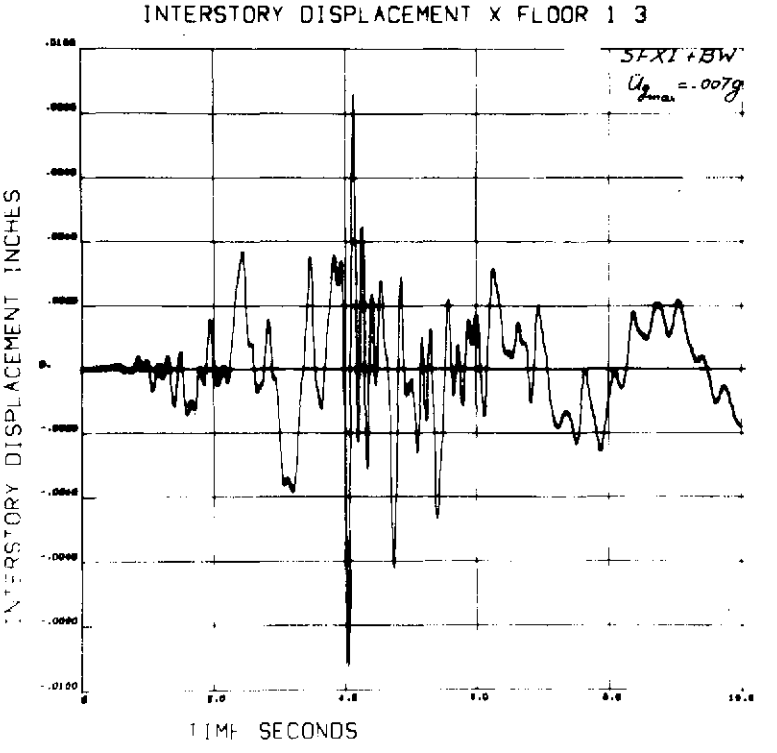
INTERSTORY DISPLACEMENT X FLOOR 1 3
SFXI+BW
$\ddot{u}_{g_{max}}$ = .007g
INTERSTORY DISPLACEMENT INCHES
TIME SECONDS

Figure C1

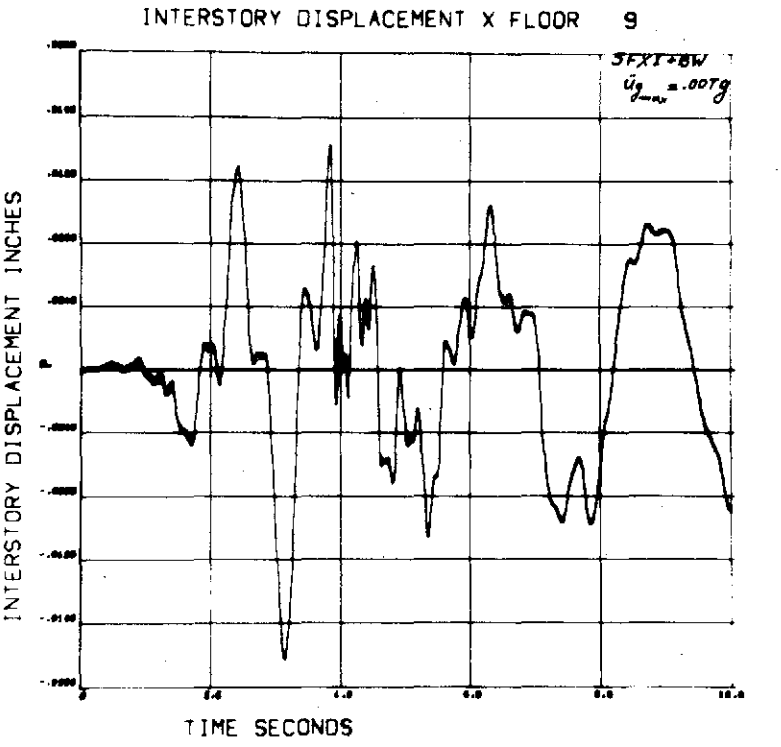
INTERSTORY DISPLACEMENT X FLOOR 9
INTERSTORY DISPLACEMENT INCHES
TIME SECONDS

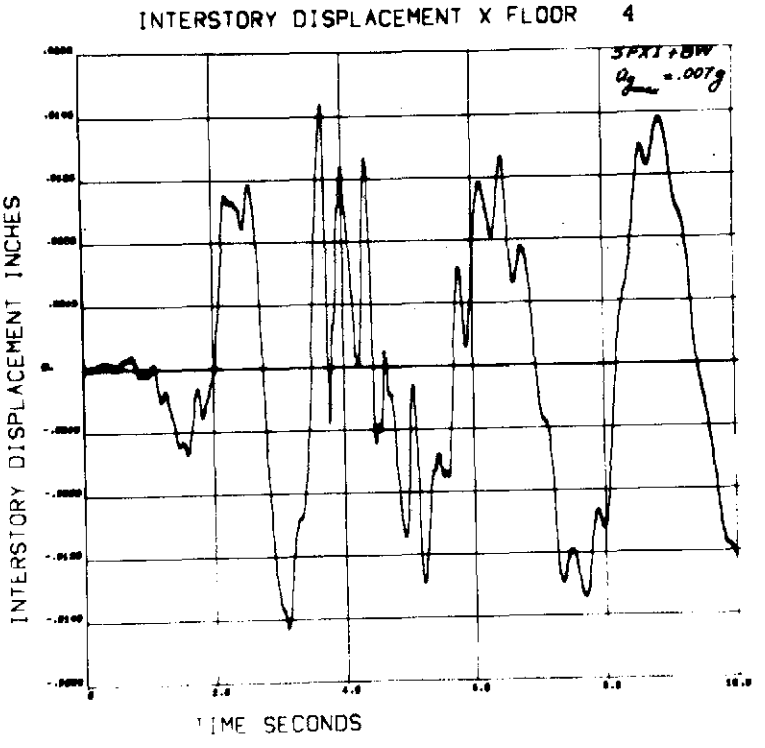
INTERSTORY DISPLACEMENT X FLOOR 4
INTERSTORY DISPLACEMENT INCHES
TIME SECONDS

Figure C2

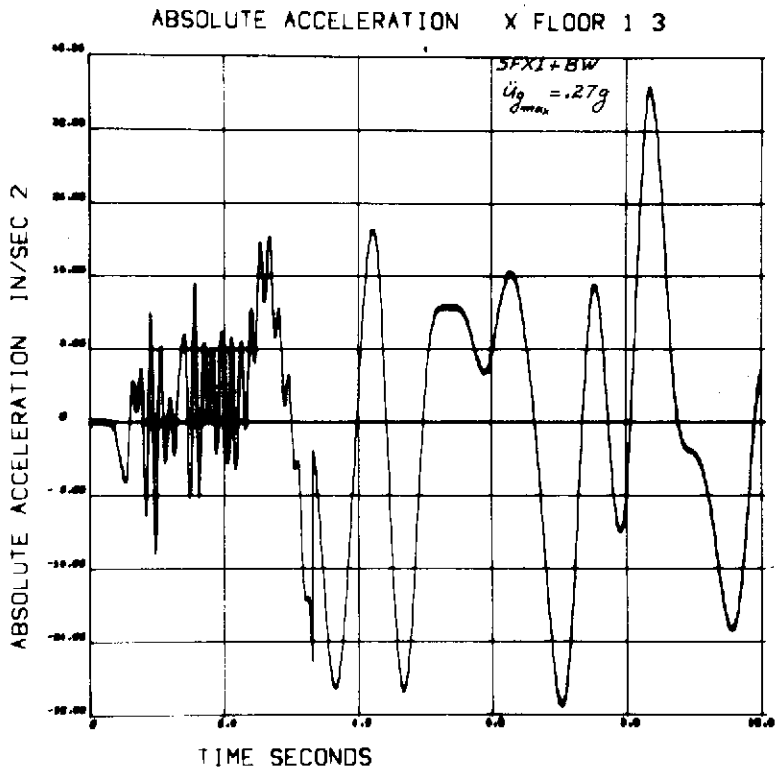
ABSOLUTE ACCELERATION X FLOOR 1 3
SFX1+BW
$\ddot{u}_{g_{max}}$ = .27g
ABSOLUTE ACCELERATION IN/SEC 2
TIME SECONDS

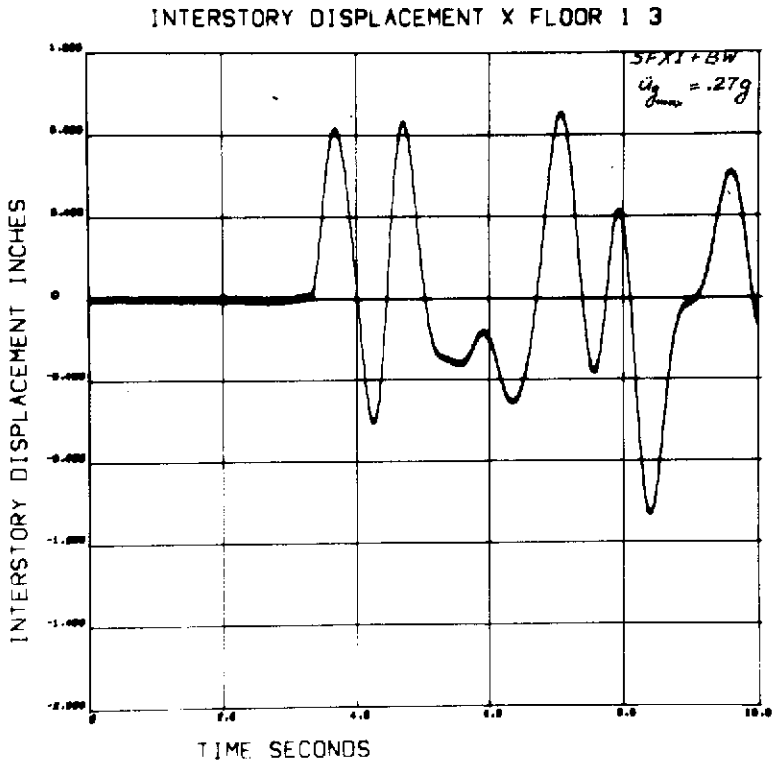
INTERSTORY DISPLACEMENT X FLOOR 1 3
SFX1+BW
$\ddot{u}_{g_{max}}$ = .27g
INTERSTORY DISPLACEMENT INCHES
TIME SECONDS

Figure C3

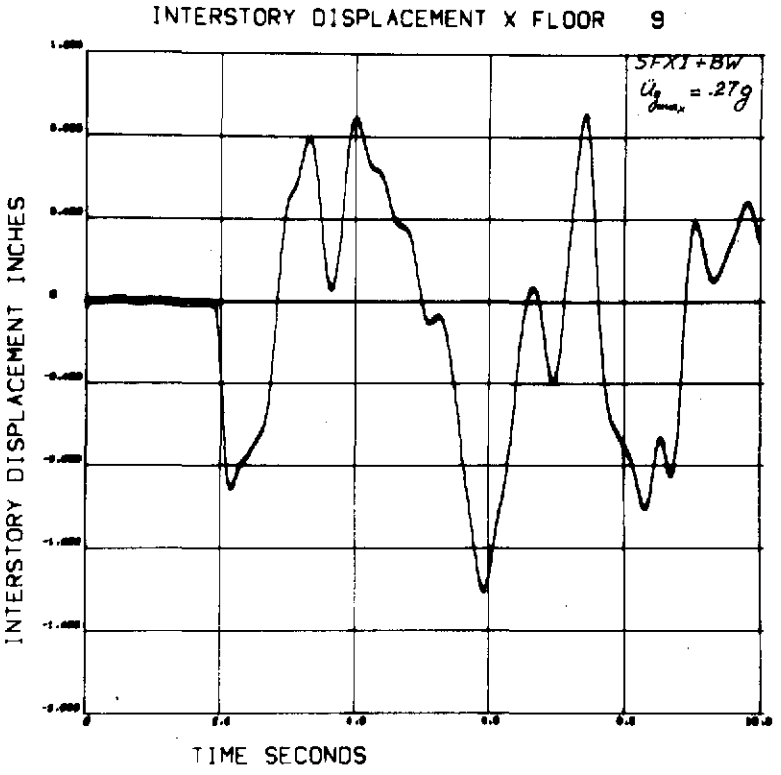
INTERSTORY DISPLACEMENT X FLOOR 9
SFX1+BW
$\ddot{U}_{g_{max_x}} = .27g$
INTERSTORY DISPLACEMENT INCHES
TIME SECONDS

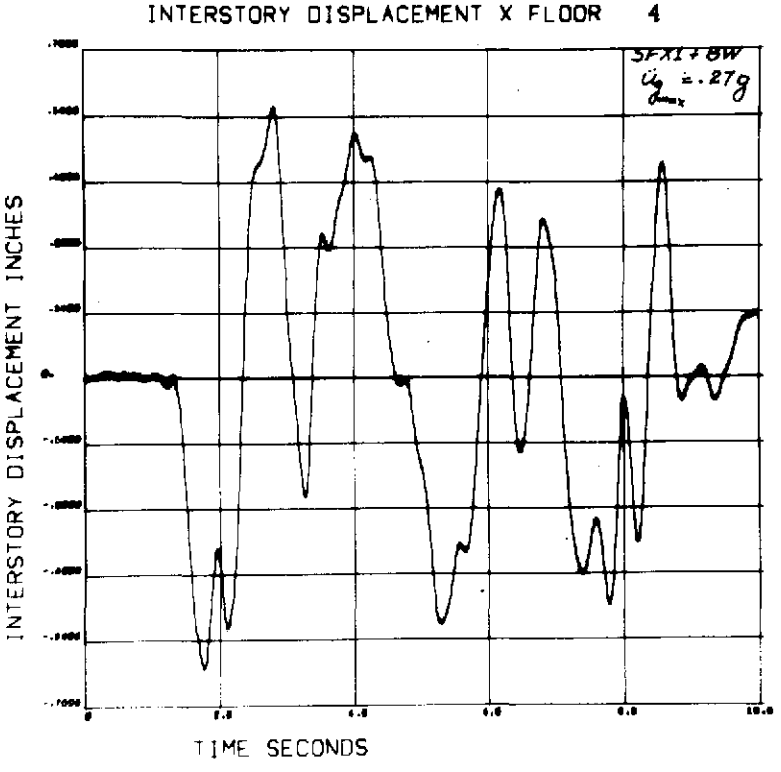
INTERSTORY DISPLACEMENT X FLOOR 4
SFX1+BW
$\ddot{U}_{g_{max_x}} = .27g$
INTERSTORY DISPLACEMENT INCHES
TIME SECONDS

Figure C4

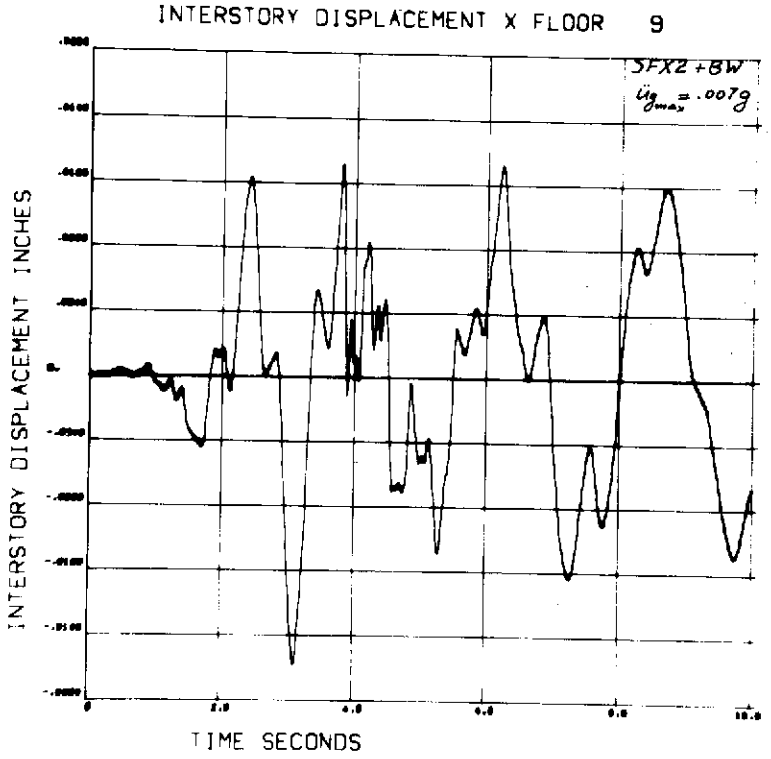
INTERSTORY DISPLACEMENT X FLOOR 9
SFX2 +BW
$\ddot{u}_{g_{max}} = .007g$
INTERSTORY DISPLACEMENT INCHES
TIME SECONDS

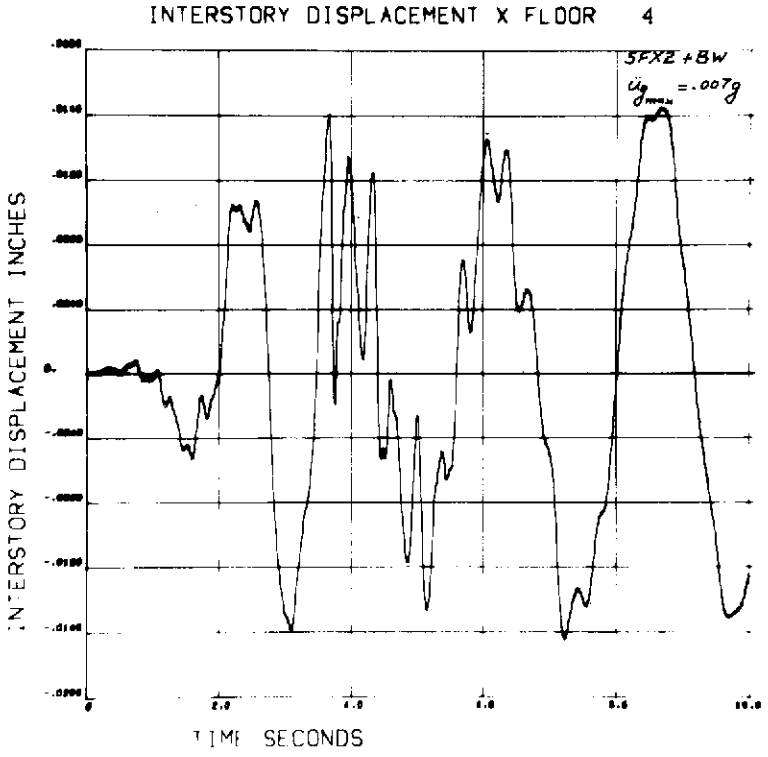
INTERSTORY DISPLACEMENT X FLOOR 4
SFX2 +BW
$\ddot{u}_{g_{max}} = .007g$
INTERSTORY DISPLACEMENT INCHES
TIME SECONDS

Figure C5

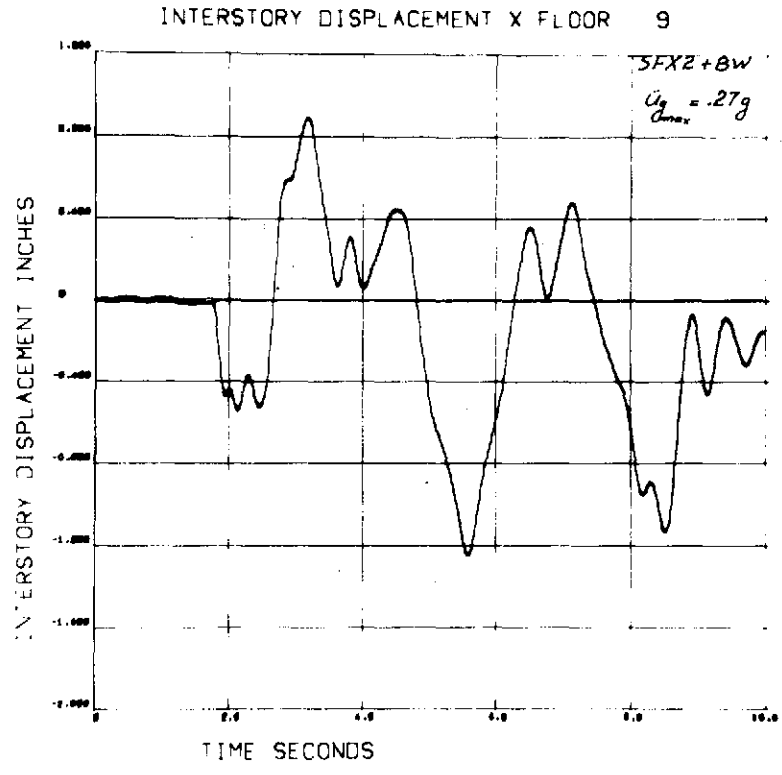
INTERSTORY DISPLACEMENT X FLOOR 9
SFX2 +BW
$\ddot{u}_{g_{max}} = .27g$
INTERSTORY DISPLACEMENT INCHES
TIME SECONDS

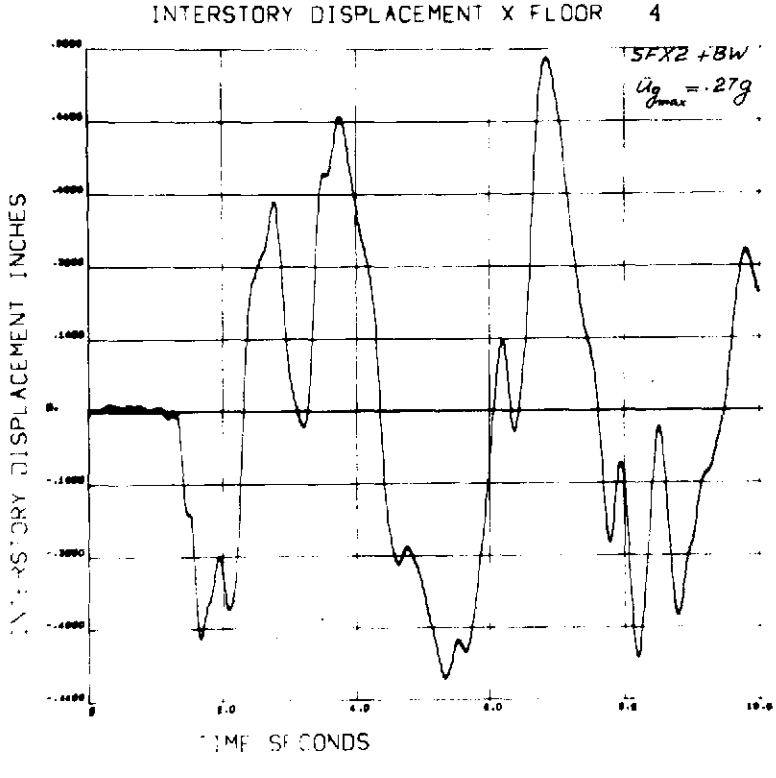
INTERSTORY DISPLACEMENT X FLOOR 4
SFX2 +BW
$\ddot{u}_{g_{max}} = .27g$
INTERSTORY DISPLACEMENT INCHES
TIME SECONDS

Figure C6

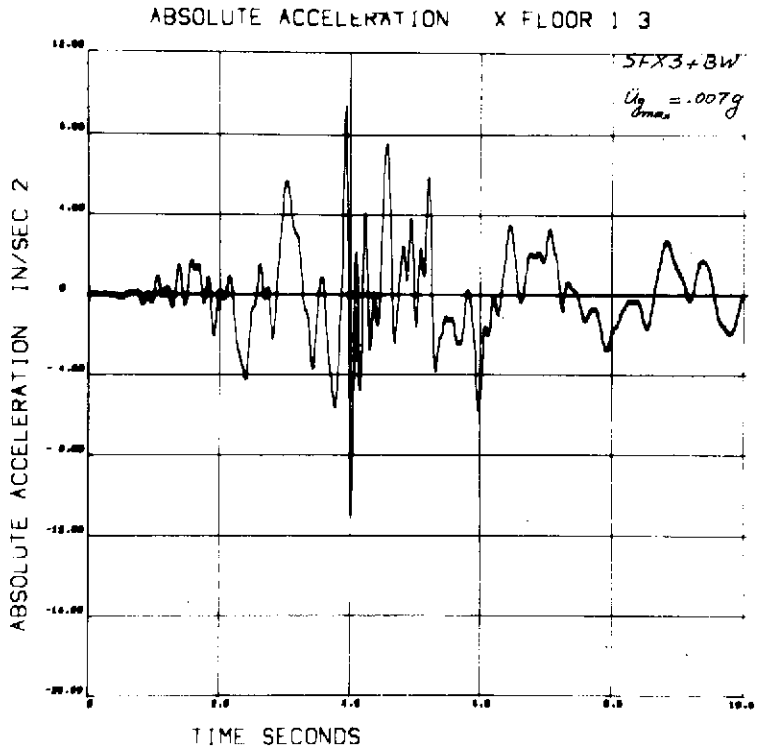
ABSOLUTE ACCELERATION X FLOOR 1 3
SFX3+BW
$\ddot{u}_{g_{max}} = .007g$
ABSOLUTE ACCELERATION IN/SEC 2
TIME SECONDS

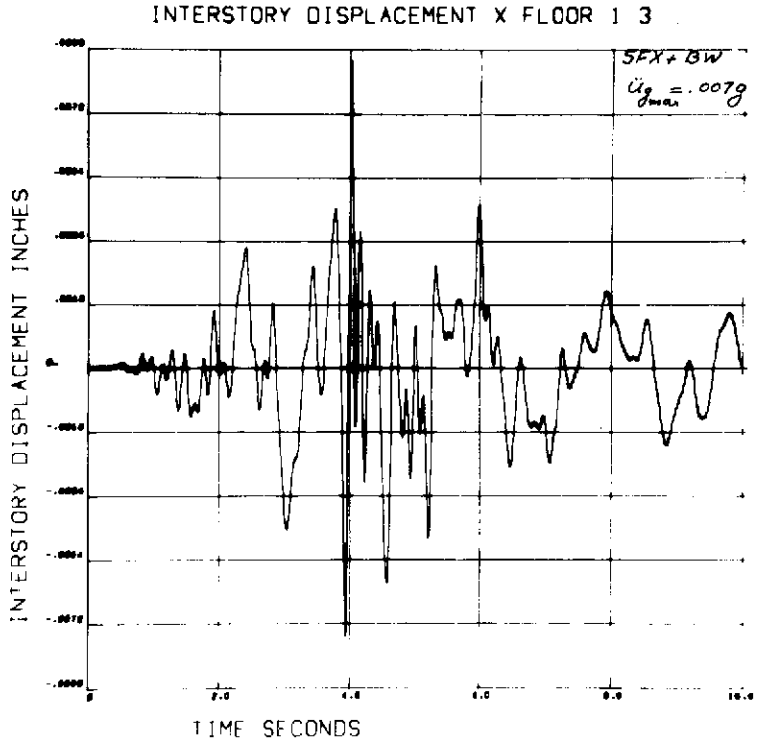
INTERSTORY DISPLACEMENT X FLOOR 1 3
SFX+BW
$\ddot{u}_{g_{max}} = .007g$
INTERSTORY DISPLACEMENT INCHES
TIME SECONDS

Figure C7

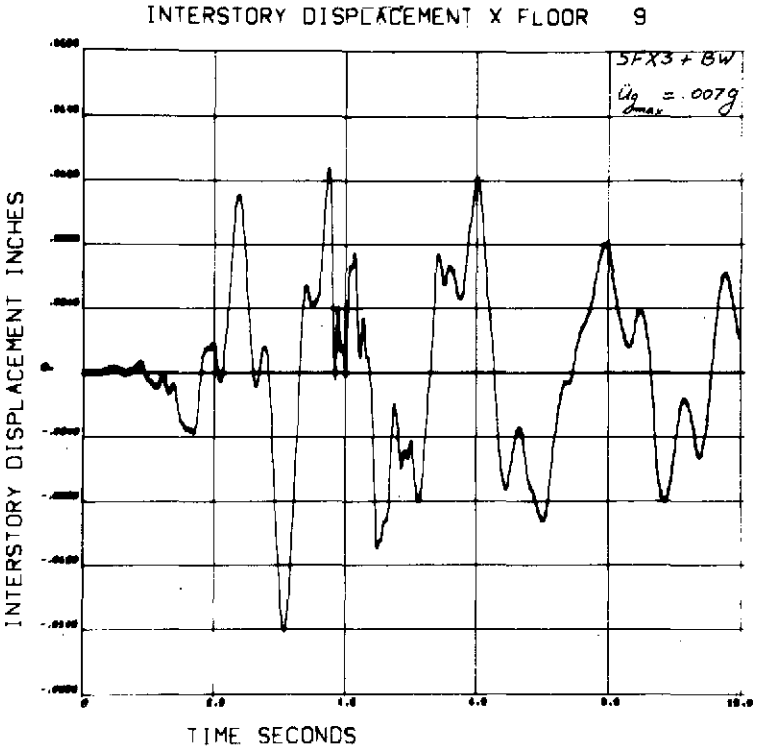
INTERSTORY DISPLACEMENT X FLOOR 9
SFX3 + BW
$\ddot{u}_{g_{max}}$ = .007g
INTERSTORY DISPLACEMENT INCHES
TIME SECONDS

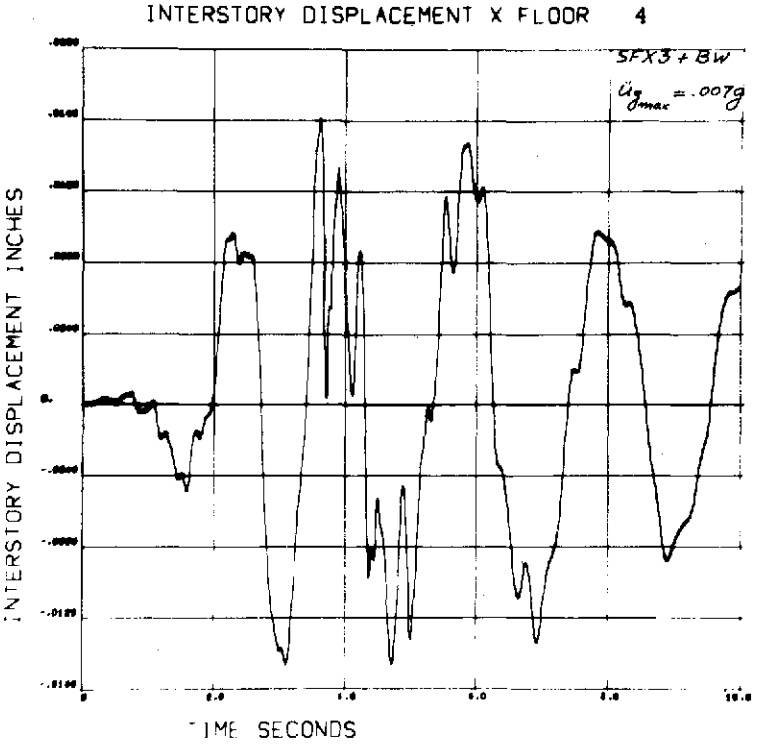
INTERSTORY DISPLACEMENT X FLOOR 4
SFX3 + BW
$\ddot{u}_{g_{max}}$ = .007g
INTERSTORY DISPLACEMENT INCHES
TIME SECONDS

Figure C8

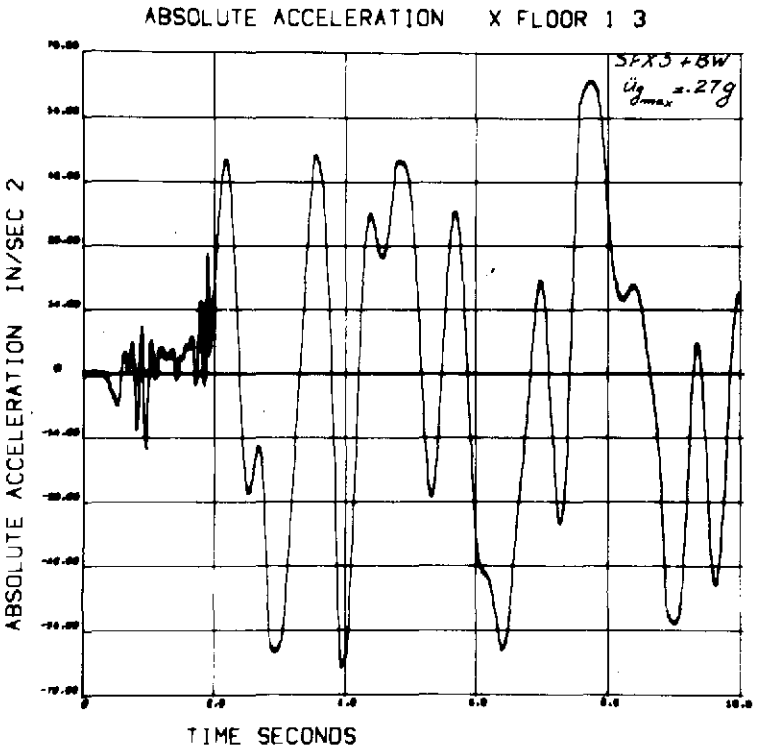
ABSOLUTE ACCELERATION X FLOOR 1 3
SFX3+8W
$\ddot{u}_{g_{max}} = .27g$
ABSOLUTE ACCELERATION IN/SEC 2
TIME SECONDS

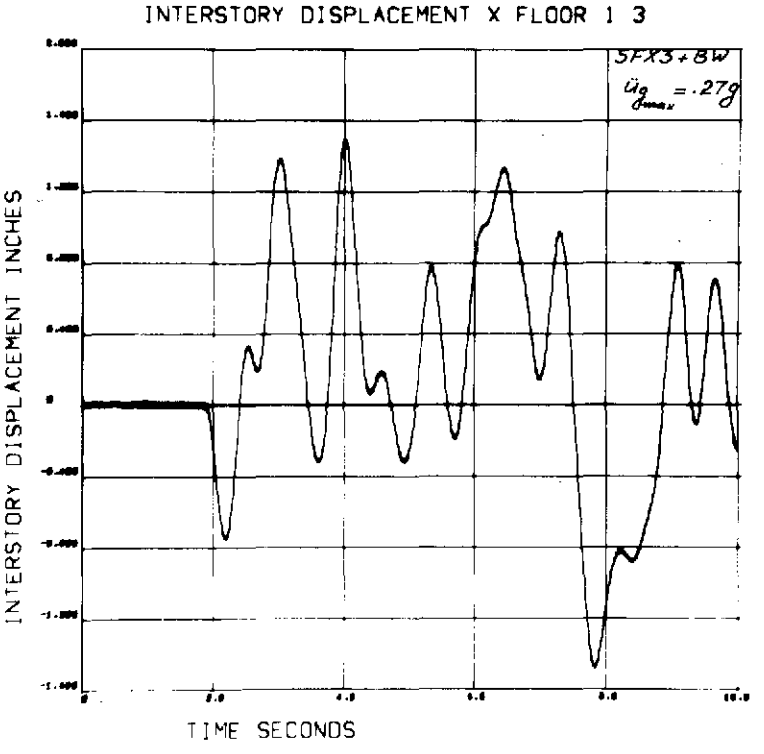
INTERSTORY DISPLACEMENT X FLOOR 1 3
SFX3+8W
$\ddot{u}_{g_{max}} = .27g$
INTERSTORY DISPLACEMENT INCHES
TIME SECONDS

Figure C9

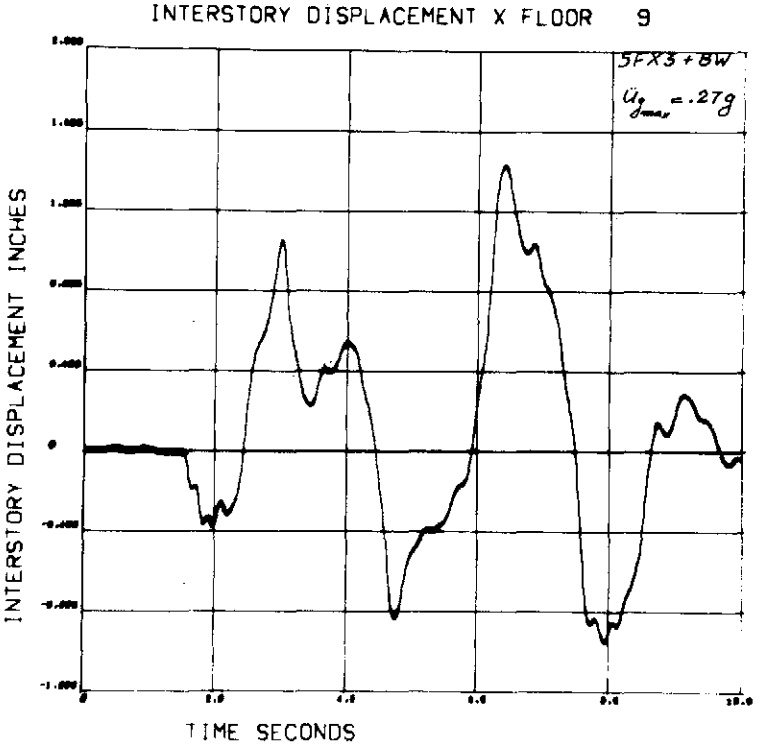
INTERSTORY DISPLACEMENT X FLOOR 9
SFX3 + BW
$\ddot{U}_{g_{max}} = .27g$
INTERSTORY DISPLACEMENT INCHES
TIME SECONDS

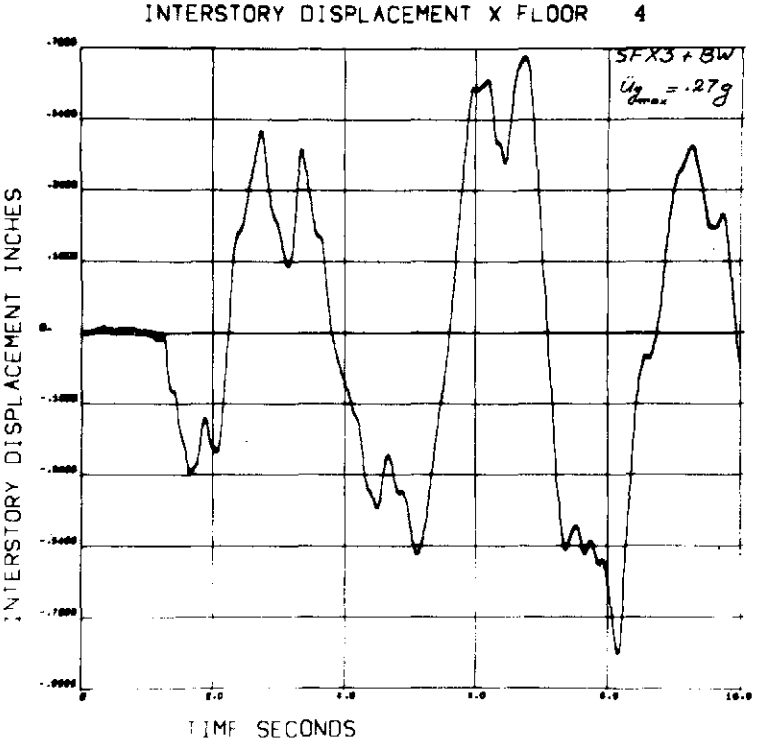
INTERSTORY DISPLACEMENT X FLOOR 4
SFX3 + BW
$\ddot{U}_{g_{max}} = .27g$
INTERSTORY DISPLACEMENT INCHES
TIME SECONDS

Figure C10

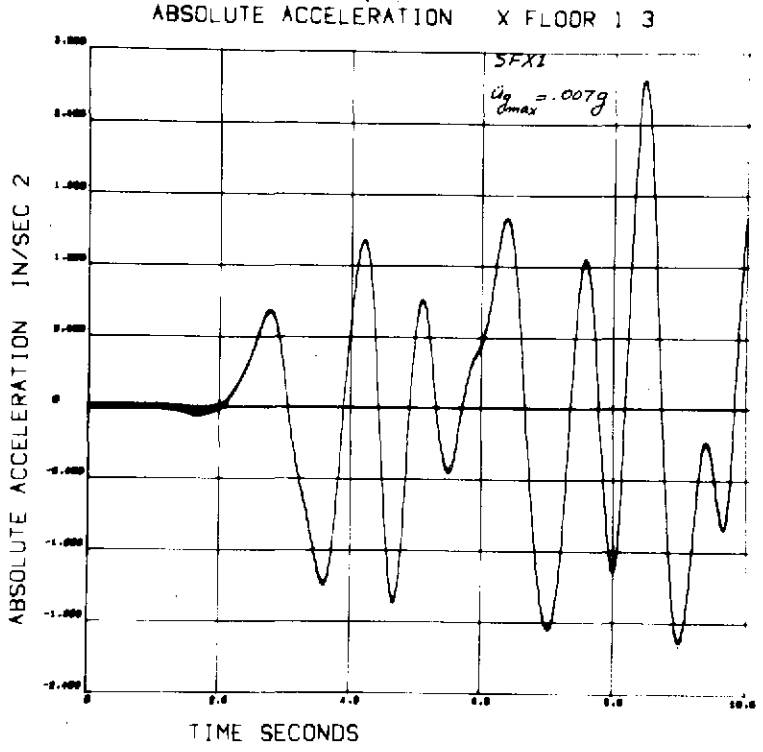
ABSOLUTE ACCELERATION X FLOOR 1 3
SFX1
$\ddot{u}_{g\,max}$ = .007g
ABSOLUTE ACCELERATION IN/SEC 2
TIME SECONDS

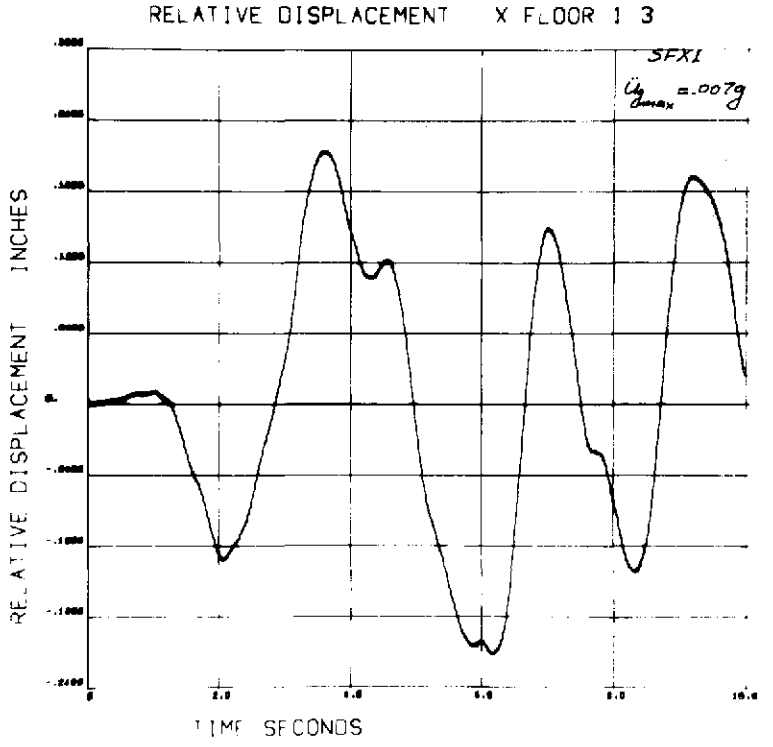
RELATIVE DISPLACEMENT X FLOOR 1 3
SFX1
$\ddot{u}_{g\,max}$ = .007g
RELATIVE DISPLACEMENT INCHES
TIME SECONDS

Figure C11

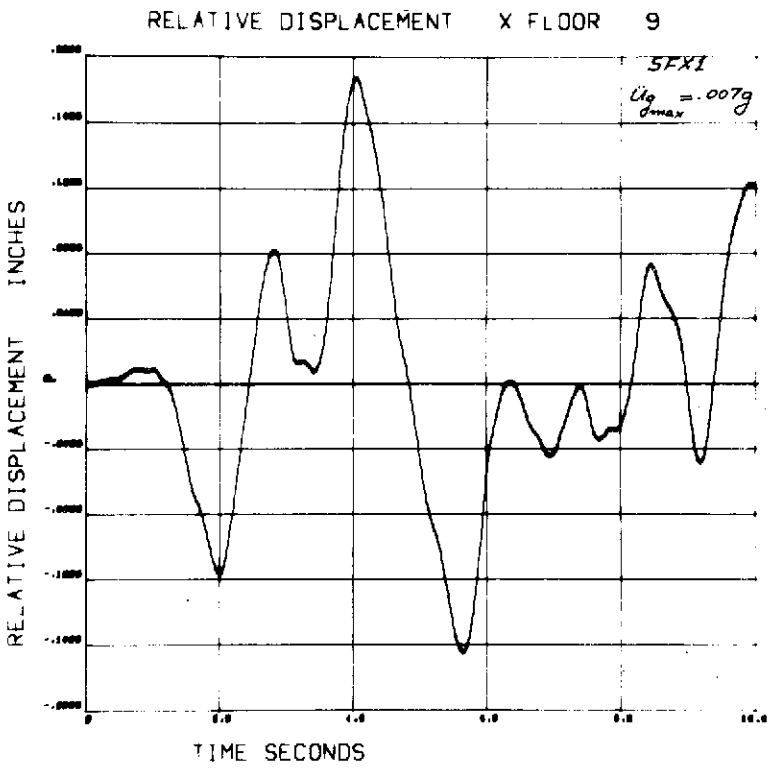
RELATIVE DISPLACEMENT X FLOOR 9
SFX1
$\ddot{U}_{g_{max}}$ = .007g
RELATIVE DISPLACEMENT INCHES
TIME SECONDS

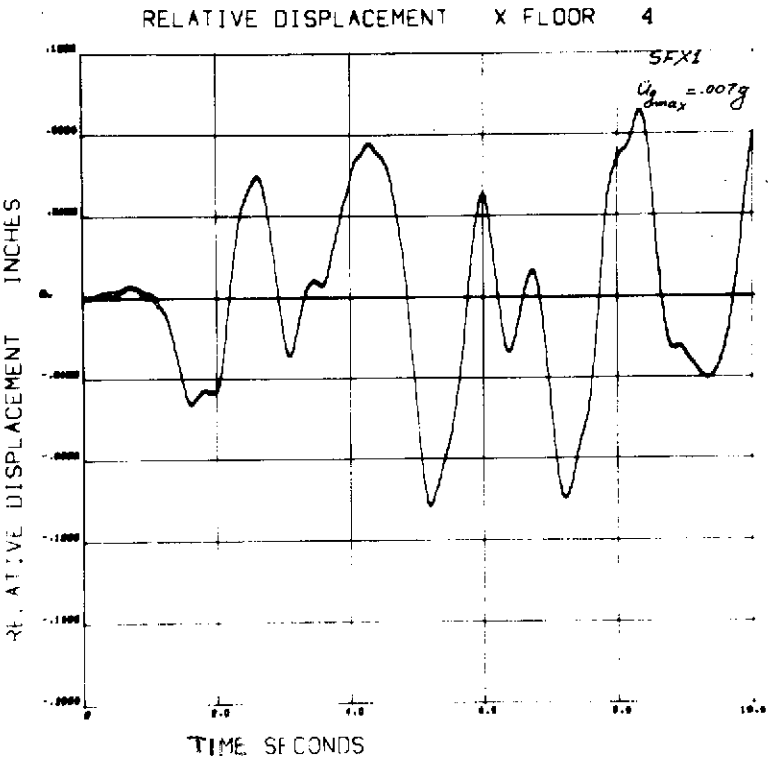
RELATIVE DISPLACEMENT X FLOOR 4
SFX1
$\ddot{U}_{g_{max}}$ = .007g
RELATIVE DISPLACEMENT INCHES
TIME SECONDS

Figure C12

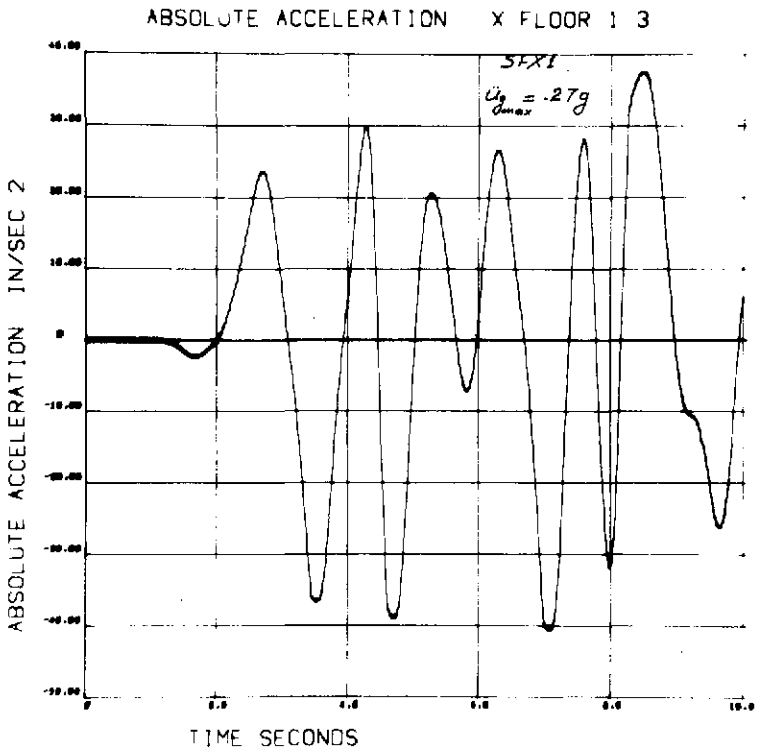
ABSOLUTE ACCELERATION X FLOOR 1 3
5FX1
$\ddot{u}_{g_{max}} = .27g$
ABSOLUTE ACCELERATION IN/SEC 2
TIME SECONDS

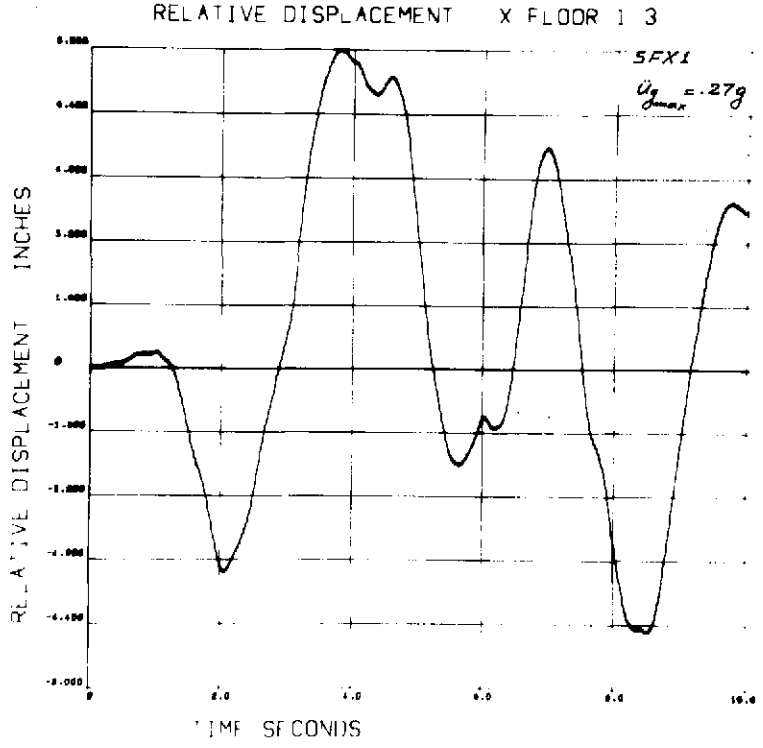
RELATIVE DISPLACEMENT X FLOOR 1 3
5FX1
$\ddot{u}_{g_{max}} = .27g$
RELATIVE DISPLACEMENT INCHES
TIME SECONDS

Figure C13

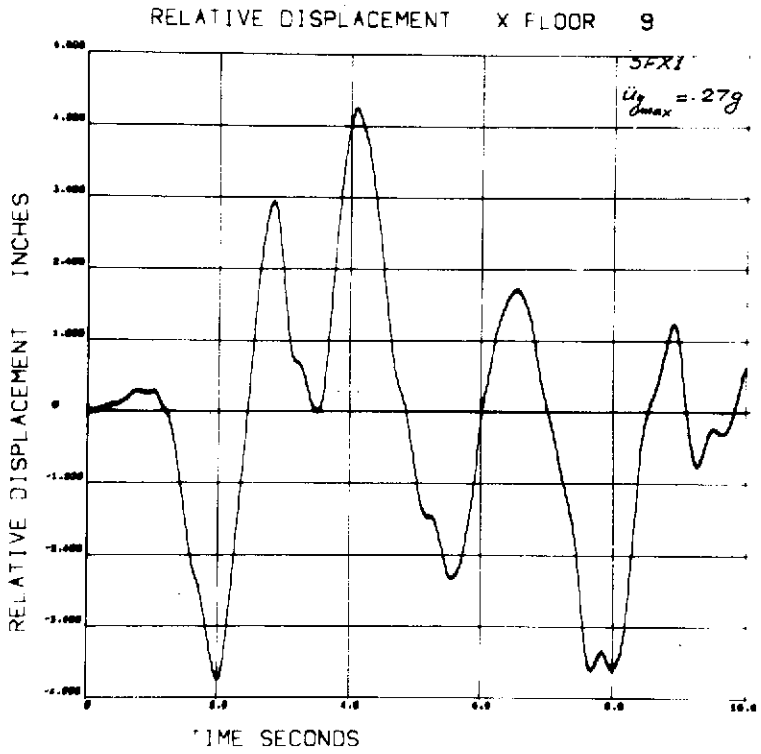
RELATIVE DISPLACEMENT X FLOOR 9
SFXI
$\ddot{u}_{g_{max}} = .27g$
RELATIVE DISPLACEMENT INCHES
TIME SECONDS

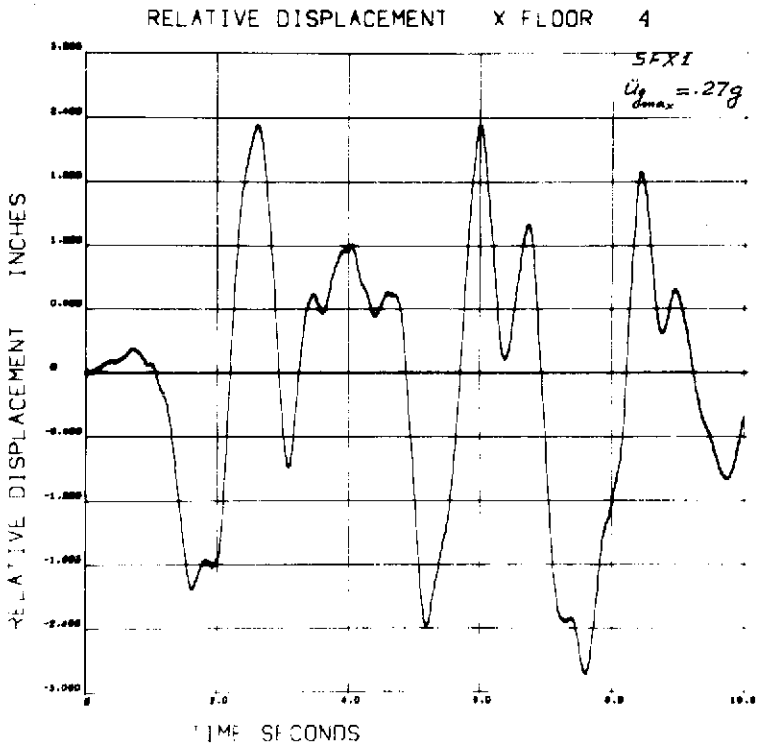
RELATIVE DISPLACEMENT X FLOOR 4
SFXI
$\ddot{u}_{g_{max}} = .27g$
RELATIVE DISPLACEMENT INCHES
TIME SECONDS

Figure C14

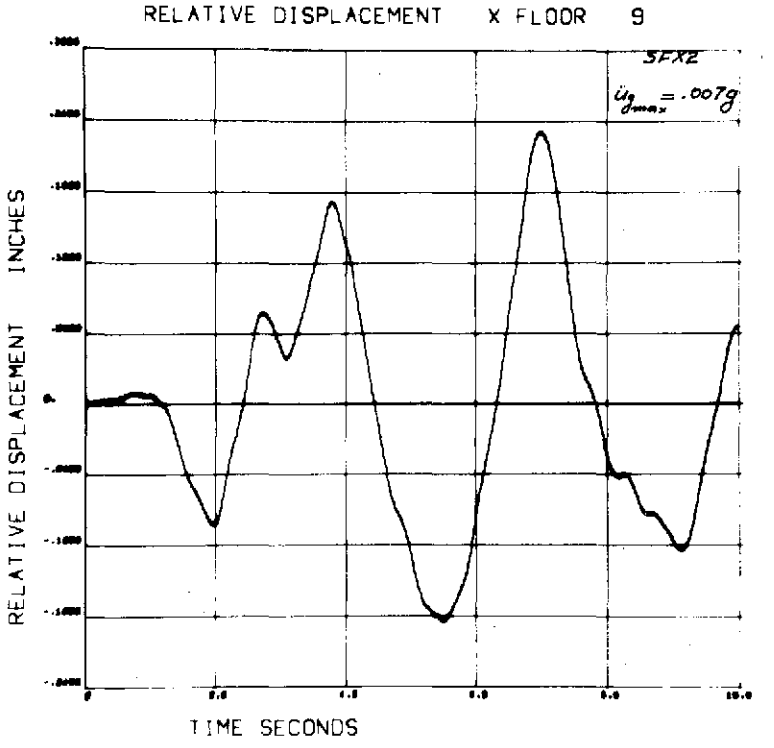
RELATIVE DISPLACEMENT X FLOOR 9
SFX2
$\ddot{u}_{g_{max}} = .007g$
RELATIVE DISPLACEMENT INCHES
TIME SECONDS

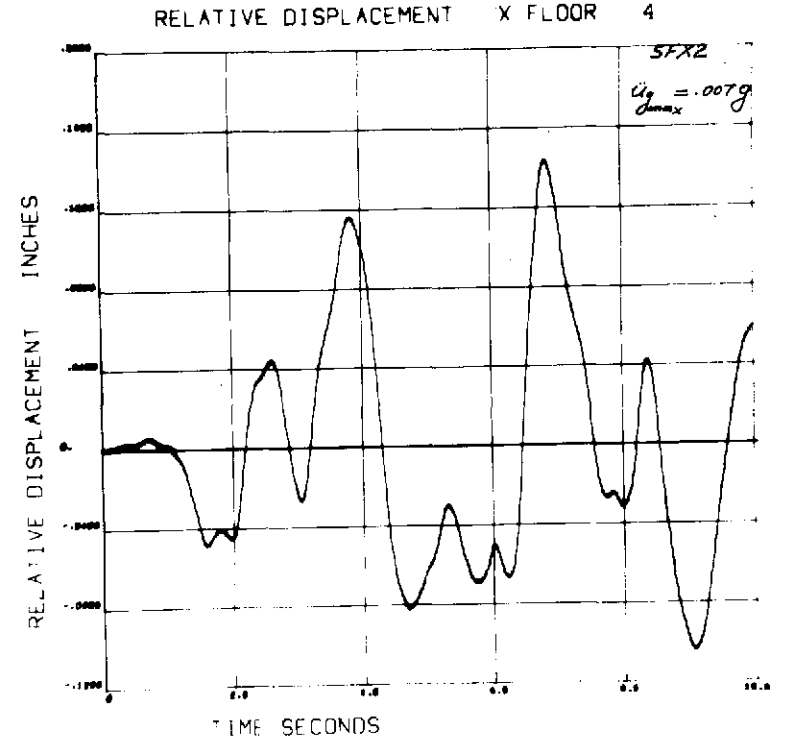
RELATIVE DISPLACEMENT X FLOOR 4
SFX2
$\ddot{u}_{g_{max}} = .007g$
RELATIVE DISPLACEMENT INCHES
TIME SECONDS

Figure C15

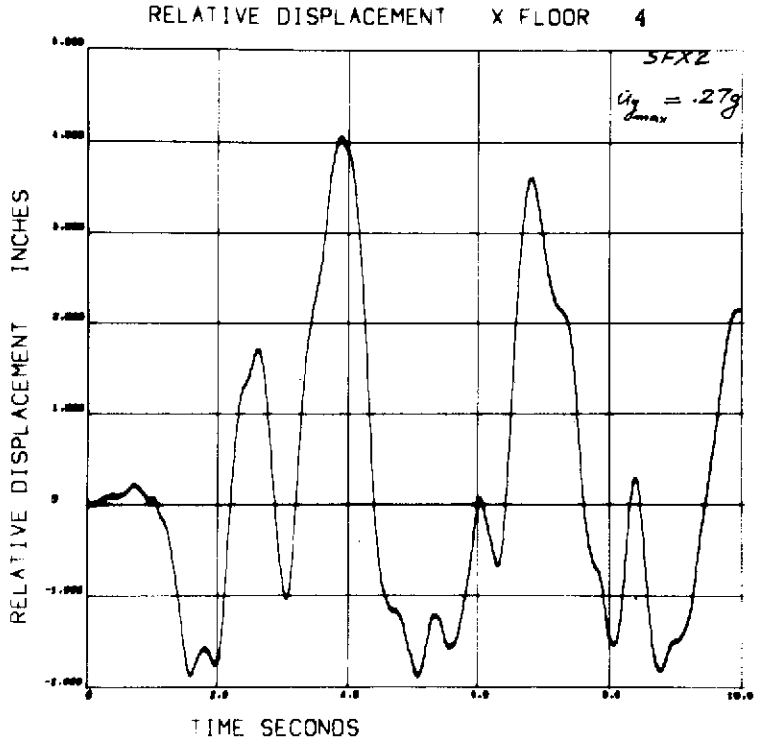
RELATIVE DISPLACEMENT X FLOOR 4
SFX2
$\ddot{u}_{g_{max}} = .27g$
RELATIVE DISPLACEMENT INCHES
TIME SECONDS

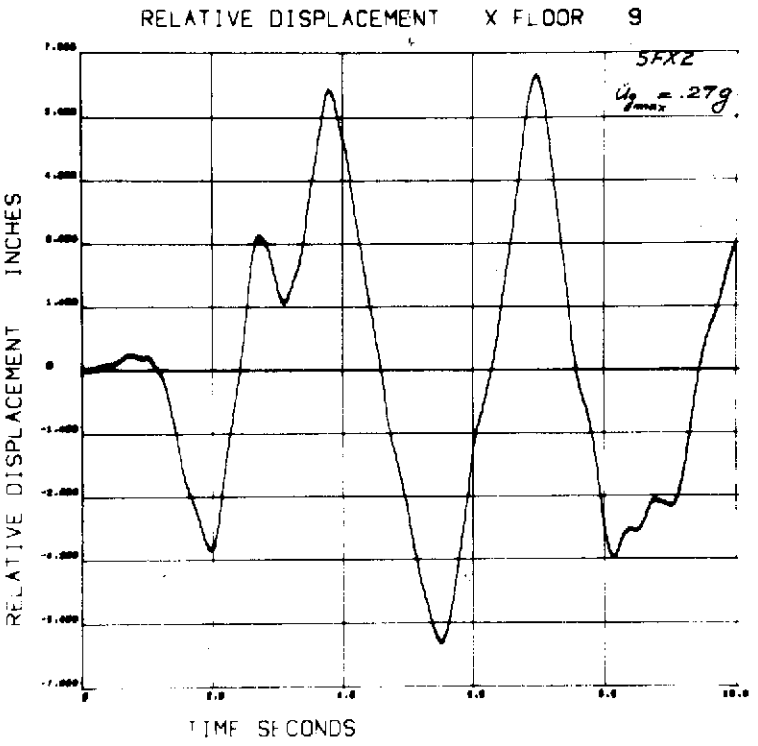
RELATIVE DISPLACEMENT X FLOOR 9
SFX2
$\ddot{u}_{g_{max}} = .27g$
RELATIVE DISPLACEMENT INCHES
TIME SECONDS

Figure C16

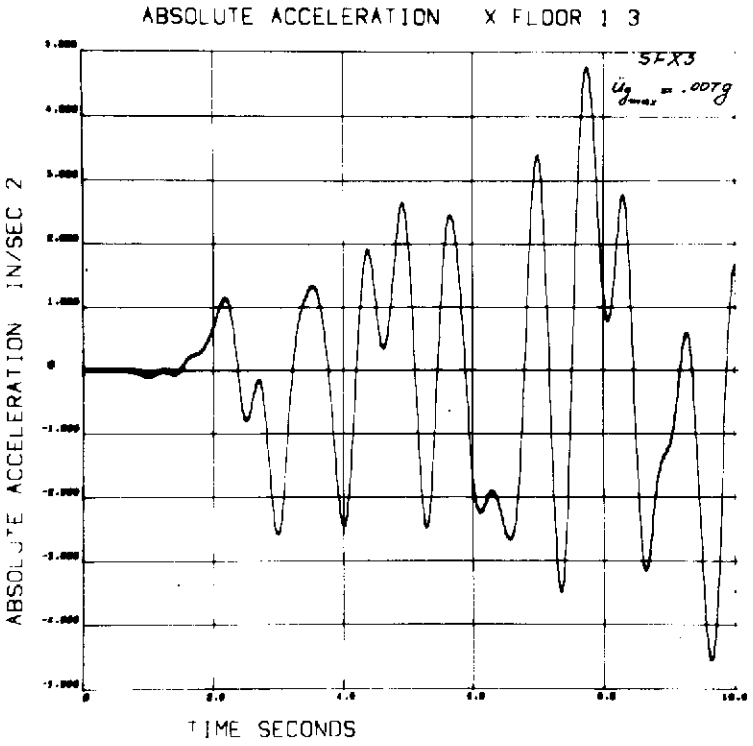
ABSOLUTE ACCELERATION X FLOOR 1 3
SFX3
$\ddot{u}_{g_{max}} = .007g$
ABSOLUTE ACCELERATION IN/SEC 2
TIME SECONDS

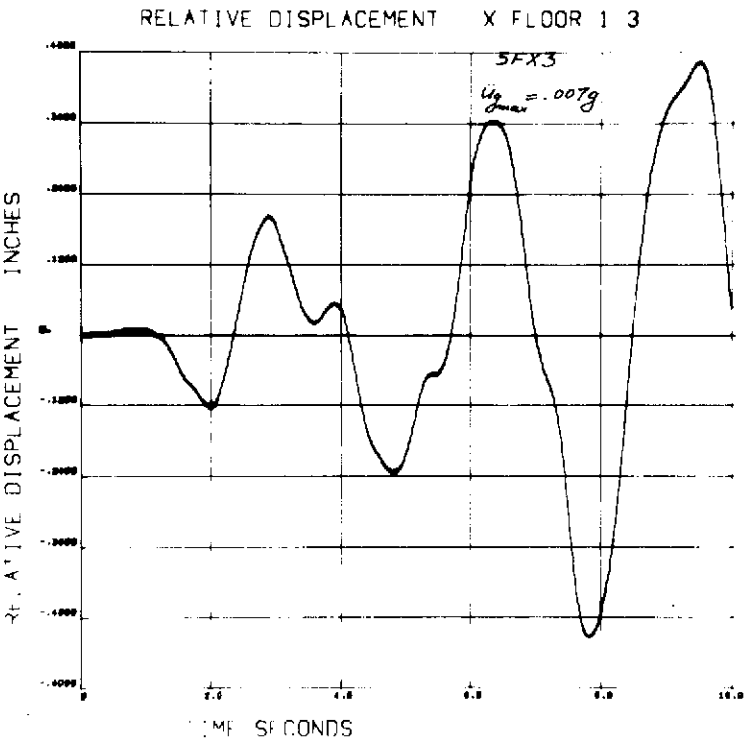
RELATIVE DISPLACEMENT X FLOOR 1 3
SFX3
$\ddot{u}_{g_{max}} = .007g$
RELATIVE DISPLACEMENT INCHES
TIME SECONDS

Figure C17

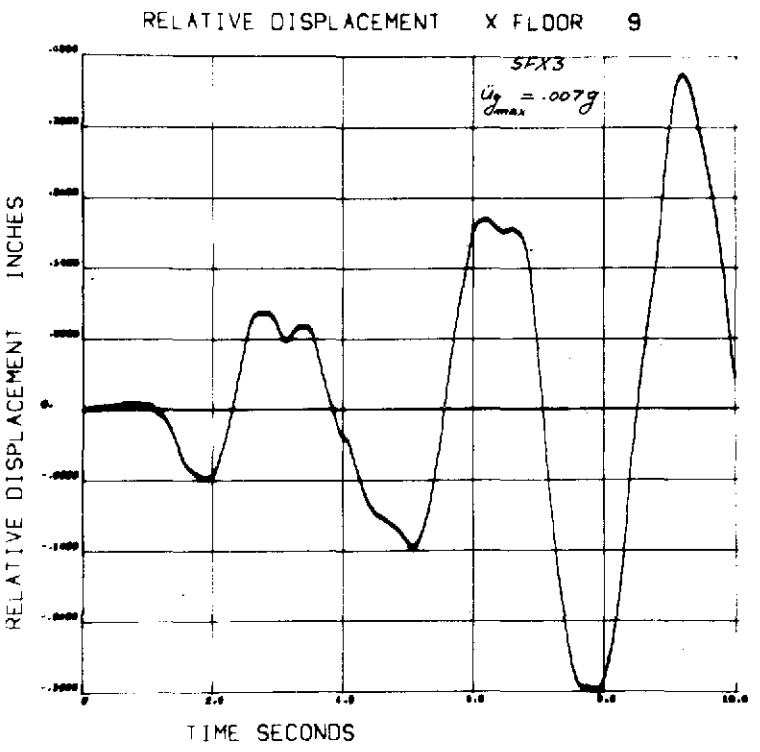
RELATIVE DISPLACEMENT X FLOOR 9
SFX3
$\ddot{u}_{g_{max}} = .007g$
RELATIVE DISPLACEMENT INCHES
TIME SECONDS

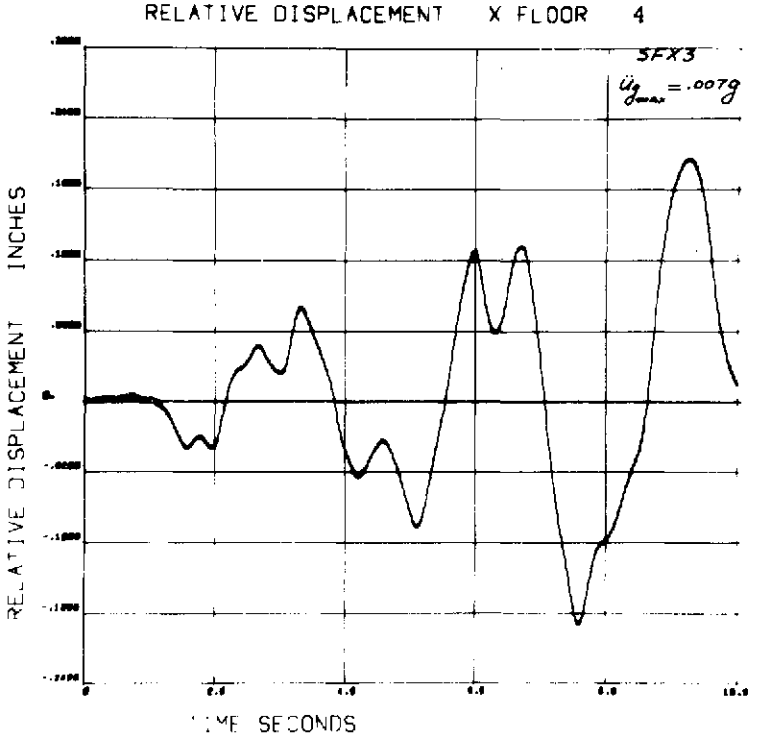
RELATIVE DISPLACEMENT X FLOOR 4
SFX3
$\ddot{u}_{g_{max}} = .007g$
RELATIVE DISPLACEMENT INCHES
TIME SECONDS

Figure C18

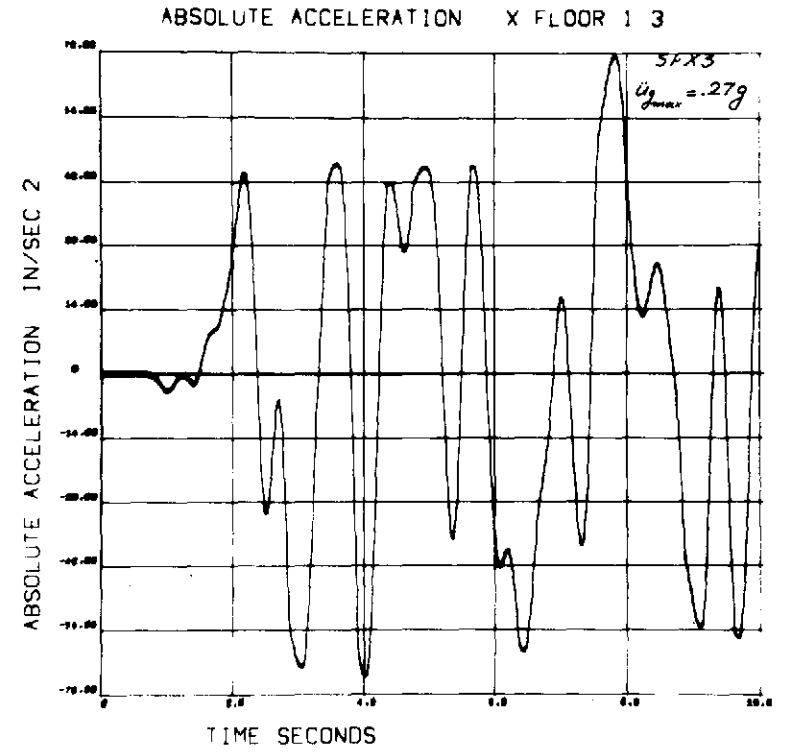
ABSOLUTE ACCELERATION X FLOOR 1 3
SFX3
$\ddot{u}_{g_{max}} = .27g$
ABSOLUTE ACCELERATION IN/SEC 2
TIME SECONDS

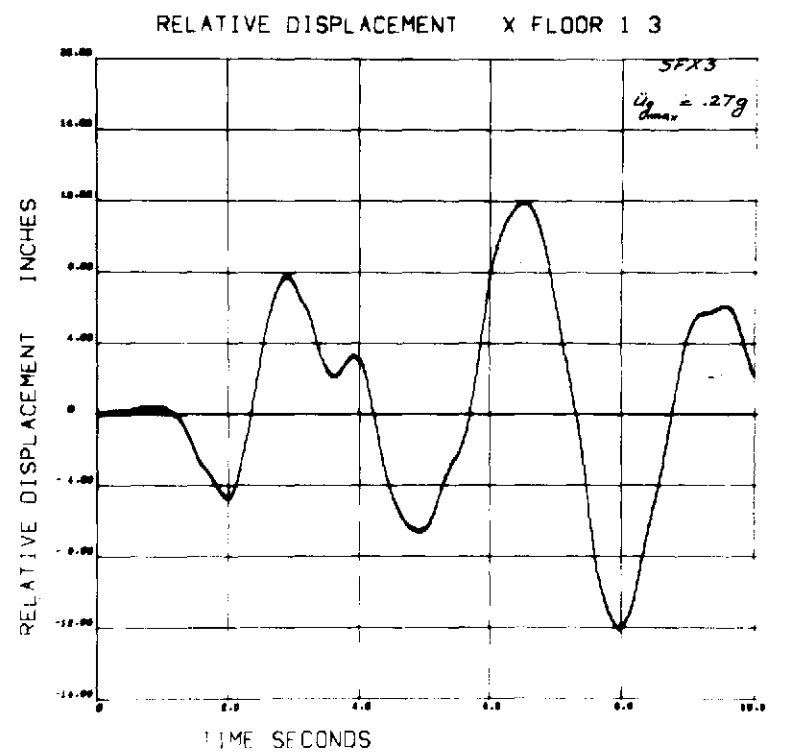
RELATIVE DISPLACEMENT X FLOOR 1 3
SFX3
$\ddot{u}_{g_{max}} = .27g$
RELATIVE DISPLACEMENT INCHES
TIME SECONDS

Figure C19

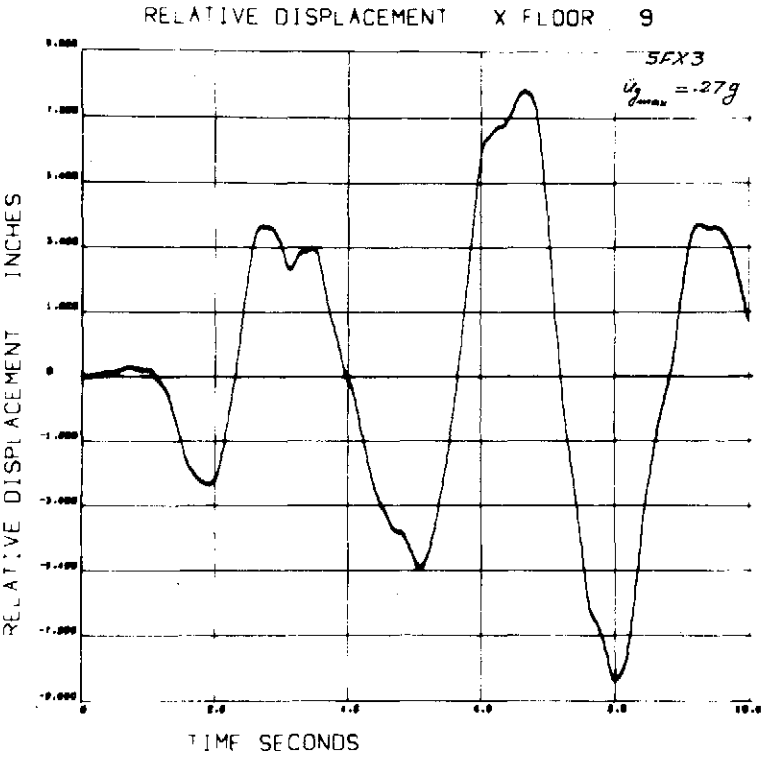
RELATIVE DISPLACEMENT X FLOOR 9
5FX3
$\ddot{u}_{g_{max}} = .27g$
RELATIVE DISPLACEMENT INCHES
TIME SECONDS

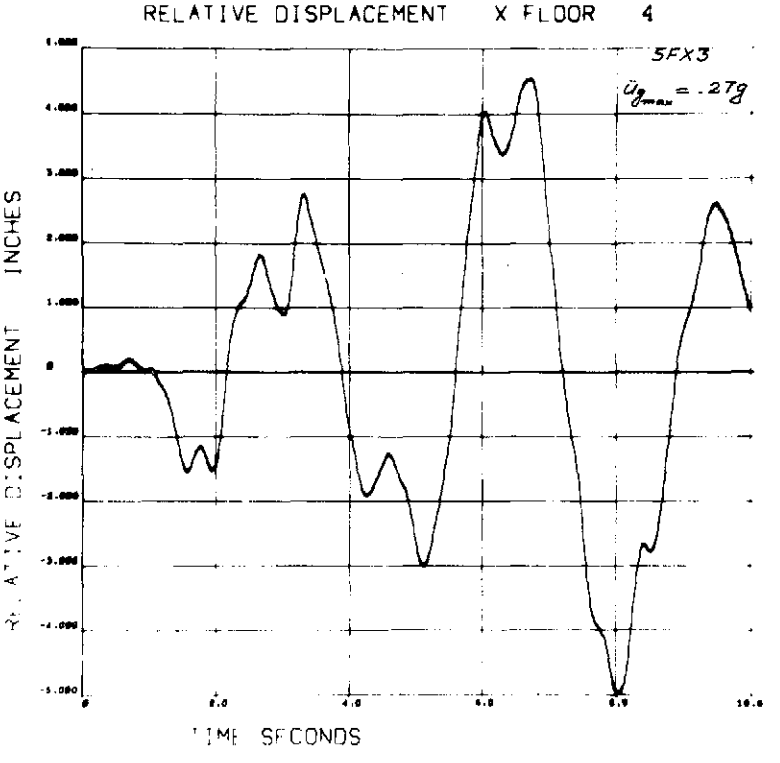
RELATIVE DISPLACEMENT X FLOOR 4
5FX3
$\ddot{u}_{g_{max}} = .27g$
RELATIVE DISPLACEMENT INCHES
TIME SECONDS

Figure C20

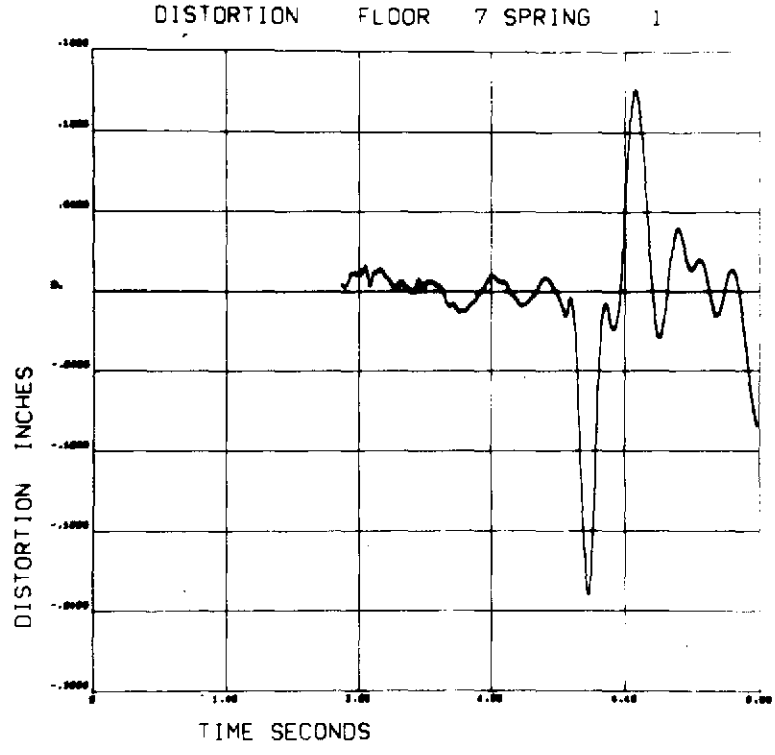
DISTORTION FLOOR 7 SPRING 1
DISTORTION INCHES
TIME SECONDS

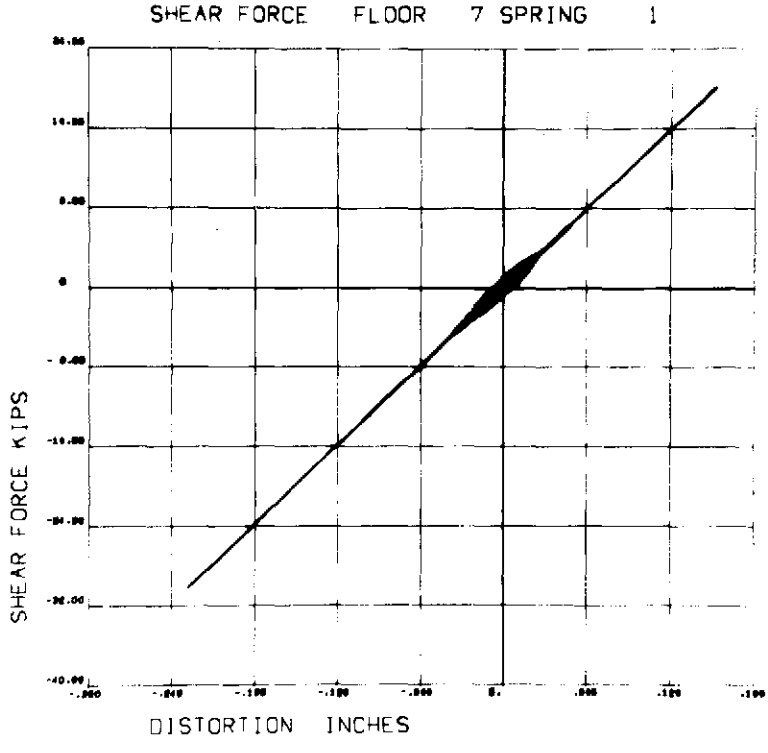
SHEAR FORCE FLOOR 7 SPRING 1
SHEAR FORCE KIPS
DISTORTION INCHES

Figure C21

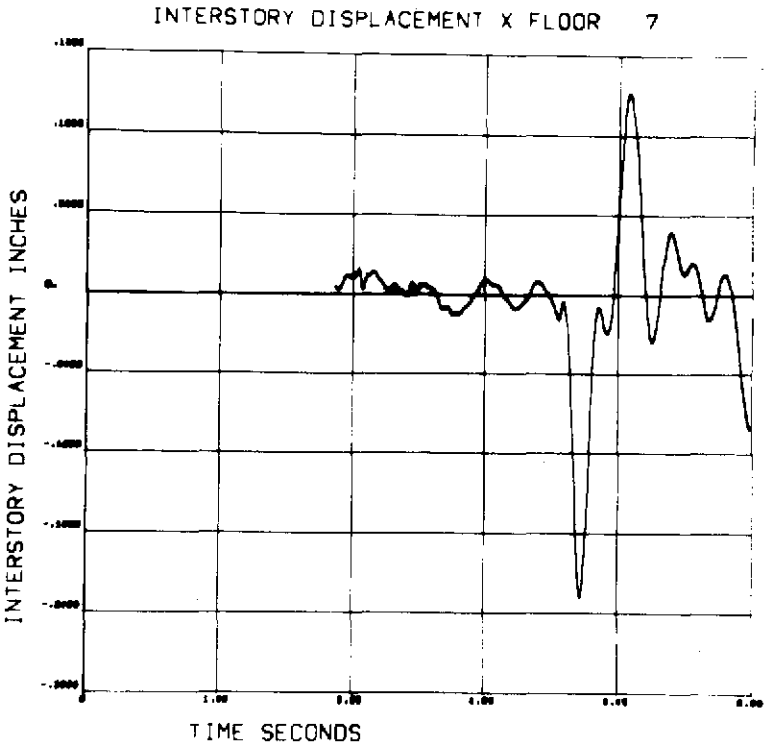
INTERSTORY DISPLACEMENT X FLOOR 7
INTERSTORY DISPLACEMENT INCHES
TIME SECONDS

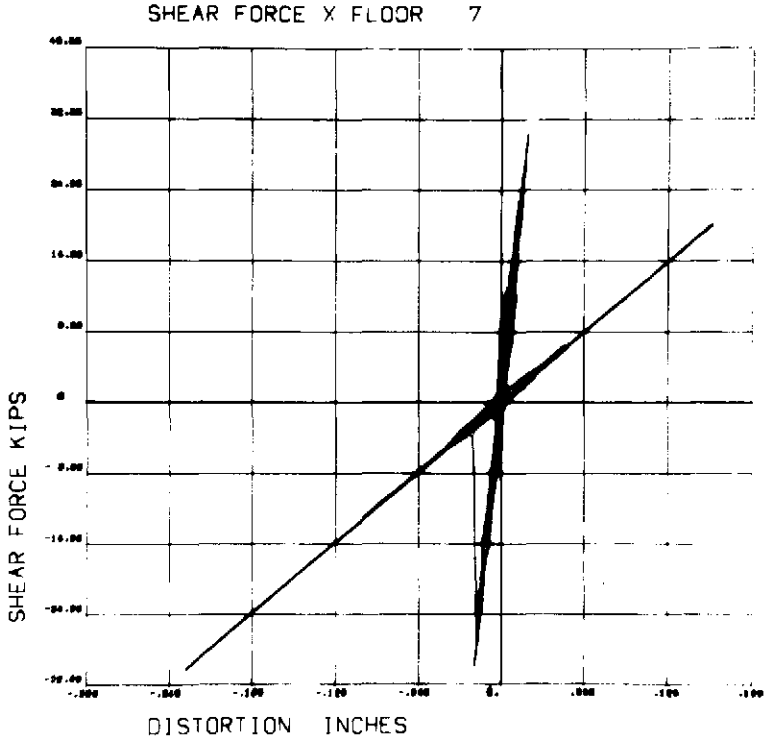
SHEAR FORCE X FLOOR 7
SHEAR FORCE KIPS
DISTORTION INCHES

Figure C22